Universitat Autònoma de Barcelona

Role of myosin VI in colorectal cancer

Irati Macaya Erro

ADVERTIMENT. L’accés als continguts d’aquesta tesi queda condicionat a l’acceptació de les condicions d’ús establertes per la següent llicència Creative Commons: http://cat.creativecommons.org/?page_id=184

ADVERTENCIA. El acceso a los contenidos de esta tesis queda condicionado a la aceptación de las condiciones de uso establecidas por la siguiente licencia Creative Commons: http://es.creativecommons.org/blog/licencias/

WARNING. The access to the contents of this doctoral thesis it is limited to the acceptance of the use conditions set by the following Creative Commons license: https://creativecommons.org/licenses/?lang=en

Role of myosin VI in colorectal cancer

By
Irati Macaya Erro

For the title of PhD
PhD program in Biochemistry, Molecular Biology and Biomedicine

Faculty of Medicine
Universitat Autònoma de Barcelona

The thesis was carried out at
Group of Biomedical Research in Digestive Tract Tumors

Center for Molecular Biology and Biochemistry Investigation in nanomedicine (CIBBIM-Nanomedicine)

Vall d'Hebron Research Institute (VHIR)

June 2018

DIRECTOR
Dr. Diego Arango Del Corro

TUTOR
Dr. Anna Meseguer Navarro

PhD CANDIDATE
Irati Macaya Erro

Lourdes eta Juanito-ri eskainia.

‘Nature was not designed to make life easy for biologists’
(Colin Tudge, 2007)

INDEX OF CONTENTS

INDEX OF FIGURES 8

INDEX OF TABLES 9

ABBREVIATIONS 10

SUMMARY 13

Resumen 13

Abstract 15

CHAPTER 1. INTRODUCTION 19

1. THE HUMAN GASTROINTESTINAL TRACT 19

1.1. The human intestine 19

1.1.1. Anatomy of the small intestine 20

1.1.2. Anatomy of the large intestine 20

1.1.3. Histology of the intestine 21

1.1.4. Small intestinal epithelium 23

1.1.5. Large intestinal epithelium 26

2. HOMEOSTASIS OF THE HUMAN INTESTINAL EPITHELIA 27

2.1. Overview 27

2.2. The stem cell niche 28

2.3. Morphogenic control of cell fate determination 29

3. HALLMARKS OF CANCER 32

4. COLORECTAL CANCER 34

4.1. Overview 34

4.2. Incidence and mortality 34

4.3. Risk factors and causes 36

4.4. Histopathological classification 37

4.5. Treatment 39

4.6. The multistep nature of colorectal cancer 39

4.7. The origin of colorectal cancer 41

4.8. Molecular pathways of colorectal cancer 42

4.8.1. Genomic instability 42

4.8.2. Oncogene and tumor suppressor gene mutations 46

5. THE MYOSIN SUPERFAMILY 51

5.1. Overview 51

5.2. Myosin functions 53
5.3. Myosins and cancer 55
6. MYOSIN VI 57
6.1. Overview 57
6.2. Mechanisms of regulation 59
6.3. Functions 63
6.3.1. Myosin VI and endocytosis 63
6.3.2. Myosin VI and secretory pathway 67
6.3.3. Myosin VI and autophagy 68
6.3.4. Myosin VI and cytokinesis 70
6.3.5. Myosin VI and migration 71
6.3.6. Myosin VI as an anchor 75
6.3.7. Nuclear role of myosin VI 76
6.4. Myosin VI and cancer 78
6.5. Myosin VI and human hereditary diseases 80
CHAPTER 2. AIMS OF THE STUDY 85
CHAPTER 3. MATERIALS AND METHODS 89
CHAPTER 4. RESULTS 109
1. Low MYO6 protein and mRNA expression in colorectal tumors is associated with poor patient prognosis. 109
2. Generation of isogenic colon cancer cell models with inducible MYO6 downregulation. 114
3. MYO6 does not regulate differentiation and polarization of colon cancer cells. 117
4. Downregulation of MYO6 expression does not affect the growth of colon cancer cells *in vitro*, but it increases their growth *in vivo*. 123
5. Downregulation of MYO6 expression does not change the metastatic potential of colon cancer cells. 131
6. Absence of MYO6 in deficient mice has no effects on intestinal tumorigenesis. 136
7. Absence of MYO6 in mouse intestinal tumor derived organoids increases Wnt signaling. 140
CHAPTER 5. DISCUSSION 145
1. MYO6 is an independent marker of prognosis in locally advanced colorectal cancer patients. 145
2. Generation of isogenic MYO6 knockdown colon cancer cell models. 147
3. MYO6 does not regulate differentiation and polarization in colon cancer cells. 147
4. Loss of MYO6 is important for the growth of colon cancer cells *in vivo*. 150

5. MYO6 does not regulate the metastatic potential in colon cancer cells. 152
6. Absence of MYO6 does not promote intestinal tumorigenesis in Snell's Waltzer mice..... 154
CHAPTER 6. CONCLUSIONS.. 159
BIBLIOGRAPHY... 163

INDEX OF FIGURES

Figure 1: The human gastrointestinal tract. 19
Figure 2: Histology of the intestine. 22
Figure 3: Small and large intestinal epithelium structure. 24
Figure 4: Organization of the different epithelial cell types of the small intestine. 25
Figure 5: Crypt organization in the small intestinal epithelium. 28
Figure 6: Key morphogen signaling pathway gradients in intestinal homeostasis. 31
Figure 7: The Hallmarks of Cancer and Enabling Characteristics. 32
Figure 8: Distribution of the expected cases and deaths for the 5 most common cancers in Europe in 2012 in males (A) and in females (B). 35
Figure 9: The growth from a polyp to a metastatic tumor. 38
Figure 10: Vogelgram: Genetic model of colorectal carcinogenesis presented by Fearon and Vogelstein in 1990. 40
Figure 11: 'Top-down' and 'bottom-up' models for adenoma origin and histogenesis in the colonic crypt. 42
Figure 12: Multiple parallel pathways for colorectal cancer development. 46
Figure 13: Genetic changes leading to deregulation of signaling pathways in CRC. 50
Figure 14: The human myosin family tree. 52
Figure 15: The structure of myosin VI. 58
Figure 16: Myosin VI protein expression levels in normal tissues. 60
Figure 17: Clathrin-coated endocytosis and the endocytic pathway. 64
Figure 18: The secretory pathway. 68
Figure 19: Steps in autophagy. 69
Figure 20: Dividing cell. 71
Figure 21: Possible roles of myosin VI during cell migration. 74
Figure 22: Organization of the structural proteins in the microvilli of the enterocytes. 76
Figure 23: Working model of myosin VI in transcription elongation. 77
Figure 24: pINDUCER10-shRNA plasmid structure. 91
Figure 25: 7xTcf-eGFP//SV40-mCherry (7TGC) plasmid structure. 92
Figure 26: Schedule of mice crosses. 104
Figure 27: Survival of colorectal cancer patients with low and high MYO6 tumor protein expression. 110
Figure 28: MYO6 tumor protein reduction along colorectal cancer progression. 112
Figure 29: Survival of colorectal cancer patients as a function of tumor *MYO6* mRNA expression. 113
Figure 30: MYO6 expression in colorectal cancer cell lines. 115
Figure 31: Confirmation of MYO6 protein expression in the selected colon cancer cell lines. 116
Figure 32: Inducible MYO6 downregulation in colon cancer cell lines. 117
Figure 33: Effects of MYO6 downregulation on the differentiation of CACO2 cells. 119
Figure 34: Effects of MYO6 downregulation on the differentiation of SW403 and LS513 cells. 121
Figure 35: Role of MYO6 downregulation on the localization of proteins of the adherens junctions in CACO2 cells. 122

Figure 36: Effects of MYO6 downregulation on the LKB1-dependent polarization in LS174T-W4 cells. 123
Figure 37: Role of MYO6 on the growth of colon cancer cells *in vitro* under normal attachment conditions. 124
Figure 38: Role of MYO6 on the colony forming ability of colon cancer cells *in vitro*. 125
Figure 39: Effects of MYO6 downregulation on the growth of CACO2 cells *in vivo*. 126
Figure 40: Effects of MYO6 downregulation on the growth of SW403 cells *in vivo*. 128
Figure 41: Effects of MYO6 downregulation on the growth of LS513 cells *in vivo*. 130
Figure 42: Role of MYO6 downregulation on the migration and invasion capability of colon cancer cells. 132
Figure 43: Role of MYO6 in the lung metastasizing capability of LS513 cells. 133
Figure 44: Role of MYO6 in the liver metastasizing capability of SW403 cells. 135
Figure 45: Characterization of *Myo6*$^{sv/sv}$ (Snell's Waltzer) mice. 136
Figure 46: Effects of *Myo6* inactivation on intestinal tumorigenesis in *Apc*$^{\mathrm{Min/+}}$ mice. 138
Figure 47: Effects of *Myo6* inactivation on AOM-induced intestinal tumorigenesis. 139
Figure 48: Effects of *Myo6* inactivation in the body weight of mice. 140
Figure 49: Role of MYO6 on Wnt signaling activation in organoids obtained from small intestinal tumors of *Apc*$^{\mathrm{Min/+}}$ mice. 141

INDEX OF TABLES

Table 1: (A) TNM and Dukes classification of colorectal cancers. (B) Definition of the different T, N and M stages. 38
Table 2: Human myosin VI isoforms. 60
Table 3: Myosin VI binding partners. 62
Table 4: Nuclear localization (NLS) and nuclear export (NES) signals predicted by bioinformatics tools within the myosin VI heavy chain. 76
Table 5: List of potential myosin VI-binding partners with nuclear functions in PC12 cells identified by mass spectrometry. 78
Table 6: Myosin VI pathogenic mutations in autosomal sensorineural hearing loss. 81
Table 7: General information of cell lines used in the study. 90
Table 8: Genetic features of colon cancer cell lines used in the study. 91
Table 9: shRNA sequences. 92
Table 10: Antibodies used in the study. 95
Table 11: Clinicopathological features of 164 Dukes' C colorectal cancer patients. 111
Table 12: Clinicopathological features of 115 Stage III colorectal cancer patients from the TCGA. 113

ABBREVIATIONS

3HB: Three-helix-bundle domain
5-FU: 5-Fluorouracil
AOM: Azoxymethane
AP: Alkaline phosphatase
APC: Adenomatous polyposis coli gene
ATP: Adenosine triphosphate
BrdU: Bromodeoxyuridine
CBC: Crypt base columnar cells
CBD: Cargo binding domain
CGN: Cis-Golgi network
CIMP: CpG island methylator phenotype
CIN: Chromosomal instability
CRC: Colorectal cancer
DMEM: Dubelcco’s Modified Eagle’s medium
DNA: Deoxyribonucleic acid
Dox: Doxycycline
DPP-IV: Dipeptidyl peptidase-4
EMT: Epithelial-mesenchymal transition
FACS: Fluorescence-activated cell sorting
FAP: Familial adenomatous polyposis
FBS: Fetal bovine serum
Fig.: Figure
GEF: Guanine nucleotide exchange factor
GFP: Green fluorescent protein
H&E: Hematoxylin and eosin
HNPCC: Hereditary non-polyposis colon cancer
ISC: Intestinal stem cells
KO: Knock-out
LI: Large intestine
LOH: Loss of heterozygosity
M cell: Microfold cell
MMR: Mismatch-repair genes
mRNA: Messenger RNA
MS: Mass spectrometry
MSI: Microsatellite instability
MSS: Microsatellite stable
MYO: Myosin
MYO6: Myosin 6/myosin VI
NaBut: Sodium butyrate
PBS: Phosphate-buffered saline
PCR: Polymerase chain reaction
PIP_2: PtdIns(4,5)P_2: Phosphatidylinositol 4,5-bisphosphate
RFP: Red fluorescent protein
RNA: Ribonucleic acid
RNAPII: RNA polymerase II complex
RNA-Seq: RNA sequencing
RPKM: Reads per kilo base per million mapped reads
RRL: Arginine-arginine-leucine motif
RT: room temperature
SAH: Single α-helix domain
SEM: Standard error of the mean
shMYO6: Short-hairpin RNA against MYO6
shNT: Non-targeting short-hairpin RNA
shRNA: Short-hairpin RNA
SI: Small insert
SI: Sucrase-isomaltase
SRB: Sulforhodamine B
SSA: Sessile serrated adenoma
TA: Transit-amplifying cells
TCGA: The cancer genome atlas
TGN: Trans-Golgi network
TMA: Tissue microarray
TNM-system: Tumor-node-metastasis system
tRFP: turbo RFP
vs: *Versus*
WB: Western blotting
WT: Wild-type
WWY: Tryptophan-tryptophan-tyrosine motif

SUMMARY

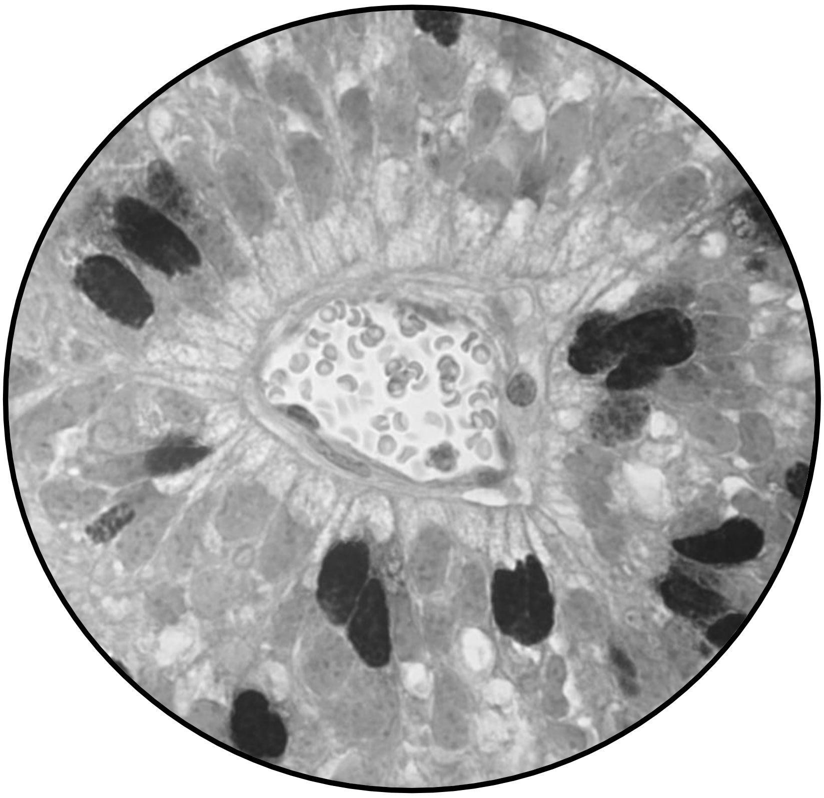

SUMMARY

Resumen

La miosina VI (MYO6) es un motor molecular que puede anclar moléculas o proporcionar tráfico de corto alcance a lo largo del citoesqueleto de actina valiéndose de la energía obtenida de la hidrólisis de ATP. La miosina VI se mueve hacia el extremo negativo de los filamentos de actina, en dirección opuesta al resto de miosinas. Se ha demostrado que la función de transporte de la miosina VI está implicada en varios procesos celulares, como la endocitosis, el tráfico endocítico y de reciclaje de vesículas, la autofagia, la exocitosis y la transcripción nuclear; y su función de anclaje se ha visto involucrada en el mantenimiento de la estructura del complejo de Golgi, de las estereocilias de las células ciliadas cocleares, de la membrana de las microvellosidades de los enterocitos, y en el mantenimiento de las uniones adherentes. La miosina VI se expresa en la mayoría de los tejidos, pero sus niveles de expresión varían considerablemente entre ellos. Además, la miosina VI puede existir en varias isoformas que se expresan diferentemente dependiendo del tipo de tejido. Estas isoformas interactúan con diferentes moléculas y, por lo tanto, llevan a cabo diferentes funciones. La miosina VI está altamente expresada en las células epiteliales del intestino delgado y grueso, estando principalmente localizada en la membrana apical y en la basolateral, aunque también está presente de forma difusa en el citoplasma. La miosina VI ha sido relacionada con determinados tipos de cáncer. En el cáncer ovárico, el de próstata y en la leucemia linfoide, se ha visto que la miosina VI está sobre-expresada, donde se le atribuye un papel en la migración y la invasión. Otros estudios también han asociado la sobre-expresión de la miosina VI con una mayor proliferación celular en cánceres como el hepático, el de mama y el de pulmón. Sin embargo, se sabe poco sobre el papel de la miosina VI en el cáncer colorrectal, el tercer tipo más común de cáncer en el mundo.

En este estudio, mediante el uso de un ‘tissue microarray’ (TMA) que contenía muestras de tejido normal de colon, tumores colorrectales primarios de estadio Dukes' C y muestras de metástasis de ganglios linfáticos, se observó que la expresión de MYO6 se reduce o se pierde con frecuencia en tumores primarios en comparación con la expresión de células epiteliales normales de colon; y que incluso aún se reduce más en las metástasis de los ganglios linfáticos, en comparación con los tumores primarios. Además, en pacientes con cáncer colorrectal localmente avanzado, la baja expresión de MYO6 en el tumor primario se asoció con una supervivencia general y una supervivencia libre de enfermedad más cortas. Para poder estudiar el posible papel de la miosina VI en el cáncer colorrectal, se diseñaron modelos celulares isogénicos inducibles por doxiciclina para reducir la expresión de MYO6. Los resultados mostraron que la inactivación de MYO6 no altera la capacidad de diferenciación/polarización de las células de cáncer de colon. Tampoco la capacidad de migración y de invasión *in vitro*, ni la habilidad de metastatizar en modelos de ratón, se vieron afectadas. Sin embargo, se observó que la reducción de la expresión de MYO6 incrementaba el crecimiento de las células de cáncer de colon en un modelo de xenoinjertos subcutáneos en ratones inmunodeficientes NOD/SCID, a pesar de no provocar ningún cambio en el crecimiento *in vitro*. Por otro lado, la ausencia de MYO6 en ratones *Apc*$^{Min/+}$ o en los tratados con AOM, no aceleró la tumorigénesis intestinal. Colectivamente, estos resultados indican que la pérdida de MYO6 es importante para promover el crecimiento de las células de cáncer colon, lo que indica un posible papel supresor tumoral de MYO6 en el cáncer colorrectal.

Abstract

Myosin VI (MYO6) is a molecular motor that can provide short range trafficking along the actin cytoskeleton by using the energy from ATP hydrolysis or anchor cargoes to actin filaments. Myosin VI moves towards the minus-end of actin filaments, in the opposite direction to the rest of myosins. The trafficking function of myosin VI has been shown to be involved in several cellular processes, such as, endocytosis, endocytic trafficking and recycling of vesicles, autophagy, exocytosis and nuclear transcription; and its anchoring function has been shown to be involved in the maintenance of Golgi complex, cochlear hair-cell stereocilia, enterocytic brush border membrane and adherens-junctions. Myosin VI is widely expressed in most tissues, but its expression levels vary considerably among them. Moreover, myosin VI can exist in several isoforms that are expressed in a tissue-specific manner. The isoforms interact with different binding partners and thus, carry out different functions. Myosin VI is highly expressed in the epithelial cells of small and large intestine, being mainly localized to the apical and basolateral membranes, although it is also present diffusely in the cytoplasm. Myosin VI has been involved in certain types of cancer. In ovarian carcinoma, prostate cancer and lymphoid leukemia myosin VI is found overexpressed with a role in migration and invasion. Other studies have also associated MYO6 overexpression with an increased cell proliferation in cancers such as, hepatocellular carcinoma, breast cancer and lung cancer. However, little is known about the role of myosin VI in colorectal cancer, the third most common type of cancer worldwide.

In this study, using a tissue microarray containing samples from normal colon tissues, primary Dukes'C colorectal tumors and lymph node metastases, MYO6 expression was observed to be frequently reduced or lost in primary tumors compared to normal colonic epithelial cells. Moreover, MYO6 levels were further reduced in regional lymph node metastases compared to primary tumors. Importantly, low tumor MYO6 expression was associated with shorter overall and disease-free survival in patients with locally advanced colorectal cancer. Therefore, to study the possible role of MYO6 in colorectal cancer, isogenic cell line systems with doxycycline-inducible MYO6 downregulation were engineered. The results showed that MYO6 inactivation does not alter the differentiation/polarization capability of colon cancer cells. The migration and invasion ability *in vitro* and the potential to metastasize in an *in vivo* mouse model were neither altered by MYO6 knockdown. Nevertheless, although no changes were observed in the growth *in vitro*, MYO6 inactivation increased the growth of colon cancer cells in a subcutaneous xenograft model in immunodeficient NOD/SCID mice. On the other hand, absence of MYO6 in *Apc*$^{\mathrm{Min/+}}$ or AOM-treated mice did not accelerate intestinal tumorigenesis. Collectively, our results indicate that loss of MYO6 provides a significant growth advantage to colon cancer cells, indicating a possible tumor suppressor role of MYO6 in colorectal cancer.

CHAPTER 1

INTRODUCTION

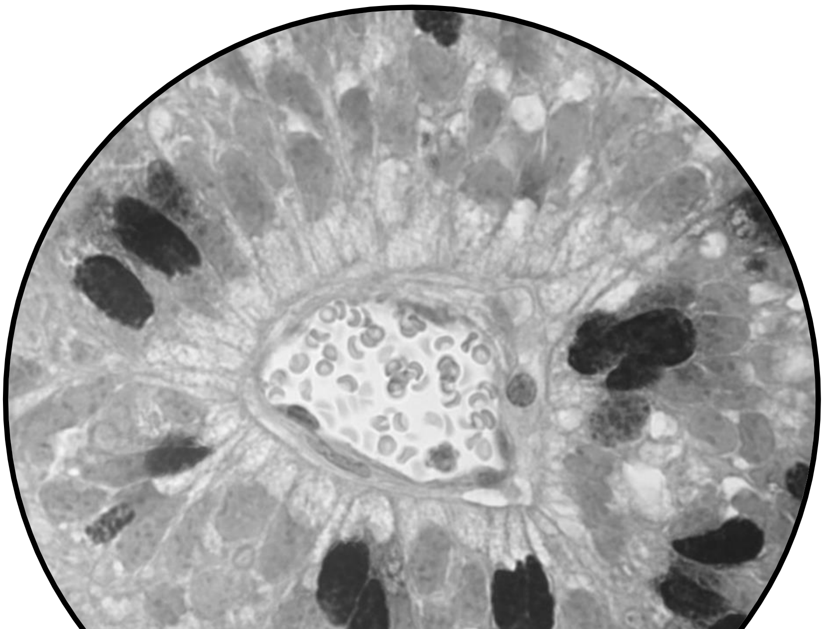

INTRODUCTION

1. THE HUMAN GASTROINTESTINAL TRACT

The human gastrointestinal tract together with a group of secretory organs forms the digestive system which is in charge of the digestion of the food and absorption of the nutrients. The gastrointestinal tract is basically a large muscular tube that extends from the mouth to the anus and through which food passes. It is made up of the oral cavity, pharynx, esophagus, stomach, small intestine, large intestine and anal canal. Several organs help in the digestion of the food by secreting enzymes directly into the gastrointestinal tract. Those organs include salivary glands, liver, gallbladder and pancreas (Feldman, Friedman, & Sleisenger, 2002) (**Fig.1**).

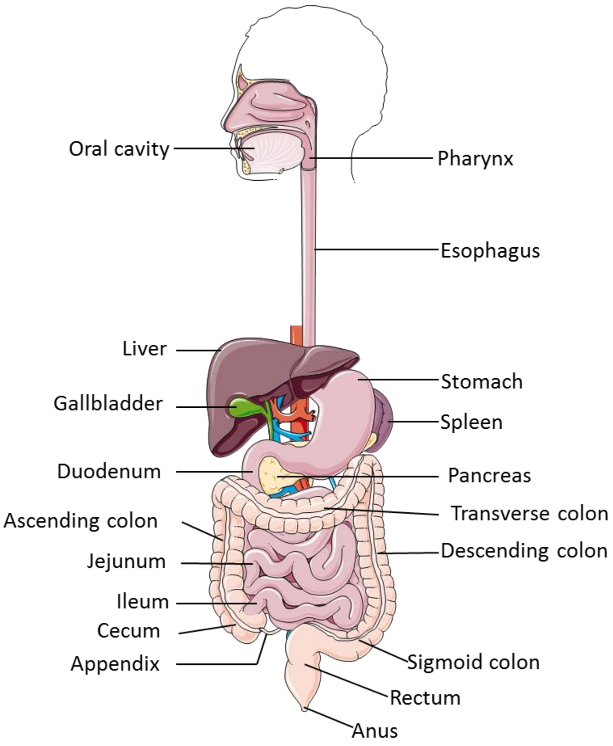
Oral cavity
Pharynx
Esophagus
Liver
Stomach
Gallbladder
Spleen
Duodenum
Pancreas
Transverse colon
Ascending colon
Descending colon
Jejunum
Ileum
Cecum
Appendix
Sigmoid colon
Rectum
Anus

Figure 1: The human gastrointestinal tract. Adapted from "Servier Medical Art," 2004.

1.1. The human intestine

The human intestine is positioned in the abdominal cavity and is composed of both, the small intestine and the large intestine. Its main function is the absorption of nutrients and water.

1.1.1. Anatomy of the small intestine

The human small intestine is the largest portion of the gastrointestinal tract with an average length of 6 m in an adult. The small intestine is responsible for absorption of nutrients, salt and water and for completion of food digestion. It is continuous proximally with the stomach and distally with the colon, being localized within the abdominal cavity. It consists of 3 parts: duodenum, jejunum and ileum (**Fig.1**). The diameter of the small intestine progressively decreases towards the distal part, being the ileum the narrowest segment (Feldman et al., 2002).

The **duodenum** is the most proximal and immobile portion of the small intestine. It is 20-25 cm long and presents a C shape. The duodenum is only covered by the peritoneum since it lacks the mesentery. Pancreatic and liver secretions directly enter into the duodenum in order to neutralize gastric acids and facilitate the digestion of proteins, carbohydrates and fats.

The rest of the small intestine is suspended (mobile part) within the peritoneal cavity by a thin, broad-based mesentery attached to the posterior peritoneal wall. The **jejunum** comprises the proximal 40% of the mobile small intestine (about 2.5 m) and it is localized in the upper left quadrant of the abdomen. The remaining 60% of the mobile small intestine is called the **ileum** and it is confined to the lower right quadrant of the abdomen. There is no clear margin between the jejunum and the ileum on external examination since the features change gradually along the small intestine. However, in overall, the jejunum has a bigger diameter, a thicker wall and it is more vascularized than the ileum.

The small intestine contains circular and longitudinal smooth muscles which by a series of contractions and relaxations (process called **peristalsis**) allow the anterograde movement of the chyme. These peristaltic movements are slower in the ileum. In addition, the luminal surface of the small bowel presents some mucosal folds called **circular folds** (also known as '*plicae circulares*' or 'valves of Kerckring') which are projected into the lumen transversally respect to the longitudinal axis. These circular folds function to slow down the movement of the chyme and increase the absorptive intestinal surface, thus facilitating a more efficient absorption of the nutrients. In the duodenum and in the proximal jejunum they are big and abundant but decrease in number and size in the distant small intestine being almost absent in the ileum. Lymphoid follicles are also scattered throughout the small intestine, finding the highest concentration in the distal ileum. Aggregates of lymphoid follicles are known as **Peyer's patches** (Drake, Vogl, & Mitchell, 2006; Feldman et al., 2002).

1.1.2. Anatomy of the large intestine

The large intestine is the last part of the gastrointestinal tract and is about 1.5 m long in an adult. It extends from the distal end of the ileum of the small intestine to the anal verge. The large intestine is responsible for the absorption of water, salts and some vitamins from the remaining waste materials that will be kept as feces before being removed by defecation. Unlike the small intestine, the large intestine does not play a major role in the absorption of nutrients. However, the flora (largely bacterial) found in the large intestine is fundamental to ferment the unabsorbed materials. The large intestine is composed of the cecum, colon, rectum and anal canal (**Fig.1**) (Feldman et al., 2002).

The first portion of the large intestine is the **cecum** which lies in the right iliac region of the pelvis and is slightly dilated compared to the rest of the large intestine. It is about 8 cm long and it is continuous with the small intestine via the ileocecal valve. The second portion of the large intestine is the **colon** which is divided into the following 4 parts: The **ascending colon** extends from the cecum for 12-20 cm along the right side of the peritoneal cavity to the undersurface of the liver. In the hepatic flexure the colon turns 90º and crosses the width of the peritoneal cavity as the **transverse colon**. This segment is about 45 cm in length. Then, at the splenic flexure the **descending colon** travels downwards until the pelvic brim, extending about 25 cm. Finally, the colon ends as S-shaped segment called **sigmoid colon** which is around 40 cm long. The **rectum**, of 10 cm, begins at the peritoneal reflection and follows the curve of the sacrum, ending at the **anal canal**.

The diameter of the large intestine is wider than that from the small intestine. Both, the small and the large intestine, have inner circular and outer longitudinal muscle layers. However, the longitudinal muscle fibers of the large intestine fuse into three discrete bands (***teniae***) positioned at 120 degree intervals respect to the intestinal circumference. In addition, the wall of the large intestine presents small pouches known as '**haustra**' conferring a segmented appearance. Fatty-filled sacs of peritoneum called **epiploic appendices** (also known as '*appendices epiploicae*' or 'omental appendices') can also be found scattered along the outside part of the large intestinal wall, except in the cecum and rectum (Drake et al., 2006; Feldman et al., 2002).

1.1.3. Histology of the intestine

The four layers of the intestinal wall are the serosa or adventitia, the *muscularis propria*, the submucosa and the mucosa, ordered from the most external to the most inner (**Fig.2**) (Standring et al., 2008). These layers are quite similar in both the large and small intestine, except for some differences that will be commented.

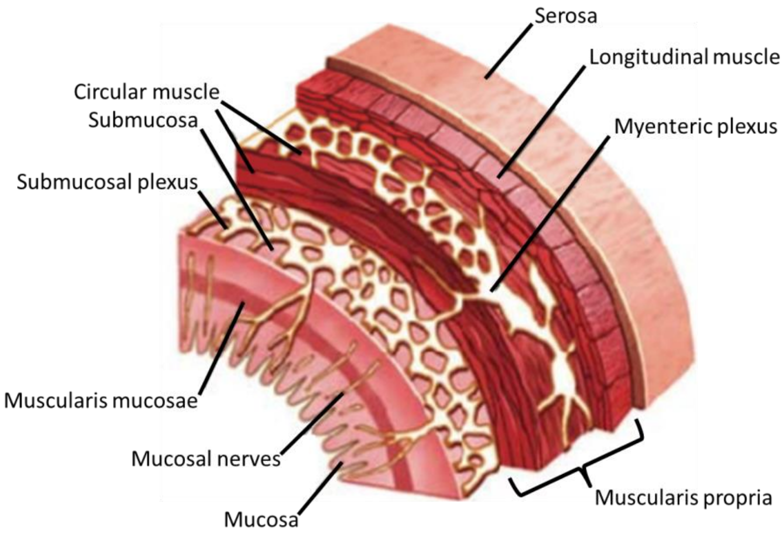

Figure 2: Histology of the intestine. Intestinal wall is composed of 4 layers: serosa or adventitia, *muscularis propia* (formed by longitudinal and circular smooth muscle layers), submucosa and mucosa. Figure adapted from Feldman et al., 2002.

The outermost layer of the intestine is the serosa or, in its absence, the adventitia. The **serosa** consists of a single layer of mesothelial cells and another single layer of connective tissue. The mesothelial layer of the serosa secrets an aqueous fluid that acts as lubricant in order to reduce the friction between different organs that are located in the peritoneal cavity. The **adventitia**, in contrast, consists only of a single layer of connective tissue. Therefore, unlike the serosa, its main function is to maintain the localization of the intestine instead of lubricate it. Most of the intestine is bounded by serosa, except the distal part of the duodenum, the ascending colon, the descending colon and the rectum, which are instead bounded by adventitia. Generally, intestinal segments that are intraperitoneal and free to move are covered by serosa, while intestinal segments that are retroperitoneal and relatively fixed in their positions are covered by adventitia.

The ***muscularis propria* or *muscularis externa*** is composed of outer longitudinal and inner circular layers of smooth muscle fibers. It is responsible for gut movement known as peristalsis. In the large intestine this muscular layer is thicker than in the small intestine and its longitudinal smooth muscle fibers form the already explained '*teniae*'.

The **submucosa** is a layer of loose connective tissue which contains blood vessels, lymphatic vessels and nerves that branch into the mucosa and *muscularis propria*. Unlike in the large intestine, in the small intestine the submucosa forms crescentic projections that give support to the mucosal circular folds.

The **mucosa** is the innermost layer of the intestinal wall and this, in turn, can be separated in three layers: the *muscularis mucosae*, the *lamina propria* and the intestinal epithelium.

The ***muscularis mucosae*** is a thin sheet of outer longitudinal and inner circular layers of smooth muscle cells that separates the mucosa from the submucosa. The contraction of the *muscularis mucosae* keeps the mucosal surface and underlying glands in a constant state of gentle agitation to expel contents of the glandular crypts and enhance contact between epithelium and the contents of the lumen.

The ***lamina propia*** or basal membrane is a connective tissue that provides mechanical support to the epithelium. It contains lymphoid tissue, capillaries, lymphatic vessels and nervous fibers. The *lamina propria* acts as the first line of immunological defense against bacterial and viral invasion. As mentioned earlier, scattered through the small intestine (but not in the large intestine) the *lamina propria* harbors aggregates of lymphocytes called Peyer's patches.

The **epithelium** is the innermost layer of the mucosa and it is in direct contact with the luminal contents of the intestine. The epithelium is formed by highly specialized epithelial cells that absorb and secrete products essential to sustain life. Notably, the epithelium of the small intestine differs from the large intestinal epithelium in the structural organization and cell composition (Drake et al., 2006; Standring et al., 2008).

1.1.4. Small intestinal epithelium

The small intestine is organized in crypts and villi. The **villi** (singular villus) are finger-like structures that extend out into the intestinal lumen. In that way, the villi increase the luminal surface area of the intestinal walls by 8-30 fold and thus, improve the absorption of nutrients. Those villi are big and numerous in the duodenum and jejunum, while in the ileum appear smaller and less abundant. The **crypts** (also known as crypts of Lieberkühn) are epithelial invaginations intercalated between the villi (**Fig.3**) (Standring et al., 2008).

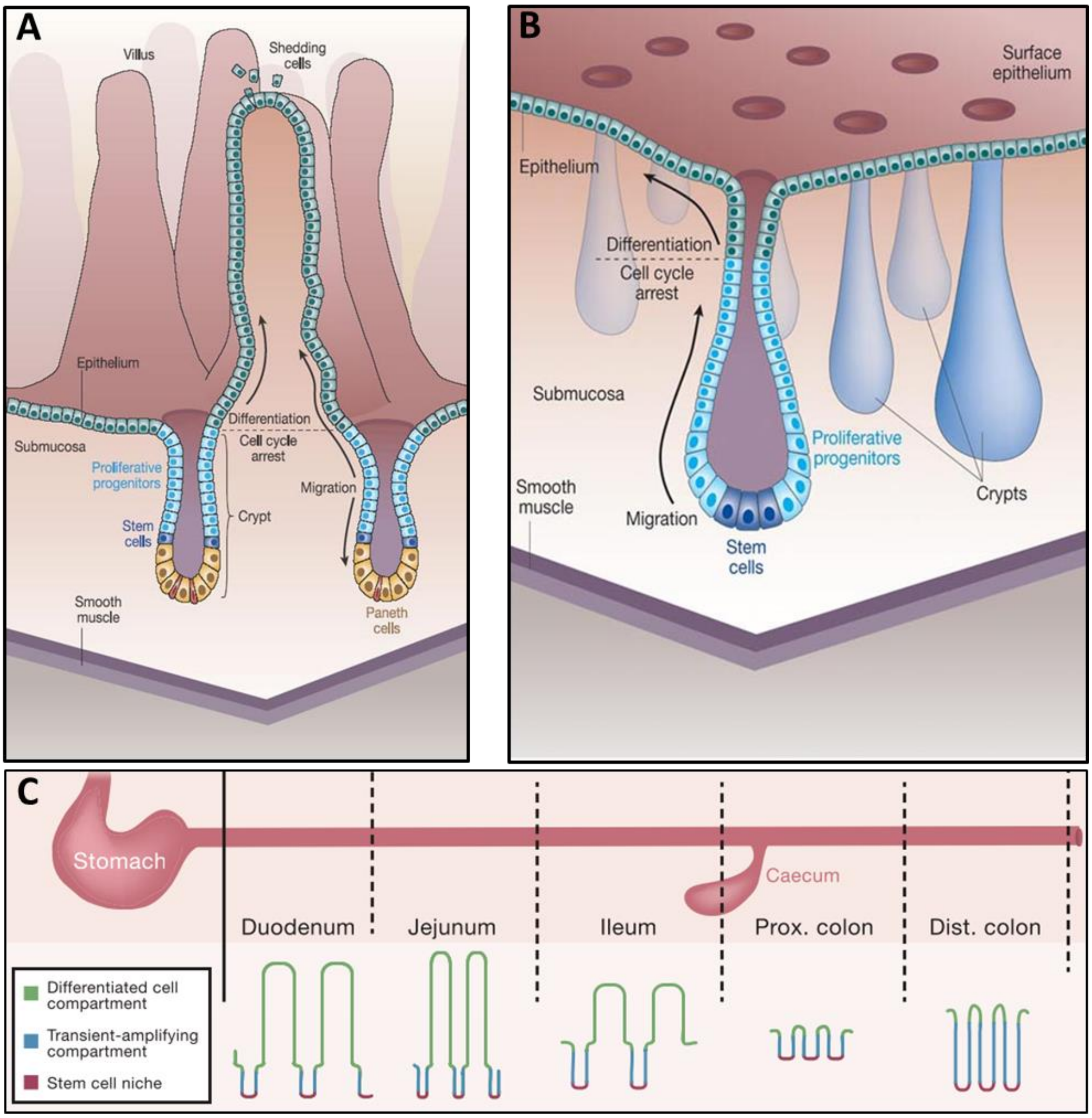
A
Villus
Shedding cells
Epithelium
Submucosa
Proliferative progenitors
Stem cells
Smooth muscle
Differentiation
Cell cycle arrest
Crypt
Migration
Paneth cells
B
Surface epithelium
Epithelium
Differentiation
Cell cycle arrest
Submucosa
Smooth muscle
Migration
Stem cells
Proliferative progenitors
Crypts
C
Stomach
Caecum
Duodenum
Jejunum
Ileum
Prox. colon
Dist. colon
Differentiated cell compartment
Transient-amplifying compartment
Stem cell niche

Figure 3: Small and large intestinal epithelium structure. A) Epithelium of the small intestine with villi and crypts. **B)** Epithelium of the large intestine only showing crypts. **C)** The intestinal epithelium presents different villus-crypt conformations along the intestinal axis. Adapted from H. Clevers & Batlle, 2013 and Reya & Clevers, 2005.

Six differentiated cell types populate the small intestinal epithelium (**Fig.4**). The most abundant cells are the enterocytes (absorptive cells) followed by goblet cells (7% of epithelial cells). **Enterocytes** are polarized epithelial cells lining the villi that are in charge of the absorption of the nutrients. They contain apical microvilli (brush border) facing the intestinal lumen which are estimated to increase the surface area of the cell between 14 and 40 times (Feldman et al., 2002). **Goblet cells** (mucosecreting cells) generate a mucus layer composed mainly by mucins that coats the intestinal surface lubricating and protecting it against the physical and chemical injury caused by ingested food, microbes and the microbial products (Kim & Ho, 2010).

Other rare secretory cell types are also scattered throughout the epithelium. They include enteroendocrine cells (1% of cell population) and tuft cells (0.4%). **Enteroendocrine cells** act as sensors of luminal contents, particularly of nutrients and by secreting a diverse array of hormones they control physiological and homeostatic functions in the digestive tract (Moran, Leslie, Levison, Worthington, & McLaughlin, 2008). **Tuft cells** are believed to secrete prostanoids and may be involved in the taste transduction pathway and in the type-2 immune response against parasitic infection (Howitt et al., 2016).

Microfold cells (M cells) are specialized epithelial cells situated over Peyer's patches. They transport antigens from the lumen to adjacent lymphoid tissues promoting the production of antibodies. Finally, **Paneth cells** are cells residing at the crypt base where they perform a dual role; they secrete antimicrobial substances and growth factors and they also nurture the intestinal stem cell (ISC) population (Feldman et al., 2002).

All differentiated cell types in the intestinal epithelium are short lived. Enterocytes, goblet cells, and the other secretory lineages are born in the crypts and migrate up towards the tip of the villi. At this location, they are extruded into the lumen. Therefore, turnover time of cells in the small intestine epithelium appears to be about 4 to 6 days. Paneth cells are the exception and are retained at the base of the crypts, where they live for 6–8 weeks (H. Clevers & Batlle, 2013).

Intestinal stem cells (ISCs) are nonmigratory, pluripotential cells located at the base of the crypt intermingled with Paneth cells (10–15 ISCs per crypt) (**Fig.4**). They are responsible for the renewal of the epithelial layer. ISCs are able to proliferate to give rise to progenitor cells (transit-amplifying (TA) cells) and self-renew. These transit-amplifying cells become progressively committed toward one of the six differentiated lineages that are present in the intestine (H. Clevers & Batlle, 2013).

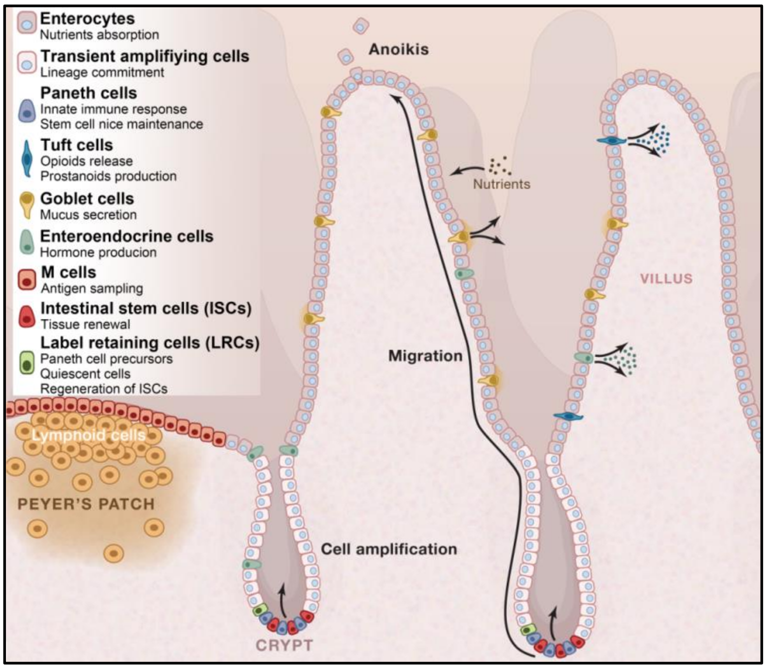
Enterocytes
Nutrients absorption
Transient amplifiying cells
Lineage commitment
Paneth cells
Innate immune response
Stem cell nice maintenance
Tuft cells
Opioids release
Prostanoids production
Goblet cells
Mucus secretion
Enteroendocrine cells
Hormone producion
M cells
Antigen sampling
Intestinal stem cells (ISCs)
Tissue renewal
Label retaining cells (LRCs)
Paneth cell precursors
Quiescent cells
Regeneration of ISCs
Anoikis
Nutrients
VILLUS
Migration
Lymphoid cells
PEYER'S PATCH
Cell amplification
CRYPT

Figure 4: Organization of the different epithelial cell types of the small intestine. Adapted from H. Clevers & Batlle, 2013.

1.1.5. Large intestinal epithelium

The large intestinal epithelium is only organized in crypts (**Fig.3**). Those crypts are longer, more abundant and more tightly packed than the ones in the small intestine. Instead of villi, there are flat epithelial surfaces between crypts covered mainly by enterocytes. The cell types in the epithelium of the large intestine are the same than in the small intestine. However, the number of goblet cells is larger and there are no Paneth cells in the crypts.

In the large bowel the cells are also generated in the crypts and extruded from the flat intercrypt region on the surface. In this case, the average lifespan of a differentiated cell appears to be 3-5 days (Standring et al., 2008).

2. HOMEOSTASIS OF THE HUMAN INTESTINAL EPITHELIA

2.1. Overview

The epithelium of the intestine represents the most rapidly self-renewing tissue of adult mammals (H. C. Clevers & Bevins, 2013). This rapid renewal of the tissue acts as a protective mechanism against the toxic contents of the gut lumen that threaten the genomic integrity of the intestinal mucosal cells. This mechanism forces epithelial cells that could have been exposed to genotoxic luminal contents to enter apoptosis and be shed into the gut lumen in 5-7 days (Biswas et al., 2015), ensuring the death of possible altered and life-threating cells.

Intestinal epithelial turnover depends on the self-renewing stem cell population mentioned above, that resides at the crypt base, safely tucked away from the shear stresses and potentially toxic agents that pass through the intestinal tract.

Crypts are considered the basic functional unit of the gut and are organized into three compartments following a bottom-to-top axis: the stem cell compartment (**stem-cell niche**) that is located at the crypt base, the transit-amplifying (TA) compartment that occupies the middle portion of the crypts, and the differentiation compartment (**Fig.5**) (H. Clevers & Batlle, 2013).

Stem cells at the base of the crypt divide slowly (with a cell cycle period of 24 h) self-renewing and giving rise to transit-amplifying cells. These TA cells are intermediate cells located in the bottom third of the intestinal crypt that undergo rapid proliferation (they divide every 12 h) generating a population of non-proliferating daughter cells which accumulate in the medium third of the crypt. These daughter cells progressively differentiate into the 6 epithelial linages (enterocytes, goblet cells, enteroendocrine cells, tuft cells, M cells and Paneth cells) while they migrate upwards through the crypt. Once differentiated, most cell types migrate upward from the upper third of the crypt to the tip of the villus, and at the top they become apoptotic and are extruded into the lumen. Exceptionally, Paneth cells migrate to the bottom of the crypt where they reside for about 6-8 weeks. In that way, the entire intestinal epithelium is renewed every 5-7 days (Pinto & Clevers, 2005).

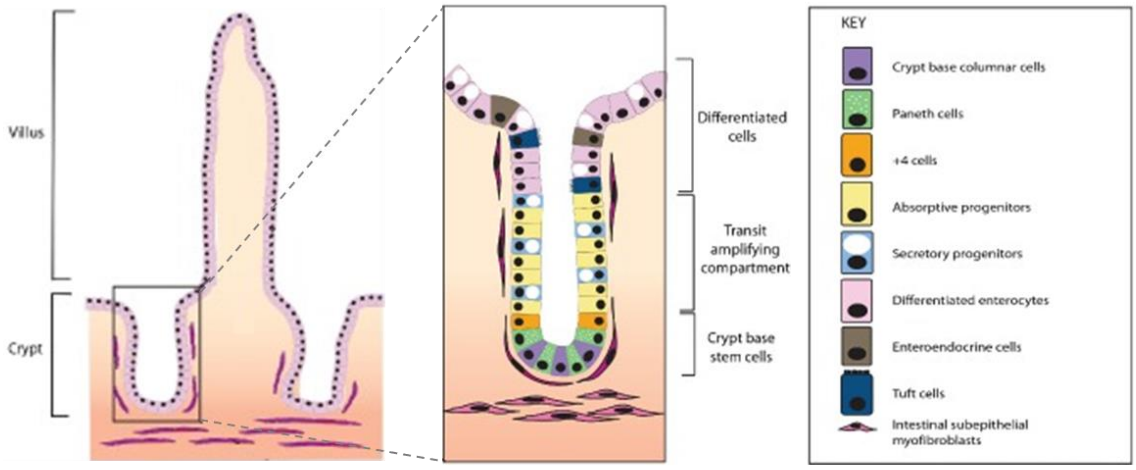
Villus
Crypt
Differentiated cells
Transit amplifying compartment
Crypt base stem cells
KEY
Crypt base columnar cells
Paneth cells
+4 cells
Absorptive progenitors
Secretory progenitors
Differentiated enterocytes
Enteroendocrine cells
Tuft cells
Intestinal subepithelial myofibroblasts

Figure 5: Crypt organization in the small intestinal epithelium. The crypt is organized into 3 compartments: the stem cell compartment, the transit-amplifying compartment and the differentiation compartment. Two types of stem cells are found in the base of the crypt: crypt base columnar (CBC) cells and stem cells at position +4. Adapted from Biswas et al., 2015.

2.2. The stem cell niche

The stem cell niche is composed of 10 to 15 stem cells and mesenchymal cells that surround the crypt base. The mesenchymal cells belong to the myofibroblast lineage and play a role in the control of stem cell behavior, maintenance of the stem cell habitus and cell migration and differentiation (Humphries & Wright, 2008). Stems cells are characterized by an undifferentiated phenotype, self-renewal capability, multipotency (capacity to differentiate into all intestinal epithelial cell types), high proliferative potential throughout life and ability to repopulate entire intestinal crypts upon injury (Pinto & Clevers, 2005).

Two distinct populations of cells with stem-like properties have been identified: crypt base columnar (CBC) cells and label-retaining cells at position +4 relative to the base of the intestinal crypt (**Fig.5**) (Biswas et al., 2015). **Crypt base columnar (CBC) cells** are intermingled with Paneth cells in the small intestine and are considered as the 'cycling stem cells' since they divide once per day. CBC cells are the ones that give rise to transit-amplifying progeny and thus, to all epithelial lineages (Barker et al., 2009; H. C. Clevers & Bevins, 2013). **Label-retaining cells at position +4** represent a quiescent and slowly cycling population of stem cells. It has been demonstrated that these cells are committed to being secretory cell precursors that retain the capability of returning to stem cell function in the event of intestinal damage and regeneration (Biswas et al., 2015).

LGR5 (leucine-rich-repeat-containing G-protein-coupled receptor 5) gene is specifically restricted to CBC cells and it has been considered as a bona fide stem cell marker in the intestine. BMI1 and TERT markers have been demonstrated to point the +4 position cells. Several other markers have been used to identify populations of cells capable of lineage tracing in the intestine such as, Hopx, Lrig1, Sox9, Ascl2, Olfm4, Prom1 and Rnf43 (Biswas et al., 2015).

Stem cell fate is not fixed, even within the confines of the stem cell niche. Intestinal stem cells form an equipotent population and undergo symmetric cell divisions. In a **symmetrical stem-cell division** any of the daughter cells can become stem cell or transit-amplifying cell. Sometimes both daughter cells become committed to differentiation and other times, both become stem cells. Therefore, one stem-cell lineage may become extinct as both daughters leave the niche (Humphries & Wright, 2008). This symmetrical stem-cell division leads to random enlargement and contraction of clones, known as **neutral drift dynamics**, and thus, it leads to stochastic clonal extinction or niche succession where one clone expands to fill the entire niche (Biswas et al., 2015; Medema & Vermeulen, 2011). This explains the monoclonal nature of the intestinal crypts.

2.3. Morphogenic control of cell fate determination

Stem cell function and daughter cell fate determination is not exclusively an intrinsic, cell autonomous property. In fact, cell fate determination depends on spatial organization of signals that emanate from supportive mesenchymal cells, as well as from differentiated epithelial progeny (Medema & Vermeulen, 2011). These signals appear in a polarized gradient pattern, resulting in several complex interactions along the crypt-villus axis that lead to restriction of certain pathways and activation of other pathways, which consequently regulate stemness, cell proliferation, differentiation and apoptosis.

Important pathways involved in cell fate determination include Wnt, BMP, Hedgehog, and Notch signaling (Biswas et al., 2015). Epithelial-mesenchymal interactions happen through the Hedgehog and BMP signaling pathways. Instead, within the epithelium, cells signal to one another through the Wnt, Notch and Eph/ephrin pathways (**Fig.6**) (Crosnier, Stamataki, & Lewis, 2006).

Hedgehog demarcates villus from crypt: Hedgehog controls tissue polarity. Sonic hedgehog (Shh) and Indian hedgehog (Ihh) ligands are secreted by the epithelium in a paracrine manner to act on the underlying mesenchymal cells. This signaling is important for homeostasis of mesenchymal cells and the development of the connective-tissue coat around the gut tube. Hedgehog signaling is also involved in the regulation of epithelial cell proliferation. The mesenchymal cells respond to the hedgehog signal from the epithelium by delivering signals back to the epithelium which increase BMP signaling. This negative feedback generates a restriction of the proliferation in the intervillus regions, which in turn, leads to the formation of the villi (Biswas et al., 2015; Crosnier et al., 2006).

BMP inhibits crypt formation: Bone morphogenetic protein (BMP) signaling is part of the TGFβ (transforming growth factor β) superfamily and it phosphorylates SMAD proteins for signal transduction. BMP2 and BMP4 ligands are expressed by the mesenchyme as a respond to hedgehog signaling and have effect on the epithelium, where they are suggested to halt the proliferation by repressing Wnt signaling and to allow the differentiation. BMPs are active in the epithelium of the villi and at the top of the crypt. However, BMPs are also produced at the crypt bottom, but here they are blocked by BMP inhibitors (such as Noggin and Gremlin1 and 2) that are specifically expressed by the mesenchyme in the intestinal stem cell region, enabling proliferation to continue. Therefore, BMP signaling blocks the formation of ectopic crypts and presents opposite gradients to Wnt signaling (Biswas et al., 2015; Crosnier et al., 2006; Medema & Vermeulen, 2011).

Wnt signaling maintains proliferation: Wnt signaling is mainly restricted to the stem and proliferative zones in the bottom third of the crypt, where it is involved in the maintenance of stem cell function and driving transit-amplifying cell proliferation (Biswas et al., 2015). WNT ligands are expressed by both epithelial and mesenchymal cells at the base of the crypt and act on the epithelial cells that present the corresponding receptor families (frizzled 5, 6 and 7, and LRP5 and 6). Those cells show an activation of the canonical Wnt pathway and thus, high levels of intranuclear β-catenin. Paneth cells residing next to ISCs are one of the main sources of WNT3a, and they consequently spatially constrain ISCs to the crypt bottom (Crosnier et al., 2006; Medema & Vermeulen, 2011).

Notch signaling determines absorptive or secretory cell fate: Notch and its ligands of the Delta and Serrate/Jagged subfamilies are transmembrane proteins that mediate communication between cells that are in contact with one another. These components of the Notch pathway are expressed in the epithelium of the crypts; not in the villar epithelium. Notch signaling determines cell fate decision between absorptive and secretory cell types. Activation of Notch leads to an absorptive differentiation and cells that scape Notch activation become secretory (Biswas et al., 2015). Moreover, Notch signaling shows a feedback inhibition process; that is, cells that receive signals through Notch downregulate their own Notch ligands and thus deprive their neighbouring cells of Notch-activating signals. Therefore, cells that become committed to a secretory fate are the ones that express Notch ligands impeding their neighbours from differentiating in the same way (Medema & Vermeulen, 2011). Notch signaling is also involved in the control of stem cells and transit-amplifying cell division. All the proliferating cells, including the stem cells, depend on Notch and WNT signals in combination to keep them in a proliferating state: neither Wnt pathway activation nor Notch pathway activation is sufficient by itself (Crosnier et al., 2006). Therefore, Notch directs proliferation when WNT signal activity is high, and directs enterocyte differentiation when WNT activity levels drop towards the top of the crypt.

Eph/ephrin signals control cell segregation: Eph receptors and their ligands (ephrins) are membrane-associated proteins that mediate communication between adjacent cells. The proper segregation and migration of the different cell types within the crypt-villus structure is controlled by Wnt signaling through ephrin B1 and its receptors EPHB2 and EPHB3 (Crosnier et al., 2006). Wnt signaling switches on expression of EPHB2 and EPHB3 and inhibits expression of ephrin B1 (Batlle et al., 2002). Moreover, there is repulsion between EPHB expressing cells and ephrin expressing cells. Therefore, Wnt activated cells by expressing EPHB2 and EPHB3 (cells located near the base of the crypts including Paneth cells) avoid becoming diluted with differentiated cells that lack Wnt activity and that, as a consequence, express ephrin B1 (cells from the crypt-villus junction and villus epithelium). In fact, EphB and ephrin genes are expressed in counter gradients along the crypt-villus axis (Batlle et al., 2002; H. Clevers & Batlle, 2006).

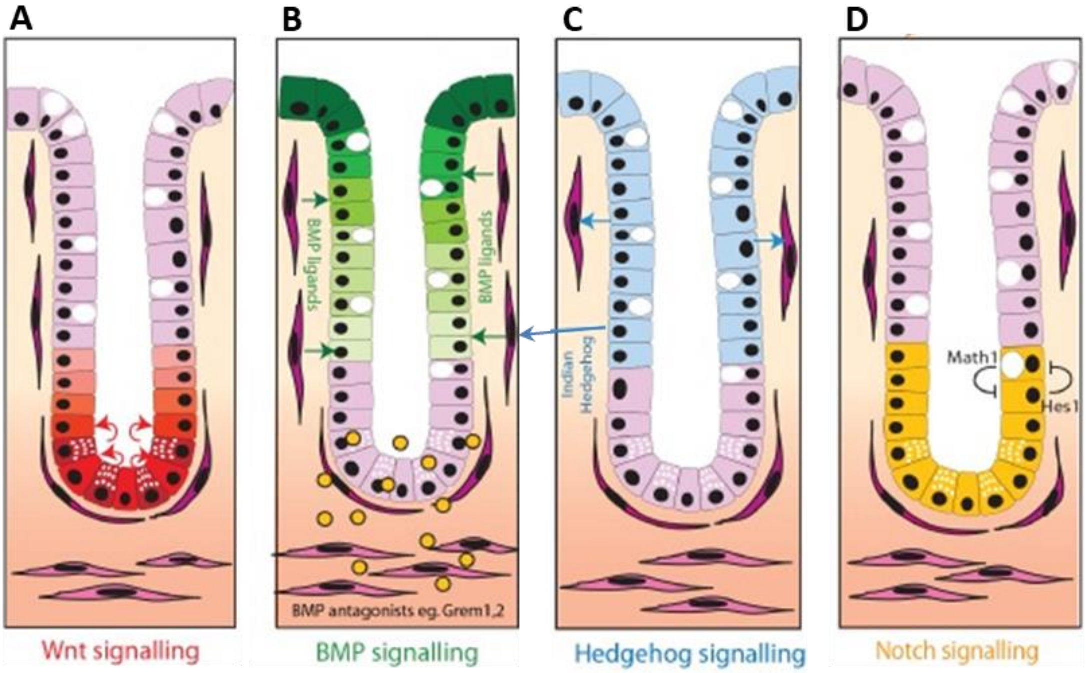

Figure 6: Key morphogen signaling pathway gradients in intestinal homeostasis. Intestinal homeostasis and cell fate determination are maintained by a complex interaction of epithelial and mesenchymal morphogen signaling pathways. Major pathways include: **A)** Wnt signaling. Wnt ligands, secreted from subepithelial myofibrobasts and Paneth cells, act predominantly at the base of the crypt (red cells) to maintain stem cell function and transit-amplifying cell proliferation; **B)** Bone morphogenetic protein signaling. BMP ligands are produced predominantly by the mesenchymal cells. BMP represses Wnt signaling and promotes cell differentiation and apoptosis, acting predominantly in the upper part of the crypt and villus (green cells). There is reduced BMP activity at the base of the crypt, due to the restricted expression of BMP antagonists from the sub-crypt myofibroblasts; **C)** Hedgehog signaling. Indian hedgehog (IHH) is expressed by epithelial cells in the upper part of the crypt (blue cells). IHH acts upon and maintains the myofibroblasts. This has a secondary effect on the epithelium through promotion of BMP ligand expression; **D)** Notch signaling. Notch regulates cell fate through cell-to-cell contact in the stem cell and transit-amplifying zone at the base of the crypt (yellow cells). Notch activation via Hes1 transcription factor and lateral inhibition via Math1 transcription factor regulate enterocyte or secretory cell fate, respectively. Adapted from Biswas et al., 2015.

3. HALLMARKS OF CANCER

The hallmarks of cancer refer to eight biological capabilities that cancer cells acquire during the multistep development of tumors and which allow them to survive, proliferate and disseminate. They include sustaining proliferative signaling, evading growth suppressors, resisting cell death, enabling replicative immortality, inducing angiogenesis, activating invasion and metastasis, reprogramming of energy metabolism and evading immune destruction. These capabilities can be acquired in the wide variety of tumors through different mechanisms and at different steps or time points of the tumorigenesis (Hanahan & Weinberg, 2000, 2011).

The gain of these hallmarks is due to two enabling characteristics: first, **genome instability**, which triggers random mutations and chromosomal rearrangements and thus, accelerates the acquisition of the cancerous abilities; and second, **inflammation** of premalignant and malignant lesions, that is driven by immune cells and which promotes tumor progression through several manners/hallmark functions (**Fig. 7**) (Hanahan & Weinberg, 2000, 2011).

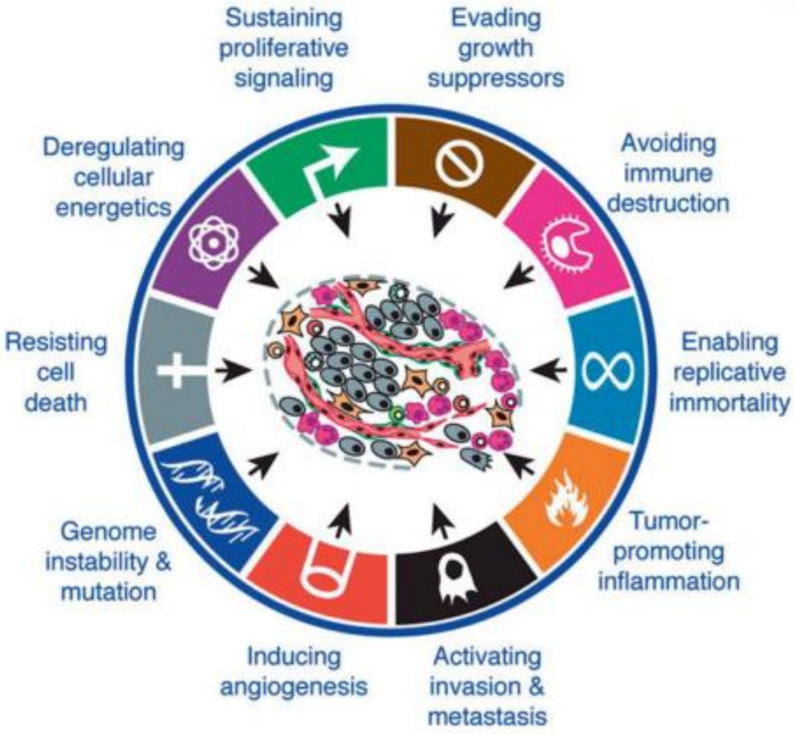
Sustaining proliferative signaling
Evading growth suppressors
Avoiding immune destruction
Enabling replicative immortality
Tumor-promoting inflammation
Activating invasion & metastasis
Inducing angiogenesis
Genome instability & mutation
Resisting cell death
Deregulating cellular energetics

Figure 7: The Hallmarks of Cancer and Enabling Characteristics. Adapted from Hanahan & Weinberg, 2011.

Sustaining proliferative signaling: Unlike the normal cells, cancer cells are able to proliferate continuously by acquiring the mechanisms that allow them to have the proliferative signaling pathways constantly activated. For instance, by increasing growth factor receptor levels at the cell surface or by expressing receptor molecules with structural alterations that enable ligand-independent firing.

Evading growth suppressors: In order to sustain proliferation, cancer cells avoid the pathways that negatively regulate it. Most of these pathways are dependent on tumor suppressors such as, *TP53* and *RB*, whose functions appear to be inactivated in tumors.

Resisting cell death (apoptosis): Tumor cells develop several strategies to prevent apoptosis when cell-integrity threatening stresses emerge, such as loss of *TP53*, increasing expression of antiapoptotic regulators (Bcl-2, Bcl-x_L) or downregulation of proapoptotic factors (Bax, Bim).

Enabling replicative immortality: Normal cells can only pass through a limited number of cell division cycles before entering senescence and later on die. Cancer cells, instead, become immortalized with no limiting number of divisions due to high expression of telomerase or activation of the 'alternative recombination-based telomere maintenance mechanism'.

Inducing angiogenesis: Like normal tissues, tumors require blood-vasculature in order to obtain nutrients and oxygen and evacuate metabolic wastes and carbon dioxide. Normal vasculature is largely quiescent, except in processes such as wound healing and female reproductive cycling where angiogenesis is activated transiently. In contrast, in tumors angiogenesis is constantly activated causing continuous sprout of new vessels and thus, sustaining tumor expansion.

Activating invasion and metastasis: Cancer cells are able to leave the primary niche and invade local tissue or even disseminate to distant tissues through blood and lymphatic vessels and form new tumors there. Being able to metastasize involves loss of adherens junctions, acquisition of a fibroblastic morphology, expression of matrix-degrading enzymes and increased motility.

Reprogramming of energy metabolism: Under aerobic conditions, normal cells process glucose until they obtain carbon dioxide. But cancer cells, even in the presence of oxygen, limit their energy metabolism largely to glycolysis (aerobic glycolysis). As a consequence, they increase glycolytic intermediates that will enter in the biosynthetic pathways, and thus, will support active cell proliferation.

Evading immune destruction: The immune system is responsible for recognizing and eliminating the great majority of incipient cancer cells. However, the tumors that have emerged have somehow succeeded in avoiding the detection by the immune system.

Note that, tumors, in addition to cancer cells, are also composed of a variety of normal cells, which form the tumor-associated stroma. These stromal cells are active participants in tumorigenesis since they contribute to the acquisition of certain hallmark capabilities by building the 'tumor microenvironment' (Hanahan & Weinberg, 2000, 2011).

4. COLORECTAL CANCER

4.1. Overview

Colorectal cancer (CRC) is a disease originating from the epithelial cells lining the colon or rectum. Colorectal cancers are the end result of a multistep process of colon neoplasia that normally extends over a period of decades. The tumorigenic process begins as an epithelial hyperplasia which results in a benign tumor (known as adenoma or polyp) that protrudes into the gut lumen. The adenoma gradually progresses increasing in size and dysplasia and finally it can turn into malignant tumor (carcinoma). Carcinomas are recognized when invasive cells breach the underlying epithelial basement membrane. Some polyps can change into cancer over the course of several years, but not all polyps become cancer (Markowitz, Dawson, Willis, & Willson, 2002).

Tumors can arise anywhere in the large intestine, but the majority appears in the distal colon (left side): 38% of CRCs develop in the rectum and 29% in the sigmoid colon (Davies, Miller, & Coleman, 2005).

Generally, colorectal cancer is a disease of age. As mentioned, its progression takes years and that is why the median age of diagnosis is about 70 years in developed countries. Incidence is low at ages younger than 50 years (Brenner, Kloor, & Pox, 2014). Taking into account the age factor and that colorectal cancers which are detected at early stages are highly curable by surgical excision, nowadays it is strongly recommended to start screenings at the age of 50 years for the adult population with an average risk. For individuals at higher risk due to family history or other predisposing factors the screenings are recommended earlier (Markowitz et al., 2002).

4.2. Incidence and mortality

Colorectal cancer is the third most common cancer type and the fourth most common cause of cancer-related death worldwide, accounting for 1.5 million new cases and 700,000 deaths per year, and exceeded only by deaths caused by lung, liver and stomach cancers. This cancer is more prevalent in developed than in developing countries (Mármol, Sánchez-de-Diego, Pradilla Dieste, Cerrada, & Rodriguez Yoldi, 2017).

In Europe, a study realized in 2012 placed colorectal cancer as one of the 5 most common cancer types. That year, 3.45 million new cases of cancer (excluding non-melanoma skin cancer) were estimated, 53% (1.8 million) occurring in men and 47% (1.6 million) in women. Among the most common diagnosed cancers were breast cancer (464,000 cases, 13.5%), colorectal cancer (447,000, 13.0%), prostate cancer (417,000, 12.1%) and lung cancer (410,000, 11.9%) which together represented half (50.5%) of total number of cancer cases in Europe in 2012. The estimated number of cancer deaths was 1.75 million, of which 56% (976,000) were in men and 44% (779,000) in women. The most frequent cause of death from cancer was lung cancer (353,000, 20%), followed by colorectal cancer (215,000 deaths, 12.2%), breast cancer (131,000, 7.5%) and stomach cancer (107,000, 6.1%) (**Fig.8**) (Ferlay et al., 2013).

In the future, total number of cancer deaths is predicted to rise up due to population ageing. However, age-standardized cancer mortality rates are expected to decrease thanks to awareness of the disease, screening, early diagnosis and patient management protocols and treatments. These favorable trends are also awaited for colorectal cancer, considering that mortality has been reduced 5% in men and 7% in women in Europe (as a whole) since 2011, except in Spain and Poland which increased, probably due to changes in dietary patterns and 'western lifestyle' risk factors (Malvezzi et al., 2015, 2016).

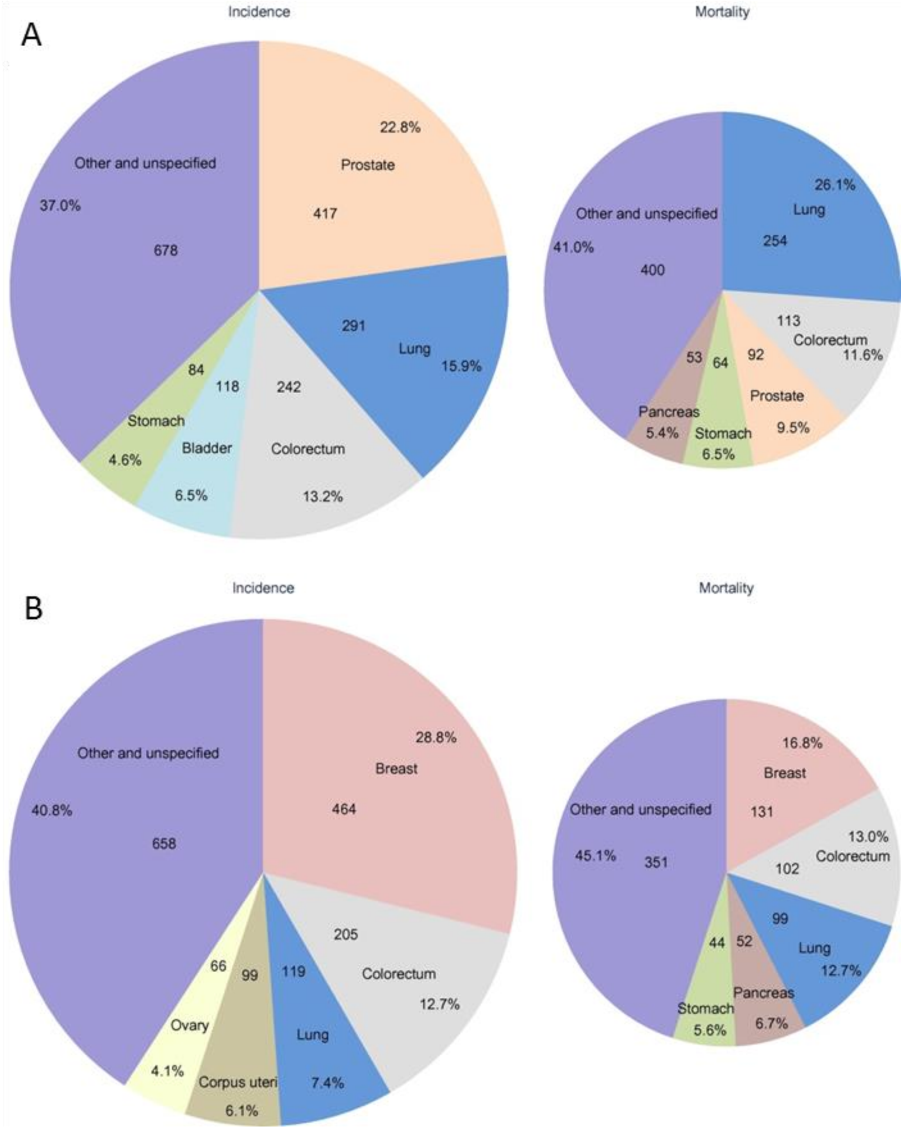

Figure 8: Distribution of the expected cases and deaths for the 5 most common cancers in Europe in 2012 in males (A) and in females (B). For each sex, the area of the segment of the pie chart reflects the proportion of the total number of cases or deaths. Numbers inside the segments represent numbers in thousands. Adapted from Ferlay et al., 2013.

4.3. Risk factors and causes

All colorectal cancers arise due to changes in the DNA and depending on how and when these mutations occur colorectal cancers can be divided into two groups: hereditary cancers and sporadic cancers.

Hereditary forms account for about 5-10% of all colorectal cancers. The two most common forms are 'hereditary non-polyposis colon cancer' (HNPCC or Lynch syndrome) and 'familial adenomatous polyposis' (FAP). Other syndromes such as Peutz-Jeghers syndrome, juvenile polyposis syndrome and Cowden syndrome are also related to increased risk of colorectal cancer (Weitz et al., 2005).

In hereditary cancer, one allele of a fundamental gene is inactivated in the germline, and when a somatic event (second hit) invalidates the functionality of the remaining wild-type allele tumor formation can occur. **FAP** is an autosomal-dominant disease. Approximately 80% of people with FAP inherit a germline mutation in the 'adenomatous polyposis coli' (*APC*) gene. FAP patients can develop more than 100 colorectal adenomas by the age of 35, which if left untreated will lead into colorectal cancer by the age of 40. **HNPCC** or **Lynch syndrome** is also an autosomal-dominant disease, but in contrast, it is caused by germline mutations in genes coding for DNA mismatch repair proteins, such as MSH2, MLH1, MSH6, PMS1 and PMS2. Consequently, the originated tumors present microsatellite instability, which means frequent mutations in short repeated DNA sequences called microsatellites. The penetrance of colorectal cancer in HNPCC is 70–85% and HNPCC patients generally develop colorectal cancer by the age of 44. In addition, these patients can also present tumors in genitourinary system, stomach, biliary system, pancreas, small intestine and central nervous system (Weitz et al., 2005).

Nevertheless, most colorectal cancer cases are **sporadic** (roughly 90% of all colorectal cancers), which means that mutations that initiate the tumor appear throughout life, mainly due to environmental exposures, though some genetic factors can also influence. Among these **environmental risk factors** are the age, male sex, smoking, excessive alcohol consumption, high consumption of red and processed meat, obesity, diabetes and sedentary lifestyle. The risk is stronger in people with inflammatory bowel diseases, such as ulcerative colitis and Crohn's colitis. Therefore, infection with *Helicobacter pylori*, *Fusobacterium spp* and other potential infectious agents could also be associated with increased risk of colorectal cancer (Brenner et al., 2014; Weitz et al., 2005). Furthermore, this risk increase is even higher for people with family history of colorectal cancer (particularly for those with multiple affected relatives or relatives diagnosed at young ages). In fact, about 20-35% of all colorectal cancer patients are estimated to have some heritable component of familial risk (**genetic risk factors**) different to the genetic aberrations that cause the hereditary colorectal cancers (familial adenomatous polyposis and hereditary non-polyposis colon cancer or Lynch syndrome). Although those genetic factors still remain poorly understood, there are evidences that show significant associations between certain single nucleotide polymorphisms (SNPs) and colorectal cancer susceptibility. However, the clinical use of these results is limited, since the relative risk associated with these variants is low. In order to further understand these familial colorectal cancers, potential roles of low-penetrance loci, gene-gene interactions, epigenetic modification or a combination of these factors in how they influence colorectal cancer risk are being investigated (Brenner et al., 2014; Stoffel & Kastrinos, 2014).

In order to prevent colorectal cancer, tobacco avoidance, physical activity, weight control and a diet rich in fruit, vegetables, cereal fiber, dairy products and fish are strongly recommended. There is also an inverse association between serum vitamin D concentrations and risk of colorectal cancer. However, endoscopy screening with the chance of removing precancerous lesions is the best method to prevent colorectal cancer appearance (Brenner et al., 2014).

4.4. Histopathological classification

Cancer staging is a classification of colorectal cancers depending on their size and spreading. It is performed for diagnostic and research purposes, and to determine the best method of treatment. Definitive staging can only be done after surgery and pathologic assessment of the local disease and the resection specimen (Compton, 2003).

In 1932 the British pathologist Cuthbert Dukes published the first classification system for colorectal cancer (Dukes, 1932). At the present time, the updated **Dukes system** divides colorectal cancer into 4 different stages: A, B, C and D. Dukes' A involves invasion into the bowel wall but not through it (the tumor is confined to the innermost lining of bowel wall); Dukes' B implicates invasion through the bowel wall, spreading into muscle layer but without involving lymph nodes; in Dukes' C there is an affectation of lymph nodes in the area; and Dukes' D indicates the presence of widespread metastases, commonly in the liver and the lungs (Haq, Schneeweiss, Kalsi, & Arya, 2009).

Currently, the Dukes system has been replaced by a more detailed staging system and is no longer recommended for use in clinical practice. Nowadays, colorectal cancers are classified according to the **TNM-system** of the 'Union for International Cancer Control' (UICC), which provides the basis for therapeutic decisions (**Table 1**). This system groups the tumors depending on the size of primary tumor and local invasion depth (T stage), nearby lymph node involvement (N stage) and presence of distant metastases (M stage). The numbers appearing after these letters (from 0 to 4) indicate increasing severity. Next, the different TNM categories are combined into an overall stage definition: Stage 0, I, II, III or IV, being Stage 0 the least advanced and Stage IV the most advanced (**Fig. 9**) (Sobin, Gospodarowicz, & Wittekind, 2010).

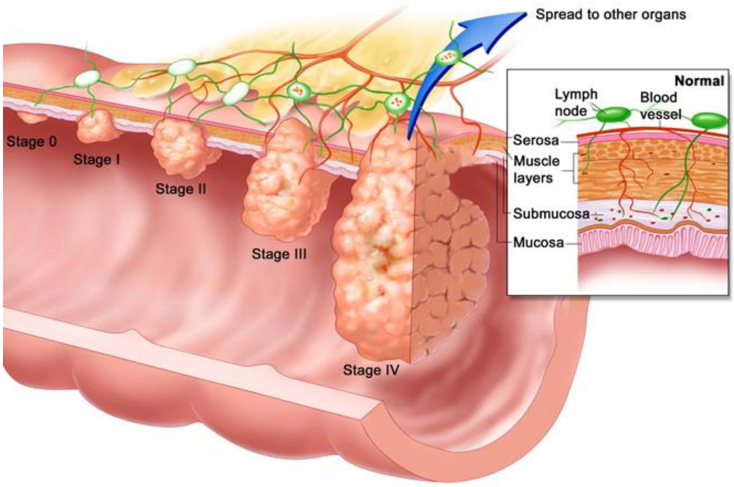

Figure 9: The growth from a polyp to a metastatic tumor. In Stage 0 (carcinoma *in situ*) abnormal cells are found in the mucosa of the colon wall. In Stage I cancer has grown in the mucosa and spread into submucosa and may also into *muscularis propria*. In Stage II cancer has spread through the muscle layer of the colon wall and grown into the serosa. In Stage III cancer has invaded nearby lymph nodes. In Stage IV cancer has metastasized to a distant organ. Figure from "Terese Winslow LLC," 2014.

Table 1: (A) TNM and Dukes classification of colorectal cancers. (B) Definition of the different T, N and M stages.

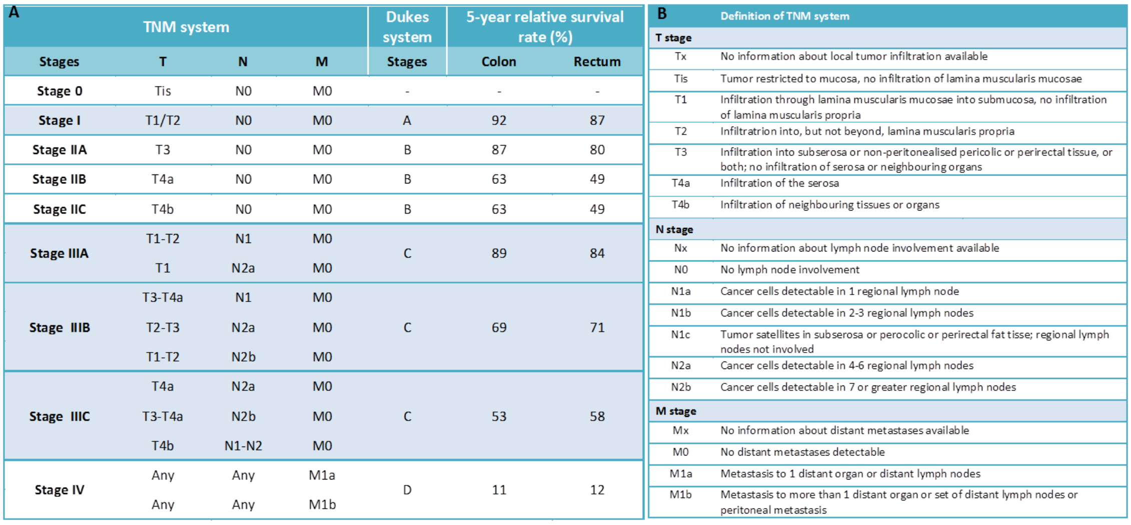

A

TNM system				Dukes system	5-year relative survival rate (%)	
Stages	**T**	**N**	**M**	**Stages**	**Colon**	**Rectum**
Stage 0	Tis	N0	M0	-	-	-
Stage I	T1/T2	N0	M0	A	92	87
Stage IIA	T3	N0	M0	B	87	80
Stage IIB	T4a	N0	M0	B	63	49
Stage IIC	T4b	N0	M0	B	63	49
Stage IIIA	T1-T2	N1	M0	C	89	84
	T1	N2a	M0			
Stage IIIB	T3-T4a	N1	M0	C	69	71
	T2-T3	N2a	M0			
	T1-T2	N2b	M0			
Stage IIIC	T4a	N2a	M0	C	53	58
	T3-T4a	N2b	M0			
	T4b	N1-N2	M0			
Stage IV	Any	Any	M1a	D	11	12
	Any	Any	M1b			

B

	Definition of TNM system
T stage	
Tx	No information about local tumor infiltration available
Tis	Tumor restricted to mucosa, no infiltration of lamina muscularis mucosae
T1	Infiltration through lamina muscularis mucosae into submucosa, no infiltration of lamina muscularis propria
T2	Infiltratrion into, but not beyond, lamina muscularis propria
T3	Infiltration into subserosa or non-peritonealised pericolic or perirectal tissue, or both; no infiltration of serosa or neighbouring organs
T4a	Infiltration of the serosa
T4b	Infiltration of neighbouring tissues or organs
N stage	
Nx	No information about lymph node involvement available
N0	No lymph node involvement
N1a	Cancer cells detectable in 1 regional lymph node
N1b	Cancer cells detectable in 2-3 regional lymph nodes
N1c	Tumor satellites in subserosa or perocolic or perirectal fat tisse; regional lymph nodes not involved
N2a	Cancer cells detectable in 4-6 regional lymph nodes
N2b	Cancer cells detectable in 7 or greater regional lymph nodes
M stage	
Mx	No information about distant metastases available
M0	No distant metastases detectable
M1a	Metastasis to 1 distant organ or distant lymph nodes
M1b	Metastasis to more than 1 distant organ or set of distant lymph nodes or peritoneal metastasis

Data taken from Brenner et al., 2014 and American Cancer Society, 2018a.

In addition to the staging, the **histological grade** of tumors also has a prognostic value. The tumor grade describes the level of resemblance that a tumor presents compared to the surrounding normal tissue when observed under the microscope. The grading scale goes from G1 to G4. G1 tumors are well differentiated and look much like normal colon tissue. In contrast, G4 tumors are undifferentiated and look very abnormal compared to normal tissue. The grades G2 (moderately differentiated) and G3 (poorly differentiated) present intermediate levels of differentiation or resemblance. However, this grading scale is commonly simplified into 'low-grade' (G1 and G2) and 'high grade' (G3 and G4) tumors. In overall, low grade tumor cells tend to grow and spread slowly and high grade tumor cells grow faster and are more invasive (Compton, 2003).

4.5. Treatment

Surgery is the basic therapy for colorectal cancer treatment. Patients with Stage 0 or I are only treated with surgery. Stage II patients, generally are just treated by surgery as well. However, adjuvant chemotherapy is also recommended for Stage II patients with T4 and advanced T3 tumors (patients with high risk of relapse). Surgical resection is highly effective for early stage colon cancers, providing cure rates of over 90% in Stage I and 75% in Stage II disease.

Surgery to remove the section of the colon containing the cancer along with nearby lymph nodes (partial colectomy) followed by adjuvant chemotherapy is the standard procedure for Stage III colorectal cancer patients, since the risk of recurrence ranges between 15-50% of the patients. Up to 73% of cases of Stage III disease are curable. Radiation therapy may be an option for people who are not healthy enough for surgery.

As adjuvant chemotherapy, either ‘FOLFOX’ (5-fluorouracil (5-FU), leucovorin and oxaliplatin) or ‘CapeOx’ (capecitabine and oxaliplatin) regimens are used most often, but some patients may get 5-FU with leucovorin or capecitabine alone based on their age and health needs.

Stage IV disease is usually incurable. These patients also have surgery to remove the section of the colon containing the cancer along with nearby lymph nodes, with the only purpose of relieving symptoms of the disease. In addition, if they present metastases easy to remove, surgical resection of those metastases is offered together with palliative chemotherapy. If the metastases cannot be resected, palliative chemotherapy is the only treatment in order to prolong survival and improve quality of life.

Some of the most commonly used palliative chemotherapies are ‘FOLFOX’, ‘FOLFIRI’ (leucovorin, 5-FU and irinotecan), ‘CapeOX’ and ‘FOLFOXIRI’ (leucovorin, 5-FU, oxaliplatin and irinotecan). Moreover, in some cases one of the above treatments can be combined with monoclonal antibodies that target ‘vascular endothelial growth factor’ (VEGF) (bevacizumab (Avastin), ziv-aflibercept (Zaltrap), or ramucirumab (Cyramza)) or ‘epithelial growth factor receptor’ (EGFR) (cetuximab (Erbitux) or panitumumab (Vectibix)). The multi-kinase inhibitor ‘regorafenib’ alone is also commonly used. Furthermore, TAS-102 (Lonsurf) has been also recently approved for the treatment of Stage IV patients who have been previously treated with any of the drugs just mentioned (American Cancer Society, 2018b; Brenner et al., 2014; Marcus et al., 2017; Markowitz & Bertagnolli, 2009).

4.6. The multistep nature of colorectal cancer

Colorectal tumorigenesis is considered a multistep process that occurs over a period of decades. Colorectal cancers arise from preexisting benign tumors (adenomas), following an ordered series of events that form the so-called ‘adenoma-carcinoma sequence’ (Fearon & Vogelstein, 1990).

The first genetic model of 'adenoma-carcinoma sequence' was presented by Fearon and Vogelstein in 1990 (**Fig. 10**). This model suggested that tumor progression implies an accumulation of multiple gene defects, each defining a different step in the 'adenoma-carcinoma sequence'. It begins with the transformation of normal colonic epithelium into an early adenoma, continues into a late adenoma and finally becomes a carcinoma (Fearon & Vogelstein, 1990).

Those gene defects refer to mutational activation of oncogenes coupled with mutational inactivation of tumor suppressor genes, being the latter more predominant during tumorigenesis. Fearon and Vogelstein identified four recurrent somatic alterations present at various stages of colorectal tumor formation: *RAS* gene mutations and deletions of chromosomes 5q, 17p, and 18q, which harbor *APC*, *TP53* and *SMAD4* tumor suppressor genes respectively. The presence of such alterations suggested that the genetic alteration itself provided the cell with a growth advantage, allowing it to outgrow other neoplastic cells within the tumor and to become the predominant cell type constituting the neoplasm (successive waves of clonal expansion). Moreover, they stated that although those recurrent genetic alterations often occur according to a preferred sequential order, the total accumulation of changes, rather than their order with respect to one another, was responsible for colorectal tumor progression (Fearon & Vogelstein, 1990).

Nowadays, it is known that at least 5 to 7 distinct mutations are required for the appearance of colorectal carcinoma and fewer changes suffice for benign tumorigenesis. Once carcinomas have formed, tumors continue to progress accumulating more alterations until they acquire the ability to metastasize and cause death. Recent genome-wide sequencing efforts calculated as many as 80 mutated genes per colorectal tumor, but a smaller group of mutations (about 15) were considered to be the true 'drivers' of tumorigenesis (Pino & Chung, 2010). Furthermore, contrarily to what Fearon and Vogelstein stated, it has also been demonstrated that for some genetic changes, their specific temporal acquisition matters. For instance, *APC* mutations initiate adenoma formation in human and mouse models, but mutational activation of *KRAS* cannot initiate cancer *in vivo*. Only when combined with a mutation in *APC* does mutant KRAS promote tumor progression (Pino & Chung, 2010).

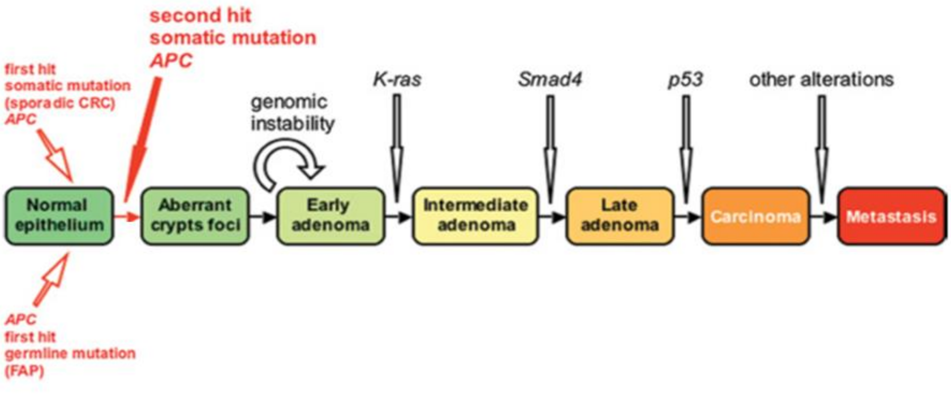

Figure 10: Vogelgram: Genetic model of colorectal carcinogenesis presented by Fearon and Vogelstein in 1990. Mutations in *APC* are required for tumor initiation. Subsequent progression towards malignancy is accompanied by genomic instability and sequential mutations in *KRAS*, *SMAD4* and *TP53* genes, as well as in other unknown genes. Adapted from Pinto & Clevers, 2005.

Many CRCs have several of the alterations described by Fearon and Vogelstein, but only some cases have all of them. This indicates that different mutations also trigger tumor development. Later in this chapter (section 4.8) other genetic and epigenetic defects that promote colorectal tumorigenesis similarly to the mutations shown in the scheme of figure 10 will be explained, as well as the different paths proposed for colorectal tumorigenesis (**Fig. 12**).

4.7. The origin of colorectal cancer

Tumors are thought to originate from a single cell. However, the cell of origin for colorectal cancer has remained unknown for a long time. Two different theories have been proposed to explain the origin and migration of intestinal tumor cells: the 'top-down' and the 'bottom-up' models (**Fig. 11**).

The **'top-down'** theory considers a progenitor or a differentiated cell as the first transformed cell. These genetically altered cells may reside in the intercryptal zones at the surface of the mucosa rather than at the base of the crypts, and they may spread laterally and downward to form new crypts by pushing the normal epithelial cells in adjacent crypts and eventually replacing them (Shih et al., 2001). This model was suggested based on the presence of dysplastic cells at the luminal surface that carried mutations in *APC*, whereas crypt cells were normal (they were genetically unrelated) (Shih et al., 2001). Moreover, it was shown that tumors can originate from mutations in short-lived progenitors, but this happens very infrequently and such adenomas develop slowly (Barker et al., 2009).

In contrast, the **'bottom-up'** theory defines an intestinal stem cell (ISC) as the cell of origin of tumor. The ISCs are found at the bottom of the crypts and their properties make them good candidates for being also cancer initiating cells: ISCs have the ability to self-renew and give rise to more differentiated daughters, have active telomerase, and are more resistant to apoptosis (Schepers & Clevers, 2012). In this model monocryptal adenomas are considered as the earliest histologically detectable precursor lesions of tumor development, in which dysplatic epithelium occupies an entire single crypt. Apparently, a stem cell acquires a second hit (*APC*) and expands to colonize the entire crypt, probably because of a selective advantage. In this scenario, in contrast to the first theory, the mutated clone further expands, not by lateral migration but by crypt fission, where the crypt divides, usually symmetrically at the base, or by budding (Humphries & Wright, 2008; Preston et al., 2003).

The 'bottom-up' theory recently received strong genetic support, since ISC-specific deletion of both functional *APC* alleles in mice leads to the very rapid development of full adenomas (Medema & Vermeulen, 2011). However, this model does not exclude the possibility that the clone later expands by lateral migration and downward spread into adjacent crypts. This lateral spread via the surface is more likely to be a phenomenon confined to the later stages of evolution of colorectal adenomas (Preston et al., 2003).

Although it is difficult to obtain definitive dynamic proof in humans, the 'bottom-up' model appears to be the most accepted theory for clonal expansion in early adenomas. This is mainly because stem cells are able to generate multiple generation of cells and are the only cells that persist long enough in the tissue to undergo the prolonged sequence of successive mutations required for carcinogenesis (Humphries & Wright, 2008).

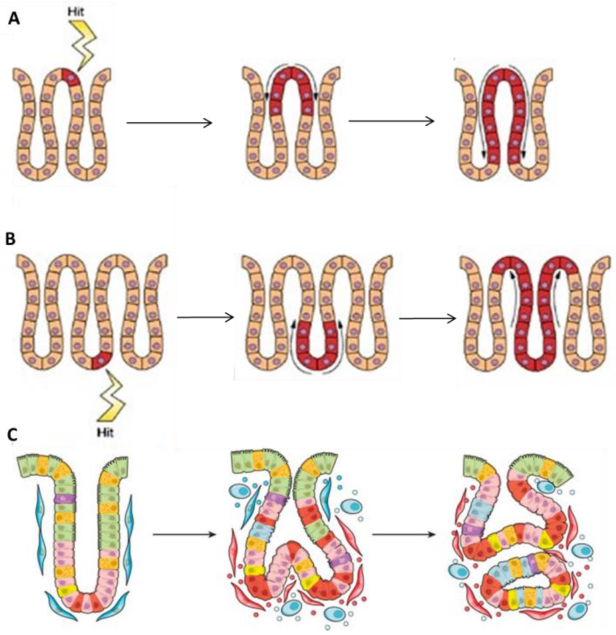

Figure 11: 'Top-down' and 'bottom-up' models for adenoma origin and histogenesis in the colonic crypt. A) The 'top-down' model suggests that the first dysplastic cell appears at, or near, the top of the crypt and it expands laterally and downward to form new crypts. **B)** In the 'bottom-up' model dysplastic cell originates at the base of the crypt, within the stem cell zone, and continues upwards so that eventually the entire crypt is dysplastic (cell migration is indicated by the arrows). **C)** Then, in contrast to the 'top-down' model, the mutated clone further expands, not by lateral migration but by crypt fission. Adapted from McDonald et al., 2006 and Medema & Vermeulen, 2011.

4.8. Molecular pathways of colorectal cancer

4.8.1. Genomic instability

Genomic instability is an important feature underlying colorectal cancer since it can drive the development of colorectal cancer by facilitating the acquisition of multiple tumor-associated mutations. The three pathogenic mechanisms that lead to this genomic instability are chromosomal instability (CIN), microsatellite instability (MSI) and epigenetic instability.

Chromosomal instability (CIN) is considered the classical mutational mechanism since it represents the cause of tumor progression of 80-85% of all colorectal cancers. CIN refers to a state of accelerated rate of gains and losses of whole or large portions of chromosomes. Thus, these colorectal cancers are characterized by containing an abnormal chromosomal content (aneuploidic tumors) and loss of heterozygosity (LOH) (Mármol et al., 2017). Karyotyping analyses of CRCs have revealed frequent losses of chromosomes 5q (harbors *APC* gene), 18q (harbors *SMAD4* and *SMAD2* genes) and 17p (harbors *TP53* gene), as well as gains of chromosomes 13 and 20 (Fearon, 2011). However, most of these types of cancers do not display microsatellite instability (MSI; see below) and so, they are called microsatellite stable (MSS) cancers.

Therefore, CIN allows cells to rapidly acquire genetic changes that are required for tumorigenesis. For instance and as mentioned above, CIN facilitates the inactivation of tumor-suppressor genes, such as, *APC*, *TP53* and *SMAD4* (Markowitz & Bertagnolli, 2009). CIN can also provide growth advantages to cancer cells by causing changes in gene expression, since the loss of some gene functions triggers a dosage compensation of the various feedback and feedforward loops that regulate most cellular pathways (Rajagopalan, Nowak, Vogelstein, & Lengauer, 2003).

CIN phenotype is a dominant trait, but the molecular basis that underlies CIN in CRC is still largely obscure and only a few genes that might cause this phenotype have been identified. Presumably, defects in genes that regulate the formation of the mitotic spindle and the proper alignment and segregation of chromosomes at mitosis may contribute to the CIN phenotype (Barber et al., 2008; Fearon, 2011). Telomere dysfunction and alterations in genes related to DNA damage response can also contribute to CIN phenotype (Pino & Chung, 2010).

The stage of tumorigenesis at which the CIN phenotype arises is controversial, with some reports suggesting that CIN initiates tumorigenesis and others proposing that CIN is acquired and has a role in maintaining the tumorigenic process. In fact, several studies have demonstrated that CIN occurs very early during tumorigenesis (Pino & Chung, 2010). APC inactivation has been suggested as one of the earliest contributors to chromosomal instability, since it has been related to defective chromosome segregation. APC has been demonstrated to play a role during mitosis by enabling proper spindle-microtubule plus-end attachments to the kinetochore of chromosomes (Fodde et al., 2001; Kaplan et al., 2001). However, mutated APC acts dominantly to interfere with microtubule plus-end attachments and to cause an increase in mitotic abnormalities; and most surprisingly, without promoting cell arrest in mitosis (Green & Kaplan, 2003; Green, Wollman, & Kaplan, 2005).

In addition to chromosomal abnormalities, the accumulation of inactivating mutations in tumor suppressor genes, such as *TGFβRII* and *PTEN*, and activating mutations in oncogenes, such as *KRAS*, *CTNNB1* and *PI3KCA*, is also characteristic of these CIN colorectal cancers. However, it is not clear whether CIN creates the appropriate environment for the accumulation of these mutations or *vice versa* (Pino & Chung, 2010).

Microsatellite instability (MSI) refers to a hypermutable phenotype caused by the loss of DNA repair mechanisms due to inactivation of genes required for repairing base-base mismatches in DNA (mismatch-repair genes; MMR). As the ability to repair DNA mismatches is defective, mutations tend to accumulate rapidly and mainly in short DNA chains or tandem repeats (two to five base-pair repeats) called microsatellites where DNA polymerase usually makes more replicating mistakes. The microsatellites are scattered throughout the genome and thus, these mutations (insertions, deletions or base changes) can affect non-coding as well as codifying regions (Mármol et al., 2017). Indeed, proto-oncogenes and tumor suppressor genes that contain repetitive DNA sequences appear to be among the major targets for somatic mutation in MSI tumors (Fearon, 2011).

Of all CRCs, approximately 15% present MSI phenotype. About 3% are hereditary CRCs coming from ‘hereditary non-polyposis colon cancer’ (HNPCC) or Lynch syndrome patients; and around 12% are sporadic colorectal cancers (Boland & Goel, 2010).

HNPCC patients can present germline inactivating mutations in *MLH1*, *MSH2*, *MSH6*, *PMS1* and *PMS2* (MMR genes), although the most common genes mutated are *MLH1* and *MSH2*. Some cases of Lynch syndrome are caused by epigenetic inactivation of *MLH1* or *MSH2* genes by promoter methylation (germline or constitutional epimutations). These constitutional epimutations show autosomal dominant inheritance (Boland & Goel, 2010). HNPCCs have at least a 100-fold increase in the rate of mutation in repetitive DNA-sequence elements compared to most CRCs. Therefore, HNPCC is a disease with very rapid tumor progression from an adenoma to carcinoma, taking only 3-5 years, instead of the 20-40 years estimated for most sporadic CRCs (Fearon, 2011).

Loss of DNA repair mechanisms in sporadic colorectal cancer is due to somatic inactivation of *MLH1* gene by biallelic silencing of the promoter region through promoter methylation. Importantly, most of the CRCs with sporadic MSI come from CIMP background (CpG island methylator phenotype; explained below) (Markowitz & Bertagnolli, 2009).

MSI cancers arise primarily in the proximal colon and unlike HNPCC patients, sporadic cases with MSI are associated with older age. In contrast to MSS tumors, MSI tumors are mainly diploid and had no apparent LOH. Histologically they are characterized by poor or mixed differentiation (high grade), high presence of tumor-infiltrating lymphocytes and expansive and cohesive pattern of invasion. In general, patients with MSI sporadic colorectal tumors have a better prognosis than those with non-MSI tumors (Boland & Goel, 2010).

In these cases, *BRAF* mutation analysis can be useful to distinguish between sporadic and Lynch syndrome-associated MSI colorectal cancers because *BRAF* oncogene mutations are almost exclusively restricted to sporadic MSI type (Brenner et al., 2014). Lynch syndrome tumors can have *KRAS* mutations but never *BRAF* mutations. Curiously, *BRAF* mutations, which are detected in sporadic but not in familial CRCs with MSI are associated with reduced mortality (Boland & Goel, 2010).

Among the genes that have been identified to be affected by MSI are regulators of cell proliferation (*CTNNB1* (codifying for β-catenin), *GRB1, TCF-4, WISP3*, activin receptor-2, insulin-like growth factor-2 receptor, *AXIN-2* and *CDX*), regulators of the cell cycle or apoptosis (*TGFβRII, BAX*, caspase-5, *RIZ, BCL-10, PTEN, hG4-1* and *FAS*), and genes related to DNA repair (*MBD-4, BLM, CHK1, MLH3, RAD50, MSH3* and *MSH6*) (Boland & Goel, 2010).

Epigenetic instability, which is responsible for the ‘CpG island methylator phenotype’ (CIMP), is the third mechanism by which a subgroup of sporadic CRCs arises (Mármol et al., 2017).

About half of all genes have a CpG island in their promoter region and its methylation is often related to transcriptional gene silencing. In adenomatous polyps and CRCs there is a generalized decrease in the total level of DNA methylation (hypomethylation) compared to adjacent normal tissues. Nevertheless, little is known about the functional contribution of DNA hypomethylation in CRC. Although the global trend in CRC cells is hypomethylation, CpG islands at various gene promoters show increased methylation, resulting in the silencing of several genes (Fearon, 2011).

The group of CRCs referred as CIMP tumors, show hypermethylation of numerous gene promoters, suggesting that the normal regulation of DNA methylation is globally disrupted (epigenetic instability) (Fearon, 2011). Those tumors represent 15% of all CRCs and show 3-5-fold higher frequency of aberrant gene methylation compared to non-CIMP colorectal cancers (Issa, 2004).

Some of the commonly methylated promoters have no apparent role in tumor development. However, methylation also occurs in promoters of known tumor suppressor genes, such as p16 and insulin-like growth factor 2, and DNA repair genes such as methylguanine methyltransferase and *MLH1*, whose inactivation triggers the tumor progression (Boland & Goel, 2010). Other commonly methylated genes include *CDKN2A* (encodes the protein INK4A/ARF28); *THBS1* (thrombosponsin 1); *HPP1* (hyperplastic polyposis gene 1); *HIC1* (hypermethylated in cancer 1) and the Wnt signaling antagonists known as SFRPs (secreted Frizzled–related proteins) (Fearon, 2011).

A subset of CIMP tumors show hypermethylation of the *MLH1* MMR gene and these tumors represent the major fraction of sporadic MSI tumors. That is, most MSI sporadic CRC arise through the process that involves the CpG island methylator phenotype (CIMP).

CIMP tumors represent clinically a distinct group since they have a distinct epidemiology, a distinct histology, distinct precursor lesions and distinct molecular features. CIMP cancers tend to appear in proximal colon and occur in older patients and more often in women. The adenomatous precursor lesions of CIMP CRCs are termed sessile serrated adenomas (SSAs). In SSAs, dysplasia is readily apparent within an architectural pattern similar to that observed in hyperplastic polyps. Genetics and epigenetics are not exclusive neither in this type of colorectal cancer. Genetically, CIMP tumors show a lack of p53 mutations and a remarkably high rate of gain-of-function mutations in KRAS or BRAF. However, among the CIMP cancers MSI-positive cases tend to have good prognosis, whereas CIMP^{+}MSI^{-} cases have a particularly poor outcome (Fearon, 2011; Issa, 2004).

Nevertheless, the molecular mechanisms for CIMP remain unknown; though, the age, environmental factors and chronic inflammation have been related with an increase in DNA methylation (Issa, 2004).

These 3 mechanisms are not mutually exclusive and therefore a tumor can occasionally exhibit features of multiple mechanisms (**Fig. 12**). For example, up to 25% of MSI colorectal cancers can exhibit chromosomal abnormalities. In addition, whereas CIMP can account for most of the MSI^{+}CIN^{-} CRCs, up to 33% of CIMP^{+} tumors can exhibit a high degree of chromosomal aberrations. Conversely, as many as 12% of CIN^{+} tumors exhibit high levels of MSI (Pino & Chung, 2010).

Consequently, CRC development, instead of being a linear progression of single events as Fearon and Vogelstein suggested, it seems that it could follow four distinct pathways that are based on different molecular mechanisms (**Fig. 12**). Depending on CIMP and MSI status, sporadic colorectal cancers can be divided into four distinct groups: CIMP^{+}MSI^{+},CIMP^{+}MSI^{-} , CIMP^{-}MSI^{+} and CIMP^{-}MSI^{-} (Issa, 2004).

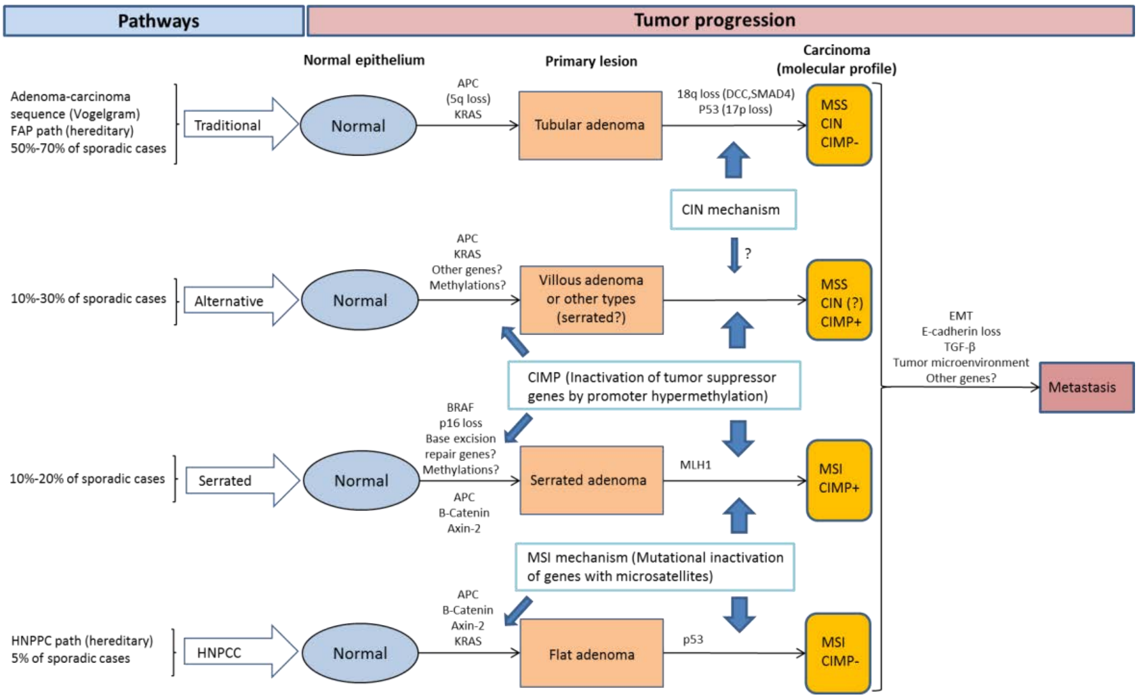
Pathways
Tumor progression
Normal epithelium
Primary lesion
Carcinoma (molecular profile)
Adenoma-carcinoma sequence (Vogelgram)
FAP path (hereditary)
50%-70% of sporadic cases
Traditional
Normal
APC (5q loss) KRAS
Tubular adenoma
18q loss (DCC,SMAD4) P53 (17p loss)
MSS CIN CIMP-
CIN mechanism
?
10%-30% of sporadic cases
Alternative
Normal
APC KRAS Other genes? Methylations?
Villous adenoma or other types (serrated?)
MSS CIN (?) CIMP+
CIMP (Inactivation of tumor suppressor genes by promoter hypermethylation)
EMT E-cadherin loss TGF-β Tumor microenvironment Other genes?
Metastasis
BRAF p16 loss Base excision repair genes? Methylations?
10%-20% of sporadic cases
Serrated
Normal
APC B-Catenin Axin-2
Serrated adenoma
MLH1
MSI CIMP+
MSI mechanism (Mutational inactivation of genes with microsatellites)
APC B-Catenin Axin-2 KRAS
HNPPC path (hereditary)
5% of sporadic cases
HNPCC
Normal
Flat adenoma
p53
MSI CIMP-

Figure 12: Multiple parallel pathways for colorectal cancer development. Sporadic colorectal cancer seems to arise from (at least) four distinct parallel models: traditional, alternative, serrated and HNPCC pathway. The sequential genetic and epigenetic changes occurring in each pathway are simplified, along with the characteristic precursor lesions (adenomas) and distinctive molecular features of the corresponding carcinomas. The estimated prevalence of the four pathways in Western population is shown. MSS, microsatellite stable; MSI, microsatellite instability; CIMP, CpG Island methylator phenotype; CIN, chromosomal instability; EMT, epithelial-mesenchymal transition; TGF-β, transforming growth factor-beta; tumor microenvironment indicates the crosstalk between cancer cells and cells of the neoplastic stroma. Adapted from Fearon, 2011; Issa, 2008 and Pancione, Remo, & Colantuoni, 2012.

4.8.2. Oncogene and tumor suppressor gene mutations

The molecular defects are of two types: alterations that lead to novel or increased function of oncogenes and alterations that lead to loss of function of tumor-suppressor genes (TSGs). The conversion of cellular genes into oncogenic variant alleles can result from specific point mutations or rearrangements that alter gene structure and function, or from chromosome rearrangements or amplifications that disrupt regulated gene expression. At present, only somatic oncogene mutations have been detected in CRCs. TSG inactivation can result from localized mutations, complete loss of the gene, or epigenetic alterations that interfere with gene expression (Fearon, 2011).

The most recurrent alterations in CRC appear in components of the Wnt, TGF-β, p53, RAS-MAPK and PI3K signaling pathways (**Fig. 13**).

4.8.2.1. Mutational inactivation of tumor-suppressor genes

Wnt pathway activation / *APC* inactivation

The activation of the Wnt signaling pathway is regarded as the initiating event in colorectal cancer (Markowitz & Bertagnolli, 2009). The main genomic aberrations in CRC related to the Wnt pathway are *APC* mutations, although many other alterations can also target this pathway.

In the **canonical or β-catenin-dependent Wnt signaling pathway,** in the absence of WNT ligand signaling, APC forms a complex with Axin, casein kinase 1 and glycogen synthase kinase 3β (GSK3β) in order to phosphorylate β-catenin and target it for ubiquitination and subsequent degradation. That is, this complex controls the levels of the β-catenin in the cytoplasm. In contrast, the binding of WNT ligands to their cognate receptors (Frizzled proteins and LRP5/6 proteins) triggers inhibitory effects on GSK3β and Axin, impeding the formation of the mentioned complex with APC. As a consequence, there is an accumulation of β-catenin in the cytoplasm, which translocate to the nucleus and bind to TCF/LEF (T cell factor/lymphoid enhancer family) DNA-binding proteins to finally activate the expression of a specific set of genes (Fearon, 2011). These genes include proto-oncogenes, such as *cMYC* and cyclin D1; genes encoding membrane factors, such as matrix metalloproteinase 7 (MMP-7), membrane-type 1 MMP (MT1-MMP), laminin-5 γ2 chain and CD44; growth factors such as FGF20 and FGF9; and Wnt pathway feedback regulators such as AXIN2, Naked-1/-2, Dickkopf-1 and WNT inhibitory factor 1 (Fearon, 2011).

As mentioned, the APC tumor suppressor controls the levels of degradation of β-catenin and also inhibits its nuclear localization. In the absence of functional APC, the coordinated phosphorylation and subsequent destruction of β-catenin are disrupted and thus, Wnt signaling is inappropriately and constitutively activated (Markowitz & Bertagnolli, 2009).

In approximately 70-80% of sporadic CRCs both *APC* alleles are mutated and most of these somatic mutations lead to premature truncation of APC protein. Moreover, germline *APC* mutations give rise to familial adenomatous polyposis (FAP) (Markowitz & Bertagnolli, 2009).

APC mutations are likely to be an early and rate-limiting event in the development of most adenomas, since both *APC* alleles appear inactivated in adenomas and carcinomas of FAP and most sporadic CRC patients (Fearon, 2011).

In some colorectal cancers with wild-type *APC*, alterations in other components of the canonical Wnt pathway that lead to pathway activation have been found. In a small subgroup of tumors mutations in β-catenin (*CTNNB1* gene) render the protein resistant to its degradation. Somatic mutations that affect the *AXIN1* or *AXIN2* genes have also been observed in several CRCs (Fearon, 2011).

TP53 inactivation

The inactivation of the p53 pathway by mutation of *TP53* is also a key genetic step in colorectal cancer. p53 tumor suppressor mediates cell-cycle arrest, cell-death checkpoints and if necessary it regulates apoptosis when multiple cellular stresses threaten the cell survival. Thus, its loss can drive tumor progression by allowing excessive proliferation and acquiring invasive properties in the face of stresses that might otherwise severely limit tumor cell survival and maintenance (Mármol et al., 2017).

Approximately 70% of CRCs show 17p LOH, which harbors *TP53* gene, and somatic mutations in the remaining *TP53* allele. A minority of CRCs lacking 17p LOH presents biallelic mutations in *TP53* gene. However, most adenomas do not have neither 17p LOH nor *TP53* mutations, suggesting that p53 inactivation is not an early step in adenoma-carcinoma transition. In fact, the inactivation of p53 often coincides with the transition of large adenomas into invasive carcinomas (Fearon, 2011).

In many colorectal cancers with mismatch-repair defects, *TP53* remains wild-type, though in these cancers the activity of the p53 pathway is probably attenuated by mutations in the *BAX* inducer of apoptosis (Markowitz & Bertagnolli, 2009).

TGF-β pathway inactivation

The mutational inactivation of TGF-β signaling is an important step in the progression of colorectal cancer. The TGF-β pathway plays a role in cellular processes such as growth, differentiation or apoptosis, and thus, its inactivation leads to an ability to evade apoptosis and to a deregulation of the cell cycle (Mármol et al., 2017). Inactivation of the TGF-β pathway coincides with the transition from adenoma to high-grade dysplasia or carcinoma (Markowitz & Bertagnolli, 2009).

Loss of chromosome 18q is one of the main genomic aberrations related to the TGF-β pathway in colorectal cancer. LOH in 18q is observed in about 70% of CRCs, 50% of large, late-stage adenomas and in fewer than 10% of small, early stage adenomas. This chromosomic location harbors two important tumor suppressor genes known as *SMAD2* and *SMAD4*, which encode proteins that function downstream of the TGF-β receptor complex. Moreover, mutations that inactivate SMAD4 are found in 10–15% of CRCs and *SMAD2* mutations are found in 5% of CRCs. Mutations inactivating the *SMAD3* gene (another downstream effector), which maps to chromosome 15, are found in 5% of CRCs.

Inactivating mutations in the TGF-β type II receptor (*TGFβIIR*) gene are found in approximately 25% of CRCs. The *TGFβIIR* gene contains a polyadenine repeat (microsatellite) which appears mutated in both alleles in most MSI colorectal cancers. But about the 15% of MSS CRCs also present somatic mutations in *TGFβIIR* gene (Fearon, 2011).

4.8.2.2. Activation of oncogene-pathways

The MAPK and PI3K pathways are both involved in cell proliferation and survival. Therefore, alterations affecting these pathways confer proliferative advantages to tumor cells. Mutations in *KRAS, BRAF* and *PIK3CA* (PI3K protein) genes are the most common activating mutations in CRC (Mármol et al., 2017)**.**

KRAS and BRAF

Oncogenic mutations of *KRAS* and *BRAF* activate the mitogen-activated protein kinase (MAPK) signaling pathway. *KRAS* somatic mutations are found in approximately 40% of CRCs. *KRAS* mutations contribute to colorectal adenoma development but are not required for adenoma initiation. Only about 10% of adenomas smaller than 1 cm present *KRAS* mutations, whereas 40-50% of adenomas greater than 1 cm show *KRAS* mutated (Fearon, 2011).

The gene for *BRAF* is mutated in approximately 5–10% of CRCs. *BRAF* mutations are detectable even in small polyps and compared to *KRAS* mutations, they are more common in serrated adenomas and cancers with the CIMP phenotype (Markowitz & Bertagnolli, 2009).

RAS proteins function downstream of several growth factor receptors, such as, the epidermal growth factor receptor (EGFR). Although *KRAS* mutations in CRC are common, activating alterations in genes encoding for growth factor receptors are quite uncommon. For instance, *EGFR* is only mutated in fewer than 5% of CRCs (Fearon, 2011).

PI3K pathway activation

15-25% of CRCs carry activating somatic mutations in *PI3KCA* gene, which encodes the catalytic subunit of phosphatidylinositol 3-kinase (PI3K) class I. These mutations activate PI3K kinase activity increasing the production of PIP3, which is a key messenger for cell growth and proliferation, survival and other processes. Although PI3K exerts its effects functionally downstream of the KRAS protein, *KRAS* mutations cosegregate to some degree with mutations in *PIK3CA*. This could be because mutant KRAS protein is apparently not very efficient in activating PI3K signaling (Fearon, 2011).

Less common genetic alterations that also activate PI3K pathway include loss of *PTEN*, an inhibitor of PI3K signaling; as well as amplification of insulin receptor substrate 2 (*IRS2*), an upstream activator of PI3K signaling; and coamplification of *AKT* and *PAK4*, which are downstream mediators of PI3K signaling (Markowitz & Bertagnolli, 2009).

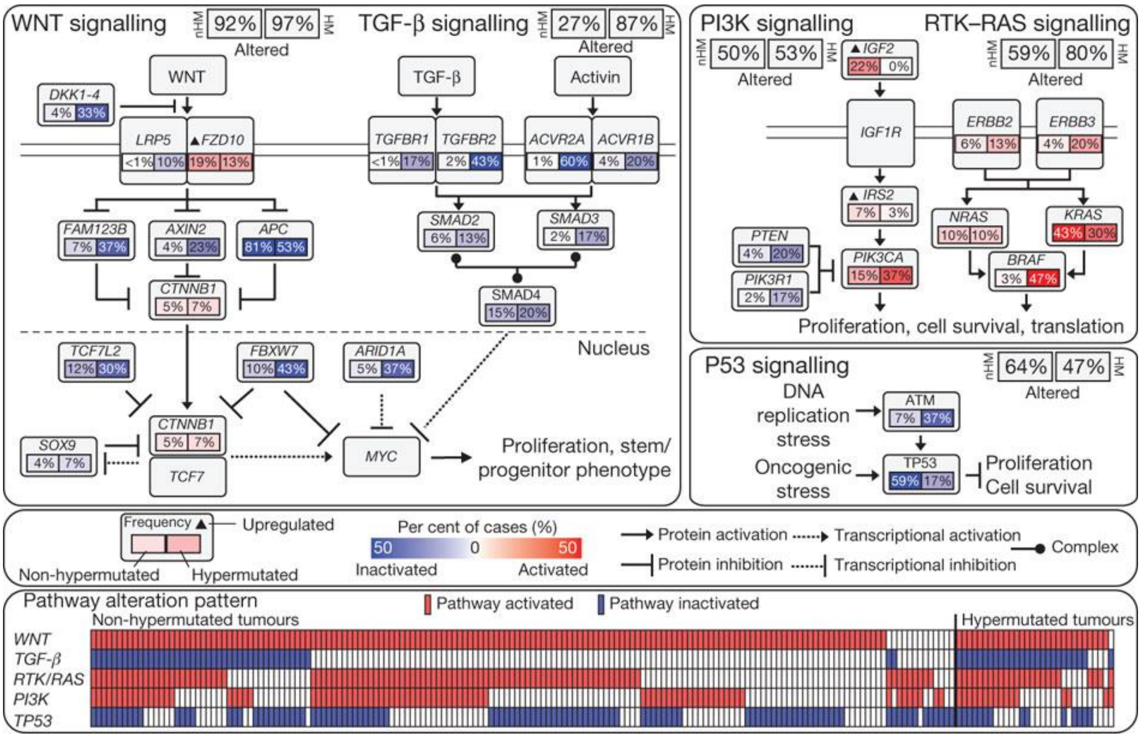
WNT signalling
nHM 92% 97% HM
Altered
TGF-β signalling
nHM 27% 87% HM
Altered
WNT
DKK1-4 4% 33%
LRP5 <1% 10%
▲FZD10 19% 13%
TGF-β
Activin
TGFBR1 <1% 17%
TGFBR2 2% 43%
ACVR2A 1% 60%
ACVR1B 4% 20%
FAM123B 7% 37%
AXIN2 4% 23%
APC 81% 53%
CTNNB1 5% 7%
SMAD2 6% 13%
SMAD3 2% 17%
SMAD4 15% 20%
Nucleus
TCF7L2 12% 30%
FBXW7 10% 43%
ARID1A 5% 37%
SOX9 4% 7%
CTNNB1 5% 7%
TCF7
MYC
Proliferation, stem/ progenitor phenotype
PI3K signalling
nHM 50% 53% HM
Altered
RTK–RAS signalling
nHM 59% 80% HM
Altered
▲IGF2 22% 0%
IGF1R
ERBB2 6% 13%
ERBB3 4% 20%
▲IRS2 7% 3%
NRAS 10% 10%
KRAS 43% 30%
PTEN 4% 20%
PIK3CA 15% 37%
PIK3R1 2% 17%
BRAF 3% 47%
Proliferation, cell survival, translation
P53 signalling
nHM 64% 47% HM
Altered
DNA replication stress
ATM 7% 37%
Oncogenic stress
TP53 59% 17%
Proliferation
Cell survival
Frequency ▲ Upregulated
Non-hypermutated
Hypermutated
Per cent of cases (%)
50 0 50
Inactivated
Activated
Protein activation
Transcriptional activation
Protein inhibition
Transcriptional inhibition
Complex
Pathway alteration pattern
Non-hypermutated tumours
Hypermutated tumours
Pathway activated
Pathway inactivated
WNT
TGF-β
RTK/RAS
PI3K
TP53

Figure 13: Genetic changes leading to deregulation of signaling pathways in CRC. The most recurrent alterations in CRC appear in components of the Wnt, RAS-MAPK, PI3K, TGF-β and p53 signaling pathways. The analyzed 224 CRC samples are separated into 'non-hypermutated tumors' with low mutation rates (nHM; 84% of the cases; mutation rate of $<8.24x10^6$) and 'hypermutated tumors' with high mutation rates (HM; 16% of the cases; mutation rate of $>12x10^6$). Genetic alterations include somatic mutations, homozygous deletions, high-level focal amplifications, and, in some cases, significant up- or downregulation of gene expression (*IGF2*, *FZD10*, *SMAD4*). Alteration frequencies are expressed as a percentage of all cases. Red denotes activated genes and blue denotes inactivated genes. Bottom panel shows for each sample if at least one gene in each of the five pathways described in this figure is altered. Source Muzny et al., 2012 from 'The Cancer Genome Network'.

5. THE MYOSIN SUPERFAMILY

5.1. Overview

Eukaryotic cells use motor proteins that move along cytoskeletal polymers to transport various intracellular cargos, including membranous organelles, protein complexes and mRNAs. There are three groups of cytoskeletal motors: myosins, kinesins and dyneins. Kinesins and dyneins move along microtubule tracks and are involved in long-distance transport. Kinesins move towards the ‘microtubule plus-end’ and dyneins towards the ‘minus-end’. Myosins, however, can anchor cargoes to actin filaments and provide shorter range trafficking along the actin cytoskeleton such as at the plasma membrane (Peckham, 2011).

The myosin superfamily is a versatile group of actin based molecular motors that need to hydrolyze ATP to generate physical force and move different cargoes inside the cell. This superfamily is divided into twenty-four classes based on head domain sequence similarity and domain organization (Syamaladevi, Spudich, & Sowdhamini, 2012).

Humans possess 40 different myosin genes representing 12 different classes (**Fig. 14**), whereas the nematode *Caenorhabditis elegans* has 17 myosin genes from 7 classes, the fly *Drosophila melanogaster* contains 13 myosin genes belonging to 8 classes, and yeast *Saccharomyces cerevisiae* presents 5 genes encoding myosins from 3 classes (Folma Buss, Spudich, & Kendrick-jones, 2004). Most eukaryotes depend on myosins, except a few taxonomic groups, namely, red algae and diplomonad protists which are not known to possess genes with myosin head domain. No classical myosins have been found in prokaryotes (Syamaladevi et al., 2012).

In humans the 40 myosin (*MYO*) genes can be grouped into conventional and unconventional myosins. The **conventional** myosins, which comprise the non-muscle myosin 2 family and the skeletal, cardiac and smooth muscle myosins (class 2), assemble to form bipolar filaments that mediate sliding and crosslinking of actin filaments to generate contractility and tension. By contrast, **unconventional** myosins do not form filaments but, rather, function as either monomeric or dimeric cargo transporters, regulators of actin organization, tethers for organelles, and/or as load-dependent tension sensors. The precise cellular functions of the different classes of unconventional myosins rely on their specific cargo-binding tail regions that mediate distinct interactions allowing them to target determined subcellular locations (Tumbarello, Kendrick-Jones, & Buss, 2013).

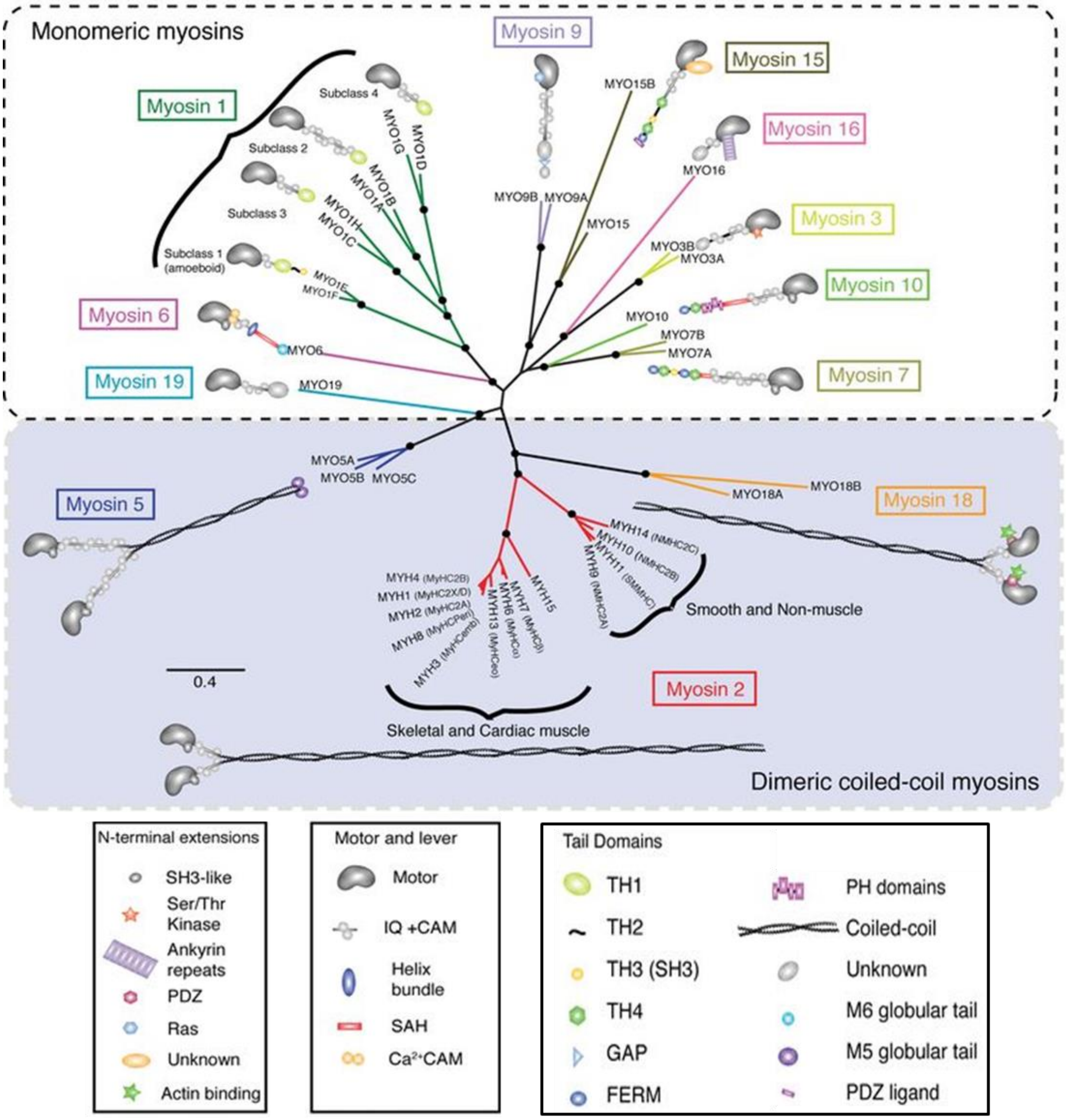
Monomeric myosins
Myosin 1
Subclass 4
Subclass 2
Subclass 3
Subclass 1 (amoeboid)
MYO1G
MYO1D
MYO1B
MYO1A
MYO1H
MYO1C
MYO1E
MYO1F
Myosin 6
MYO6
Myosin 19
MYO19
Myosin 9
MYO9B
MYO9A
Myosin 15
MYO15B
MYO15
Myosin 16
MYO16
Myosin 3
MYO3B
MYO3A
Myosin 10
MYO10
MYO7B
MYO7A
Myosin 7
MYO5A
MYO5B
MYO5C
Myosin 5
MYO18A
MYO18B
Myosin 18
MYH14 (NMHC2C)
MYH10 (NMHC2B)
MYH11 (SMMHC)
MYH9 (NMHC2A)
Smooth and Non-muscle
MYH4 (MyHC2B)
MYH1 (MyHC2X/D)
MYH2 (MyHC2A)
MYH8 (MyHCPeri)
MYH3 (MyHCemb)
MYH13 (MyHCeo)
MYH6 (MyHCα)
MYH7 (MyHCβ)
MYH15
0.4
Myosin 2
Skeletal and Cardiac muscle
Dimeric coiled-coil myosins
N-terminal extensions
SH3-like
Ser/Thr Kinase
Ankyrin repeats
PDZ
Ras
Unknown
Actin binding
Motor and lever
Motor
IQ +CAM
Helix bundle
SAH
Ca2+CAM
Tail Domains
TH1
TH2
TH3 (SH3)
TH4
GAP
FERM
PH domains
Coiled-coil
Unknown
M6 globular tail
M5 globular tail
PDZ ligand

Figure 14: The human myosin family tree. The human myosins are divided into 12 different classes. Myosins acting as dimers are shown in the bottom part of the tree (blue box), while monomeric myosins appear in the upper part (white box). Note that, myosin 6, myosin 7 and myosin 10 classes may act as both monomers and dimers. Structural components of the myosins are defined in the boxes at the bottom. Figure taken from Peckham, 2011.

Myosins are typically 1,000-2,000 residues long and their protomer consists of a long polypeptide known as the 'heavy chain' and smaller polypeptides called 'myosin light chains'.

The **heavy chain** comprises three regions (Krendel & Mooseker, 2005):

- An N-terminal **motor or head domain** which contains an ATP-binding site responsible for ATP hydrolysis and an actin-binding site.
- A **neck region** (C-terminal portion of the head) containing from one to six IQ motifs (with the consensus sequence [I,L,V]QxxxRGxxx[R,K]) where the 'myosin light chains'

bind. It acts as a lever arm that amplifies smaller movements within the catalytic domain.

- A variable C-terminal **tail** that can present a coiled-coil region (responsible for dimerization of heavy chains) and/or a globular cargo binding domain (responsible for cargo binding). Conventional myosins (myosin 2 family) possess long coiled-coil tails which enable them to assemble and form filaments, but lack the C-terminal globular domain. The C-terminal tails of unconventional myosins do contain globular cargo-binding domain but only some unconventional myosins present a coiled coil or similar regions.

The **myosin light chains** are regulatory proteins that bind to the IQ motifs of the neck region modulating the function and dynamics of the myosin heavy chains. Among this proteins are calmodulin or calmodulin-like proteins or other members of the E-F hand family of proteins (Krendel & Mooseker, 2005).

As mentioned before, within unconventional myosins only myosin 5 and myosin 18 contain an α-helical coiled-coil domain and have been shown to form dimers. Three further classes (myosin 6, myosin 7 and myosin 10) contain stable SAH domains (single α-helix; similar but not a real coiled-coil region) and therefore it seems that they can act as both monomers or dimers depending on the function (Peckham, 2011). However, most unconventional myosins do not have these helical regions and are believed to operate as single molecules (Krendel & Mooseker, 2005).

5.2. Myosin functions

The first myosin to be described was muscle **myosin 2**, which is responsible for muscle contraction. These myosins form bipolar filaments and when they slide between them, they induce the contraction of the muscle fibers by forcing two sets of actin filaments of opposite polarity to slide toward each other. Later, myosins from the class 2 were also discovered in non-muscle cells and were shown to use the ‘sliding-filament-type motility’ to provoke the constriction of the cleavage furrow during cytokinesis and the contraction of the apical actin ring associated with adherens junctions in polarized epithelia.

From that moment on, several studies have reported the presence of different mysosins and their involvement in a wide variety of intracellular functions. Below, some myosins are described as examples for each cellular function.

Cell migration and adhesion

Cell migration occurs mainly due to actin polymerization, actomyosin contractility and establishment of cell adhesions as points of support and push. Several myosins have been reported to be involved in such processes. **Myosin 2** is present in actin stress fibers in the rear of the cell during cell migration (Maupin, Phillips, Adelstein, & Pollard, 1994; Saitoh et al., 2001) and thus, it may be responsible for the forward movement of the cell body and tail retraction. It also coordinates directional motility by preventing the formation of lateral pseudopods and only limiting pseudopodial/lamellipodial protrusion to the leading edge of the cell (Lo et al., 2004). **Myosin 10** has been shown to bind integrins and its overexpression enhances the formation of filopodia and promotes integrin recruitment into filopodia (H. Zhang et al., 2004). Therefore, it may link elongating actin filaments to matrix-bound integrins, or it may stabilize filopodia by promoting integrin concentration at the filopodial tip to establish strong adhesion to the substrate. In *Dictyostelium amoebae*, **myosin 7** forms part of both, cell-cell and cell-substrate adhesions, and as a result of defects in adhesion, myosin 7-null cells are deficient in cell migration (Tuxworth et al., 2001).

Signal transduction

Myosins can also play important roles in cell-signaling pathways. For instance, **myosin 9** family members contain an active 'GTPase activation protein (GAP) domain' in their tail domain for the G protein Rho (Post, Bokoch, & Mooseker, 1998; Reinhard et al., 1995). **Myosin 3** contains an active protein kinase domain at its NH_2 terminus (Komaba, Inoue, Maruta, Hosoya, & Ikebe, 2003) and it has been involved in phototransduction in *Drosophila* (Cronin, Diao, & Tsunoda, 2004; S. J. Lee & Montell, 2004). **Myosin 5a** has been shown to play a role in regulating apoptosis by binding proapoptotic protein Bmf and sequestering it to actin filaments (Puthalakath et al., 2001).

Membrane traffic

Myosins are implicated in endocytosis, exocytosis and intracellular transport of a variety of membranous organelles and also in their capture and retaining at specific subcellular regions. **Myosin 1** has been involved in vesicle scission from the cell membrane in yeast (Jonsdottir & Li, 2004) and myosin 1c has been found to promote insulin-stimulated exocytosis of glucose transporter GLUT4 in mouse adipocytes (Bose et al., 2004). **Myosin 2b** is known to participate in calcium-stimulated exocytosis in fibroblasts (Togo & Steinhardt, 2004). Myosins of the **myosin 5** family are in charge of the transport of various types of organelles: melanosomes, phagosomes, smooth endoplasmic reticulum, endocytic vesicles and recycling vesicles (Langford, 2002; Reck-Peterson, Provance, Mooseker, & Mercer, 2000); and they also play a role in exocytosis, such as, in the case of insulin secretion by pancreatic β-cells (Varadi, Tsuboi, & Rutter, 2005). Myosin 5a also acts as an anchor by tethering melanosomes to the tips of dendrites (X. Wu et al., 2001). **Myosin 7a** is involved in the centripetal transport of phagosomes to provoke the fusion with lysosomes (Gibbs, Kitamoto, & Williams, 2003). **Myosin 18a** has been found to anchor the Golgi complex to actin filaments in HeLa cells (Dippold et al., 2009). **Myosin 19** is the responsible for mitochondria transport in mammalian neurons (Quintero et al., 2009).

Protein, RNA and non-membranous organelle localization

Myosins are involved in determining intracellular localization of proteins, multiprotein complexes, RNA and non-membranous organelles. **Myosin 1a** is involved in localizing sucrase-isomaltase to the brush border of intestinal epithelial cells; and as the major calmodulin-binding protein within the brush border of enterocytes, myosin 1a is also required to recruit high amounts of calmodulin, which is necessary for correct dietary uptake of Ca^{2+} (Tyska et al., 2005; Tyska & Mooseker, 2004). **Myosin 5a** is known to directly bind to microtubules and interact with microtubule-dependent motor kinesin and with intermediate filaments. Thus, it may serve as a linker between actin-, microtubule-, and intermediate filament-based cytoskeletal systems (Langford, 2002; Rao et al., 2002; Waterman-Storer et al., 2000). In neurons, myosin 5a has been shown to be part of a polyribosome-associated mRNA/protein (mRNP) complex containing Puralpha, mStaufen and fragile X protein (Ohashi et al., 2002). In budding yeast *Saccharomyces cerevisiae*, the **class 5 myosin Myo4p** plays a role in the transport and localization of several mRNAs from the mother cell to the tip of bud (Gonsalvez, Urbinati, & Long, 2005). **Myosin 2** is implicated in centrosome separation, where it is the responsible for the final position of centrosomes after nuclear envelope breakdown (Rosenblatt, Cramer, Baum, & McGee, 2004). **Myosin 10** is involved in transport of integrins and Mena/VASP proteins to the tips of filopodia (Tokuo & Ikebe, 2004; H. Zhang et al., 2004).

Nuclear functions

Several myosins have been found in the nucleus, where they interact with nuclear actin and regulate the cell cycle and the transcription of certain genes (De Lanerolle, 2012). **Myosin 1** is regarded as the mediator of ribosomal RNA genes transcription (Philimonenko, Janáček, Harata, & Hozák, 2010). **Myosin 2** serves as another core transcription factor to mediate the assembly of precursor complex for gene transcription (Q. Li & Sarna, 2009). **Myosin 5b** interacts with RNA polymerase I and newly transcribed ribosomal RNA (Lindsay & McCaffrey, 2009).

5.3. Myosins and cancer

In recent years, increasing evidence indicates that myosins play multi-functional and crucial roles during tumorigenesis. Below, some myosins shown to be involved in tumor progression are mentioned.

MYO1A was discovered to act as a tumor suppressor in intestinal epithelial cells. Knockdown of MYO1A in colon cancer cell lines resulted in decreased polarization and differentiation, enhancement of anchorage-independent growth, and increased tumorigenicity. Genetically- or chemically-induced tumors showed faster progression in *Myo1a*-knockout mice than in the animals expressing *Myo1a*. Moreover, colorectal cancer patients with low tumor MYO1A expression were associated with faster tumor progression and poor prognosis (Mazzolini et al., 2012). **MYO1E** expression has been shown to correlate with poor prognosis in patients with invasive breast cancer (Hallett, Dvorkin-Gheva, Bane, & Hassell, 2012). A mutation in ***MYH11*** gene (expressing the smooth-muscle **myosin 2** heavy chain) results in human colorectal cancer formation (Vickaryous et al., 2008). **MYO5A** is highly expressed in metastatic cancer cell lines derived from lung, colon, breast and prostate; and its knockdown disrupted tumor cell spreading and migration *in vitro* and decreased pulmonary metastasis of tumor cells in a chick embryo chorioallantoic membrane model *in vivo*. The expression of MYO5A was also elevated in metastatic colorectal cancer tissues (Lan et al., 2010). A ***MYO7A*** polymorphism has been linked to malignant melanoma risk (Fernandez et al., 2009). Genetic variants of ***MYO9B*** have been related to esophageal adenocarcinoma and 'Barrett's esophagus' precancerous lesion (Menke et al., 2012). In cancer cells, upregulation of **MYO10** expression promotes cell adhesion inhibition, protrusion formation (filopodia) and, tumor progression and metastasis development (Arjonen et al., 2014). High expression of MYO10 is observed in primary glioblastomas (Mischel et al., 2003), acute lymphoblastic leukemia (Ross et al., 2003) and aggressive subtypes of breast cancer (Cao et al., 2014). ***MYO18B*** gene is frequently mutated or hypermethylated in lung cancers and expression of MYO18B in lung cancer cells suppressed anchorage-independent growth (Nishioka et al., 2002). *MYO18B* mutations and epigenetic modifications have also been detected in ovarian and colorectal cancer, where MYO18B exhibits reduced expression (Nakano et al., 2005; Yanaihara et al., 2004).

6. MYOSIN VI

6.1. Overview

Human myosin VI gene is located in chromosome 6 at q14.1 position and it consists of 36 coding exons ("Ensembl," 2018). Besides myosin 9b, which may move towards both plus and minus ends (Krendel & Mooseker, 2005), myosin VI, with ~150 kDa, is the only myosin that moves towards the minus-end of actin filaments, in the opposite direction to the rest of myosins (Wells et al., 1999). Actin filaments present a polarity, with plus (or barbed) and minus (or pointed) ends. The polarity of actin filaments inside the cells is not well established, but it seems that most actin filaments have their plus ends towards the plasma membrane and towards the surface of internal organelles such as the phagosome or the Golgi complex (Krendel & Mooseker, 2005). Therefore, as a retrograde motor, myosin VI would move away from the plasma membrane into the cell and away from the surface of internal organelles (Folma Buss & Kendrick-Jones, 2008). Thus, it is likely to have unique cellular functions and properties.

Structurally, myosin VI differs from the other myosins principally in the presence of several 'unique inserts' along its different regions. Myosin VI is composed of the following basic domains: 1) An N-terminal canonical 80 kDa motor domain with ATP binding and acting binding sites. In this motor domain there is a **22 amino acid insert** that controls the nucleotide on and off rates and thus, it adjusts myosin VI functions (Sweeney et al., 2007). 2) A short neck or 'lever-arm' region with a single IQ motif that binds calmodulin. Between the motor domain and the 'lever-arm' there is a unique insert of 53 amino acids called the **'reverse gear'** which is responsible for the retrograde movement of myosin VI along actin filaments (Wells et al., 1999) and which is bound to a non-exchangeable calmodulin subunit (Bahloul et al., 2004). 3) A tail domain formed in its N-terminus of a three-helix-bundle (3HB) and a stable single α-helix (SAH) that enable dimerization in determined conditions (Fili et al., 2017; Mukherjea et al., 2009; Spink, Sivaramakrishnan, Lipfert, Doniach, & Spudich, 2008); and of a C-terminal cargo binding domain (CBD) that contains the sites by which myosin VI interacts with its binding partners (Folma Buss & Kendrick-Jones, 2008). Within the tail region there are two inserts, the **'large insert'** (LI) and the **'small insert'** (SI), which through alternative splicing can generate five different myosin VI isoforms (see 'mechanisms of regulation' section) (Folma Buss & Kendrick-Jones, 2008) (**Fig. 15**).

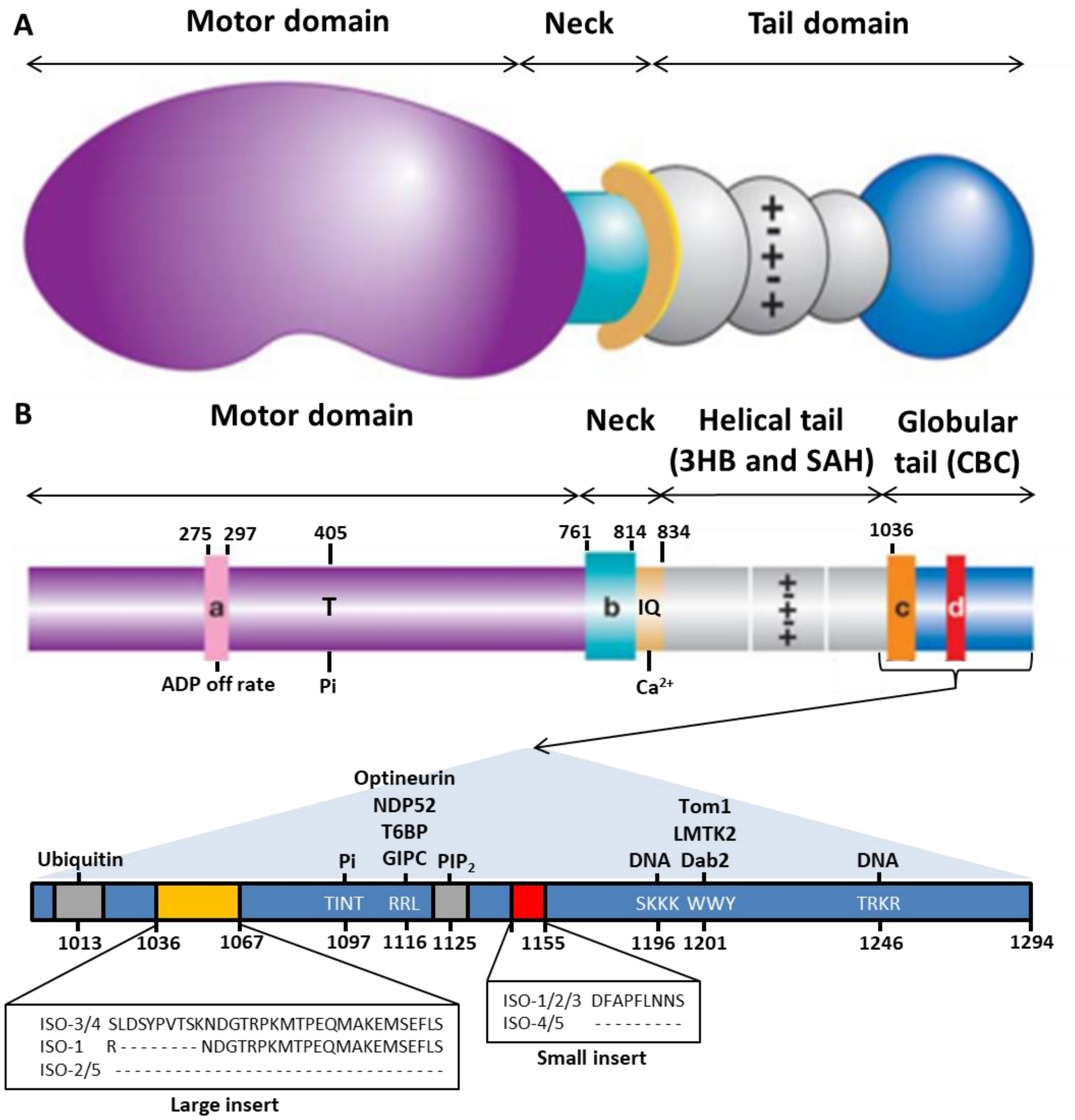
A
Motor domain
Neck
Tail domain
+
-
+
-
+
B
Motor domain
Neck
Helical tail (3HB and SAH)
Globular tail (CBC)
275
297
405
761
814
834
1036
a
T
b
IQ
c
d
ADP off rate
Pi
Ca2+
Optineurin
NDP52
T6BP
GIPC
Tom1
LMTK2
Ubiquitin
Pi
PIP2
DNA
Dab2
DNA
TINT
RRL
SKKK
WWY
TRKR
1013
1036
1067
1097
1116
1125
1155
1196
1201
1246
1294
ISO-3/4 SLDSYPVTSKNDGTRPKMTPEQMAKEMSEFLS
ISO-1 R - - - - - - - - NDGTRPKMTPEQMAKEMSEFLS
ISO-2/5 -
Large insert
ISO-1/2/3 DFAPFLNNS
ISO-4/5 - - - - - - - - -
Small insert

Figure 15: The structure of myosin VI. Amino acid (aa) numbering refers to isoform 3. **A)** Domain organization of myosin VI showing the motor domain, neck region with a single IQ motif, and the tail domain composed of the helical tail (the three-helix-bundle (3HB) and the single-α helix (SAH)) and the globular tail (cargo binding domain; CBD). **B)** Structural components of myosin VI pointing the potential regulatory sites. a-d represent the positions of unique inserts to myosin VI: **a-** twenty-two aa insert in the motor domain (275–297); **b-** fifty-three aa insert in the neck region (reverse gear) (761–814); **c-** large (1036–1067) and **d-** small (1147–1155) splice inserts in the tail domain giving rise to five different isoforms (ISO) of myosin VI. A threonine (T) at position 405 in the motor domain and two threonines (1097 and 1100) in the TINT sequence of the CBD can undergo phosphorylation. The cargo-binding domain also contains two protein interaction motifs (RRL and WWY), two DNA interaction sites (SKKK and TRKR), as well as regions for ubiquitin and PIP_2 binding. Adapted from Folma Buss & Kendrick-Jones, 2008; Folma Buss et al., 2004; Fili et al., 2017; and Tumbarello et al., 2012.

6.2. Mechanisms of regulation

How myosin VI is regulated inside the cell remains largely unknown. Nonetheless, it is most likely that several regulatory mechanisms are involved in modulating its activity since myosin VI is related with a wide variety of cellular functions that require a tight spatial and temporal specificity. Some probable regulatory mechanisms are shown below:

Isoforms

Myosin VI can exist in several isoforms that differ in the inserts of the tail due to the alternative splicing that undergoes the gene at the tail-codifying region. Exons 29, 30 and 31 which encode the large insert (LI; 32 amino acids) and exon 34, which encodes the small insert (SI; 9 amino acids), are the exons that can be alternatively spliced ("Ensembl," 2018). In humans, there are at least five known myosin VI isoforms with either only the large insert, only the small insert, both inserts, or no-inserts in the tail domain (F. Buss et al., 1998; F Buss, Arden, Lindsay, Luzio, & Kendrick-Jones, 2001; T Hasson & Mooseker, 1994; Tumbarello et al., 2013). The large insert shows two different variations depending on whether exon 29 is spliced or not. The longest version contains 32 amino acids (exons 29-30-31) and it is present, for instance, in the isoform expressed in the intestine (isoform 3). The other version is formed by 23 amino acids (exons 30-31) and it is part of isoform 1, which is found in the brain (Folma Buss et al., 2004) (**Table 2**). However, it is likely that more isoforms exist since other splice variants of large insert have been already reported, although they are not annotated in the Ensembl platform. Exons 29, 30 and 31 have been also shown to rearrange like '29-30' (Puri et al., 2010) and only 31 (Dance et al., 2004).

Although myosin VI is widely expressed in most tissues (**Fig. 16**), as mentioned above, the isoforms are expressed in a tissue-specific manner. The isoforms with the large insert are preferentially expressed in polarized epithelia containing microvilli, such as liver, kidney and intestine, whereas the isoforms with the small or no-inserts are preferentially expressed in unpolarized tissues such as testis and lung (F Buss et al., 2001). Moreover, different isoforms can be expressed in the same cell type or tissue at the same time or at different time points depending on certain conditions. For instance, when CACO2 cells (epithelial colorectal adenocarcinoma cells) are polarized or highly differentiated the isoform with 'both inserts' (isoform 3) is expressed and when they are unpolarized or undifferentiated the isoforms with the small insert (isoform 2) and no-inserts (isoform 5) are expressed (F Buss et al., 2001).

None of the tail inserts contain any obvious structural motif or binding site, but they have been shown to control the overall structural conformation of myosin VI protein and thus the binding to some of its specific partners (Folma Buss & Kendrick-Jones, 2008; Wollscheid et al., 2016). Therefore, the tissue-specific expression of the isoforms seems to be a mechanism to control motor-cargo interactions and their subsequent cellular localization and function.

Table 2: Human myosin VI isoforms. Information about the different protein isoforms and their corresponding gene transcripts is shown.

Isoforms	Large insert[2]	Small insert	UniProt Reference	Length (aa[3])	Missing aa (nº)	Transcript Reference	Translating sequence (bp[4])	Lacking exons[5]
Isoform 1	Yes - Short	Yes	Q9UM54	1285	1037-1045 (9)	202[a]	3858	29
Isoform 2	No	Yes	Q9UM54	1262	1037-1068 (32)	204 / 207[a]	3789	29, 30, 31
Isoform 3 (Canonical)[1]	Yes - Large	Yes	A0A0D9SGC1	1294	- (0)	208[a]	3885	-
Isoform 4	Yes - Large	No	Q9UM54	1285	1147-1155 (9)	007[b]	3858	34
Isoform 5	No	No	A0A0A0MRM8	1253	1037-1068; 1147-1155 (41)	201[a]	3762	29, 30, 31, 34

[1] Canonical isoform: Protein sequence of reference for being the longest isoform. The amino acids that are missing in the rest of the isoforms are based on the amino acid numbering of the isoform 3. [2] Large insert versions: Short: 23 aa; Large: 32 aa. [3] aa – amino acids. [4] bp – base pairs. [5] Ensembl exon numbering for *MYO6* gene. Protein information taken from UniProt database ("UniProt," 2014). Transcript information taken from [a] Ensembl ("Ensembl," 2018) and [b] GeneBank ("GenBank," 2017) databases.

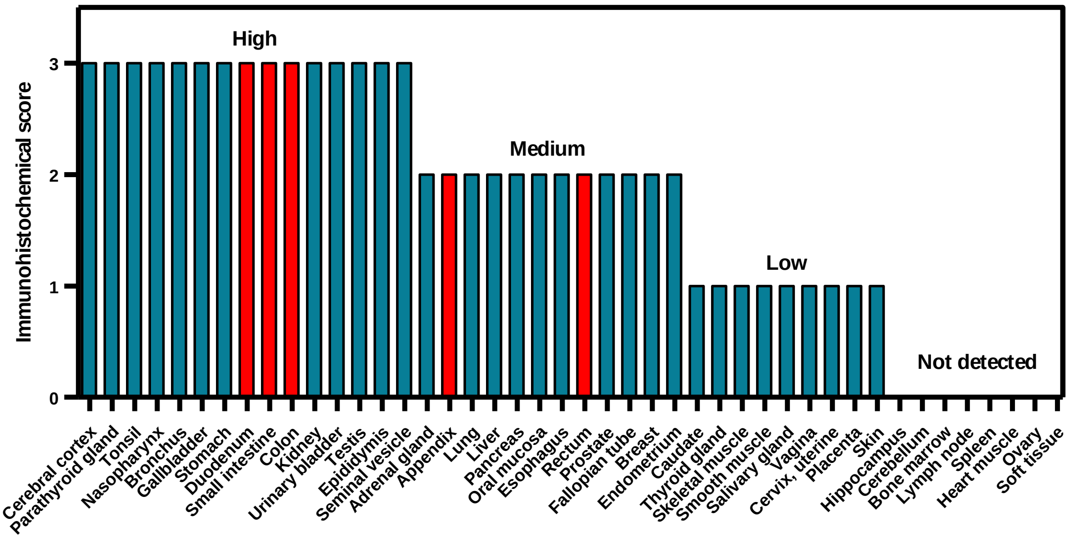

Figure 16: Myosin VI protein expression levels in normal tissues. Myosin VI protein expression assessed by immunohistochemistry in a panel of 44 normal tissues. For each tissue, the mean score of samples from three different individuals stained with two different antibodies (HPA035483 and CAB010762) is shown. Different MYO6 staining levels (immunohistochemical scores) are shown: 0: not detected; 1: low; 2: medium; 3: high. Tissues corresponding to intestine are indicated in red. Information taken from "The human protein atlas," 2017.

Phosphorylation of potential sites in the motor domain and tail region

Phosphorylation of two threonines ($T^{1089}INT^{1092}$) in the C-terminal region of myosin VI tail by PAK3 kinase has been demonstrated to regulate the binding of optineurin to myosin VI, only permitting the binding when myosin VI is not phosphorylated (Sahlender et al., 2005). Phosphorylation at these sites does not regulate myosin VI binding to any of the other binding partners so far tested.

The threonine T405 of the head domain of myosin VI is also a target of phosphorylation. The phosphorylation of this threonine by PAK1 (a Rac- and cdc42-activated kinase) is related with the recruitment of myosin VI into the ruffling membrane at the leading edge (F. Buss et al., 1998).

Ca^{2+} binding to the calmodulin subunit in the lever-arm region

The reverse gear (between the motor and neck domains) contains a bound calmodulin, but as the calcium that is bound to it is not-exchangeable, it seems that this calmodulin plays only a structural role (Bahloul et al., 2004).

In the neck region myosin VI has a single IQ motif which also binds a calmodulin. Batters et al. stated that the binding of calcium to this calmodulin affects the structure and thus, possibly certain functions of myosin VI. Basically, they found that the calmodulin of the lever arm, in the absence of Ca^{2+}, binds simultaneously to both, the IQ motif and part of the CBD in the tail (the region that contains the RRL motif and phospholipid binding motif) keeping myosin VI in a folded, inactive conformation. In presence of Ca^{2+}, calmodulin suffers a reorientation that prevents its interaction with the tail and enables myosin VI to adopt an accessible, active conformation (Batters, Brack, Ellrich, Averbeck, & Veigel, 2016; Masters, Kendrick-Jones, & Buss, 2016).

This fits with previous data showing that calcium is necessary for some functions. For instance, myosin VI only binds PtdIns(4,5)P_2-containing liposomes in the presence of calcium (Spudich et al., 2007) and in neurosecretory cells, recruitment of myosin VI to secretory granules depends on Ca^{2+} (Tomatis et al., 2013).

Although, several other studies also confirmed the folded conformation of myosin VI as a mechanism to regulate the binding to specific molecules (Song, Sader, White, Kendrick-Jones, & Trinick, 2010; Spink et al., 2008), Fili et al. recently observed that Ca^{2+} had no discernible impact on myosin VI unfolding (Fili et al., 2017), in contrast to Batters (Batters et al., 2016). They showed that some binding partners were responsible for unfolding myosin VI and exposing binding sites that were masked in the folded conformation (Fili et al., 2017).

Binding to specific adaptors and binding partners

In the CBD of myosin VI, at least seven adaptor proteins compete to interact with two binding interfaces that contain the amino acid motifs RRL or WWY (Spudich et al., 2007). The region containing the RRL motif interacts with ‘nuclear dot protein 52’ (NDP52), ‘Traf6-binding protein’ (T6BP), optineurin and ‘GAIP-interacting protein C-terminus’ (GIPC); and the region containing the WWY motif is required for binding to TOM1, DAB2 and ‘lemur tyrosine kinase-2’ (LMTK2) (Bunn, Jensen, & Reed, 1999; Chibalina, Seaman, Miller, Kendrick-Jones, & Buss, 2007; Morris et al., 2002; Morriswood et al., 2007; Sahlender et al., 2005; Spudich et al., 2007; Tumbarello et al., 2012). For other myosin VI adaptor molecules, such as SAP97 (H. Wu, Nash, Zamorano, & Garner, 2002), otoferlin (Heidrych et al., 2009), phospholipase Cδ3 (Sakurai, Hirata, Yamaguchi, Nakamura, & Fukami, 2011) and Dock7 (Ł. Majewski, Sobczak, Havrylov, Jóźwiak, & Rędowicz, 2012), the exact binding domain has not yet been determined. The two subdomains containing the RRL and WWY protein-protein interaction sites are linked by a phospholipid binding motif that interacts specifically and with high affinity to PtdIns(4,5)P_2 (Spudich et al., 2007). The CBD also contains a conserved ubiquitin-binding motif (Penengo et al., 2006); however, ubiquitylated proteins that specifically bind to myosin VI have not yet been identified. In close proximity to the WWY motif, 2 sites (SKKK and TRKR), which likely form a single binding surface, are required for interacting with DNA (Fili et al., 2017) (**Table 3**).

Recently, several new potential myosin VI binding partners have been identified through mass spectrometry–based proteomic screen. Among them are molecules implicated in endocytosis and vesicular trafficking, several GEFs and nuclear factors. However, their function and direct interaction with myosin VI need to be studied more thoroughly (L. Majewski et al., 2018; Wollscheid et al., 2016).

Table 3: Myosin VI binding partners. Their binding site on myosin VI and their cellular functions are shown.

Binding partner	Interaction motif	Function	References
Optineurin	RRL	Autophagy receptor, innate immunity, exocytosis/secretion, Golgi morphology, signaling	(Sahlender et al., 2005)
T6BP	RRL	Autophagy receptor, innate immunity, cell signaling, secretion, cell adhesions and ruffling	(Morriswood et al., 2007)
NDP52	RRL	Autophagy receptor, innate immunity, cell signaling, secretion, cell adhesions and ruffling	(Morriswood et al., 2007)
TOM1	WWY	Autophagy, endocytosis and cargo sorting	(Tumbarello et al., 2012)
GIPC	RRL	Endocytosis, cargo sorting, cell migration and cytokinesis	(Aschenbrenner, Lee, & Hasson, 2003; Arden, Puri, Sui-Yan Au, Kendrick-Jones, & Buss, 2007)
LMTK2	WWY	Endocytosis and cargo sorting	(Chibalina et al., 2007)
DAB2	WWY	Endocytic adaptor, clathrin-mediated endocytosis, cell adhesion and movement	(Morris et al., 2002; Spudich et al., 2007)
SAP97	Unknown	Trafficking and endocytosis of AMPA receptors and cell-cell adhesion	(Nash et al., 2010)
Ortofelin	Unknown	Exocytosis/secretion	(Heidrych et al., 2009)
Phospholipase Cδ3	Unknown	Membrane anchoring, signaling	(Sakurai et al., 2011)
Dock7	Unknown	GEF of Rho-family GTPases, cytoskeleton remodeling	(Ł. Majewski et al., 2012)
PtdIns(4,5)P_2	phospholipid binding motif	Endocytosis, signaling	(Spudich et al., 2007)

The spatial and temporal regulation and coordination of motor-cargo attachment is likely to involve several mechanisms, including tissue-specific expression of motor protein isoforms and the stoichiometric concentration of adaptor proteins.

6.3. Functions

Myosin VI has been related to several intracellular functions in mammalian cells. The most important roles of myosin VI are involved in processes such as clathrin-mediated endocytosis; cargo secretion and Golgi complex maintenance; migration; autophagy; cargo tethering; cytokinesis; and transcription. The specific functions of myosin VI known so far are explained below with more detail.

6.3.1. Myosin VI and endocytosis

Overview of endocytosis

Endocytosis is a fundamental process that occurs at the plasma membrane of the cells and which is required for regulated uptake of macromolecules such as proteins, nutrients and cell surface receptors (**Fig. 17**). Therefore, the cells through the endocytic pathway, control the reutilization or degradation of membrane components and this in turn has influence over important processes such as nutrient uptake, immunity, signaling, adhesion, membrane turnover and development (Scott, Vacca, & Gruenberg, 2014).

There are several endocytic mechanisms for internalizing molecules from the cell surface (Doherty & McMahon, 2009). The best characterized endocytic process is the **'receptor-mediated endocytosis'** (also known as clathrin-mediated endocytosis) which involves the internalization of receptors and their ligands by clathrin-coated pits. It implies the following sequence of steps: 1) selection and clustering of cell-surface receptors; 2) coat assembly and formation of the coated pit; 3) invagination of the plasma membrane; 4) membrane scission generating the clathrin-coated vesicle; and 5) movement of vesicles away from the plasma membrane (Folma Buss et al., 2004).

All the internalized macromolecules are delivered to a common **early endosome**. This early endosome is a pleomorphic and persistent organelle that acts as a first sorting station in the cell for membrane-associated molecules (The term 'early endosome' actually describes two distinct endosomal organelles, the **sorting endosome** and the **endocytic recycling compartment** (ERC) and both together form an extensive network of interconnected tubulo-cisternal elements) (Maxfield & McGraw, 2004). A few minutes after arrival to the early endosome, the material destined for degradation or recycling is segregated. Some receptors and proteins are recycled back to the plasma membrane directly or indirectly through the recycling endosome, while other molecules are sent towards lysosomes for degradation (Scott et al., 2014).

Before degradation, some activated signaling receptors or receptors that need to be downregulated are separated into intraluminal vesicles (ILVs) originated from luminal invaginations of the early endosome membrane. Vacuolar regions that contain those intraluminal vesicles detach from the early endosome and become free multivesicular bodies (MVBs) (also called endosomal carrier vesicles (ECVs)) which eventually fuse with the **late endosome**. Ligands after receptor uncoupling such as LDL, and endocytosed solutes are also degraded via ILV-MVBs route (Scott et al., 2014).

The late endosome is formed by highly pleomorphic multivesicular regions and very dynamic tubulo-cisternal elements. As the early endosome, the late endosome also functions as a sorting station, since it sorts materials for lysosomal degradation or for other destinations such as extracellular release as exosomes. The late endosome also plays a role in the autophagy pathway, since the autophagosome fuses with the late endosome to acquire degradative capacity (Scott et al., 2014).

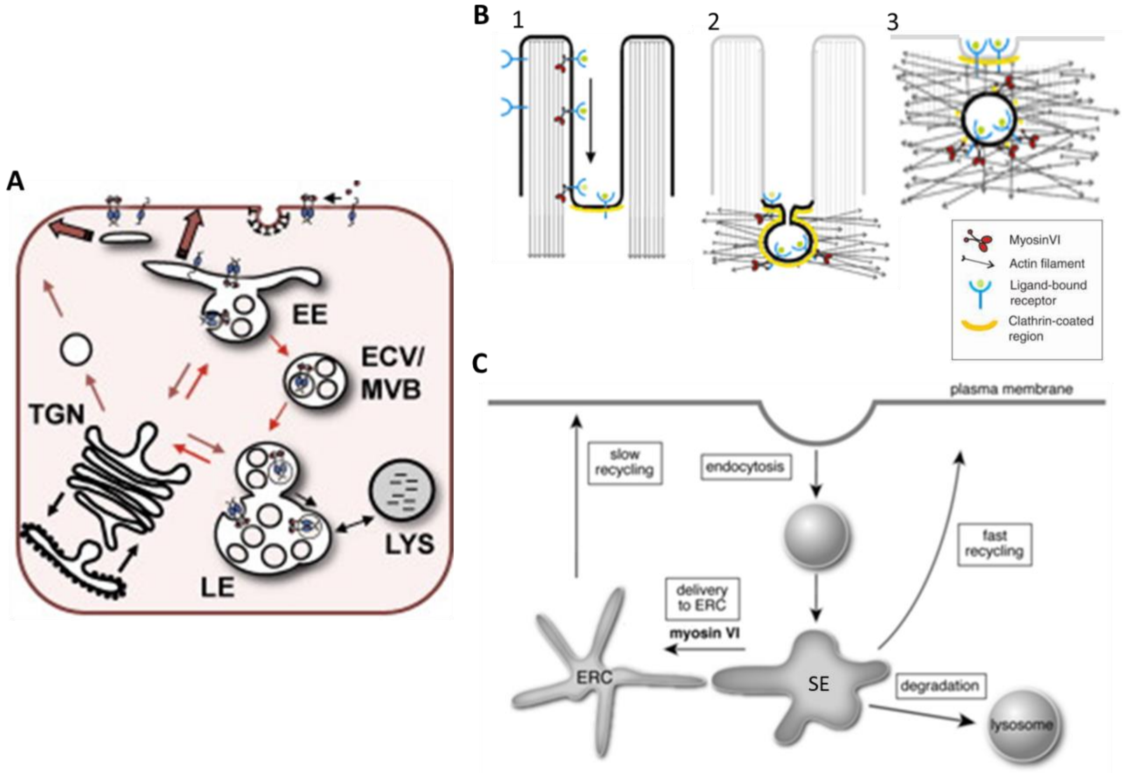

Figure 17: Clathrin-coated endocytosis and the endocytic pathway. A) The endocytic pathway. Molecules are internalized into vesicles originated from the plasmatic membrane and delivered to the early endosome (EE). Some proteins are recycled back to the membrane and others are sent for degradation to lysosomes (LYS) passing first through multivesicular bodies (MVB or endosomal carrier vesicles (ECV)) and late endosome (LE). TGN: trans-Golgi network. **B)** Roles of myosin VI in the clathrin-coated endocytosis. 1- Myosin VI transports ligand-bound receptors down the microvilli and recruits receptors in clathrin-coated pits. 2- Myosin VI participates in the formation of clathrin-coated vesicles. 3- Myosin VI transports uncoated vesicles through the actin mesh. **C)** Myosin VI is also involved in transporting cargo from the sorting endosome (SE) to the endocytic recycling compartment (ERC).

Roles of myosin VI in endocytosis and endocytic pathway

In mammalian cells the cortical actin network underlying the plasma membrane is important for endocytosis. In polarized as well as in unpolarized cells actin filaments are involved in the early stages of endocytosis, specifically in receptor clustering and spatial organization of the endocytic machinery; and also in vesicle scission and the transport of vesicles away from the plasma membrane (Folma Buss et al., 2004).

As actin-based motor, myosin VI has been demonstrated to be required in four distinct stages of endocytosis (**Fig. 17**): 1) Clustering of ligand-bound receptors into clathrin-coated pits. 2)

Formation of clathrin-coated vesicles. 3) Transport of uncoated vesicles through actin-rich terminal web towards the early endosome. 4) Transport of cargo from the sorting endosome to the endocytic recycling compartment (Tama Hasson, 2003). A more detailed description can be found below:

1. Clustering of ligand-bound receptors into clathrin-coated pits

A study done in the intestinal brush border ‘Na^+/H^+ exchanger NHE3’ presented evidence that myosin VI moves cargo down the microvillus length to inter-microvillar region of intestinal cells (Chen et al., 2014). Moreover, they also demonstrated that NHE3 localization and anchoring in the microvillus of intestinal cells is dependent on myosin VI, although NHE3 itself does not bind myosin VI. Most probably, myosin VI may bind NHE3 indirectly through adaptors.

2. Formation of clathrin-coated vesicles

The first indications that myosin VI could be involved in the formation of clathrin-coated vesicles were presented by Buss (F Buss et al., 2001), since they demonstrated that 1) myosin VI with the large insert localized to clathrin-coated pits/vesicles and that 2) the myosin VI tail domain with the large insert acted as a dominant-negative inhibiting transferring endocytosis. Therefore, as it is a minus end directed motor, myosin VI was believed to move the clathrin-coated vesicles towards the minus end of actin filaments, away from the plasma membrane and into the cell.

Subsequent studies have proven the direct binding of myosin VI and **disabled 2 (DAB2)** (Morris et al., 2002; Spudich et al., 2007), both co-localizing in clathrin-coated pits/vesicles. It was already known that DAB2 is involved in clathrin-coated vesicle formation by directly binding to clathrin adapter AP-2 and clathrin heavy chain (Tama Hasson, 2003). The WWY (1183-1185) motif was identified as DAB2 binding site in myosin VI C-terminal tail (Spudich et al., 2007).

Interestingly, the large insert in the globular tail region of myosin VI identified as being required for localization to apical surfaces in polarized cells is not necessary for DAB2 interaction. Namely, in *in vitro* binding assays, DAB2 can associate with both splice forms of myosin VI (with and without LI) (Morris et al., 2002). However, *in vivo*, the association of endogenous DAB2 and myosin VI only occurs in polarized epithelial cells, where the large insert form of myosin VI is expressed and localized to apical coated pits/vesicles (F Buss et al., 2001; Morris et al., 2002)**.** In fibroblasts or unpolarized cells, the endogenous myosin VI lacks the large insert that directs it to coated pits, and therefore only a very small amount of the endogenous myosin VI colocalizes with clathrin and AP-2, despite DAB2 being also present in coated pits in non-polarized cells (Aschenbrenner et al., 2003). In addition, in unpolarized cells, overexpressed GFP-tagged myosin VI containing the large insert also colocalizes with endogenous DAB2 (Morris et al., 2002).

Therefore, the large insert in the tail enhances binding to clathrin-coated pits/vesicles, but by itself is not sufficient, indicating that the large insert does not contain all the targeting information. Considering these data, yet-uncharacterized mechanism must regulate myosin VI targeting to DAB2 in clathrin-coated pits, specifically recruiting the longer splice version (Tama Hasson, 2003; Morris et al., 2002).

It has also been discovered that myosin VI binds with high specificity to **PtdIns(4,5)P_2**-containing liposomes, showing little or no binding to other phosphoinositides. PtdIns(4,5)P_2 (PIP_2) is known to bind and recruit many endocytic proteins to the plasma membrane and regulate the formation, scission and uncoating of clathrin-coated vesicles. The binding site for PtdIns(4,5)P_2 is established in the myosin VI C-terminal tail as WKSKNKKR (1124–1131) (Spudich et al., 2007). Mutations in the PtdIns(4,5)P_2 binding-site reduced substantially the recruitment of both, full-length myosin VI and its tail domain to clathrin-coated structures compared with the wild-types (Spudich et al., 2007).

Thus the targeting and functional role of myosin VI in clathrin-coated pits/vesicles is mediated by the binding to both DAB2 and PtdIns(4,5)P_2 and requires the presence of the large insert in the tail domain.

3. Transport of uncoated vesicles through actin-rich terminal web towards the early endosome

Unpolarized cells or epithelial cells under non-polarizing conditions express the myosin VI isoforms without the large insert (F Buss et al., 2001). Although these cells lack microvilli, they do exhibit dense cortical actin networks. In these cells myosin VI is found in peripheral areas, recruited to newly uncoated endocytic vesicles, but it is not present on clathrin-coated pits (Aschenbrenner et al., 2003). The association to the vesicles is transient, since myosin VI leaves upon fusion with the early endosome. The adaptor protein GIPC, known to be binding partner of myosin VI (Morris et al., 2002), is also present on the uncoated vesicles, colocalizing with myosin VI. This suggets that GIPC may be involved in the recruitment of myosin VI to the uncoated vesicles or that GIPC is recruited along with myosin VI to the vesicle surface (Aschenbrenner et al., 2003). The disruption of myosin VI function provokes that the transferrin-containing uncoated vesicles remain 'stuck' at the cell periphery, dramatically delaying the delivery of the transferrin cargo to the early endosome. Remarkably, under these conditions initial rates of transferrin uptake into clathrin-coated vesicles are normal. Consequently, myosin VI (without LI) is necessary for the efficient and appropriate traffic of nascent endocytic vesicles (Aschenbrenner et al., 2003).

4. Cargo transport from early sorting endosome to endocytic recycling compartment

It has been demonstrated that myosin VI by binding directly to 'lemur tyrosin kinese 2' (LMTK2) is required for the transport of cargos, such as transferrin receptor, from the early sorting endosome to the endocytic recycling compartment. LMTK2 binds to the WWY site in the C-terminal of myosin VI tail and it does it regardless of whether it contains the large insert or not. When either myosin VI or LMTK2 is depleted by siRNA, the transferrin receptor is trapped in swollen endosomes and the tubule formation in the endocytic recycling pathway is dramatically reduced (Chibalina et al., 2007).

As explained before, Aschenbrenner et al. (2003) observed that the disruption of myosin VI activity leads to accumulation of transferrin positive vesicles in the cortical actin network delaying its trafficking. However, with longer time the transferrin receptor still reaches to swollen early endosome. Nevertheless, in these myosin VI knockdown cells, a major drawback appears with the block of transferrin receptor transport from the early sorting endosome to the endocytic recycling compartment (Chibalina et al., 2007).

6.3.2. Myosin VI and secretory pathway

Overview of secretory pathway and Golgi complex

The Golgi complex is of great importance in the secretory pathway. Proteins after being synthesized in the endoplasmic reticulum pass through the Golgi complex in order to undergo post-translational changes and be sorted for specific cell compartment. Golgi complex appears as a series of flattened and stacked membrane cisternae, which can be grouped into cis, medial and trans Golgi compartments. Complex networks of membrane tubules and vesicles flank both sides of Golgi apparatus: the cis-Golgi network (CGN) and the trans-Golgi network (TGN) (Ladinsky, Mastronarde, McIntosh, Howell, & Staehlin, 1999). In the TGN cargos are sorted into different vesicles for delivery to targeted locations in the cell depending on whether they are carried through the basolateral or apical trafficking pathways (**Fig. 18**) (Griffiths & Simons, 1986).

Roles of myosin VI in the secretory pathway and Golgi complex maintenance

Myosin VI is localized within the Golgi complex and within flanking TGN and CGN (F. Buss et al., 1998) by interacting with its binding partner optineurin. Optineurin binds myosin VI in the RRL sequence of the globular tail and the presence of the large insert is not required for this binding (Sahlender et al., 2005).

Myosin VI has been demonstrated to be involved in the **steady-state organization of the Golgi complex**, since in fibroblasts derived from Snell's Waltzer mice, where myosin VI is absent, the Golgi complexes are smaller and more fragmented compared to the fibroblasts of the wild-type mice. However, there are no differences in the overall morphology of individual Golgi stacks at ultrastructural level (Warner et al., 2003).

In addition to this structural role in maintaining Golgi complex morphology, myosin VI has also been shown to be fundamental in the secretory pathway for the **delivery of cargo from the Golgi complex to the plasma membrane**. The absence of myosin VI reduces significantly the level of secretion of a secreted form of alkaline-phosphatase (expressed from a exogenous construct introduced to the cells) from the TGN to the plasma membrane (Sahlender et al., 2005; Warner et al., 2003).

In polarized epithelial cells myosin VI is required for the **sorting of newly-synthesized 'tyrosine motif containing' proteins** specifically to the basolateral domain (Au, Puri, Ihrke, Kendrick-Jones, & Buss, 2007). The myosin VI isoform with no insert in the tail domain is the isoform required for this function, and it forms a complex with optineurin and RAB8 to mediate the sorting in the AP-1B–dependent biosynthetic sorting pathway.

Moreover, it has also been demonstrated that myosin VI and optineurin are required for **polarized delivery of epidermal growth factor receptor (EGFR)** into the leading edge of motile cells through the anterograde trafficking pathway (Chibalina, Poliakov, Kendrick-Jones, & Buss, 2010).

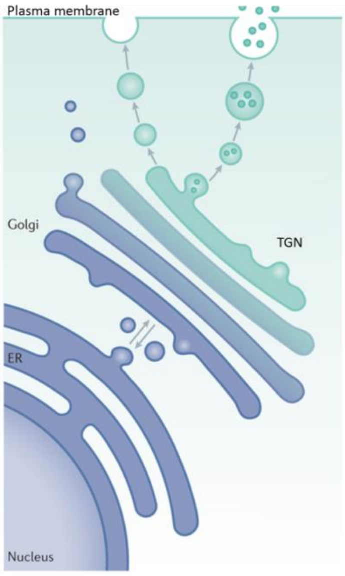

Figure 18: The secretory pathway. Proteins synthesized in the endoplasmic reticulum (ER) pass through the Golgi complex to undergo post-translational changes. Once in the trans-Golgi network (TGN) they are sorted into different vesicles for basolateral or apical delivery. Adapted from Lamb, Yoshimori, & Tooze, 2013.

6.3.3. Myosin VI and autophagy

Overview of autophagy

Autophagy is a fundamental catabolic pathway in eukaryote cells that is required for degradation of cytoplasmic proteins and organelles. Autophagy is characterized by the formation of a double-membrane vesicle termed autophagosome, which sequesters cytoplasmic material and delivers it to lysosomes for degradation (Weidberg, Shvets, & Elazar, 2011; Z. Yang & Klionsky, 2010).

Autophagy receptors recognized ubiquitinated cargoes and recruit them to LC3-positive membranes to start forming the autophagosome (Tumbarello et al., 2012). Then the autophagosome expands and matures by taking membranes derived from the plasma membrane, endoplasmic reticulum, Golgi complex, mitochondria, early and late endosomes and from multivesicular bodies. Subsequently, the autophagosome fuses with lysosomes to allow cargo breakdown. The resulting macromolecules are transported back into the cytosol through membrane permeases for reuse (**Fig. 19**) (Z. Yang & Klionsky, 2010).

Basal autophagy is important for maintaining cellular homeostasis through the elimination of damaged organelles, long-lived proteins, protein aggregates and pathogens. If an environmental stress appears, such as nutrient starvation, hypoxia, oxidative stress, pathogen infection, radiation or anticancer drug treatment, autophagy is enhanced as a cytoprotective response. However, dysregulated or excessive autophagy may lead to cell death (Z. Yang & Klionsky, 2010).

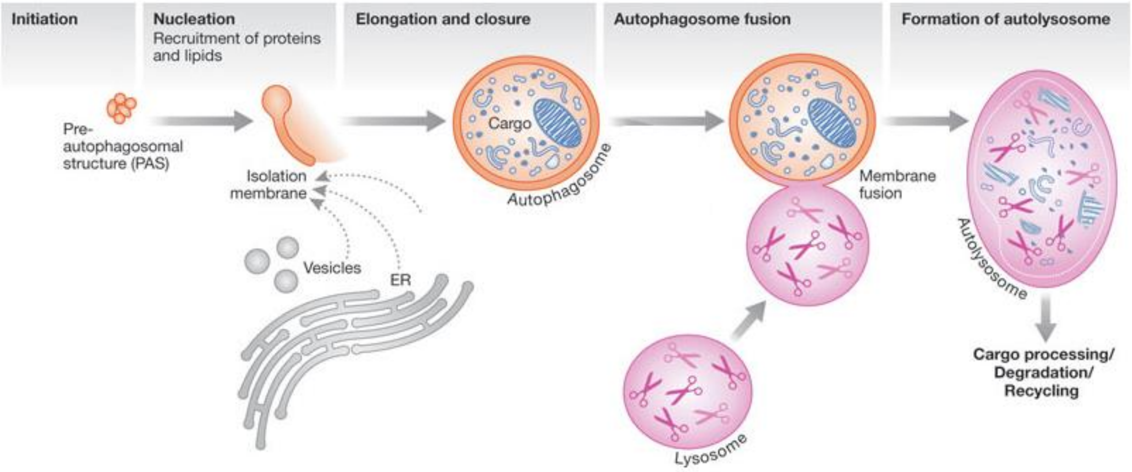
Initiation
Nucleation
Recruitment of proteins and lipids
Elongation and closure
Autophagosome fusion
Formation of autolysosome
Pre-autophagosomal structure (PAS)
Isolation membrane
Vesicles
ER
Cargo
Autophagosome
Membrane fusion
Lysosome
Autolysosome
Cargo processing/ Degradation/ Recycling

Figure 19: Steps in autophagy. Initiation: activation of protein complexes that lead to the initiation of isolation membrane formation. Nucleation: recruitment of proteins and lipids for autophagosome biogenesis. Membrane elongation and closure: the isolation membrane expands either by direct flow of membranes from a source such as the endoplasmic reticulum (ER) or by vesicle fusion to finally form the autophagosome that will surround the cargos. Autophagosome and lysosome fusion: the autophagosome fuses with the lysosome to form an autolysosome, in which the cytosolic cargos are degraded and recycled. Adapted from Subramani & Malhotra, 2013.

Role of myosin VI in autophagy

Myosin VI has been demonstrated to be involved in autophagy in concert with some of its known adaptor proteins NDP52, optineurin, T6BP and TOM1. During autophagy myosin VI facilitates the delivery of TOM1-positive endosomes to autophagosomes by docking to NDP52, T6BP and optineurin and thereby promoting autophagosome maturation and its fusion with lysosome (Tumbarello et al., 2012).

TOM1 belongs to 'endosomal sorting complex required for transport' (ESCRT) class 0 protein family. It is found on endosomes from which mediates the endosomal localization of myosin VI by interacting with its WWY motif. A loss of myosin VI function results in a decrease in endosome-autophagosome fusions (Tumbarello et al., 2012).

Recruitment of myosin VI to autophagosomes occurs by binding to **NDP52, T6BP** and **optineurin** and it requires the myosin VI RRL motif (Morriswood et al., 2007; Sahlender et al., 2005). NDP52, T6BP and optineurin are characterized as cargo-selective receptors in autophagy and they contain an ubiquitin-binding domain (UBD) and a LC3-interaction region (LIR). They participate in the autophagosome biogenesis as adaptors between ubiquitilated cargo and LC3-associated autophagocytic membranes facilitating autophagosome formation.

Therefore, acting also as myosin VI receptors they enable the delivery and docking of myosin VI associated endosomes and probably other fusion events required for autophagosome maturation.

Myosin VI depletion leads to an abundant accumulation of autophagosomes due to autophagosome-lysosome fusion defects. This failure may be caused by defects in autophagosome maturation due to lack of docking of endosomal membranes containing Tom1 (Tumbarello et al., 2012).

6.3.4. Myosin VI and cytokinesis

Overview of cytokinesis

Cytokinesis is the process of division of the cytoplasm and the plasma membrane in the late stage of mitosis. During cytokinesis an actomyosin II contractile ring is formed, which is progressively constricted while targeted membranes are added to the division site (Glotzer, 2005). This membrane delivery is first required during cleavage furrow ingression to increase the surface area of the two daughter cells and later during the abscission process to seal the two newly formed cells (Albertson, Riggs, & Sullivan, 2005; Strickland & Burgess, 2004). Membrane vesicles targeted to the cleavage furrow come from the secretory pathway (Skop, Bergmann, Mohler, & White, 2001), endocytic pathway and from vesicles of the recycling compartment (**Fig. 20**) (Fielding et al., 2005; Gerald, Damer, O'Halloran, & De Lozanne, 2001; Schweitzer & D'Souza-Schorey, 2002; Wilson et al., 2005).

Role of myosin VI in cytokinesis

In cells undergoing cytokinesis myosin VI is present on the walls of the ingressing cleavage furrow and on vesicles moving into and out of the midbody region (cytoplasmic bridge that connects the two daughter cells). It has been shown that myosin VI is required for membrane delivery into the cleavage furrow in the final stages of cell-cell abscission and most probably it carries out this function in association with its binding partner GIPC. Inhibition of myosin VI activity can lead to defects in cytokinesis such as multinucleation or abscission failure and cell death (Arden et al., 2007).

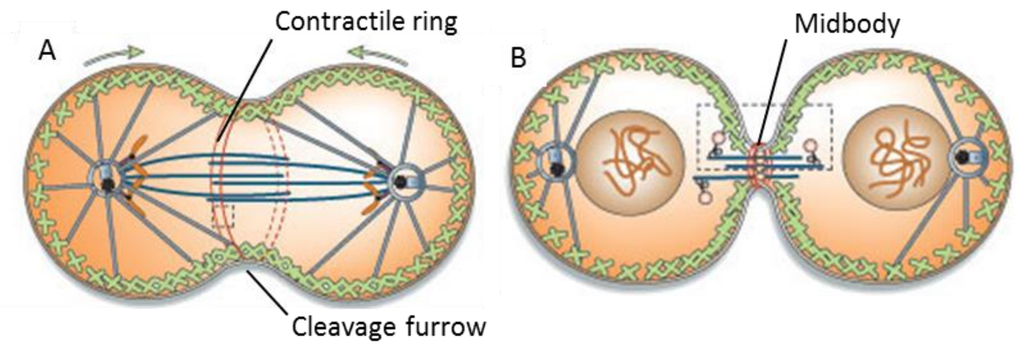

Figure 20: Dividing cell. A) Late anaphase. The cleavage furrow advances while the contractile ring of actomyosin II begins to contract. **B)** Telophase/cell–cell abscission. The contractile ring contracts (furrow ingression) developing a barrier between the daughter cells and constricting the spindle mid-zone into a structure called the midbody. During abscission the furrow 'seals' by a mechanism that involves vesicle transport/exocytosis, completely separating the daughter cells. Adapted from Scholey, Brust-Mascher, & Mogilner, 2003.

6.3.5. Myosin VI and migration

Overview of migration

Cell migration is a fundamental cellular process in embryonic development, tissue repair and immune response among other cellular functions. Moreover, changes in the migratory behavior of cells are linked to many pathological processes such as tumor metastasis (Chibalina, Puri, Kendrick-Jones, & Buss, 2009).

Cellular motility involves cell polarization, the formation of extended protrusions in the direction of the migration, the assembly of adhesions and actin-myosin structures at the leading edge, as well as the disassembly of focal adhesions and retraction at the rear end of the cell. Therefore, the process of cell migration depends on the coordinated action of actin remodeling, membrane trafficking and cell adhesion to a substrate (Ridley, 2003).

The direction of movement is determined by the leading edge of the cell which contains actin-based membrane protrusions known as lamellipodia and filopodia (Chhabra & Higgs, 2007). The formation of these plasma membrane extensions is closely regulated by two different subclasses of Rho-GTPases, Rac and Cdc42 (Heasman & Ridley, 2008). Some downstream effectors of Rac and Cdc42 activate the actin-related proteins 2 and 3 (Arp2/3 complex) triggering the actin polymerization and the formation of lamellipodia and filopodia (Pollard & Borisy, 2003).

The spatial and temporal coordination of actin polymerization and the formation of stable contacts with the underlying substrate are necessary to generate force to push the plasma membrane forward (Chibalina et al., 2009). In order to create those new focal adhesions there is a constant need for delivery of extracellular matrix receptors into the leading edge. These receptors can be supplied by transporting them directly from the Golgi complex via the biosynthetic pathway or by recycling through endocytosis the receptors that are left at the rear part of the cell as the cell moves forwards and bringing them to the front (Folma Buss, Luzio, & Kendrick-jones, 2002).

Roles of myosin VI in migration

Several studies have suggested the involvement of myosin VI in cell migration. Buss et al. demonstrated that myosin VI was recruited into membrane ruffles of the leading edge of fibroblasts after EGF stimulation (F. Buss et al., 1998).

Later, a good evidence of myosin VI involvement in cell motility came from the study of the migration of border cells in *Drosophila* ovaries. Border cells are a small subgroup of migratory epithelial follicle cells that during the oogenesis detach from their epithelial neighbors and migrate towards the oocyte. Myosin VI is expressed in the border cells throughout their migration and is found within the extended protrusions at the leading edge. But when myosin VI expression is missing, the protrusions are lost and migration is severely inhibited (Geisbrecht & Montell, 2002).

Although myosin VI has been demonstrated to be required for cell migration, the underlying molecular mechanisms and regulation of myosin VI function in cell motility in mammalian cells are poorly understood. So far, a number of possible mechanisms have been suggested (**Fig. 21**): 1) stabilization of cell-cell and cell-ECM junctions at the leading edge and generation of protrusive force to push actin filaments outwards; 2) regulation of actin dynamics; 3) endocytosis and recycling of adhesion molecules into the leading edge; and 4) delivery of newly synthesized cell adhesion and signaling receptors from the Golgi complex to the leading edge.

1. Maintenance of cell contact sites

During the process of migration the assembly of new cell-cell and cell-extracellular matrix (ECM) junctions at the leading edge is essential for cells to move. Myosin VI has been shown to have a role in E-cadherin-based cell-cell adhesion in both mammalian and *Drosophila* cells.

In the border cells of *Drosophila* ovaries, myosin VI was isolated in a complex with the adhesion proteins E-cadherin and β-catenin. Moreover, E-cadherin and β-catenin protein levels were specifically reduced in cells lacking myosin VI. This effect was specific of cell-cell junctions (adherent junctions) since the levels of proteins of focal adhesion complexes were unchanged (Geisbrecht & Montell, 2002). These data suggested that myosin VI is required for border cell migration either by stabilizing E-cadherin and β-catenin complexes or by generating a protrusive force that would move actin filaments outwards while binding to these stationary adhesion complexes in the plasma membrane (Chibalina et al., 2009).

In early *Drosophila* embryogenesis myosin VI seems to be also crucial for maintenance of cell-cell contacts during dorsal closure. During this process myosin VI is recruited into filopodia and lamellipodia at the leading edge of the moving epithelial sheets. The absence of myosin VI leads to a detachment of the cells from the epithelial cell layer and results in defects in movement of these epithelial cells (Millo, Leaper, Lazou, & Bownes, 2004).

In mammalian epithelial cells, myosin VI has also been shown to be recruited to cadherin-dependent cell-cell contacts as the epithelial monolayers mature, regulating the morphogenesis of those cell-cell contacts. Myosin VI forms a biochemical complex with E-cadherin and vinculin (an actin binding protein that connects adhesion receptors to the actin cytoskeleton). When myosin VI is depleted from these cells, vinculin is lost from adhesion sites weakening the adhesion complex and reducing the stability of perijunctional actin cytoskeleton**.** This results in a loss of cohesive forces in the epithelial layers which is a prerequisite for invasive cancer cell migration**.** In contrast to *Drosophila* cells, in mammalian epithelial cells, myosin VI depletion does not affect the total or surface levels of E-cadherin, the cellular expression of catenins or their binding to E-cadherin and neither the total cellular levels of vinculin (Maddugoda, Crampton, Shewan, & Yap, 2007).

2. Regulation of actin filament dynamics at the leading edge of motile cells

Actin cytoskeleton is fundamental in migration since it supports several mechanical events such as membrane protrusion, contractility and anchorage. Myosin VI has been proposed to stabilize actin filaments and regulate actin dynamics during migration, since it has been reported to be involved in these processes in mammalian and *Drosophila* cells.

In *Drosophila* testis cells, myosin VI has been found to remain bound to F-actin in the front of growth cones maintaining actin cone organization as the cones move. The loss of myosin VI in *Drosophila* testis leads to a loss of actin filaments as well as actin regulatory proteins such as cortactin and Arp2/3 from the growth cone and consequently it leads to defects in sperm individualization. Therefore, myosin VI may protect the actin cone structure either by cross-linking actin filaments or by anchoring regulatory molecules (cortactin and Arp2/3) at the cone front that, in turn, regulate actin assembly and organization. (Isaji, Lenartowska, Noguchi, Frank, & Miller, 2011; Noguchi, Lenartowska, & Miller, 2006).

In MCF7 mammary epithelial cancer cells, myosin VI has been suggested to regulate perijunctional organization of F-actin, since myosin VI depletion leads to a looser organization of F-actin packing in the junctions, without any concomitant change in total cellular F-actin levels (Maddugoda et al., 2007).

3. Endocytosis and recycling of cell adhesion molecules into the leading edge

During cell migration extracellular matrix receptors such as integrins are selectively inserted into the leading edge of the cell to form adhesion complexes with the underlying substrate. Substrate adhesion coupled to a protrusive force at the leading edge is then believed to move the cell forward (Gupton & Waterman-Storer, 2006). The temporal and spatial organization of adhesion receptors at the leading edge are tightly controlled by cycles of receptor endocytosis and recycling. Thus, the inhibition of endosomal trafficking or recycling disrupts cell polarity and directed migration (Caswell & Norman, 2008). Myosin VI has been reported to play important roles in the endocytic and recycling pathways (Chibalina et al., 2007) and in addition, myosin VI and its interacting protein GIPC have been shown to be involved in the endocytosis of activated α5β1 integrin, thereby linking myosin VI directly to focal adhesion turnover (Valdembri et al., 2009).

4. Delivery of adhesion or signaling receptors from the Golgi complex to the leading edge

Directed migration is controlled by polarized signaling at the leading edge. That is, the spatial restriction of signaling receptors and pathways at the leading edge stabilizes selected lamellipodia and thereby maintains the orientation and direction of movement. This selective delivery of proteins to the leading edge of the cell can be accomplished by the transport of newly synthesized adhesion or signaling receptors through the anterograde secretion pathway from the trans-Golgi network into the lamellipodium (Chibalina et al., 2010).

Myosin VI has been shown to be involved in constitutive secretion of cargo from the Golgi complex to the plasma membrane together with its binding partner optineurin (Sahlender et al., 2005). Furthermore, Chibalina et al. have demonstrated that myosin VI and optineurin are required for the polarized delivery of epidermal growth factor receptor (EGFR) into the leading edge of a migrating cell, which is important for the generation of directionally persistent migration (Chibalina et al., 2010). Therefore, myosin VI could be required in cell migration due to its involvement in polarized delivery of proteins such as EGFR.

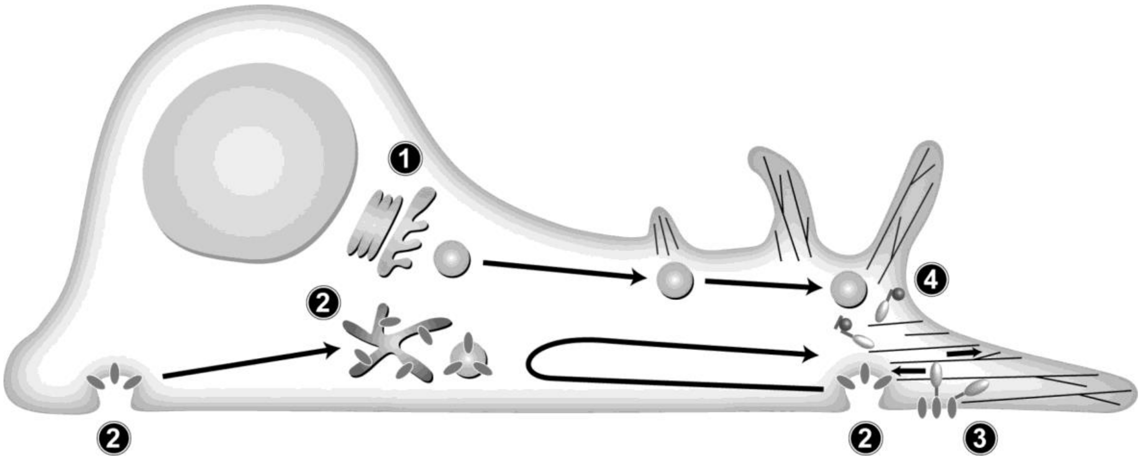

Figure 21: Possible roles of myosin VI during cell migration. 1) The localization of myosin VI around the Golgi complex and its function in the secretory pathway suggests that it might regulate the delivery of newly synthesized adhesion or signaling receptors from the *trans*-Golgi network into the leading edge. **2)** At the plasma membrane and in endosomes, myosin VI might participate in cell-adhesion receptor endocytosis and recycling. **3)** At the leading edge, myosin VI could provide a protrusion force by moving towards the minus end of actin filaments and, while binding to stationary cell-adhesion receptors, it could move the polymerizing actin filaments towards the membrane and thus enhance protrusion. **4)** Also at the front of the moving cell, myosin VI may recruit Arp2/3 or upstream signaling molecules such as a Rac-activating factor or Rac itself into the leading edge. Figure taken from Chibalina et al., 2009.

All these data suggest that myosin VI may play a key role in coordinating several aspects of the process of cell migration. However, further work is needed to establish the exact functions that myosin VI carries out in migration.

6.3.6. Myosin VI as an anchor

Several studies have proposed a tethering role for myosin VI in addition to its motor role. *In vitro* experiments showed that myosin VI molecules are able to remain tightly bound for minutes to actin filaments when a backward force is applied to them (Altman, Sweeney, & Spudich, 2004). Therefore, it is believed that myosin VI when acting as an anchor binds stably to actin filaments for long periods while tethers other molecules to these actin structures. So, myosin VI may likely contribute to the stabilization of specialized actin structures and to the maintenance of cellular components in particular locations.

One such example is the role of myosin VI in the maintenance of 'cochlear hair cell stereocilia'. Stereocilia are specialized actin-based structures with finger-like shape found at the apical part of cochlear hair cells. The actin bundles that form the core of the stereocilia are anchored in the dense actin meshwork, known as terminal web, which is located at the base of stereocilia. In these cells myosin VI is enriched at the terminal web region where it plays an essential role in organizing and maintaining the structural integrity of stereocilia by stabilizing membrane-cytoskeletal attachments at the base of the stereociliary bundles (Salles et al., 2014). In Snell's Waltzer mice and in mutant zebrafish, where myosin VI is absent, after birth the stereocilia of the hair cells become progressively more disorganized and irregular, and the membrane near the base of the stereocilia appears raised. At later stages stereocilia fuse together and finally, hair cells die triggering a complete degeneration of inner ear (neurosensory epithelium) (Seiler et al., 2004; Self et al., 1999).

It has been reported a similar tethering role of myosin VI in the enterocytes of the intestine. In these cells myosin VI is primarily localized in the sub-apical/terminal web region underlying the microvilli (T Hasson & Mooseker, 1994). Microvilli are apical actin structures similar to stereocilia that form the brush border of enterocytes. In this context, myosin VI is also required for proper tethering of the brush border membrane to the terminal web and thus, for the maintenance of overall microvilli ultrastructure (**Fig. 22**). When myosin VI is missing, the microvilli show defects such as, lifting of the plasma membrane off of the actin cytoskeleton in the inter-microvillar region, fusion of microvilli and disorganized morphology of the terminal web (Hegan, Giral, Levi, & Mooseker, 2012).

As explained in previous sections, myosin VI has also been demonstrated to have an anchoring activity in the maintenance of Golgi complex morphology (Sahlender et al., 2005; Warner et al., 2003); in epithelial junction maintenance by stabilizing cadherin/catenin complexes or other adhesion molecules such as vinculin (Geisbrecht & Montell, 2002; Maddugoda et al., 2007); and in maintaining actin cone organization during *Drosophila* spermatogenesis by tethering molecules that regulate actin assembly or organization (Isaji et al., 2011; Noguchi et al., 2006).

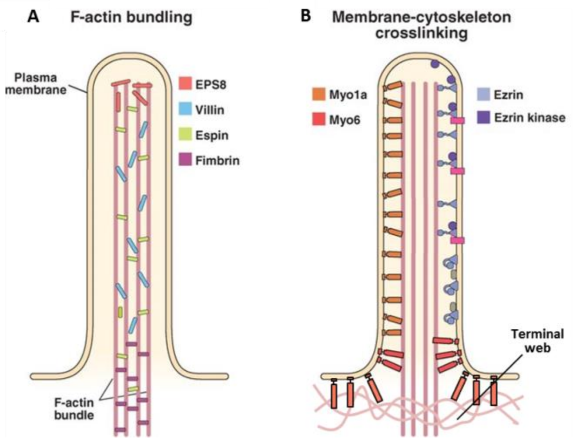

Figure 22: Organization of the structural proteins in the microvilli of the enterocytes. A) Bundling of actin filaments in the microvillar actin core is performed by villin, espin, fimbrin, and EPS8. **B)** Membrane-cytoskeleton cross-linking is mediated by myosin 1a, myosin 6 and the active form of ezrin. Note that myosin 6 is mainly found in the terminal web. Adapted from Crawley, Mooseker, & Tyska, 2014.

6.3.7. Nuclear role of myosin VI

Myosin VI has been demonstrated to be also present in the nucleus of cells where it interacts with RNA polymerase II (RNAPII) being able to modulate RNAPII-dependent transcription (Fili et al., 2017; Vreugde et al., 2006).

The myosin VI non-insert isoform is the isoform recruited to the nucleus (Fili et al., 2017). Seven potential **nuclear localization signal (NLS)** regions and one potential **nuclear export sequence (NES)** region have been identified in myosin VI structure (**Table 4**), which seem to be functional as the nuclear presence of myosin VI was affected by the inhibitors of nuclear import (ivermectin) and export (leptomycin B) (L. Majewski et al., 2018; Vreugde et al., 2006). Moreover, myosin VI can be translocated from the cytoplasm to the nucleus very rapidly upon cell stimulation (for instance, PC12 cells (rat pheochromocytoma derived cells) upon KCl stimulation) and, upon p53 stabilization and DNA damage in a p53-dependent manner (Jung, Liu, Zhou, & Chen, 2006; L. Majewski et al., 2018).

Table 4: Nuclear localization (NLS) and nuclear export (NES) signals predicted by bioinformatics tools within the myosin VI heavy chain.

Putative sites	Amino acid residues predicted by bioinformatics tools	Location within the myosin VI heavy chain
Nuclear localization signal (NLS)	PRKSKLA	Motor domain
	RRHK	IQ motif
	RKRR	Helical tail domain
	RRRK	Helical tail domain
	RKKR	Helical tail domain
	RRLKVYHAWKSKNKKRN	Globular tail domain
	PQSKKKG	Globular tail domain
Nuclear export sequence (NES)	LALRI	Helical tail domain

Information taken from Majewski et al., 2018.

Inside the nucleus myosin VI is recruited to RNAPII complex at intragenic and promoter regions of certain **transcriptionally active genes** (Vreugde et al., 2006). Myosin VI forms a bipolar interaction with the RNAPII complex, by coupling its motor domain to RNAPII-bound **nuclear actin** and its CBD to **DNA** and/or **binding partners**. It binds DNA through two adjacent loops in its CBD (**Fig. 15**) and the binding is regulated through intra-molecular backfolding. When myosin VI is backfolded upon itself (CBD and the N-terminus tail can form an interaction), DNA-binding sites appear to be occluded impeding the binding to DNA. **NDP52**, a known binding partner of myosin VI, is able to trigger a conformational change in myosin VI by binding it in the RRL-motif, leading to an unfolded state that permits the DNA binding (**Fig. 23**) (Fili et al., 2017; Zhu, Zeng, Huang, & Hao, 2004). Depletion of all three molecules, myosin VI, NDP52 and actin, separately, decreases transcription (steady-state mRNA levels) of RNAPII target genes *in vivo* and *in vitro* (Fili et al., 2017; Vreugde et al., 2006; Zhu et al., 2004).

Furthermore, myosin VI not only interacts with RNAPII complex, but also with certain nuclear receptors for specific gene targeting. It has been shown that myosin VI is able to modulate 'androgen or estrogen-regulated gene expression' by coupling to androgen and estrogen receptors (**Fig. 23**) (Fili et al., 2017; Loikkanen et al., 2009).

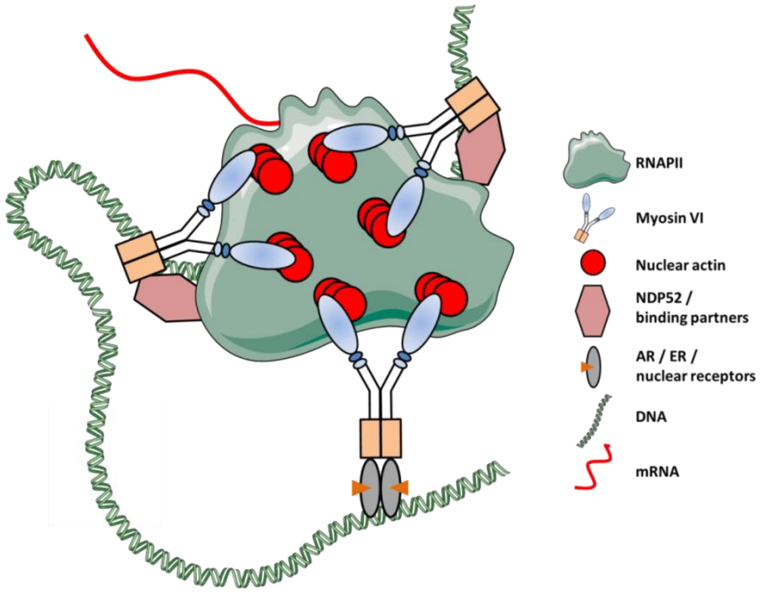

Figure 23: Working model of myosin VI in transcription elongation. Myosin VI is recruited to a specific location by nuclear receptors such as androgen (AR) or estrogen receptors (ER). Myosin VI gets unfolded by NDP52 (or probably also by other binding partners) which enables the binding to DNA by its CBD and the binding to RNA Polimerase II complex (RNAPII) through nuclear actin by its motor domain. Adapted from Fili et al., 2017.

Recently, myosin VI has been found to colocalize in the nucleus not only with transcriptionally active regions, but also with **PML bodies** (promyelocytic leukaemia bodies – structures involved in processes such as chromatin reconstruction and DNA repair) and **speckles** (protein structures involved in pre-mRNA processing) (L. Majewski et al., 2018). Furthermore, through mass spectrometry analysis, several potentially novel myosin VI partners that are involved in processes associated with gene expression, post-transcriptional events and intranuclear transport have been identified (**Table 5**). For instance, among them are three heterogeneous nuclear ribonucleoproteins (hnRNPU, hnRNPK and hnRNPM; involved in pre-mRNA metabolism and transport), histone H1d (involved in chromatin organization) and nucleolin (involved in nucleolar processes) (L. Majewski et al., 2018). Therefore, myosin VI might facilitate nuclear activities by transporting substrates and products into and out the nucleus; and might be involved in other functions such as RNA maturation and chromatin organization.

Table 5: List of potential myosin VI-binding partners with nuclear functions in PC12 cells identified by mass spectrometry.

Human gene name	Name
XRCC5	X-ray repair complementing defective repair in Chinese hamster cells 5
LRCH3	leucine-rich repeats and calponin homology (CH) domain-containing protein 3
G22P1	G22p1 – ATP-dependent DNA helicase activity
LRCH1	leucine-rich repeats and calponin homology (CH) domain-containing protein 1
DDX17	DEAD (Asp-Glu-Ala-Asp) box polypeptide 17
NCL	nucleolin
DDX3Y	hypothetical protein LOC364073
DDX3X	DEAD (Asp-Glu-Ala-Asp) box polypeptide 3, X-linked
HNRNPU	SP120 /heterogeneous nuclear ribonucleoprotein U
WRN	similar to Werner syndrome ATP-dependent helicase homolog
***PABP* family**	rCG31475
DDX5	DEAD (Asp-Glu-Ala-Asp) box polypeptide 5
HNRNPK	heterogeneous nuclear ribonucleoprotein K
HIST1H1D	histone (H1d)
RPA1	replication protein A1
HNRNPM	heterogeneous nuclear ribonucleoprotein M isoform b

Asp: Aspartic acid; Glu: Glutamic acid; Ala: Alanine. Information taken from Majewski et al., 2018.

6.4. Myosin VI and cancer

Myosin VI has already been involved in certain types of cancer. The first report linking myosin VI to cancer was carried out in **ovarian carcinoma**. Myosin VI protein was found to be absent or weakly expressed in normal ovary and benign ovarian cystadenomas. However, myosin VI was expressed in ovarian cancers at levels that strongly correlated with the aggressiveness of clinical behavior (tumor grade), being highly expressed in high-grade ovarian carcinomas. Using cell line models from ovarian carcinomas, it was shown that the inhibition of myosin VI expression impaired cell spreading and migration ability *in vitro*, but it did not alter cell proliferation rate. Moreover, *in vivo* dissemination of intraperitoneally injected ovarian carcinoma cells throughout the bowel of nude mice was substantially reduced when myosin VI expression was inhibited. Therefore, in this study, high myosin VI expression was suggested to be related with enhanced migration capability, although, the precise mechanism by which myosin VI promoted ovarian cancer cell migration was not defined (Yoshida et al., 2004).

Further studies in ovarian cancer revealed that myosin VI isoform 2 (without large insert and with small insert) was almost exclusively expressed in ovarian tumors compared to normal ovarian epithelium, in which other isoforms were also expressed. Furthermore, among the seven ovarian cancer cell lines examined for isoform expressions, OVCAR-5 was the only cell line expressing also other myosin VI isoforms, while the rest selectively expressed isoform 2. Moreover, as observed by Yoshida et al. (Yoshida et al., 2004), depletion of myosin VI in ovarian cancer cells severely impaired their ability to migrate, except for the case of OVCAR-5, in which migration efficiency was unaffected (Wollscheid et al., 2016). Hence, only ovarian cancer cells that selectively express myosin VI isoform 2 were deficient in cell migration upon myosin VI depletion. This suggested that cancer cells positively select isoform 2 because it confers them with a migratory advantage, and thus, it may promote tumor progression and metastasis.

However, using data from The Cancer Genome Atlas (TCGA) database, it was shown that the selective expression of 'myosin VI isoforms without the large insert' (such as, isoform 2) was highly frequent event in certain tumors (such as, head and neck squamous cell carcinoma and lung squamous cell carcinoma) if compared to their normal tissues, but not in other tumor types (Wollscheid et al., 2016). Therefore, the function of the 'isoforms without large insert' may be critical and positively selected only in specific types of cancers.

Myosin VI was also demonstrated to be involved in **prostate cancer**. Myosin VI was found to be overexpressed at mRNA and protein level in prostate cancer specimens compared to normal prostate epithelium, which showed negative or weak myosin VI staining in tissue microarrays (TMA). Notably, medium-grade prostate cancers exhibited the most consistent cancer-specific myosin VI protein overexpression, whereas prostate cancers associated with more aggressive histological features continued to overexpress myosin VI but to a lesser extent. Therefore, contrary to ovarian cancers, myosin VI expression did not correlate with prostate cancer aggressiveness. However, when compared with the normal tissue, myosin VI protein expression was statistically higher in premalignant lesions, suggesting that overexpression of myosin VI is an early event during prostate carcinogenesis (Dunn et al., 2006). As observed in ovarian cancer, the inhibition of myosin VI expression resulted in impaired cell migration, but did not affect the proliferation rate of prostate cancer cells (LNCaP) *in vitro*. In addition, reduction of myosin VI expression significantly decreased the number of soft agar colonies, associating myosin VI to anchorage-independent growth. Exceptionally, myosin VI knockdown also resulted in a nearly 10-fold increase of TXNIP expression, which is a known tumor suppressor, suggesting a role for myosin VI in maintaining the malignant phenotype of human prostate cancer cells (Dunn et al., 2006).

In an attempt to find an explanation to how myosin VI promotes migration in prostate cancer, subsequent studies found that myosin VI overexpression enhanced secretion of 'prostate-specific antigen' (PSA) and 'vascular endothelial growth factor' (VEGF) in LNCaP prostate cancer cells, two molecules related with tumor progression (Puri et al., 2010). PSA can increase cellular migration by promoting epithelial-mesenchymal cell transition and by cleaving extracellular matrix proteins; and VEGF can promote tumor growth by stimulating vascularization and tumor angiogenesis. Therefore, myosin VI overexpression was suggested to be linked to elevated protein secretion in prostate cancer. Notably, enhanced myosin VI expression did not show a major impact on clathrin-mediated endocytosis (Puri et al., 2010).

It is known that androgens are a prerequisite for the development of prostate cancer and that the action of androgens on gene expression is mediated via the androgen receptor (AR). Myosin VI positively correlated with the presence of androgen receptor in prostate cancer cell lines (Dunn et al., 2006), and it was showed that expression of AR decreased as a result of myosin VI knockdown (Loikkanen et al., 2009). Moreover, it was demonstrated that AR and myosin VI interact in the same transcription complex inside the nucleus and that myosin VI is able to modulate androgen-dependent gene expression, suggesting another mechanism by which increased myosin VI expression could promote prostate cancer progression (Loikkanen et al., 2009).

In **lymphoid leukemia cells** myosin VI was also reported to be fundamental for spontaneous cell migration *in vitro*. Myosin VI was found to be localized in membrane ruffles at the leading edge of motile cells, but its exact function remained poorly understood (Jbireal, Strell, Niggemann, Zänker, & Entschladen, 2010).

More recent researches involving **hepatocellular carcinoma** (Ma et al., 2015); **breast cancer** (H. Wang, Wang, Zhu, & Yang, 2015); **lung cancer** (Yu, Zhu, Chang, Wang, & Shen, 2015); **prostate cancer** (D. Wang et al., 2016); **gastric cancer** (Z. Wang, Ying, Wu, Wang, & Li, 2016); **oral squamous carcinoma** (X. Zhang, Huang, Hu, & Liu, 2016); and **colon cancer** (You et al., 2016) also suggest a role of myosin VI in tumor progression. In all these types of cancer, myosin VI expression appeared to be significantly increased compared to the surrounding normal tissues. Moreover, although the data shown in these articles is quite **weak**, they all agree that the downregulation of myosin VI leads to a significant reduction in cell proliferation and colony forming capacity as well as a slight arrest in cell cycle progression and an increase in the number of apoptotic cells. However, the exact mechanisms by which myosin VI could be inducing tumor progression have not been yet described.

6.5. Myosin VI and human hereditary diseases

Hearing loss is a complex and heterogeneous disease presenting various phenotypes as a result of both genetic and environmental factors. Approximately 70% of cases affected by **hereditary hearing loss (HHL)** can be classified as non-syndromic hearing loss (NSHL) (with the absence of abnormalities in other organs), whereas the remaining 30% are classified as syndromic. The vast majority of NSHL cases (80%) are transmitted as **autosomal recessive traits** (ARNSHL **-** Autosomal recessive sensorineural hearing loss; 64 known genes). The remaining 20% show an **autosomal dominant** pattern of inheritance (ADNSHL - Autosomal dominant sensorineural hearing loss; 36 known genes) while a small proportion is X-linked (4 known genes) or mitochondrial (8 known mutations) (Alkowari et al., 2017).

Mutations in myosin VI have been associated with autosomal dominant (DFNA22 deafness locus on Chr. 6q13) and recessive (DFNB37 deafness locus on Chr. 6q13) hearing loss. So far, 20 different mutations have been described in several European and Asiatic families: 16 mutations in DFNA22 and 4 mutations in DFNB37 (**Table 6**).

Table 6: Myosin VI pathogenic mutations in autosomal sensorineural hearing loss.

Locus	Exon	Domain	Nucleotide change	Amino acid change	Hereditary form	Reference
DFNB37	2	Motor	c.36-37insT		Recessive	(Ahmed et al., 2003)
DFNB37	3	Motor	c.178G>C	p.E60Q	Recessive	(Alkowari et al., 2017)
DFNA22	8	Motor	c.613C>T	p.R205X	Dominant	(Choi et al., 2013)
DFNA22	8	Motor	c.614G>A	p.R205Q	Dominant	(Kwon et al., 2014; M Miyagawa, Nishio, Kumakawa, & Usami, 2015)
DFNB37	8	Motor	c.647A>T	p.E216V	Recessive	(Ahmed et al., 2003)
DFNA22	9	Motor	c.737A>G	p.H246R	Dominant	(Mohiddin et al., 2004)
DFNA22	9	Motor	c.862_865delACAA	p.D288DfsX17	Dominant	(Shearer et al., 2010)
DFNA22	10	Motor	c.884_893delGCAAAGTCC	p.R295LfsX13	Dominant	(Vona et al., 2014)
DFNA22	12	Motor	c.1325C>T	p.C442Y	Dominant	(Melchionda et al., 2001)
DFNA22	19	Motor	c.1975C>T	p.R659X	Dominant	(Maiko Miyagawa, Naito, Nishio, Kamatani, & Usami, 2013; M Miyagawa et al., 2015)
DFNA22		Intron 23	c.IVS23+2321T>G		Dominant	(Hilgert et al., 2008)
DFNA22	24	IQ motif	c.2473C>T	p.R825X	Dominant	(Kwon et al., 2014)
DFNA22	25	After IQ motif	c.2545C>T	p.R849X	Dominant	(Sanggaard et al., 2008)
DFNA22	26	Coiled-coil	c.2752insA	p.Q918fsX941	Dominant	(Kwon et al., 2014)
DFNA22	27	Coiled-coil	c.2944C>T	p.Q982X	Dominant	(T. Yang, Wei, Chai, Li, & Wu, 2013)
DFNA22	28	Coiled-coil	c.2971C>T	p.R991X	Dominant	(Kwon et al., 2014)
DFNA22	32	Globular	c.3361A>T	p.K1121X	Dominant	(M Miyagawa et al., 2015)
DFNB37	34	Globular	c.3496C>T	p.R1166X	Recessive/Dominant	(Ahmed et al., 2003; M Miyagawa et al., 2015)
DFNA22	34	Globular	c.3610C>T	p.R1204W	Dominant	(Oonk et al., 2013)
DFNA22	35	Globular	c.3667G>A	p.D1223N	Dominant	(Shearer et al., 2010)

Hearing loss caused by myosin VI was found to be progressive. Depending on the mutation the hearing loss could be from mild to profound, and the onset age of the disease varied considerably among the patients, being generally postlingual, although prelingual cases were also reported (M Miyagawa et al., 2015). Most of the patients with a myosin VI mutation were found to have non-syndromic hearing loss. However, there were patients that presented, in addition to deafness, **vestibular dysfunction** (Ahmed et al., 2003), **facial dysmorphology** (Ahmed et al., 2003), **retinitis pigmentosa** (Ahmed et al., 2003) or **hypertrophic cardiomyopathy** (Mohiddin et al., 2004), suggesting that mutations in myosin VI might also cause these diseases.

However, it is intriguing that mutations in myosin VI, which is widely expressed in several non-auditory tissues, apparently do not trigger severe clinical consequences in other organs or tissues.

CHAPTER 2

AIMS OF THE STUDY

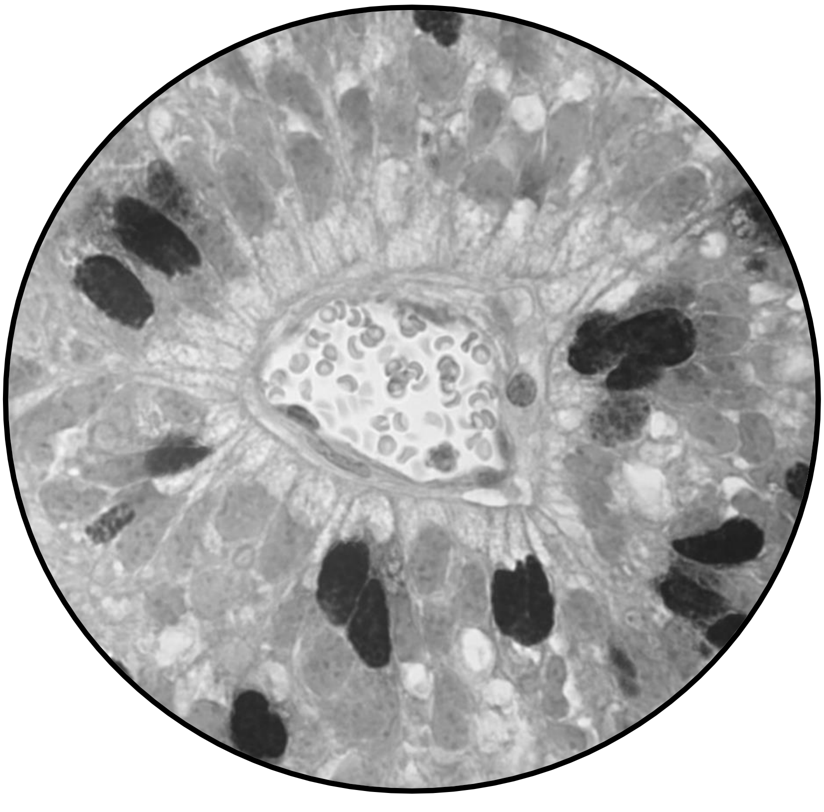

AIMS OF THE STUDY

Previously in our lab, myosin IA was found to be a regulator of differentiation/polarization of colon cancer cells and its loss was demonstrated to promote intestinal tumorigenesis. Similar to myosin IA, myosin VI is highly expressed in the apical microvilli of enterocytes and the loss of either of these myosins has been shown to result in important structural and compositional defects in intestinal microvilli (Hegan et al., 2012; Mazzolini et al., 2012), suggesting that myosin VI could also play a role in the progression of colorectal cancer. Moreover, myosin VI has been reported to be involved in the progression of ovarian and prostate cancers (Dunn et al., 2006; Yoshida et al., 2004). However, no studies have been performed investigating the functional role of the loss of MYO6 in colorectal tumorigenesis.

Therefore, the specific aims of this study were:

1. To evaluate the association between primary tumor MYO6 expression and survival or clinicopathological features of colorectal cancer patients.

2. To investigate the role of MYO6 in the a) differentiation, b) proliferation and c) metastatic potential of colon cancer cells using isogenic MYO6 knockdown cell line systems.

3. To investigate the effects of MYO6 inactivation on the intestinal tumorigenesis using *Myo6* knock-out mice.

CHAPTER 3

MATERIALS AND METHODS

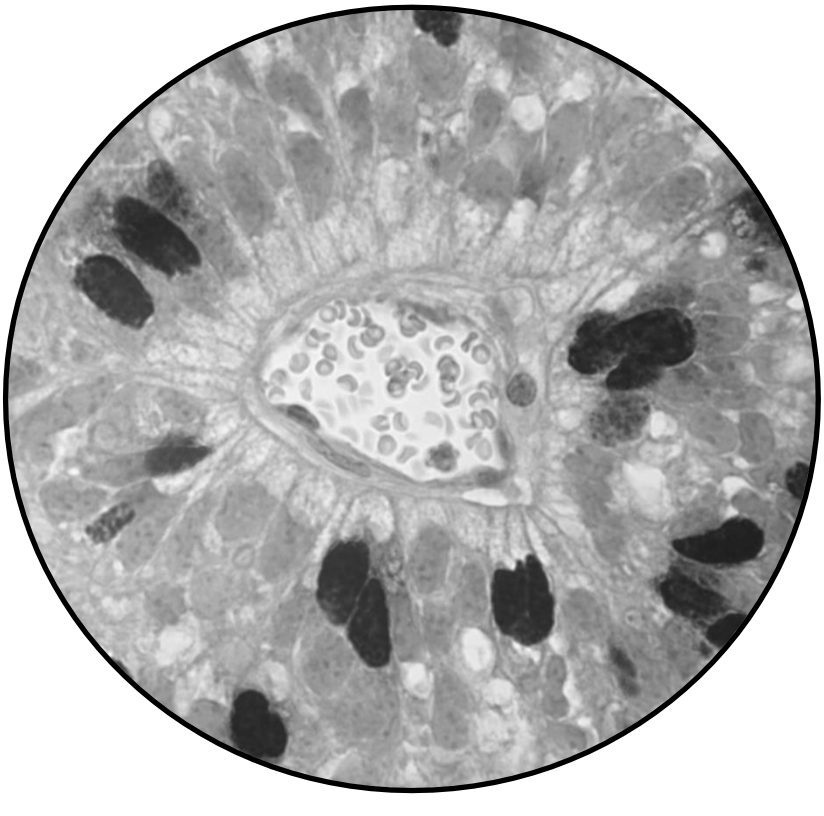

MATERIALS AND METHODS

Clinical samples – 91 normal colon tissue samples, 164 primary colorectal tumors and 16 lymph node metastases from Dukes' C colorectal cancer (CRC) patients were collected at collaborating medical institutions in Spain and Finland, together with their respective clinical data. Informed consent for genetic analysis of the tumor/tissue sample was obtained from each patient, according to protocols approved by the 'Human Investigations and Ethical Committee' in the appropriate institution. All samples were formalin-fixed, paraffin-embedded and used for immunohistochemical assessment of MYO6 expression in a **tissue microarray (TMA)**. Among the 164 Dukes' C colorectal cancer patients from which the primary tumors were collected, 77 patients had surgery as the only form of treatment and 82 patients received additionally 5-FU-based adjuvant chemotherapy. The mean follow up of patients was 9.2 years (range from 6.8 to 11.2 years), thus allowing the analysis of long-term survival.

TMA was assembled as described previously (Arango et al., 2005). Briefly, areas containing a high proportion of tumor cells were selected after histological examination of hematoxylin-eosin stained sections of primary tumor and metastasis samples. Triplicate 0.6 mm cores were arrayed in a paraffin block using a Beecher Instruments tissue arrayer (Silver Spring, MD). Four µm sections of the tissue microarray were mounted on slides coated with (3-aminopropyl)triethoxysilane (Sigma-Aldrich). For immunohistochemical analysis, the commercial NovoLink polymer detection system (Novocastra Laboratories) was used according to the instructions of the manufacturer. For MYO6 detection, anti-MYO6 mouse monoclonal antibody was used at 1:400 dilution (SC-58808 – Santa Cruz Biotechnology) (**Table 10**).

Tissue microarray (TMA) analysis: MYO6 expression was evaluated in samples of normal colon tissues, primary tumors and lymph node metastases, all of them in triplicate, with the investigator blinded to the sample identity and the clinical data. MYO6 staining intensity levels were scored using a semiquantitative scale ranging from 0 (absence of MYO6 immunostaining) to 3 (high immunostaining). **1)** The average MYO6 immunostaining in normal colon tissues, primary tumors and lymph node metastases is shown. **2)** Based on MYO6 staining value of the primary tumor, patients were dichotomized as high or low MYO6. This dichotomization depended on the 'cutoff value' calculated by the 'Cutoff finder' program, which is based on the statistical engine R (http://molpath.charite.de/cutoff/) (Budczies, Klauschen, & Denkert, 2013). This program identifies the cutoff staining level that maximizes the survival differences between patients with high and low MYO6 tumor expression. Survival differences (Kaplan-Meier plots) as a function of tumor MYO6 protein expression are shown.

In addition, clinical data and 'primary tumor *MYO6* mRNA expression' from 115 Stage III CRC patients were downloaded from 'The Cancer Genome Atlas' (TCGA) database ("TCGA Colon and Rectal Cancer (COADREAD) - Xena Functional Genomics Explorer," 2016). *MYO6* mRNA expression from the tumors was obtained through **RNA sequencing** (Illumina RNA-Seq).

TCGA RNA sequencing data analysis: Patients were dichotomized as high or low *MYO6* basing on the tumor *MYO6* mRNA expression. This dichotomization depended on the cutoff value formerly calculated by the 'Cutoff finder' program (R package) (http://molpath.charite.de/cutoff/) (Budczies et al., 2013), which finds the cutoff expression value that results in the best survival differences between patients with high and low tumor *MYO6* mRNA expression. Survival differences (Kaplan-Meier plots) as a function of tumor *MYO6* mRNA expression are shown.

Colorectal cancer cells' expression data – *MYO6* mRNA expression analyzed by **RNA sequencing** (Illumina HiSeq2000) for 51 CRC cell lines was taken from Mouradov et al., 2014. MYO6 protein expression assessed by **Shotgun mass spectrometry proteomics** for 48 CRC cell lines (data not published) was a kind gift from Dr. John M. Mariadason (Olivia Newton-John Cancer Research Institute, Melbourne, Australia).

Cell lines – CACO2, SW403, LS513 and LS174T-W4 human colon cancer cell lines and HEK293T human embryonic kidney cell line were purchased from American Type Culture Collection (ATCC) repository. Features of these cell lines are described in **Tables 7** and **8**. Cells were cultured in Dubelcco's Modified Eagle's medium (DMEM – Life Technologies) supplemented with 10% fetal bovine serum (FBS – Sigma-Aldrich) and 1x antibiotic-antimycotic (10,000 U/mL of penicillin, 10,000 μg/mL of streptomycin and 25 μg/mL of amphotericin B; Life Technologies); and maintained in a humidified incubator at 37ºC and 5% CO_2.

Table 7: General information of cell lines used in the study.

Cell line	Age	Gender	Ethnicity	Primary Site	Histology / disease	Tumor source	Cell type
CACO2	72	Male	Caucasian	Colon	Colorectal Adenocarcinoma	Primary	Epithelial adherent
SW403	51	Female	Caucasian	Colon	Colorectal Adenocarcinoma	Dukes' C Grade III Primary	Epithelial adherent
LS513	63	Male	Caucasian	Cecum	Colorectal Carcinoma	Dukes' C Primary	Epithelial adherent
LS174T-W4	58	Female	Caucasian	Colon	Colorectal Adenocarcinoma	Dukes' B Primary	Epithelial adherent
HEK293T	Fetus	Female	Unknown	Embryonic kidney	-	-	Epithelial adherent

Information taken from "ATCC," 2017.

Table 8: Genetic features of colon cancer cell lines used in the study.

Cell line	MSI/MSS[a]	MLH1 methylation[b]	CIMP status[b]	BRAF[b]	KRAS[b]	TP53[b]	APC[b]	TGFBR2[b]	PIK3CA[b]	PTEN[b]	SMAD4[b]	TCF7L2[b]	CTNNB1[b]
CACO2	MSS	Neg	CIMP-	WT	WT	Mut	Mut	WT	WT	WT	Mut	WT	Mut
SW403	MSS	Neg	CIMP-	WT	Mut	Mut	Mut	WT	WT	WT	WT	WT	WT
LS513	MSS	Neg	CIMP+	WT	Mut	WT	WT	WT	WT	WT	WT	WT	WT
LS174T-W4	MSI	Pos	CIMP-	WT	Mut	WT	WT	Mut	Mut	WT	WT	Mut	Mut

MSS: Microsatellite stable; MSI: Microsatellite instable; CIMP: CpG island methylator phenotype; Neg: negative; Pos: Positive; WT: wild-type; Mut: mutant. a) Mazzolini et al., 2011 and b) Mouradov et al., 2014.

Lentiviral vectors – pINDUCER10 vector was used to generate colon cancer cell lines with inducible MYO6 downregulation (Meerbrey et al., 2011). pINDUCER10 plasmid is a Tet-on system, in which the rtTA (reverse tetracycline-controlled transactivator) protein binds the operator TRE (tetracycline response element) only if bound by tetracyclines. Thus, the introduction of doxycycline to the system initiates the transcription of the cassette, in this case the ‘turbo red fluorescent protein’ (tRFP) and the short-hairpin RNA (shRNA) (**Fig. 24**). In all *in vitro* experiments the concentration of doxycycline (Doxycycline hyclate – Sigma-Aldrich) used to activate the expression of the shRNA was 1 µg/mL.

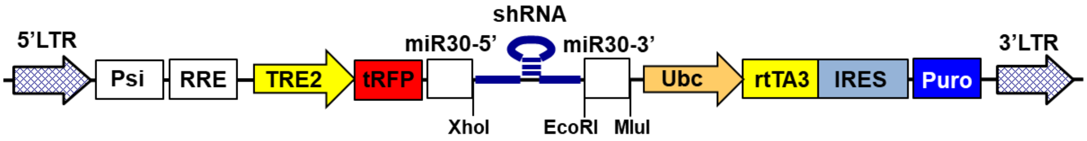

Figure 24: pINDUCER10-shRNA plasmid structure. LTR: Long terminal repeat; Psi: Retroviral Psi packaging element; RRE: Rev Response Element; TRE2: Tetracycline response element; tRFP: Turbo red fluorescent protein; Ubc: Ubiquitin C promoter; rtTA3: Reverse tetracycline-controlled transactivator; IRES: internal ribosome entry site; Puro: Puromycin resistance gene. XhoI, EcoRI and MluI: targets for the indicated restriction enzymes. miR30: backbone of the miR30 microRNA.

Four different shRNAs against *MYO6*, which were already designed by the ‘RNAi codex’ platform (Olson, 2006; “RNAi Codex,” 2009), were used: MYO6_HP_901211, MYO6_HP_850067, MYO6_HP_57574 and MYO6_HP_775475, hereafter named sh52, sh53, sh54 and sh55, respectively (**Table 9**). ‘RNAi codex’ platform designs the shRNAs within the miR-30 miRNA context. As control shRNA (non-targeting shRNA), a sequence against firefly luciferase was selected and designed within the miR-30 miRNA backbone by using ‘RNAi oligo retriever’ web server (http://cancan.cshl.edu/RNAi_central/RNAi.cgi?type=shRNA) (“RNAi Central shRNA retriever,” 2009), hereafter named shNT (**Table 9**). Finally, all the shRNAs were cloned into pINDUCER10 following the protocol described before (Paddison et al., 2004).

Table 9: shRNA sequences. sh52, sh53, sh54 and sh55 against MYO6. shNT against firefly luciferase.

Plasmid	RNAi codex	Sequence 5’-3’
sh52	MYO6_HP_901211	TGCTGTTGACAGTGAGCG**ACGGAACAAATGGCCAAAGAAA**TAGTGAAGCCACAGATGTA**TTTCTTTGGCCATTTGTTCCGG**TGCCTACTGCCTCGGA
sh53	MYO6_HP_850067	TGCTGTTGACAGTGAGCG**CCCATACTTTGACATACCTAAA**TAGTGAAGCCACAGATGTA**TTTAGGTATGTCAAAGTATGGA**TGCCTACTGCCTCGGA
sh54	MYO6_HP_57574	TGCTGTTGACAGTGAGCG**CGGTGTTAATGAAGTGCATTAT**TAGTGAAGCCACAGATGTA**ATAATGCACTTCATTAACACCT**TGCCTACTGCCTCGGA
sh55	MYO6_HP_775475	TGCTGTTGACAGTGAGCG**CCGAGCTGAAGCCTGCATTAAA**TAGTGAAGCCACAGATGTA**TTTAATGCAGGCTTCAGCTCGA**TGCCTACTGCCTCGGA
shNT		TGCTGTTGACAGTGAGCG**AGCTCCCGCTGAATTGGAATCC**TAGTGAAGCCACAGATGTA**GGATTCCAATTCAGCGGGAGCC**TGCCTACTGCCTCGGA

In bolt sense and antisense sequences.

All constructions were confirmed by **DNA sequencing** under BigDye^{TM} Cycling conditions on an Applied Biosystems 3730x1 DNA analyzer (Macrogen Inc). For that, 5 μL of plasmid (≃200 ng) with 5 μL of 5 μM sequencing primer (pINDUCER10_Revers; 5’- CGCGTGTTTAAACGCATTAG -3’) were sent to Macrogen.

7xTcf-eGFP//SV40-mCherry (7TGC) vector (Addgene; #24304) (Fuerer & Nusse, 2010) was used to infect organoid cells from mouse small intestinal tumors. This vector contains an SV40-mCherry cassette which allows the discrimination between infected and uninfected cells, by expressing constitutively a red fluorescence protein (mCherry). Upstream from this cassette, it also contains a green fluorescence protein (eGFP) gene under the control of a minimal promoter containing ‘Tcf-binding sites’ (7xTcf-eGFP reporter cassette). Thus, in the presence of Wnt signal, cells will express GFP, in addition to mCherry (**Fig. 25**).

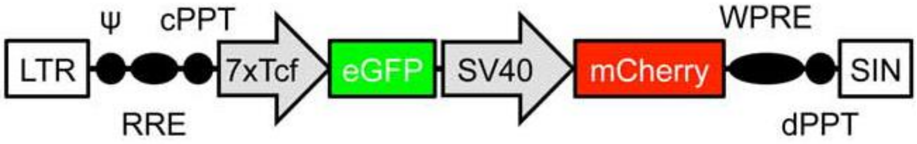

Figure 25: 7xTcf-eGFP//SV40-mCherry (7TGC) plasmid structure. LTR: Long Terminal Repeat; ψ: packaging signal; RRE: Rev Response Element; cPPT: central PolyPurine Tract; WPRE: Woodchuck hepatitis Post-transcriptional Regulatory Element; dPPT: distal PolyPurine Tract; SIN: Self Inactivated (LTR).

Lentiviral infection of colon cancer cells – CACO2, SW403, LS513 and LS174T-W4 colon cancer cell lines were stably infected with lentivirus containing pINDUCER10-shRNAs against MYO6 and control shRNA, and subsequently selected with puromycin. Production of lentiviral supernatants was carried out as follows: HEK293T packaging cells were plated in a 10 cm plate (4x10^{6} cells) to have them ≃80% confluent on the following day. Twenty-four hours after seeding, HEK293T cells were transfected with 2.5 μg of packaging plasmid (psPAX2 – Addgene; #12260), 3.4 μg of envelope plasmid (pMD.G2 – Addgene; #12259) and 9.8 μg of lentiviral plasmid (pINDUCER10-shMYO6 (sh52, sh53, sh54 and sh55)/shNT) using polyethylenimine (PEI – Polysciences) (4 μg PEI : 1 μg total DNA) in DMEM medium. The following day (≃16 h after transfection), the medium was replaced with 7 mL of 5% FBS-DMEM medium containing 5 mM sodium butyrate (Acros organics) and the cells were allowed to produce viral particles. From this point on, biosecurity level-2 conditions were applied. Twenty-four hours after medium renewal, the medium containing the viral particles was collected and kept at 4ºC. Cells were re-fed as described above and kept in culture for 24 additional hours. The second batch of medium containing viral particles was collected and mixed with the stored first batch, and then filtered with 0.45 μm PVDF filters (Millipore) and kept at -80ºC until infection.

The day previous to the infection, cells of interest were seeded in 6 well-plates in order to reach ≃40% confluence the following day. Cells were infected with the lentiviral particles overnight (3 mL of the virus-containing medium mixed with 1 mL of fresh DMEM medium) together with 5 μg/mL hexadimethrine bromide (Polybrene – Sigma-Aldrich). Forty-eight hours later, medium containing puromycin (Sigma-Aldrich; CACO2: 18 μg/mL; SW403: 4 μg/mL; LS513: 2 μg/mL; LS174T-W4: 3 μg/mL) was applied to the cells and renewed every 3 days until selection was finished.

Cell protein extraction and quantification – ***Extraction:*** After being washed with ice-cold PBS (Phosphate buffered saline solution – Fisher Scientific), cells were scraped directly from the plate using rubber scrapers and harvested with cold PBS in eppendorfs. Then, cells were centrifuged at 4ºC-2000 rpm for 5 min, resuspended in radioimmunoprecipitation (RIPA) lysis buffer (0.1% SDS (Sigma-Aldrich), 1% NP40 (Panreac), 0.5% Na-deoxycholate (Sigma-Aldrich) and 50 mM Tris-HCl (pH 7.5; Fisher Scientific) in water) supplemented with protease inhibitors (cOmplete™ ULTRA Tablets, Mini, EDTA-free, EASYpack Protease Inhibitor Cocktail – Sigma-Aldrich) and kept for 30 min on ice. Next, samples were sonicated for 10 seconds 3 times at 20-50 kHz on ice and spun-down for 20 min at 4ºC-14.000 rpm. Supernatants, which contained the proteins, were transferred to new precooled eppendorfs and stored at -80ºC. ***Quantification:*** Protein concentration was quantified using 'Bicinchoninic acid (BCA) Protein Assay Kit' (Thermo Scientific). The protocol was as follows: Two μL of protein sample diluted in distilled water (final volume 25 μL) were mixed with 200 μL of BCA solution in a 96 well-plate. A series of protein standards (bovine serum albumin (BSA) diluted in distilled water) was run alongside with the protein lysates for the establishment of a standard curve. The plate was dark-incubated at 37ºC for 30 min. The absorbance was read at 562 nm on a plate reader (Epoch – BioTek Instruments). Protein concentrations were determined using the BSA standard curve method.

Western blotting (WB) – ***Gel electrophoresis:*** Thirty μg of protein were mixed with loading dye (Laemlli buffer 4X: 250 mM Tris pH 6.8 (Sigma-Aldrich), 4.2% SDS (Sigma-Aldrich), 20% Glycerol (Sigma-Aldrich), 0.008% bromophenol blue (Sigma-Aldrich), 10% 2-mercaptoethanol (Sigma-Aldrich)) and denatured at 95ºC for 5 min. Then, proteins were separated by SDS-PAGE (Sodium dodecyl sulfate - polyacrylamide gel electrophoresis) electrophoresis in polyacrylamide gels (4% acrylamide stacking gel; 10% acrylamide running gel; Acrylamide – Fisher Scientific). The electrophoresis chamber was filled with running buffer (0.25 M Tris, 1.92

M Glycine (Fisher Scientific) and 34.6 mM SDS (Sigma-Aldrich)) and the current was set to 120 V, allowing the proteins to run until the loading dye went out from the gel. ***Protein transfer to filters:*** Proteins were electrophoretically transferred from the gel to a polyvinylidene fluoride (PVDF; Amersham – GE Healthcare Life Sciences) membrane. For that purpose, the gel and the membrane were stacked as a ‘sandwich’ together with filters and sponges in the following order: sponge, Whatman filter (VWR), polyacrylamide gel, PVDF membrane, Whatman filter and sponge. The transfer was carried out in a tank containing ice-cold transfer buffer (0.21 M Tris and 1.92 M Glycine). The proteins were allowed to transfer for 90-120 min at 110 V and 4ºC. ***Blocking and blotting:*** The membrane with the transferred proteins was blocked with 5% skim milk in PBS-0.1% Tween (Sigma-Aldrich) for 1 h at room temperature in order to prevent unspecific binding of the antibodies. Next, the membrane was cut and incubated overnight at 4ºC with primary antibodies (Anti-MYO6 1:500; Anti-tubulin 1:10,000; **Table 10**). The following day, unbounded primary antibodies were removed by washing the membranes 3 times for 10 min with PBS-0.1% Tween under agitation. Membranes were then incubated with secondary antibodies conjugated with horseradish peroxidase (Anti-mouse 1:5,000; Anti-rabbit 1:5,000; **Table 10**) for 1 h at room temperature and washed again with PBS-0.1% Tween 3 times for 10 min. ***Detection:*** Finally, proteins were detected using ‘Enhanced chemiluminescence system’ kit (ECL – GE Healthcare) and blue-light sensitive autoradiography films (AGFA (CP-BU)). Summarizing, the membrane was incubated with an equal volume of detection reagent A and reagent B (which contain a light-emitting non-radioactive substrate for horseradish peroxidase) for 1 min. Then, AGFA films were exposed to the membrane to detect the chemiluminescent signal and after an automated film development (Curix 60 – AGFA healthcare) the bands were visualized. Quantification of band intensity was done using ImageJ program (NIH-National Institutes of Health).

Table 10: Antibodies used in the study.

Antibody	Source	Reference	Host	Application (dilution)
MYO6	Santa Cruz	SC-50461 H-215	Rabbit, polyclonal	WB (1:500)
MYO6	Santa Cruz	SC-58808 MUD-19	Mouse, monoclonal	IHC (1:400)
β-Tubulin	Sigma-Aldrich	T4026	Mouse, monoclonal	WB (1:10,000)
BrdU	Developmental Studies	G3G4	Mouse, monoclonal	IHC (1:15)
Caspase 3	R&D Systems	AF835	Rabbit, polyclonal	IHC (1:500)
Swine Polyclonal Anti-Rabbit Immunoglobulins	Dako	P0217	Swine, polyclonal	WB (1:5,000)
Goat Polyclonal Anti-Mouse Immunoglobulins	Dako	P0447	Goat, polyclonal	WB (1:5,000)
β-catenin	BD Biosciences	610154	Mouse, monoclonal	IF (1:100)
E-cadherin	BD Biosciences	610181	Mouse, monoclonal	IF (1:500)
Goat Polyclonal Alexa Fluor® 488 conjugated Anti-mouse immunoglobulins	Thermo Fisher	R37120	Goat, polyclonal	IF (1:500)

WB: Western Blot; IHC: Immunohistochemistry. IF: Immunofluorescence. Antibodies for WB are diluted in '5% skim milk - PBS-0.1% Tween'. Antibodies for IHC and IF are diluted in PBS.

FACS analysis – pINDUCER10-shMYO6 (sh53, sh54, sh55)/shNT transduced CACO2, SW403 and LS513 cells were treated with doxycycline (1 µg/mL) for 48 h and analyzed by FACS (Fluorescence-activated cell sorting) using BD FACSCalibur™ flow cytometer, in order to determine the percentage of infected (tRFP-positive) cells within the populations. Percentage of tRFP-positive cells was determined using the 'FCS Express 3' program (De Novo Software). Parental cell lines (no-infected original colon cancer cell lines) were used as gating controls to establish the threshold of tRFP signal.

Enzymatic activity assays – Specific enzymatic activity assays were used to assess the capability of differentiation of CACO2, SW403 and LS513 derivative cells. Cells were treated with or without 1 µg/mL of doxycycline for 72 h prior to the seeding to induce MYO6 downregulation.

CACO2 cells ($5.5x10^5$; sh53, sh54, sh55 and shNT) were seeded with or without doxycycline (1 µg/mL) onto 6 well-plates and allowed to spontaneously differentiate by confluence over time. Medium with or without doxycycline (1 µg/mL) was renewed every 2-3 days. Cells were harvested directly from the plates with rubber scrapers at days -1, 0, 2, 5, 7, 14 and 21, being '-1' the day previous to 100% confluence and 0 the first day of 100% confluence. Cell pellets were kept at -80ºC.

A different approach was followed to induce differentiation in SW403 and LS513 cell lines since they do not differentiate under confluent culture conditions. Cells (SW403: $1.25x10^6$; LS513: $4x10^6$ (sh53, sh54, sh55 and shNT)) were seeded with or without doxycycline (1 μg/mL) onto 6 well-plates. The following day, cells were treated with 0 mM or 5 mM sodium butyrate, a potent inducer of differentiation in colorectal cancer cells (NaBut – Fisher Scientific), for 72 h and finally harvested by gentle scraping and kept at -80ºC.

Proteins from cells were extracted using mannitol buffer pH 7.4 (50 mM D-Mannitol (Sigma-Aldrich), 2 mM Tris (Sigma-Aldrich), 0.1% Triton x-100 (Sigma-Aldrich)) supplemented with protease inhibitors (cOmplete™ ULTRA Tablets, Mini, EDTA-free, EASYpack Protease Inhibitor Cocktail – Sigma-Aldrich). Alkaline phosphatase (AP), sucrase-isomaltase (SI) and dipeptidyl peptidase-4 (DPP-IV) activities were assessed as follows. All these experiments were carried out three independent times in triplicate.

Alkaline phosphatase (AP) activity assay: Twenty-five μg of protein in 50 μL of mannitol buffer were mixed with 200 μL of p-Nitrophenyl phosphate (NPP – Fisher Scientific) substrate solution in a 96 well-plate and incubated in the dark at 37ºC. After 1 h of incubation, absorbance was measured in a microplate reader (Epoch – BioTek Instruments) at 405 nm.

Sucrase-isomaltase (SI) activity assay: Twenty-five μg of protein in 12.5 μL of mannitol buffer were incubated for 5 min at 37ºC. Then, 12.5 μL of substrate solution (0.056 M maltose (Sigma-Aldrich) in 0.1 M sodium maleate buffer pH 6.0 (Sigma-Aldrich)) were added and incubated for 1 h at 37ºC. The reaction was stopped by heating the samples at 100ºC for 2 min. Next, 250 μL of TGO solution (4% glucose oxidase (Sigma-Aldrich), 0.2 % o-dianisidine (Sigma-Aldrich), 0.2% Triton x-100 (Sigma-Aldrich), 0.1% peroxidase (Sigma-Aldrich) in a final volume of 50 mL Tris 0.5 M pH 7.0) were added and the plate was left incubating for 1 h at 37ºC. After incubation the absorbance was measured at 420 nm in a microplate reader.

Dipeptidyl peptidase-IV (DPP-IV) activity assay: Twenty-five μg of protein in 90 μL of mannitol buffer were mixed with 10 μL of 1.4 M glycine-NaOH pH 8.7 (Fisher Scientific) and 100 μL of substrate (3 mM glycyl-L-proline-p-nitroanilide (Santa Cruz Biotechnology) in 2% Triton x-100 (Sigma-Aldrich)), and incubated at 37ºC for 30 min or until the most differentiated samples turned yellowish. The reaction was stopped by adding 800 μL of 32% trichloroacetic acid (TCA – VWR) and spinning down at 4000 rpm for 10 min at room temperature. Fifty μL of the supernatant were mixed with 50 μL of cold 0.2% sodium nitrite ($NaNO_2$; Sigma-Aldrich) in 96 well-plates and then incubated at 4ºC for 10 min. Next, 50 μL of 0.5% ammonium sulfamate (Sigma-Aldrich) were added. Two min later, 100 μL of 0.05% NED (N-(1-Naphthyl)ethylenediamine dihydrochloride; Sigma-Aldrich) were added and the plate was incubated in the dark at 37ºC. After 15 min of incubation, absorbance was measured at 492 nm in a microplate reader.

Immunofluorescence in CACO2 cell line – CACO2-sh53 cells were seeded in gelatin-coated glass coverslips and cultured with and without 1 µg/mL doxycycline for 21 days to let them become polarized. Next, cells were fixed in 4% paraformaldehyde (PFA – Sigma-Aldrich) for 10 min, permeabilized with 0.5% Triton X-100 (Sigma-Aldrich) for 5 min and incubated with blocking solution (1% BSA – Fisher Scientific) for 30 min. Cells were then incubated with primary antibodies (E-cadherin 1:500; β-catenin 1:100; **Table 10**) overnight at 4ºC. Finally, cells were incubated with secondary antibody (Anti-mouse Alexa Fluor® 488 conjugate 1:500; **Table 10**) for 1 hour and stained with DAPI (90 µM; Sigma-Aldrich) for 5 min. Images were taken with a confocal fluorescence microscope (FV1000 Olympus) at 100X magnification.

Polarization assay – LS174T-W4 colon cancer cells were stably infected with lentivirus containing pINDUCER10-shRNAs against MYO6 (sh53 and sh54) and control shRNA (shNT), and subsequently selected with puromycin (Sigma-Aldrich; 3 µg/mL) as explained in 'Lentiviral infection of colon cancer cells' section. LS174T-W4 cells have been previously modified to overexpress the pseudokinase STRAD in an inducible manner and LKB1 constitutively (Baas et al., 2004). LKB1 is a serine/threonine kinase that when is activated is able to promote polarization of colon cancer cells in the absence of cell-cell and cell-extracellular-matrix contacts. Therefore, upon doxycycline treatment, STRAD activates LKB1, triggering a complete polarization of LS174T-W4 cells which can be visualized by the formation of an apical brush border. LS174T-W4-shNT, sh53 and sh54 cells were treated with 1 µg/mL doxycycline for 72 h previous to the seeding to induce MYO6 downregulation. Next, cells were trypsinized and seeded on gelatin-coated glass coverslips, and incubated with 1 µg/mL doxycycline for 48 h to induce polarization (cells lose the cell polarity acquired during the previous 72 h of doxycycline treatment when they are trypsinized). Then, cells were fixed in 4% paraformaldehyde (PFA; Sigma-Aldrich) for 10 min, permeabilized with 0.1% Triton X-100 (Sigma-Aldrich) for 5 min and stained with ALEXA-488 labeled phalloidin (0.1 µM; Cytoskeleton) for 30 min and with DAPI (90 µM; Sigma-Aldrich) for 1 min in the dark. Coverslips were mounted with ProLong® Gold antifade reagent (Life technologies). Number of polarized LS174T-W4 derivative cells was scored using a fluorescent microscope (Olympus BX61). At least a total of 500 cells (polarized and unpolarized) were counted blinded from the sample identity in three independent experiments carried out in triplicate. The percentage of polarized cells (polarized *versus* total number of cells) is shown.

***In vitro* proliferation assays – Cell counting:** Seventy-two hours previous to the seeding, cells were treated or not with 1 µg/mL of doxycycline to induce MYO6 downregulation. Cells (CACO2: 3x10^4; SW403: 6x10^4; LS513: 8x10^4 (sh53, sh54, sh55 and shNT)) were seeded in 24 well-plates with medium containing or not doxycycline (1 µg/mL) (3 replicates per cell line, condition (± Dox) and time point) and allowed to adhere overnight. For cell counting, cells were trypsinized and stained with trypan blue (Serva). Viable cells were counted using a hemocytometer (Fuchs-Rosenthal – Marienfeld) at days 1, 2, 3, 4 and 5. The number of cells was plotted *versus* time and used to assess the proliferation of each cell line. The average of three independent experiments is shown. **Sulforhodamine B (SRB) staining:** SRB dye stains protein contents of cells and the absorbance measurement at 590 nm can be used for cell density calculation (Skehan et al., 1990). Seventy-two hours previous to the seeding, cells were treated or not with 1 μg/mL of doxycycline to induce MYO6 downregulation. Cells (CACO2: 2.5 x10^3; SW403: 1.5x10^4; LS513: 3x10^3 (sh53, sh54, sh55 and shNT)) were seeded in 96 well-plates with medium containing or not doxycycline (1 μg/mL) (8 replicates per cell line and condition (± Dox) in each plate). Seven plates were seeded in order to evaluate proliferation for 7 consecutive days. Fifty μL of fresh medium with or without doxycycline was added at day 4 to the plates evaluated at days 5, 6 and 7. All plates were fixed with 50 μL of 50% trichloroacetic acid (w/v) (TCA – Fisher Scientific) for 1 h at room temperature (RT), washed with tap water and air dried. Then, plates were stained with 50 μL of 0.4% (w/v) sulforhodamine B (SRB – Sigma-Aldrich) in 1% acetic acid (VWR) for 30 min at RT, washed with 1% acetic acid to remove excess of SRB and air dried. Eventually, SRB precipitates were solubilized with 200 μL of 10 mM Tris buffer (pH 10) (Fisher Scientific) and the absorbance was measured in a microplate reader (Epoch – BioTek Instruments) at 590 nm. Absorbance was plotted *versus* time and used to assess the proliferation of each cell line. The average of three independent experiments is shown.

Clonogenicity assay – Seventy-two hours previous to the seeding, cells were treated or not with 1 μg/mL of doxycycline to induce MYO6 downregulation. Cells (CACO2: 5x10^2; SW403: 2.5x10^4; LS513: 5x10^2 (sh53, sh54, sh55 and shNT)) were seeded into 6 well-plates with medium containing or not doxycycline (1 μg/mL) and let them form individual colonies for 15, 22 and 12 days, respectively. Medium, with or without doxycycline (1 μg/mL), was renewed every 4 days. Once the colonies were visible, they were fixed with methanol-acetic acid solution (3:1 v/v) (Methanol – Fisher scientific; Acetic acid – VWR) for 5 min and stained with 1% crystal violet - 25% methanol (Crystal violet – Fisher Scientific) for 10 min. Dye excess was removed by extensive wash of plates with tap water. The plates were scanned and the number of macroscopically visible colonies was scored using ImageJ program (NIH-National Institutes of Health). Three independent experiments were carried out in triplicate.

Soft Agar colony formation assay (anchorage independent growth assay) – Seventy-two hours previous to the seeding, cells were treated or not with 1 μg/mL of doxycycline to induce MYO6 downregulation. Cells (LS513: 3.5×10^3 (sh53, sh54, sh55 and shNT)) were resuspended in 20% FBS-DMEM medium containing 0.3% agar (Agar noble – BD Biosciences) with or without doxycycline (1 μg/mL) and then plated onto 6 well-plates on top of 20% FBS-DMEM medium containing 0.6% agar, also with or without doxycycline. Cultures were maintained at 37ºC in a 5% CO_2 incubator for 15 days. Once a week, 0.5 mL of 20% FBS-DMEM medium with or without doxycycline (1 μg/mL) was added to the cells. At the end of the experiment the colonies were stained overnight with nitroblue tetrazolium chloride (1 mg/mL; Sigma-Aldrich) and the number of macroscopically visible colonies was scored using 'NICE colony counter' program (NIST – National Institute of Standards and Technology). Three independent experiments were carried out in triplicate.

Wound-healing assay – LS513 cells (sh53, sh54, sh55 and shNT) were treated with or without doxycycline (1 μg/mL) for 72 h to induce MYO6 downregulation. Cells (6x10^6) were seeded with and without doxycycline (1 μg/mL), as corresponding, onto 6 well-plates in order to achieve about 90% confluence the following day. The cell monolayer was scratched with a sterile micropipette tip and the wound region was allowed to heal by cell migration. The area that remained clear of cells after 7, 24, 31, 48 and 72 h was quantified with 'TScratch program' (ETH Zurich University) and compared with the area of the wound at time zero. Percentage of migrated area *versus* time is shown. The average of three independent experiments in triplicate is shown.

Transwell migration assay (Boyden chamber method) – The ability of cells to migrate through filters stimulated by a FBS concentration gradient was determined using a 24 well-plate Boyden chamber (Beckton Dickinson; 8 μm pore size). Cells were treated with or without 1 μg/mL of doxycycline for 72 h prior to the seeding to induce MYO6 downregulation. Cells (CACO2: 1x10^5; SW403: 1x10^5 (sh53, sh54, sh55 and shNT)) were seeded in 200 μL of DMEM containing 1% FBS with or without doxycycline (1 μg/mL) in the upper compartment of the transwell. The lower compartment was filled with 600 μL of DMEM-10% FBS, acting as a chemoattractant. CACO2 and SW403 were allowed to migrate for 3 and 4 days, respectively. At the end of the experiment, cells from the transwell were fixed with cold 100% methanol (Fisher Scientific) for 5 min and stained with 1% crystal violet - 25% methanol (Fisher Scientific) for 10 min. Excess of crystal violet was washed out by submerging the transwell in water. Cells that did not migrate and therefore did not pass through the membrane were removed with cotton swabs. The number of migrating cells was scored by direct counting using an inverted microscope (Eclipse TE2000-S – Nikon) at 20X magnification. Three independent experiments were carried out in triplicate.

Matrigel invasion assay – The ability of cells to invade through matrigel-coated filters was determined using a 24 well-plate Boyden chamber (Beckton Dickinson; 8 μm pore size). Cells were treated with or without 1 μg/mL of doxycycline for 72 h prior to the seeding to induce MYO6 downregulation. CACO2 cells (1x10^5; sh53, sh54 and shNT) were resuspended in 100 μL of DMEM-1% FBS with 10% of matrigel (1 mg/mL; Corning) and seeded onto the membrane of Boyden Chambers. The matrigel was allowed to solidify at 37ºC for 20 min. Then the upper compartment of the transwell was filled with 100 μL of DMEM-1% FBS and the lower compartment with 600 μL of DMEM-10% FBS, generating an FBS based chemoattraction. Media from both compartments contained or not 1 μg/mL of doxycycline, as corresponding. Then, cells were let to invade for 4 days. The invading cells were fixed with cold 100% methanol (Fisher Scientific) for 5 min and stained with 1% crystal violet – 25% methanol (Crystal violet – Fisher Scientific) for 10 min. Excess of crystal violet was washed out by submerging the transwell in water. The cells that did not invade and therefore did not pass through the membrane were removed with cotton swabs. The total number of invading cells was scored using an inverted microscope (Eclipse TE2000-S – Nikon) at 20X magnification. Three independent experiments were carried out in triplicate.

Xenograft and metastasis models – All animal experiments were carried out under protocols approved by the Institutional Ethical Animal Care and Use Committee of Vall d'Hebron Research Institute and the appropriate governmental agency. Mice were housed under pathogen-free conditions in a temperature-controlled room on a 12/12 hour light/dark schedule with food and water *ad libitum*.

For ***subcutaneous xenograft models*** 8-10 NOD/SCID mice (Charles River; 6-8 weeks old) were used per experiment. Sh53 and shNT cells were treated for 72 h with 1 μg/mL of doxycycline previous to the injection, in order to downregulate MYO6 expression. Cells (CACO2: $6x10^6$; SW403: $3x10^6$; LS513: $2x10^6$) were resuspended in 100 μL PBS (Fisher Scientific) and subcutaneously injected in the rear flanks of mice using 25-gauge needles (BD Microlance). Animals were injected with both sh53 and shNT cells, in the left and in the right flanks, respectively, in order to minimize inter-animal variations. Doxycycline (1 mg/mL; Vibracin – Pfizer) was administered with the drinking water (it also contained sucrose in order to reduce the bitter taste produced by doxycycline, which may lead to reduced drinking; 25 mg/mL; Fisher Scientific) of all animals and it was newly prepared every 3-4 days. The tumor size was measured twice per week for a total of 18 weeks in the case of CACO2 xenografts, 4 weeks for SW403 xenografts and 5 weeks for LS513 xenografts. Tumor volume was calculated based on tumor dimensions, measured using calipers, and expressed in cubic millimeters according to the formula: $V = 0.5a \times b^2$, where a and b are the long and short diameters of the tumor, respectively. The average tumor size for each cell line *versus* time is represented once the tumors achieved a consistently detectable size (CACO2: 100 mm^3; SW403: 30 mm^3; LS513: 30 mm^3). For CACO2 cells a bigger tumor size was considered as consistently detectable, because tumors at the beginning were rather flat and size measurements took longer to be reproducible over time. SW403 and LS513 formed quite defined subcutaneous masses and reproducible size measurements were more easily obtained over time. Kaplan-Meier curves showing the 'xenograft-tumor free survival' for each cell line are also shown (the event was considered when the tumors reached the threshold of 'detectable size' determined above). At the end of the experiment, animals were injected with bromodeoxyuridine (BrdU – Sigma-Aldrich) and two hours later euthanized. Then the tumors were excised and measured. For immunohistological analysis, xenograft tumor samples were formalin-fixed (10% neutral buffered formalin – DiaPath), and paraffin-embedded (Klinipath).

For ***lung metastasis model*** 16 NOD/SCID mice were used (Charles River; 6-8 weeks old). Animals were divided into two groups: 'doxycycline +' group and 'doxycycline -' group. LS513-sh53 cells ($2x10^6$) were resuspended in 100 μL PBS and intravenously injected in each animal through the tail vein using a 30-gauge needle (BD Microlance). For the animals of the 'doxycycline +' group, cells were treated with 1 μg/mL of doxycycline for 72 h previous to the injection; and doxycycline was administered with the drinking water (1 mg/mL; Vibracin – Pfizer) and newly prepared every 3-4 days, as described for the xenograft experiments. Animals from the 'doxycycline -' group were given drinking water containing sucrose (25 mg/mL; Fisher Scientific; it reduces the bitter taste) and lactose (1 mg/mL; Sigma-Aldrich; excipient of the doxycycline pills). Mice were monitored twice a week until they showed signs of advanced metastasis-related morbidity (hunched posture, poor hair coat, weight loss, respiratory distress at rest) (7 weeks). Mice were euthanized and the lungs were formalinperfused and excised, separated into lobes and formalin-fixed. Finally, formalin-fixed lungs were paraffin-embedded, sectioned and stained with hematoxylin and eosin (H&E; Hematoxylin – Quimica clínica aplicada S.A; Eosin – Millipore). Images from lung sections were taken and the metastatic area was quantified using ImageJ program (NIH-National Institutes of Health). The average number and area of lung metastatic lesions for each cell line is shown.

For ***liver metastasis model*** 13 NOD/SCID mice were used (Charles River; 10 weeks old; 7 males and 6 females, equitably distributed into the groups) and divided into 'doxycycline +' and 'doxycycline -' groups. Cells for animals of the 'doxycycline +' group were treated with 1 μg/mL of doxycycline for 72 h previous to the injection. SW403-sh53 cells ($2x10^6$) were resuspended in 150 μL PBS and directly injected in the spleen of the mouse following the procedure described in Soares et al., 2014. Briefly, animals were anesthetized with isuflorane (Aerrane – Baxter) and a left subcostal incision in line with the left ear, through the skin and through the peritoneum was made. Spleen was exposed and cut from the middle after placing two ligating clips (Horizon – Teleflex) in the center of it. The upper pole of the spleen was put back into the peritoneum. Cells were then slowly injected into the exposed hemispleen with a 30-gauge needle (BD Microlance). After 1 min to let the cells exit the spleen towards the liver, splenic blood vessels were occluded using two Horizon clips and the exposed hemispleen was cut above them and removed. Finally, peritoneum was closed with a 6-0 running stitch (B Braun – Optilene), and the skin with 4-0 running stitch (B Braun – Novosyn). Animals were administered 0.1 mg/kg buprenorphine (Buprecare – Divasa-Farmavic) subcutaneously to alleviate post-surgical pain. For animals from the 'doxycycline +' group, doxycycline was administered with the drinking water (1 mg/mL; Vibracin – Pfizer) during all the course of the experiment and it was newly prepared every 3-4 days, as described for the xenograft experiments. Animals from the 'doxycycline -' group were given drinking water containing sucrose (25 mg/mL; Fisher Scientific; it reduces bitter taste) and lactose (1 mg/mL; Sigma-Aldrich; excipient of the doxycycline pills). Mice were monitored twice a week. After 10 weeks of experiment mice were euthanized and the liver was excised and formalin-fixed. Presence of liver metastases was assessed macroscopically under a stereomicroscope (OLYMPUS SZH stereo-zoom microscope, magnification 7.5X). Finally, formalin-fixed livers were paraffin-embedded, sectioned and stained with hematoxylin and eosin (H&E; Hematoxylin – Quimica clínica aplicada S.A; Eosin – Millipore). Images from liver sections were taken and the metastatic area was quantified using ImageJ program (NIH-National Institutes of Health). Metastatic incidence (presence/absence of metastatic lesions) and the average liver metastatic area per animal group are shown.

Histology and immunohistochemistry in mouse samples – Intestines and subcutaneously grown xenograft tumors, once excised from the animals, were fixed overnight with 10% neutral buffered formalin (DiaPath) and then dehydrated by serial immersions of 1 h in 50%, 70%, 96% and 100% ethanol (Comercial Bellés). Excess of ethanol was removed by incubation in xylene (Comercial Bellés) three times for 1 h at room temperature and then tumors were immersed in 65ºC paraffin (Klinipath) overnight. Tissues were then included in paraffin blocks. Tumor sections (3 μm) were cut and placed on poly-L-Lysine coated microscope slides and incubated at 60ºC for 1 h. Then, sections were dewaxed by immersion in xylene (2 x 5 min) and hydrated by serial immersions in 100% ethanol (5 min), 96% ethanol (5 min), 70% ethanol (5 min), 50% ethanol (5 min) and distilled water.

For **immunohistochemistry** (IHC) of bromodeoxyuridine (BrdU), caspase 3 and MYO6, the NovoLink polymer detection system (Novocastra Laboratories) was used according to the instructions of the manufacturer. Briefly, first, antigen retrieval was done by heating samples at 180ºC for 4 min in 10 mM citrate buffer pH 6.0 (2 mM citric acid, 8 mM sodium citrate) in a pressure cooker. After endogenous peroxidase blocking, samples were incubated with their corresponding primary antibody overnight at 4ºC (**Table 10**). Then, incubation with the second antibody (Novolik polymer) for 30 min at room temperature was done and the peroxidase activity of this second antibody was revealed by adding DAB solution (3, 3 -diaminobenzidine) to the samples. Finally, slides were counterstained with Harry's hematoxylin (Quimica clínica aplicada S.A), dehydrated with serial immersions in 50%, 70%, 96% and 100% ethanol and xylene; and mounted with DPX mounting medium (Panreac Química).

BrdU-positive cell counting: BrdU staining was performed to assess proliferation in tumors grown as subcutaneous xenografts. Animals were intraperitoneally injected with 100 mg/Kg bromodeoxyuridine (BrdU; Sigma-Aldrich) 2 hours before being euthanized. BrdU is a synthetic nucleoside analogous to thymidine that can be incorporated into the newly synthesized DNA of replicating cells during S phase (Lehner et al., 2011). Therefore, anti-BrdU immunohistochemistry was used to determine the number of cells in S-phase of cell cycle during these 2 hours. Images from BrdU-stained xenograft tumor samples were taken (40x magnification) and the number of BrdU-positive cells per field was counted using ImageJ program (NIH-National Institutes of Health). Three images per tumor sample, in five different animals per group were counted. The average percentage of BrdU-positive cells per tumor group is shown.

Caspase 3-positive cell counting: Caspase 3 staining was performed to analyze apoptosis in tumors grown as subcutaneous xenografts. Caspase 3 is a protease associated with the initiation of the death cascade and therefore is an important marker of the apoptotic signaling pathway (Porter & Jänicke, 1999). Images from caspase 3-stained xenograft tumor samples were taken (40x magnification) and the number of caspase 3-positive cells per field was counted using ImageJ program (NIH-National Institutes of Health). Three images per tumor sample, in five different animals per group were counted. The average percentage of caspase 3-positive cells per tumor group is shown.

Mice DNA extraction and genotyping – *Myo6*$^{sv/sv}$ mice can be distinguished from their wild-type or heterozygous littermates from the first week of age due to their abnormal behavior, but still all the mice were subjected to genotyping by PCR. ***Extraction:*** Mice tissue samples were obtained from ears. Seventy-five μL of base solution (25 mM NaOH, 0.2 mM EDTA, pH 12) were added to samples and heated at 95ºC for 30 min. After cooling the samples to room temperature or below, 75 μL of neutralization solution (40 mM Tris-HCl, pH 5) were added. Samples were centrifuged at 2500 rpm and stored at 4ºC. ***Genotyping by PCR:*** **1) *Myo6* gene genotyping –** *Myo6* genomic DNA was amplified with primers that flank the deletion in the *sv* allele (*Myo6* mutant allele). *Myo6*$^{+/+}$ mice displayed a genomic fragment of 190 bp, *Myo6*$^{sv/sv}$ mice displayed a 400 bp fragment, and DNA from *Myo6* heterozygous mice generated both fragments. Primers were as follows: primer '*Myo6 mice WT-Reverse*' is 5'-CTGAACTTTCTTCCAGCGACT-3', primer '*Myo6 mice-Forward*' is 5'-TTGGGATGTGAAATCCATGT-3' and primer '*Myo6 mice mut-Reverse*' is 5'-AAGCTCAGGCAGGAATCTGA-3'. The PCR reaction mixture contained 200 ng genomic DNA, 1x PCR buffer, 2 mM $MgCl_2$, 0.5 mM dNTPs, 1 μM '*Myo6 mice WT-Reverse*' and '*Myo6 mice mut-Reverse*' primers, 2 μM '*Myo6 mice-Forward*' primer and 0.0025 U/μL Taq-polymerase (Bio-Taq – Ecogen). PCR was performed as follows: 2 min of denaturation at 94°C; followed by 10 cycles of 30 s denaturation at 94°C, 30 s annealing at 65°C and 1 min extension at 68°C; followed by 28 cycles of 30 s denaturation at 94°C, 30 s annealing at 60°C and 1 min extension at 72°C; and finally 2 additional minutes at 72°C. **2)** ***Apc*** **gene genotyping –** *Apc* genomic DNA was amplified with primers that flank the deletion in the *Apc*$^{\mathrm{Min}}$ allele. *Apc*$^{+/+}$ mice displayed a genomic fragment of 600 bp and *Apc*$^{\mathrm{Min}/+}$ mice displayed a 340 bp fragment in addition to the 600 bp fragment. Primers were as follows: primer '*Apc-Forward*' is 5'-TTCCACTTTGGCATAAGGC-3', primer '*Apc-Reverse WT*' is 5'-GCCATCCCTTCACGTTAG-3' and primer '*Apc-Reverse mut*' is 5'-TTCTGAGAAAGACAGAAGTTA-3'. The PCR reaction mixture contained 200 ng genomic DNA, 1x PCR buffer, 2 mM $MgCl_2$, 0.5 mM dNTPs, 0.6 μM 'A*pc-Forward*' and '*Apc-Reverse WT*' primers, 1.2 μM '*Apc-Reverse mut*' primer and 0.0025 U/μL Taq-polymerase (Bio-Taq – Ecogen). PCR was performed as follows: 3 min of denaturation at 94°C; followed by 35 cycles of 30 s denaturation at 94°C, 1 min annealing at 55°C and 1 min extension at 72°C; and finally 2 additional minutes at 72°C.

Tumorigenesis studies using *Myo6* knock-out mouse – Mice were housed in a temperature-controlled room on a 12/12 hour light/dark schedule with food and water *ad libitum*. All studies were performed with the approval of the Institutional Ethical Animal Care and Use Committee of the Vall d'Hebron Research Institute.

C57BL/6J x STOCK *Tyr*$^{c\text{-}ch}$ *Bmp5*^{se} +/+ *Myo6*^{sv}/J strain mice (Stock Nº: 000578) (also called Snell's Waltzer mice) were purchased from The Jackson Laboratory (Bar Harbor, Maine, USA). This strain is the final result of a mix of different genetic backgrounds in which B10.HA(33NX), SEC/1 and C57BL/6J strains are involved. Mice contain an intragenic deletion of 1.1 Kb in *Myo6* gene (*sv* recessive mutation; chromosome 9). *Myo6* mRNA is expressed at very low levels in *sv* homozygous (*Myo6*$^{sv/sv}$) mice. Sequence analysis of *Myo6* transcripts identified a 130 bp deletion corresponding to nucleotides 2456-2585. The deletion results in a frame shift which introduces a stop codon at the beginning of the MYO6 neck protein domain. No MYO6 protein is detected in any tissue of *Myo6*$^{sv/sv}$ mice (Avraham et al., 1995).

The **C57BL/6J-Apc$^{\mathrm{Min}}$/J** strain was also obtained from The Jackson Laboratory (Stock Nº: 002020). Mice carry the *Apc*^{Min} heterozygous mutation in the tumor-suppressor gene *Apc* (Adenomatous polyposis coli; Chromosome 18). The mutation, T2549A, converts Leu850 into a stop codon (Su et al., 1992). The *Apc*$^{\mathrm{Min}}$ mutation in a C57BL/6J background causes the development of multiple adenomas and tumors in the intestine which in turn, cause anemia (Moser, Pitot, & Dove, 1990).

Female *Myo6*$^{sv/+}$*;Apc*$^{+/+}$ mice of the strain 'B6 x STOCK Tyr$^{\mathrm{c\text{-}ch}}$ Bmp5$^{\mathrm{se}}$ +/+ Myo6$^{\mathrm{sv}}$/J' (mixed background) were crossed with male *Myo6*$^{+/+}$*;Apc*$^{\mathrm{Min}/+}$ mice of the strain 'C57BL/6J-Apc$^{\mathrm{Min}}$/J' to obtain *Myo6*$^{sv/+}$;*Apc*$^{Min/+}$ males and *Myo6*$^{sv/+}$;*Apc*$^{+/+}$ females that were subsequently crossed to obtain *Myo6*$^{sv/sv}$;*Apc*$^{Min/+}$, *Myo6*$^{+/+}$;*Apc*$^{Min/+}$, *Myo6*$^{sv/sv}$;*Apc*$^{+/+}$ *and Myo6*$^{+/+}$;*Apc*$^{+/+}$ offspring, all of them with the same contribution of 'mixed' and C57BL/6J genetic background (**Fig. 26**).

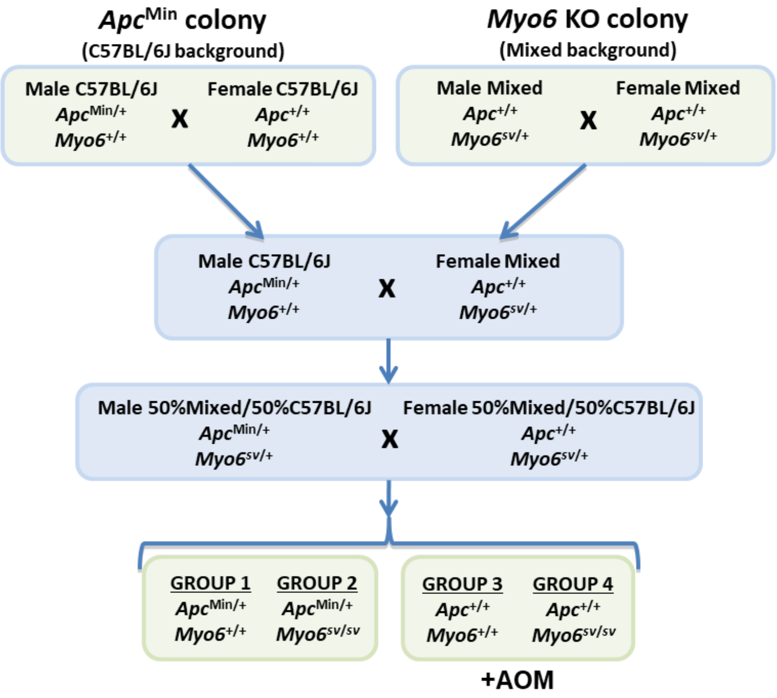
ApcMin colony
(C57BL/6J background)
Myo6 KO colony
(Mixed background)
Male C57BL/6J
ApcMin/+
Myo6+/+
X
Female C57BL/6J
Apc+/+
Myo6+/+
Male Mixed
Apc+/+
Myo6sv/+
X
Female Mixed
Apc+/+
Myo6sv/+
Male C57BL/6J
ApcMin/+
Myo6+/+
X
Female Mixed
Apc+/+
Myo6sv/+
Male 50%Mixed/50%C57BL/6J
ApcMin/+
Myo6sv/+
X
Female 50%Mixed/50%C57BL/6J
Apc+/+
Myo6sv/+
GROUP 1
ApcMin/+
Myo6+/+
GROUP 2
ApcMin/+
Myo6sv/sv
GROUP 3
Apc+/+
Myo6+/+
GROUP 4
Apc+/+
Myo6sv/sv
+AOM

Figure 26: Schedule of mice crosses. Mixed background refers to the genetic background obtained from the mix of B10.HA(33NX), SEC/1 and C57BL/6J strains. KO: Knock-out. AOM: azoxymethane.

In order to study the effects of the loss of MYO6 on the intestinal tumorigenesis, *Myo6*$^{sv/sv}$;*Apc*$^{Min/+}$ and *Myo6*$^{+/+}$;*Apc*$^{Min/+}$ mice were used, in which the initiation of tumorigenesis is established by mutated *Apc* allels. As an alternative method to initiate tumorigenesis, ten-week old *Myo6*$^{sv/sv}$;*Apc*$^{+/+}$ *and Myo6*$^{+/+}$;*Apc*$^{+/+}$ mice were intraperitoneally injected with the intestine-specific carcinogen azoxymethane (10 mg/Kg; AOM – Sigma-Aldrich) weekly for 12 weeks and euthanized 9 weeks after the last AOM injection.

Survival assay: *Myo6*$^{sv/sv}$;*Apc*$^{Min/+}$ and *Myo6*$^{+/+}$;*Apc*$^{Min/+}$ mice (11 per group) were let to live until they looked sick (endpoint criteria: weight loss, abnormal posture, decline in the activity and whitish legs). Animals were euthanized and their age (survival days/lifespan) was annotated. The survival of both groups is shown in a Kaplan-Meier plot.

Tumor number, size and localization: **1)** 110 day-old *Myo6*$^{sv/sv}$;*Apc*$^{Min/+}$ and *Myo6*$^{+/+}$;*Apc*$^{Min/+}$ mice (5 animals per group) were euthanized. The small and large intestines were dissected, opened longitudinally and the contents carefully removed. The intestines were fixed overnight with 10% neutral buffered formalin (DiaPath). Then, number, size and localization of intestinal tumors were scored under a stereomicroscope (OLYMPUS SZH stereo-zoom microscope, magnification 7.5X). **2)** AOM treated animals (*Myo6*$^{sv/sv}$;*Apc*$^{+/+}$ *and Myo6*$^{+/+}$;*Apc*$^{+/+}$) at the end of the experiment (31 week-old) were also euthanized and the number, size and localization of intestinal tumors were also assessed.

Culture of organoids derived from mouse intestinal tumors – Cells from small intestinal tumors from female *Apc*$^{\text{Min/+}}$ mice, which were wild-type or knock-out for *Myo6* gene were used to culture organoids. Briefly, animals (older than 5 months) were euthanized and their small intestines dissected in order to cut areas with tumors. From each animal, between 2 and 25 tumors were dissected out, pooled together and incubated with quelation buffer (2 mM EDTA (Omnipur), 5.6 mM sodium phosphate dibasic (Sigma-Aldrich), 8mM potassium phosphate monobasic (Sigma-Aldrich), 96.2 mM sodium choride (Sigma-Aldrich), 43.4 mM sucrose (Millipore), 54.9 mM D-sorbitol (Fisher Scientific), 0.5 mM DL-dithiothreitol (Fluka) in water) for 1 h on ice. Next, tumors were cut into small pieces and incubated with digestion solution (2.5% fetal bovine serum (Sigma-Aldrich), 100 U/mL penicillin (Life Technologies), 100 µg/mL streptomycin (Life Technologies), 0.25 µg/mL amphotericin B (Life Technologies), 2U/mL type I collagenase (Fisher Scientific) 0.062 U/mL type II dispase (Sigma-Aldrich) in DMEM-F12 medium (Life Technologies)) for 3 h at 37ºC. Big tumor pieces were allowed to decant and supernatant was filtered through a 100 µm pore-size filter (Sysmex). Finally cells were centrifuged, resuspended in IntestiCult medium (STEMCELL Technologies) containing 50% matrigel (Corning) and seeded onto plates following the instructions of the manufacturer (STEMCELL Technologies). In brief, 80 µL of cell-matrigel mixture were seeded per well onto 24 well-plates and allowed to solidify for 15 min. 500 µL of IntestiCult medium were then added into wells. Once the cells formed organoids, DMEM-F12-20%FBS medium was used to culture the organoids instead of IntestiCult medium (*Apc* mutated organoids are able to survive in a medium without WNT and R-spondin factors) (Miyoshi & Stappenbeck, 2013; Toshiro Sato et al., 2011). For the experiments described, tumor organoids from three *Myo6* wild-type animals were pooled together and compared to the phenotype of pooled tumor organoids from three *Myo6* knock-out mice.

Wnt signaling detection assay – Organoid tumor cells that were wild-type or knock-out for *Myo6* gene (*Myo6*$^{-/-}$;*Apc*$^{\text{Min/-}}$ or *Myo6*$^{+/+}$;*Apc*$^{\text{Min/-}}$) were stably transduced with a lentiviral vector containing a Wnt/β-catenin reporter GFP gene driven by a minimal promoter containing 7 tandem repeats of the consensus β-catenin/TCF4 binding site, and a constitutive SV40 promoter driving the expression of the red fluorescent protein mCherry. (7TGC Wnt reporter; Addgene; #24304). Viral particles were obtained as previously explained in 'Lentiviral infection of colon cancer cells' section (but 7TGC lentiviral plasmid instead of the pINDUCER10-shRNA). The infection procedure was carried out as described previously (Maru, Orihashi, & Hippo, 2016). Briefly, organoid cells were seeded on top of a matrigel layer and covered with IntestiCult medium containing the lentiviral particles. The following day, viruses were removed and cells were covered with a matrigel layer, and on top of it new IntestiCult medium was added to let the cells form organoids and expand. In order to determine relative levels of Wnt activity in *Myo6* wild-type and knock-out intestinal organoids, 5×10^4 infected cells were seeded onto 24 well plates with 50% matrigel containing DMEM-F12 -20% FBS medium (DMEM-F12 – Life Technologies; FBS – Sigma-Aldrich) and grown for 5 days. Then, organoids were dissociated into individual cells and analyzed by FACS (Fluorescence-activated cell sorting) using BD FACSCalibur™ flow cytometer, in order to determine the percentage of 7TGC-infected (mCherry-positive) and Wnt activated (GFP-positive) cells. Data obtained from the flow cytometer was analyzed using the 'FCS Express 3' program (De Novo Software). Percentage of

Wnt-activated (GFP-positive) cells within the 7TGC-infected cell population (mCherry-positive) is shown. Relative levels of Wnt signaling (average GFP intensity) in both wild-type and knock-out *Myo6* organoid cells are also shown. Four independent experiments were carried out.

CHAPTER 4

RESULTS

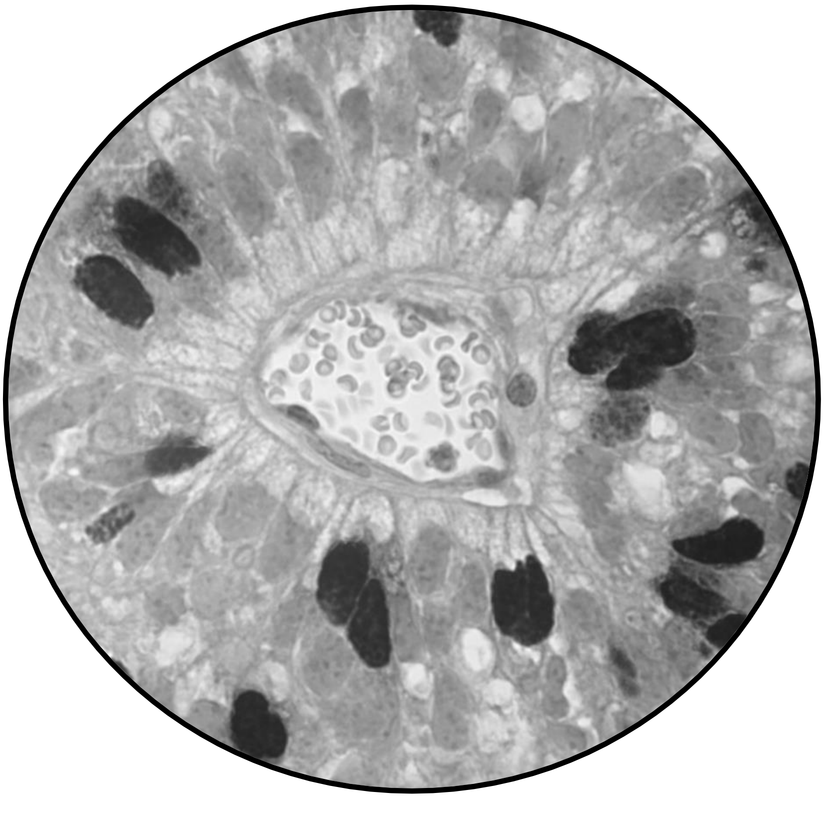

RESULTS

1. Low MYO6 protein and mRNA expression in colorectal tumors is associated with poor patient prognosis.

A tissue microarray (TMA) containing triplicate tumor samples from 164 Dukes' C colorectal cancer (CRC) patients was used to investigate possible associations between **MYO6 tumor protein expression** and patient 'overall' and 'disease-free' survival. Among these patients, after potentially curative surgery, 82 received 5-FU-based adjuvant chemotherapy and 77 did not receive any adjuvant treatment. For the remaining 5 patients there were no data regarding adjuvant chemotherapy. Samples were collected between 1994 and 1998 in Finland, and at that time it was not mandatory to treat Dukes' C patients with adjuvant chemotherapy.

MYO6 protein expression of these tumor samples was determined by immunohistochemistry using a commercially available monoclonal antibody that specifically recognizes MYO6 (**Table 10**). The specificity of the antibody on formalin-fixed, paraffin-embedded samples was verified by immunostaining normal intestinal tissue from wild-type and *Myo6* knock-out mice (Snell's Waltzer mice) (**Fig. 27A**); and also by immunostaining samples of tumor xenografts formed by colon cancer cell lines that were engineered to downregulate MYO6 expression (**Fig. 27B**).

The relative intensity of MYO6 immunostaining in each sample of the tissue microarray was assessed blinded from the clinical data of the patients using a semiquantitative scale ranging from 0 (no staining) to 3 (strong staining) (**Fig. 27C**). High variability in MYO6 expression was observed among the different primary colon tumor samples.

In order to study possible survival differences (Kaplan-Meier plots) depending on MYO6 tumor protein expression, patients were dichotomized as high or low MYO6. To identify the cutoff staining level that maximizes survival differences between patients with high and low tumor levels, 'Cutoff finder' package was used. This program is based on the 'R' statistical engine and analyzes the survival curves for every possible grouping of patients as a function of the threshold for classifying high/low MYO6 expression. The best survival differences were obtained with a cutoff staining value of 2.4 (**Fig. 27D-E**). Therefore, tumors with staining levels of 2.4 or lower (128 of 164 tumors, 78%) were considered as low MYO6, and staining intensities higher than 2.4 (36 of 164 tumors, 22%) were considered as high MYO6.

For this cutoff value, patients with low MYO6 tumor protein expression showed significantly worse overall and disease-free survival than patients with high MYO6 tumor protein expression (Log-rank test p=0.01 and p=0.03, respectively; **Fig. 27D-E**). The median overall survival (length of time from surgery to the point at which half of the patients are still alive) of patients with low MYO6 expression was 2.6 years, whereas for patients with high MYO6 expression it was >9 years; and the median disease-free survival (time from surgery to the point at which half of the patients have relapsed) was 1.7 and >9 years for patients with low and high tumor MYO6 expression, respectively. These data indicate that low expression of tumor MYO6 protein could be used as a marker of poor prognosis in Dukes' C colorectal cancer patients after surgery.

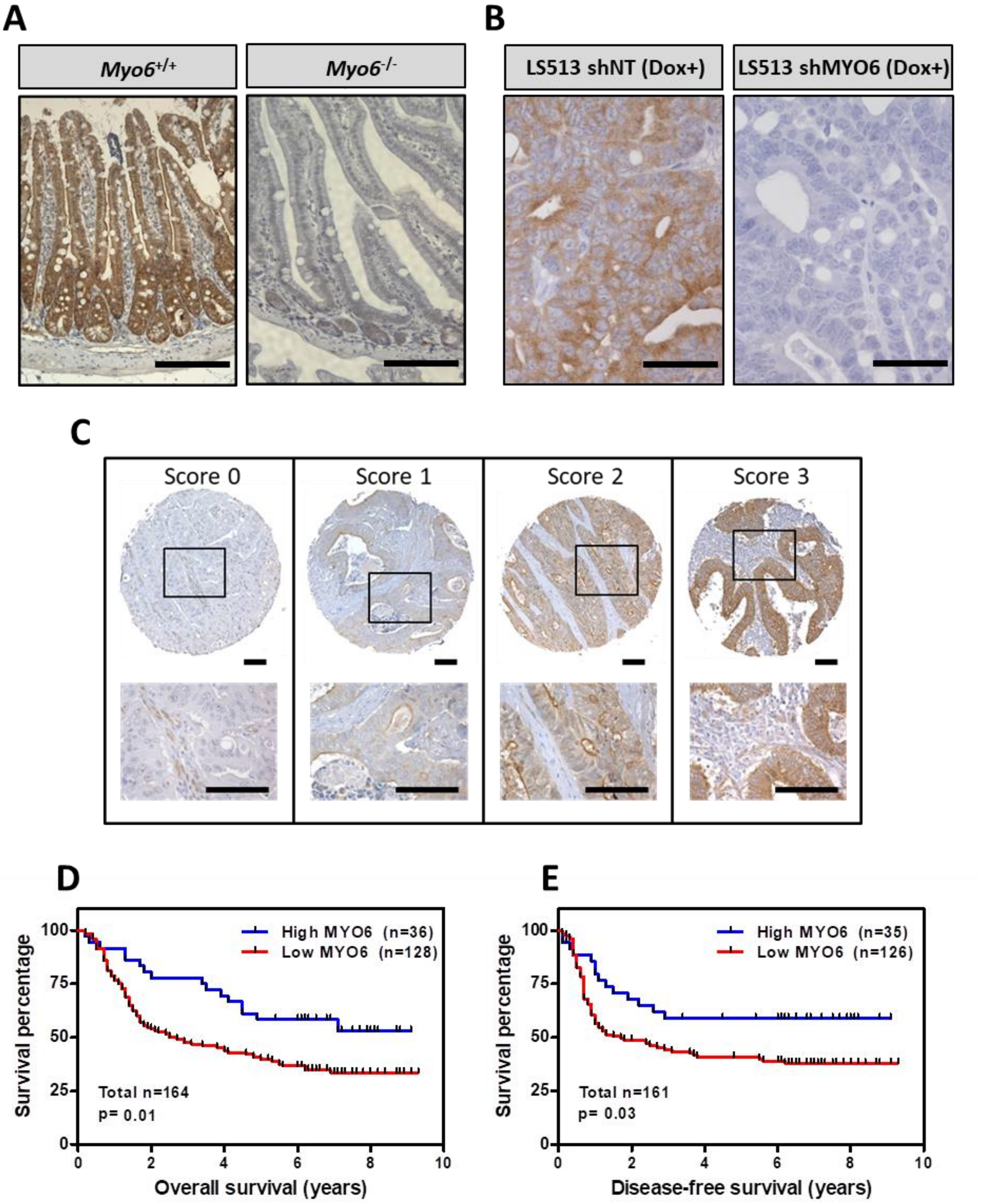
A
Myo6+/+
Myo6-/-
B
LS513 shNT (Dox+)
LS513 shMYO6 (Dox+)
C
Score 0
Score 1
Score 2
Score 3
D
Survival percentage
High MYO6 (n=36)
Low MYO6 (n=128)
Total n=164
p= 0.01
Overall survival (years)
E
Survival percentage
High MYO6 (n=35)
Low MYO6 (n=126)
Total n=161
p= 0.03
Disease-free survival (years)
0
25
50
75
100
0
2
4
6
8
10

Figure 27: Survival of colorectal cancer patients with low and high MYO6 tumor protein expression. (A-B) Validation of the antibody against MYO6 by immunostaining **A)** normal small intestine samples from wild-type (*Myo6*$^{+/+}$) and *Myo6* knock-out (*Myo6*$^{-/-}$) mice (Scale bar: 100 μm) and **B)** subcutaneous xenograft tumor samples generated from LS513 cells with inducible MYO6 downregulation in NOD/SCID mice (Scale bar: 50 μm). shNT: control non-target shRNA; shMYO6: cells with shRNA against *MYO6*. Dox+: doxycycline treated. **C)** Expression of MYO6 protein was assessed by immunohistochemistry in a cohort of 164 Dukes' C colorectal tumor samples. Representative images of the different MYO6 staining levels (scores) are shown: 0: no staining; 1: low; 2: moderate; 3: high. Higher magnification pictures of the indicated regions are shown. Scale bars: 100 μm. **(D-E)** Kaplan-Meier plots showing **D)** overall and **E)** disease-free survival of 164 and 161 Dukes' C colorectal cancer patients, respectively, as a function of MYO6 tumor protein expression. Cutoff value= 2.4. n: number of patients. Log-rank test p values are shown.

No significant associations were observed between MYO6 protein expression and other clinicopathological variables, such as, patient sex, age, tumor location (colon/rectum), histological grade, adjuvant treatment; or molecular features of the tumors, such as, DNA replication error (RER) status (MSS/MSI), *TP53* status (wild-type/mutant), *KRAS* status (wild-type/mutant) and loss of 18q chromosome (**Table 11**).

Table 11: Clinicopathological features of 164 Dukes' C colorectal cancer patients.

	Total	High MYO6	Low MYO6	p value
Sex, n (%)				
Female	81 (49.4)	19 (52.8)	62 (48.5)	0.71[a]
Male	83 (50.6)	17 (47.2)	66 (51.5)	
Age (years), mean±SD	65.21	64.9±12.1	65±13.0	0.91[b]
Site, n (%)				
Colon	98 (60.2)	22 (61.2)	76 (59.9)	1[a]
Rectum	65 (39.8)	14 (38.8)	51 (40.1)	
Degree of differentiation, n (%)				
Good	20 (12.4)	6 (16.7)	14 (11.2)	0.64[c]
Moderate	121 (74.6)	25 (69.4)	96 (76.1)	
Poor	21 (12.9)	5 (13.8)	16 (12.6)	
Follow up (years), mean±SD	9.2	9.1±1.1	9.2±1.0	0.52[b]
Adjuvant treatment, n (%)				
Yes	83 (51.9)	14 (40)	69 (55.2)	0.13[a]
No	77 (48.1)	21 (60)	56 (44.8)	
RER status, n (%)				
MSI	21 (12.9)	2 (5.6)	19 (15)	0.17[a]
MSS	142 (87.1)	34 (94.4)	108 (85)	
***TP53* status, n (%)**				
Wild type	18 (45)	2 (18.2)	16 (55.2)	0.07[a]
Mutant	22 (55)	9 (81.8)	13 (44.8)	
***KRAS* status, n (%)**				
Wild-type	35 (64.9)	9 (69.3)	26 (63.5)	1[a]
Mutant	19 (35.1)	4 (30.7)	15 (36.5)	
Allelic loss of chromosome 18q, n (%)				
LOH	47 (44.4)	10 (41.7)	37 (45.2)	0.82[a]
No LOH	59 (55.6)	14 (58.3)	45 (54.8)	

[a]Fisher's exact test; [b]Mann-Whitney test; [c]Chi-square test. RER: DNA replication error; MSS: Microsatellite stable; MSI: Microsatellite instability; LOH: Loss of heterozygosity; n: Number of patients. SD: Standard deviation.

The TMA used also contained triplicate samples of normal colon tissues (n=91) and regional lymph node metastases (n=16) from a subset of the 164 Dukes' C colorectal cancer patients included. This allowed the comparison of MYO6 protein expression among samples representing different stages of tumor progression. The expression of MYO6 was significantly reduced in primary tumors compared to normal tissues (Student's t-test, $p<0.0001$). Moreover, lymph node metastases were found to have significantly lower MYO6 protein expression than primary tumors (Student's t-test, $p<0.0001$), further suggesting that reduced MYO6 is associated with tumor spread/progression and poor prognosis (**Fig. 28**).

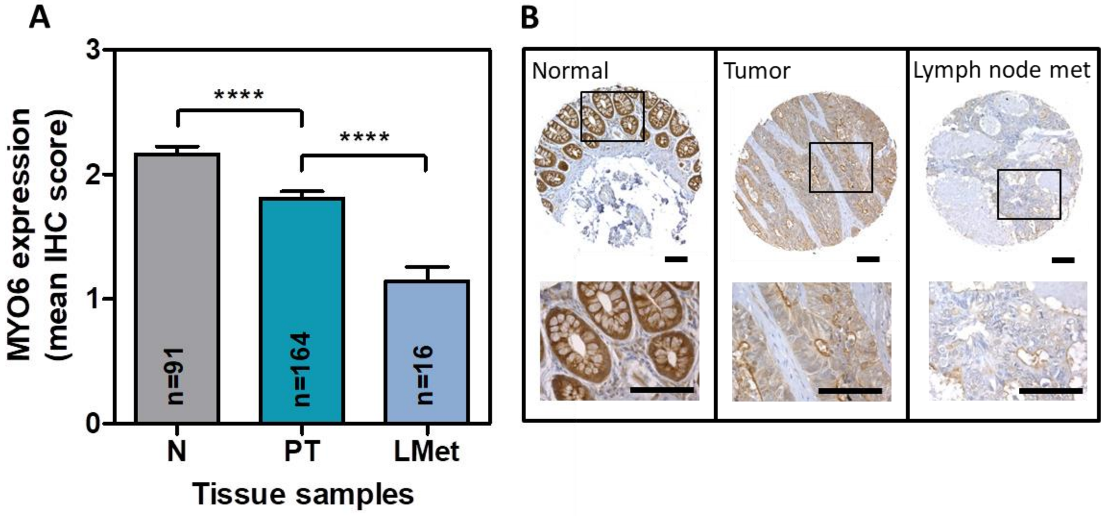

Figure 28: MYO6 tumor protein reduction along colorectal cancer progression. A) Average (±SEM) of MYO6 protein immunostaining levels in normal colon samples (N), colorectal primary tumors (PT) and regional lymph node metastases (LMet). n: number of samples. IHC: immunohistochemistry. ****$p<0.0001$; Student's t-test. **B)** Representative images of MYO6 staining levels in normal colon, primary tumor and regional lymph node metastasis samples from the same patient. Higher magnification images of the indicated regions are shown in the lower panels. Scale bars: 100 μm.

Collectively, these results show that low tumor expression of MYO6 protein identifies a subset of patients with poor prognosis after surgery treatment and that are at high risk of recurrence (five-year recurrence rate of 61.5% and 43.7% in patients with low and high tumor MYO6 expression, respectively).

Next, the association between ***MYO6* tumor mRNA expression** and patient survival was further studied using a cohort of 115 Stage III CRC patients from the 'The cancer genome atlas' (TCGA) program. Samples were collected between 1999 and 2013 and tumor *MYO6* mRNA expression data was obtained through RNA sequencing as previously described in detail ("TCGA Colon and Rectal Cancer (COADREAD) - Xena Functional Genomics Explorer," 2016).

As described above for MYO6 protein expression, to investigate possible survival differences depending on *MYO6* tumor mRNA expression, patients were divided into two groups: low *MYO6* mRNA and high *MYO6* mRNA. As in the case of the tissue microarray, the cutoff value that gives the best survival differences between low and high *MYO6* tumor mRNA patients was obtained by using the 'Cutoff finder' R package. Patients with *MYO6* mRNA expression of 11.12 RPKM (reads per kilo base per million mapped reads) or lower (56 of 115 tumors, 48.7%) were considered as low *MYO6* and patients with *MYO6* mRNA expression higher than 11.12 RPKM (59 of 115 tumors, 51.3%) were considered as high *MYO6* (*MYO6* mRNA expression ranges from 9.57 to 12.12 RPKM). Patients with tumors expressing low expression of *MYO6* mRNA showed significantly shorter overall survival compared to patients with high *MYO6* tumor mRNA expression (Log-rank test, p=0.03; **Fig. 29A**). The median overall survival of patients with low *MYO6* expression was 3.8 years, whereas for patients with high *MYO6* expression it was >10 years. This is in good agreement with the overall survival difference observed for Dukes' C CRC patients depending on MYO6 tumor protein expression (**Fig. 27D**). A corresponding trend was observed for disease-free survival, although it did not reach statistical significance (Log-rank test, p=0.12; **Fig. 29B**).

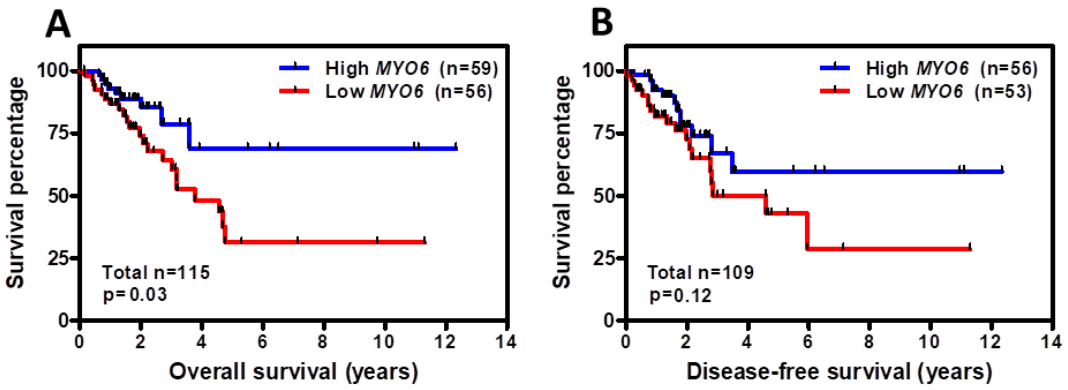

Figure 29: Survival of colorectal cancer patients as a function of tumor *MYO6* mRNA expression. (A-B) Kaplan-Meier plots showing **A)** overall survival and **B)** disease-free survival of 115 and 109 Stage III colorectal cancer patients, respectively, as a function of *MYO6* tumor mRNA expression (RNA sequencing). Cutoff value: 11.12 RPKM. n: number of patients. Log-rank test p values are shown.

No significant associations were observed between *MYO6* mRNA expression and other clinicopathological variables, such as, patient sex, age and tumor location (colon/rectum); or molecular features of the tumors, such as, DNA replication error (RER) status (MSS/MSI) and *KRAS* status (wild-type/mutant) (**Table 12**).

Table 12: Clinicopathological features of 115 Stage III colorectal cancer patients from the TCGA.

	Total	High MYO6	Low MYO6	p value
Sex, n (%)				
Female	53 (46.1)	25 (42.4)	28 (50)	0.46[a]
Male	62 (53.9)	34 (57.6)	28 (50)	
Age (years), mean±SD	63.3	64.5±12.8	62.1±14.3	0.43[b]
Site, n (%)				
Colon	79 (68.7)	38 (64.5)	41 (73.3)	0.32[a]
Rectum	36 (31.3)	21 (35.5)	15 (26.7)	
Follow up (years), mean±SD	2.4	2.5±2.5	2.4±2.5	0.55[b]
RER status, n (%)				
MSI	29 (25.5)	14 (23.8)	15 (27.3)	0.67[a]
MSS	85 (74.5)	45 (76.2)	40 (72.7)	
***KRAS* status**				
Wild type	10 (55.6)	3 (50)	7 (58.4)	1[a]
Mutant	8 (44.4)	3 (50)	5 (41.6)	

[a]Fisher's exact test; [b]Mann-Whitney test; RER: DNA replication error; MSS: Microsatellite stable; MSI: Microsatellite instability; n: Number of patients. SD: Standard deviation.

These data further support the value of low MYO6 expression as a marker of poor prognosis for locally advanced colorectal cancer patients.

2. Generation of isogenic colon cancer cell models with inducible MYO6 downregulation.

As described above, low tumor MYO6 expression is associated with poor prognosis in colorectal cancer patients. However, it was not clear whether MYO6 was able to directly modulate the progression of colorectal tumors or was just a marker of prognosis but not causally related to tumor progression.

Therefore, in order to investigate whether reduced MYO6 expression plays a direct role in colorectal cancer tumorigenesis, cell line systems with doxycycline-inducible MYO6 knockdown were engineered. For this purpose, cell lines showing relatively high MYO6 expression were stably transduced with lentiviral vectors that contained shRNAs against *MYO6* (pINDUCER10-sh53, sh54 and sh55) or with the corresponding non-targeting control vector (pINDUCER10-shNT).

The expression of MYO6 was assessed in a panel of colorectal cancer cell lines at the protein ($n=48$; Shotgun mass spectrometry (MS) proteomics) or mRNA ($n=51$; RNA sequencing) level. As observed in the primary CRC tumors, significant variability was detected in the expression of MYO6 in these cell lines (**Fig. 30A-B**). The levels of MYO6 mRNA (RNA-Seq) and protein (Shotgun-MS proteomics) showed a significant correlation (Pearson's $r=0.66$ and $p<0.0001$; **Fig. 30C**).

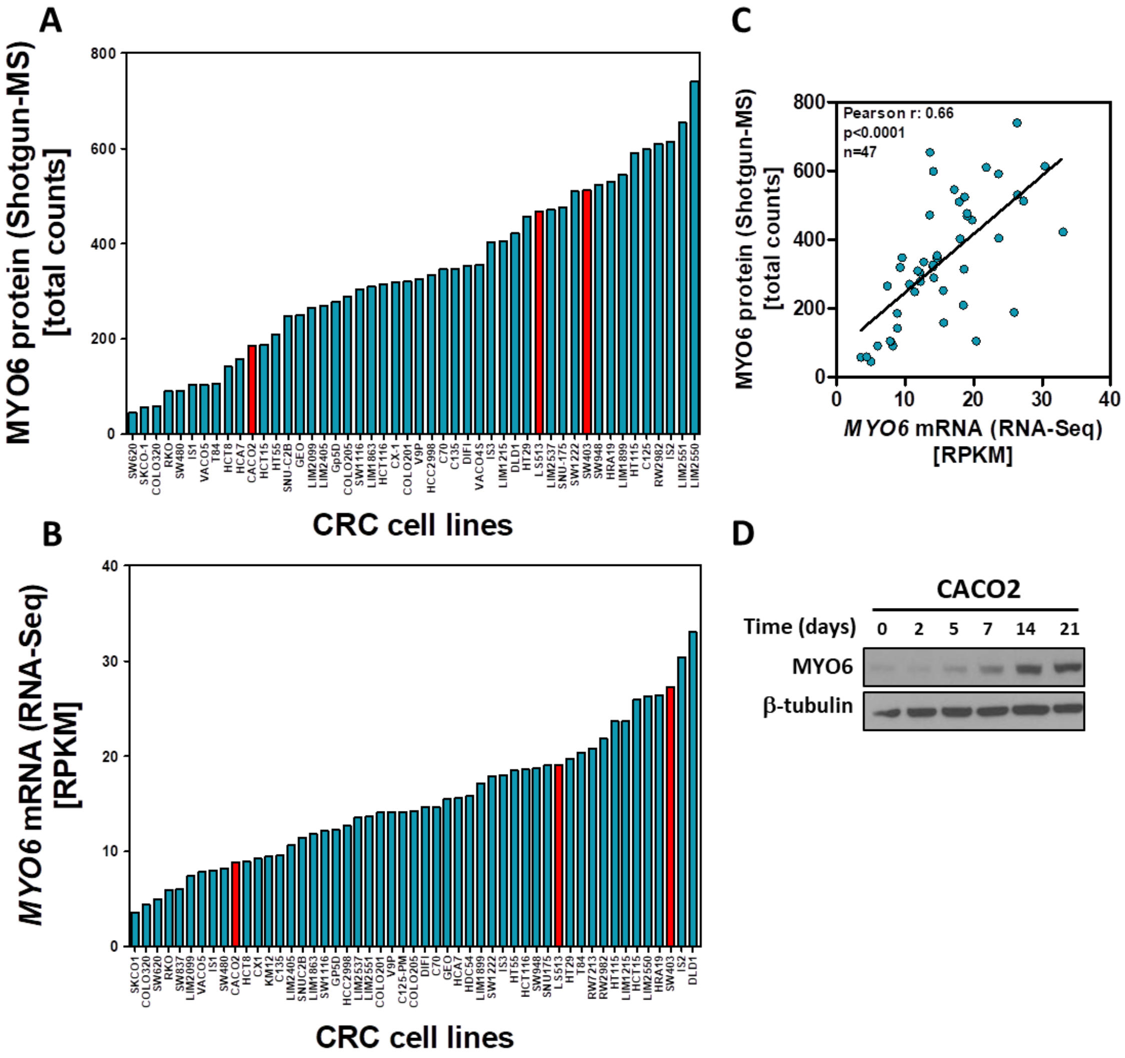

Figure 30: MYO6 expression in colorectal cancer cell lines. A) MYO6 protein expression in a panel of 48 CRC cell lines obtained by Shotgun mass spectrometry (MS) proteomics. **B)** *MYO6* mRNA expression in a panel of 51 CRC cell lines assessed by RNA sequencing (RNA-Seq). The colon cancer cell lines that were selected for targeted MYO6 downregulation are indicated in red. **C)** Correlation between MYO6 expression data from Shotgun-MS proteomics and RNA sequencing. Pearson's r and p values are shown. n: number of analyzed CRC cell lines. **D)** MYO6 protein expression of CACO2 cells at different days of confluence, assessed by western blotting. β-tubulin expression is shown as a loading control.

Based on these MYO6 expression data, two cell lines (**SW403** and **LS513**) with relatively high MYO6 expression were selected for targeted downregulation of MYO6. In addition, **CACO2** cell line, which showed intermediate MYO6 expression, was also selected. CACO2 cells increase considerably the expression of MYO6 when become differentiated (**Fig. 30D**) and also form a well-structured brush border, which makes them suitable to study the role of MYO6 in polarization/differentiation during tumor progression. MYO6 expression of these cell lines (among others) was further verified by western blot (WB) (**Fig. 31A-B**) and shown to correlate significantly with both Shotgun-MS and RNA-Seq MYO6 expression data mentioned above (WB *vs* RNA-Seq: Pearson's r=0.86 and p=0.0004; WB *vs* Shotgun-MS: Pearson's r=0.85 and p=0.001; **Fig. 31C-D**). Importantly, none of the three cell lines presented mutations in *MYO6* gene (Mouradov et al., 2014). Features, such as, age, gender, ethnicity and primary site; and mutational status of the main ‘colorectal cancer related genes’ such as, *TP53*, *APC* and *KRAS*, of these cell lines are shown in ‘material and methods’ section (**Tables 7 and 8**).

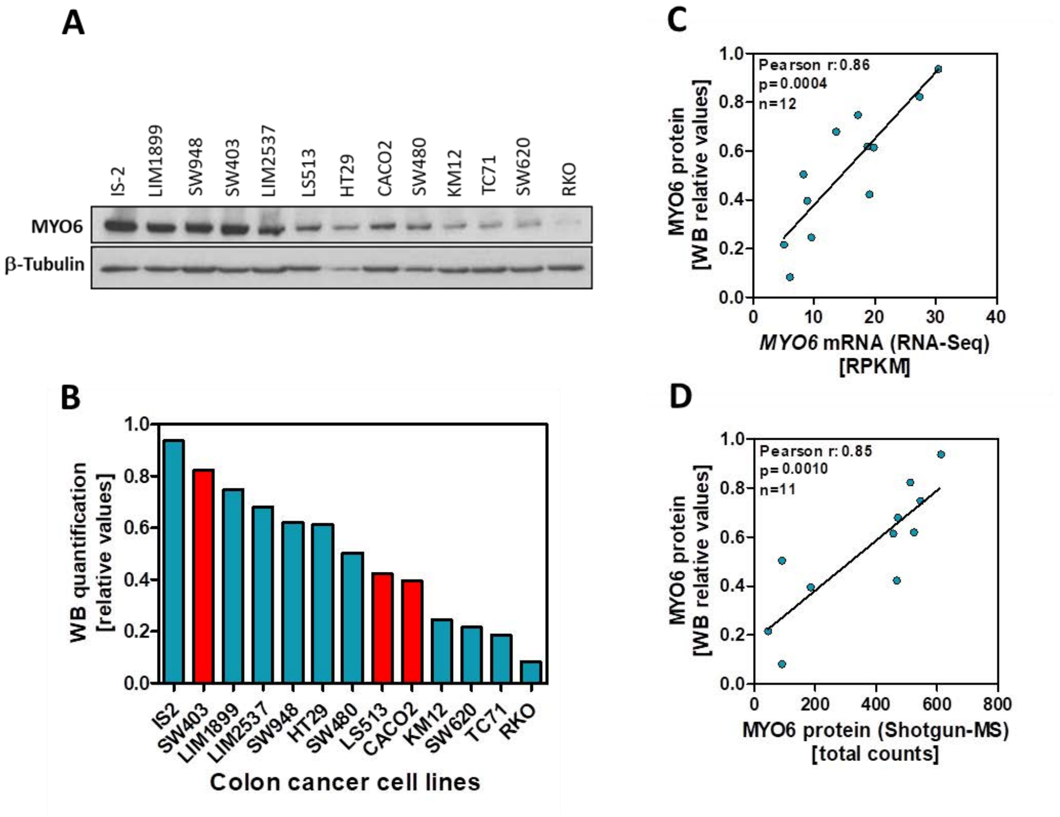

Figure 31: Confirmation of MYO6 protein expression in the selected colon cancer cell lines. A) MYO6 protein expression of 13 colon cancer cell lines assessed by western blotting (WB). β-tubulin expression is shown as a loading control. Cells were collected at 80% confluence. **B)** MYO6 protein expression of these 13 colon cancer cell lines was quantified using ImageJ program and normalized to β-tubulin expression. Colon cancer cell lines selected for MYO6 knockdown are indicated with red. **(C-D)** Correlations between MYO6 expression data obtained from **C)** ‘western blot quantification’ and RNA sequencing (RNA-Seq); and **D)** ‘western blot quantification’ and Shotgun-MS proteomics. n: number of colon cancer cell lines. Pearson’s r and p values are shown.

After lentiviral transduction and puromycin selection (see ‘materials and methods’ section), the percentage of transduced cells in the newly engineered cell lines was analyzed by flow-cytometry through detection of ‘turbo red-fluorescence protein’ (tRFP) after 48 h of doxycycline treatment. Doxycycline, in addition to inducing shRNA expression, also induces tRFP expression which acts as a transduction reporter in the infected cells. The percentage of transduced cells (cells expressing tRFP) was higher than 90% in all engineered derivative cell lines (**Fig. 32A-C**). MYO6 downregulation was confirmed by western blotting after 72 h of 1 μg/mL doxycycline treatment (**Fig. 32D-F**). Note that sh53, sh54 and sh55 downregulate MYO6 in CACO2 cells, while sh52 did not have any effects on MYO6 expression, and was not further used.

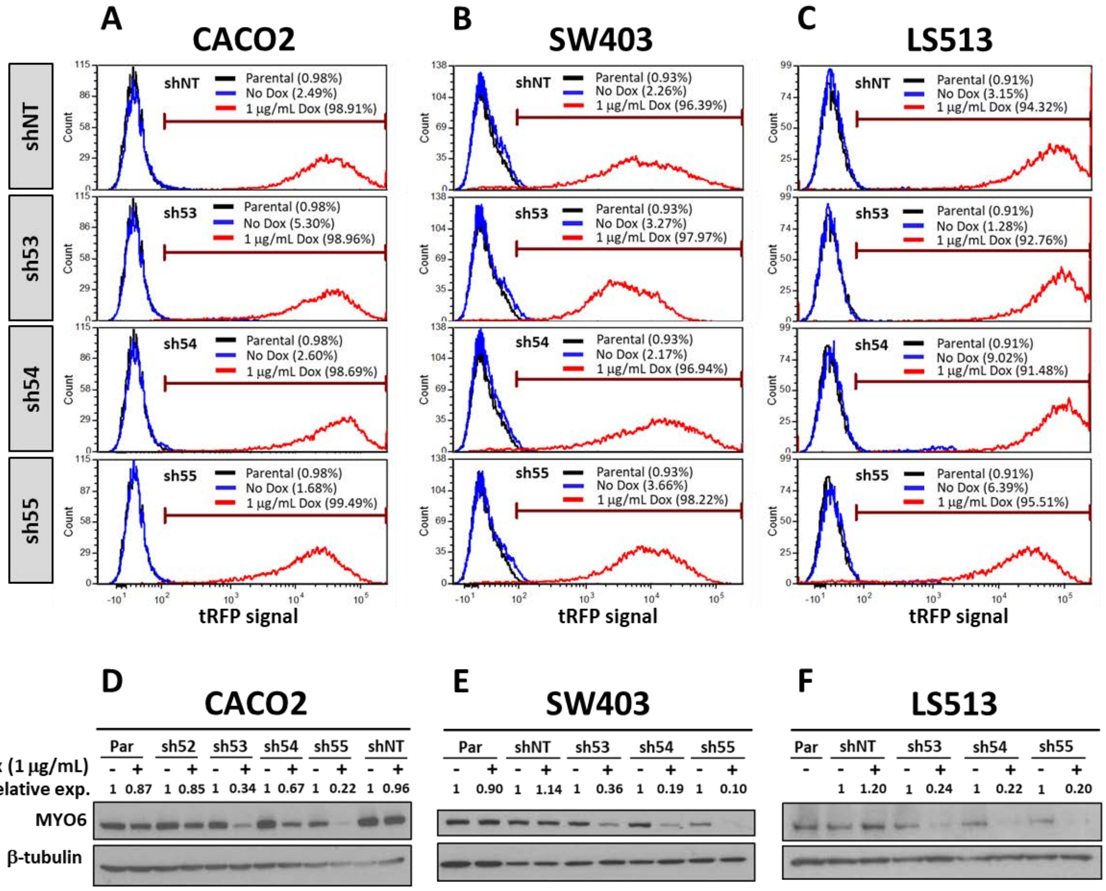

Figure 32: Inducible MYO6 downregulation in colon cancer cell lines. (A-C) Flow cytometry analysis of tRFP-positive cells in the shNT, sh53, sh54 and sh55 cell populations engineered from **A)** CACO2, **B)** SW403 and **C)** LS513 cell lines. The percentage of positive cells is indicated. 'Parental' refers to the no-transduced original colon cancer cell line. tRFP: turbo red-fluorescent protein. **(D-F)** Western blot analysis showing MYO6 downregulation after 72 h of 1 μg/mL doxycycline (Dox) treatment in **D)** CACO2, **E)** SW403 and **F)** LS513. MYO6 expression was quantified in the different cell lines using ImageJ program and normalized to β-tubulin expression. The relative MYO6 expression, normalized to 'Dox-' conditions for each cell line, is indicated. β-tubulin expression is shown as a loading control. Par: Parental.

3. MYO6 does not regulate differentiation and polarization of colon cancer cells.

During colon cancer development cancer cells become less differentiated and can acquire mesenchymal traits. This loss of differentiation implies a loss of polarization (loss of basal-apical polarity and the acquisition of more spindly/fibroblastic morphology) and a loss of 'tissue specific functions'. Moreover, the loss of differentiation is usually accompanied by faster proliferation rate, increased resistance to apoptosis and higher migration and invasion capacity (Wodarz & Näthke, 2007). Hence, poorly differentiated cancer cells show a more aggressive phenotype. Loss of cell polarity is commonly observed in advanced tumors (carcinomas) and is associated with local invasion and formation of distant metastasis (Hanahan & Weinberg, 2011; Wodarz & Näthke, 2007). However, loss of polarization and differentiation is also important in the early stages of intestinal tumorigenesis (Mazzolini et al., 2012).

MYO6 has been reported to be important for the polarized structure of ‘cochlear hair cells’, since its absence triggers a progressive disorganization of the hair cells’ stereocilia, which leads to the death of cochlear hair cells and a complete degeneration of the neurosensory epithelium, finally causing deafness (M Miyagawa et al., 2015; Seiler et al., 2004; Self et al., 1999). MYO6 is also required for the maintenance of overall microvilli ultrastructure in enterocytes, although its absence does not trigger such a dramatic consequence as in cochlear hair cells (Hegan et al., 2012).

As loss of differentiation is a critical event during cancer development and MYO6 has been reported to be involved in the polarization of normal intestinal epithelial cells, we wanted to study whether MYO6 could regulate the differentiation of colon cancer cells.

Normal enterocytes (absorptive cells) during the process of differentiation from the proliferative crypts to the mature flat colonic mucosa, develop a well-structured brush border with high expression of their associated hydrolases (Mariadason, Rickard, Barkla, Augenlicht, & Gibson, 2000). Among these enzymes are alkaline phosphatase (AP), sucrase-isomaltase (SI) and dipeptidyl peptidase-IV (DPP-IV), which are frequently used as markers of cell differentiation in colorectal cancer cells (Matsumoto et al., 1990). In order to investigate if MYO6 regulates cell differentiation, the **activities of AP, SI and DPP-IV** were analyzed in the isogenic cell line systems engineered.

CACO2 cells are able to spontaneously differentiate *in vitro* when cultured in **confluence** for 2-3 weeks. Studies demonstrated that these cells upon differentiation express several morphological and biochemical features specific of mature small intestinal enterocytes or fetal colonocytes, such as, cylindrical polarized morphology with microvilli on the apical side, tight junctions between adjacent cells and high expression of hydrolases such as alkaline phosphatase, sucrase-isomaltase and dipeptidyl peptidase-IV (Sambuy et al., 2005).

Therefore, CACO2 derivative cell lines were cultured in confluence up to 21 days in order to induce them differentiation, and cell pellets were collected at days -1 (pre-confluence), 0 (first day of 100% confluence), 2, 5, 7, 14 and 21 (days post-confluence). Once the proteins were extracted with mannitol buffer the different enzymatic assays were carried out. No changes were found in the differentiation capability of cells with reduced expression of MYO6 compared to their corresponding controls, as assessed by AP activity (**Fig. 33A**), SI activity (**Fig. 33B**) and DPP-IV activity (**Fig. 33C**). Note that, CACO2-sh55 cells showed atypical differentiation kinetics in these conditions, for reasons that were not further investigated. The downregulation of MYO6 in the isogenic CACO2 derivative cells was confirmed by western blotting during the course of these experiments (**Fig. 33D-G**).

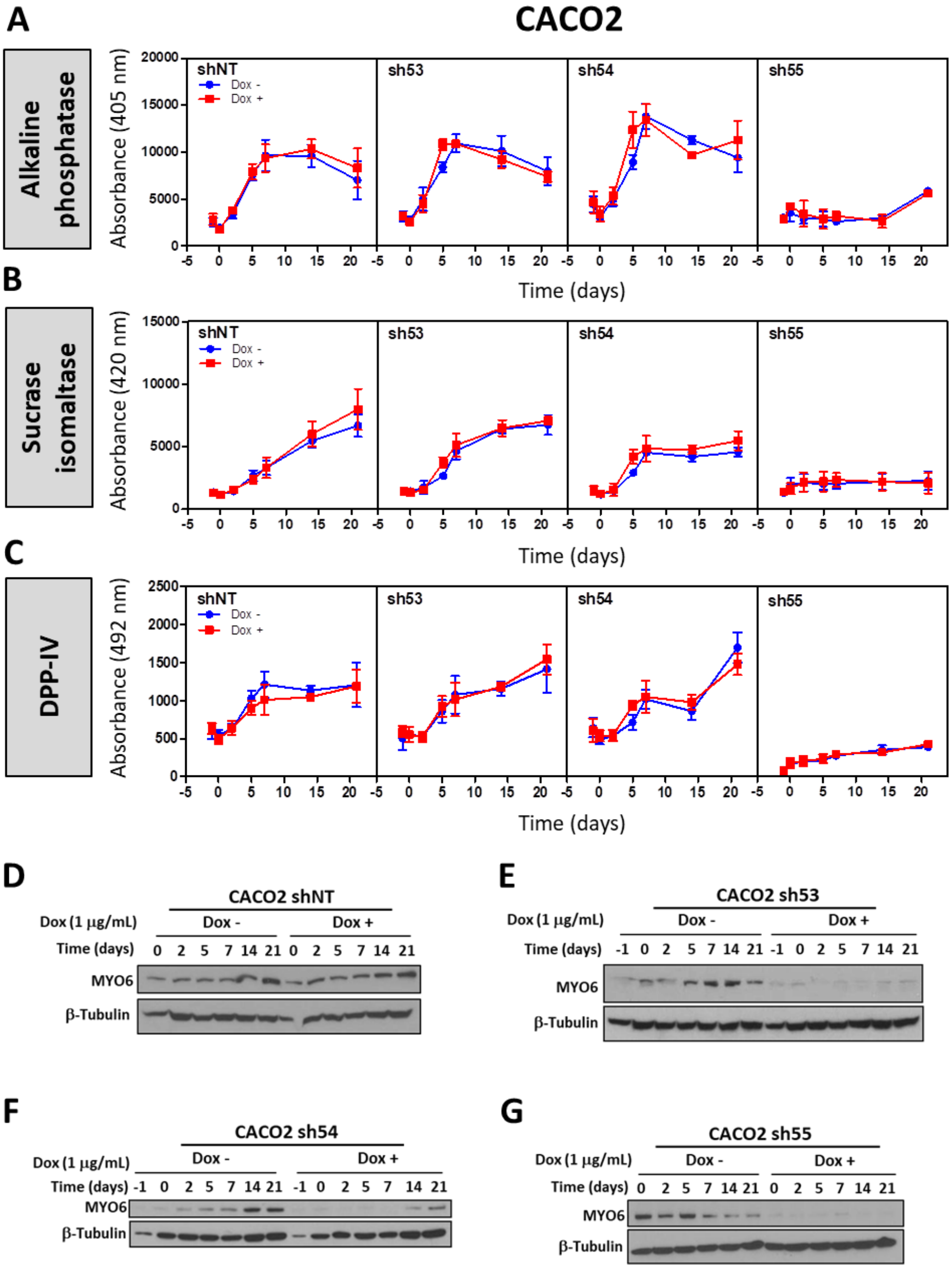

Figure 33: Effects of MYO6 downregulation on the differentiation of CACO2 cells. (A-C) Enzymatic activity of **A)** alkaline phosphatase, **B)** sucrase-isomaltase and **C)** dipeptidyl peptidase-IV (DPP-IV) in CACO2 derivative cell lines (treated with (Dox +) or without (Dox -) 1 μg/mL doxycycline) at different days of confluence. Day '-1' is the day previous to confluence, day 0 is the first day of 100% confluence and days 2, 5, 7, 14 and 21 are the days after reaching 100% confluence. The average enzymatic activity (±SEM) of 3 independent experiments each run in triplicate is shown. **(D-G)** MYO6 protein expression of **D)** CACO2-shNT, **E)** CACO2-sh53, **F)** CACO2-sh54 and **G)** CACO2-sh55 cells at different days of confluence, assessed by western blotting. β-tubulin expression is shown as a loading control.

Unlike CACO2 cells, most colorectal cancer cell lines are unable to undergo enterocytic differentiation spontaneously under confluent culture conditions (Chantret, Barbat, Dussaulx, Brattain, & Zweibaum, 1988). However, treatment with certain synthetic or biological factors can induce partial differentiation of colon cancer cells (Sambuy et al., 2005).

Butyrate is a short-chain fatty acid produced by intestinal bacteria through carbohydrate fermentation (mainly from dietary fiber). Butyrate is an important energy source for intestinal epithelial cells and plays a role in the maintenance of colonic homeostasis. *In vitro* exposure of a wide variety of colorectal cancer cells to butyrate leads to a more differentiated phenotype, an inhibition of cell proliferation and an induction of apoptosis (Hamer et al., 2008). Butyrate-induced differentiation is more rapid and includes many, but not all the phenotypic changes observed during spontaneous CACO2 cell differentiation. Although alkaline phosphatase is the hydrolase most robustly induced by butyrate, its increase varies among the different colorectal cancer cell lines (Chung, Song, Erickson, Sleisenger, & Kim, 1985). The induction of SI and DPP-IV is usually not as robust as AP induction and several colorectal cancer cell lines show a lack of responsiveness of SI or DPP-IV activities to butyrate (Chung et al., 1985).

Because **SW403** and **LS513** cells do not differentiate spontaneously upon confluence (data not shown), the differentiation was induced by adding **sodium butyrate** (NaBut) to the medium for 72 h. The activity of AP and DPP-IV was significantly upregulated by sodium butyrate (compare 0 mM and 5 mM NaBut conditions), although no changes were observed in the activity of SI (not shown). However, cells with downregulated MYO6 expression (Dox +; 5 mM NaBut) showed the same increase in AP (**Fig. 34A-B**) and DPP-IV (**Fig. 34C-D**) activity as their respective controls (Dox -; 5 mM NaBut), indicating that reduced MYO6 levels do not interfere with the differentiation program of colon cancer cells (understood as the regulation of tissue specific functions).

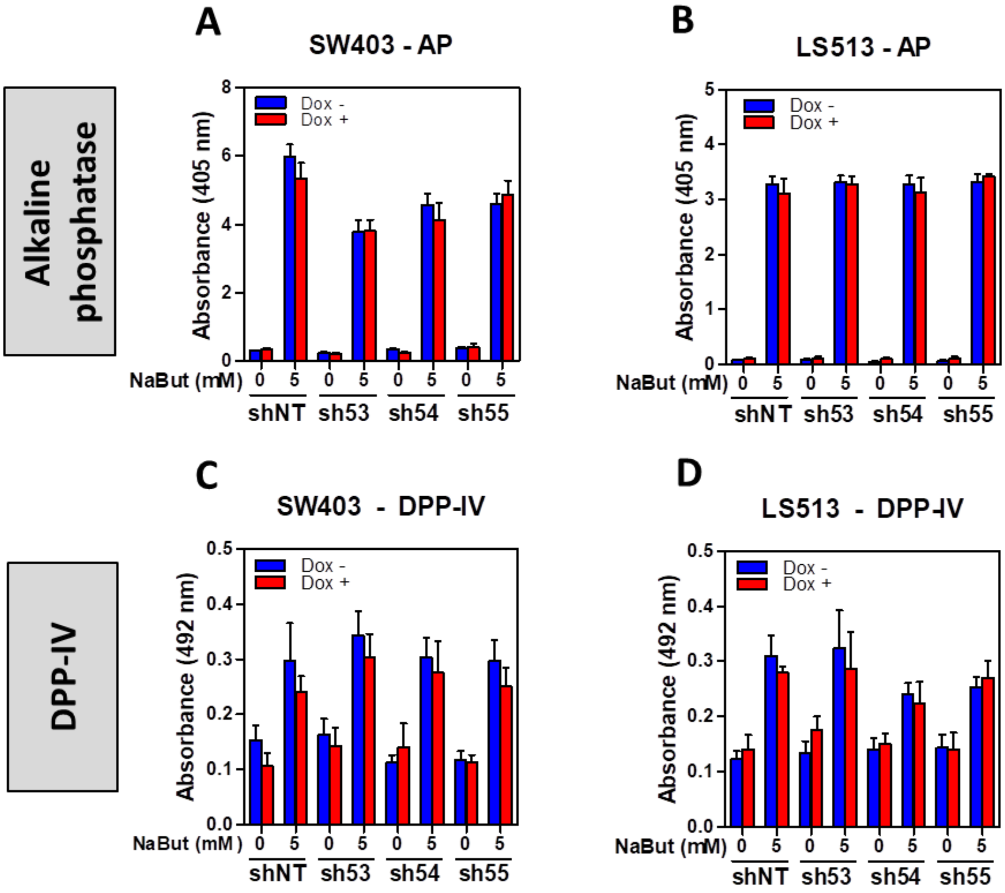

Figure 34: Effects of MYO6 downregulation on the differentiation of SW403 and LS513 cells. (A-B) Enzymatic activity of alkaline phosphatase (AP) in **A)** SW403 and **B)** LS513 derivative cell lines after induction with sodium butyrate (NaBut; 5 mM for 72 h). **(C-D)** Enzymatic activity of dipeptidyl peptidase-IV (DPP-IV) in **C)** SW403 and **D)** LS513 derivative cell lines after induction with sodium butyrate (NaBut; 5 mM for 72 h). All cell lines were treated with (Dox +) or without (Dox -) 1 μg/mL doxycycline. The mean (±SEM) of three independent experiments each carried out in triplicate is shown. No significant differences were observed (Student's t-test $p > 0.05$).

The formation of cell-cell adherens junctions is believed to be the first required condition to promote the establishment of polarity in epithelial cells. In fact, loss of cell polarity is frequently related to alterations in their attachment to other cells (loss of cell-cell adhesions). In these adherens junctions, E-cadherin, which is considered a key factor, forms a complex with β-catenin, p120-catenin and α-catenin (Jeanes, Gottardi, & Yap, 2008). This complex, in addition to providing a physical link between adjacent cells and intracellular structures, also supports the assembly of signaling complexes (Van Roy & Berx, 2008; Wodarz & Näthke, 2007). The loss of overall E-cadherin expression or loss of its normal localization at cell-cell contacts has been associated with tumor progression to a more invasive cancer phenotype (Jeanes et al., 2008). Moreover, cells that contained E-cadherin mutants lacking β-catenin-binding domain were found to be poorly adhesive (Nagafuchi & Takeichi, 1989).

Myosin VI has been shown to bind and stabilize E-cadherin and β-catenin complexes in *Drosophila* border cells (a kind of follicle cells) (Geisbrecht & Montell, 2002). Furthermore, in MCF7 breast adenocarcinoma cells, myosin VI has also been shown to localize to adherens junctions through its interaction with E-cadherin, where it contributes to the maturation of cadherin-dependent cell-cell contacts during polarization (Maddugoda et al., 2007).

Therefore, in order to investigate a possible role of MYO6 in colon cancer cell polarity, cell localization of **E-cadherin** and **β-catenin** were analyzed. E-cadherin and β-catenin expression has been reported to be increased during the differentiation process of CACO2 cells (Mariadason et al., 2001). Therefore, CACO2-sh53 cell line was cultured for 21 days in order to differentiate cells. Then, cells were immunostained against E-cadherin and β-catenin and analyzed under confocal fluorescence microscope. No differences were observed in the intensity or localization of E-cadherin and β-catenin between CACO2 cells with endogenous MYO6 expression and reduced MYO6 expression (**Fig. 35**).

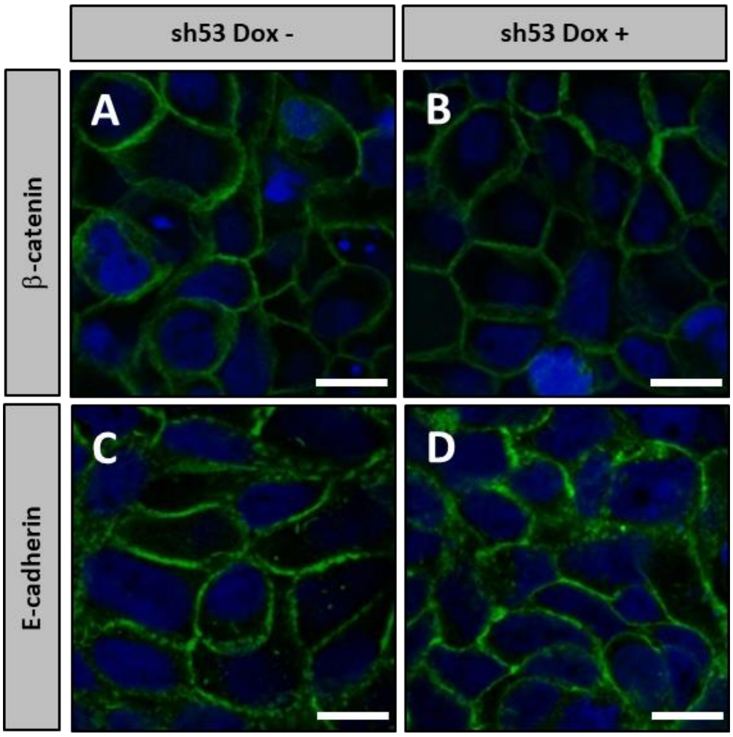

Figure 35: Role of MYO6 downregulation on the localization of proteins of the adherens junctions in CACO2 cells. Immunostaining of β-catenin **(A-B)** and E-cadherin **(C-D)** in CACO2 cells with endogenous MYO6 expression (sh53 Dox -) and with reduced MYO6 expression (sh53 Dox +). Dox -: no doxycycline treatment. Dox +: Doxycycline treated. Scale bars: 10 μm.

The *LKB1* gene encodes a serine/threonine kinase that is found mutated in the germline of the majority the 'Peutz-Jeghers cancer syndrome' (PJS) patients. These patients are characterized by the presence of hamartomas (benign tumors with disorganized differentiated cells) in the gastrointestinal tract. LKB1 has been found to have a key role in mammalian intestinal epithelial cell polarization. Strikingly, LKB1 activation promotes the polarization of colon cancer cells in the absence of cell-cell and cell-extracellular-matrix contacts. Moreover, cells form an actin-rich apical brush border and localize the tight junction component ZO-1 and the adherens junction component p120 in circles around the brush border (Baas et al., 2004). Therefore, to study the possible involvement of MYO6 in the polarization process of colon cancer cells through the **LKB1-dependent pathway**, LS174T-W4 cell line was used. This cell line has been modified to overexpress the pseudokinase STRAD in an inducible manner and LKB1 constitutively. Upon doxycycline treatment, STRAD activates LKB1, triggering a complete polarization of the cells which can be visualized by the formation of an apical brush border (**Fig. 36B**). Reduction of MYO6 expression (**Fig. 36A**) did not affect the percentage of polarized LS174T-W4 cells upon doxycycline treatment (**Fig. 36C**), indicating that MYO6 does not regulate LKB1 dependent polarization.

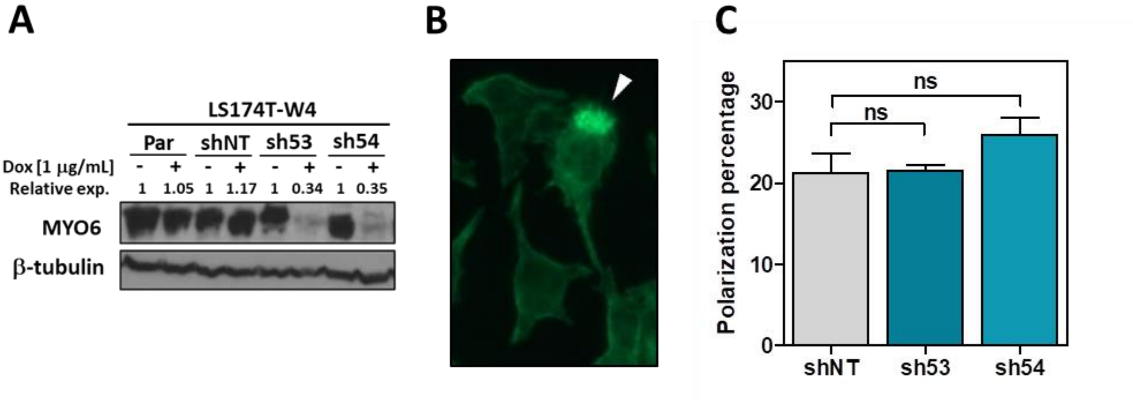

Figure 36: Effects of MYO6 downregulation on the LKB1-dependent polarization in LS174T-W4 cells. A) Western blot showing downregulation of MYO6 expression in LS174T-W4 derivative cell lines after 72 h of 1 μg/mL doxycycline (Dox) treatment. MYO6 expression was quantified in the different cell lines using ImageJ program and normalized to β-tubulin expression. The relative MYO6 expression, normalized to 'Dox -' conditions for each cell line, is indicated. β-tubulin expression is shown as a loading control. Par: Parental. **B)** Representative image of polarized LS174T-W4 cells after activation of the LKB1/STRAD pathway by 48 h of doxycycline treatment, as revealed by the apical accumulation of actin (white arrowhead; F-actin staining with rhodamine-phalloidin-Alexa488). **C)** Percentage of polarized LS174T-W4 cells after MYO6 downregulation (sh53 and sh54). The knockdown was induced with 1 μg/mL doxcycycline for 72 h. Then, cells were trypsinized and seeded on glass coverslips and allowed to polarize for another 48 h in presence of doxycycline. Average (±SEM) of three different experiments each carried out in triplicate is shown. ns: $p>0.05$; Student's t-test.

Collectively, these results indicate that the loss of MYO6 does not contribute to the loss of differentiation and polarization of colon cancer cells.

4. Downregulation of MYO6 expression does not affect the growth of colon cancer cells *in vitro*, but it increases their growth *in vivo*.

The ability to sustain **rapid uncontrolled growth** is one of the hallmarks of cancer development and it is acquired during the initial phases of tumorigenic process (Hanahan & Weinberg, 2011). Thus, the engineered cell line systems were used to study the possible role of MYO6 on the growth of colon cancer cells *in vitro*, as determined by directly counting the number of cells over time (**Fig. 37A-C**) or by using sulforhodamine B (SRB) staining (**Fig. 37D-F**) as a surrogate cell growth. In both procedures, MYO6 reduction did not affect the growth rate of any of the three cell lines studied. Note that the CACO2-sh55 cell line showed limited growth capability under the low seeding density conditions used, for reasons that were not further investigated.

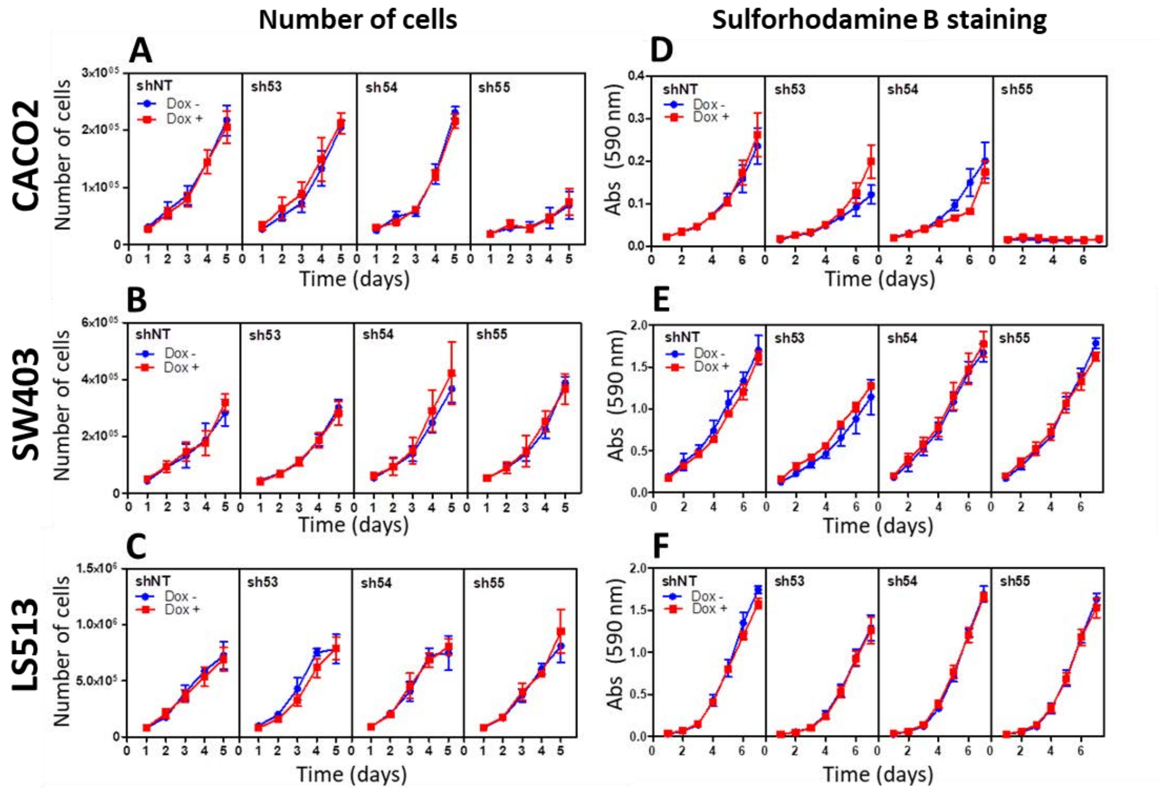

Figure 37: Role of MYO6 on the growth of colon cancer cells *in vitro* under normal attachment conditions. (A-C) Effects of MYO6 downregulation on the growth of **A)** CACO2, **B)** SW403 and **C)** LS513 cells assessed by direct cell counting at the indicated time points after seeding on cell culture plates. The mean (±SEM) of three independent experiments each run in triplicate is presented. **(D-F)** Effects of MYO6 downregulation on the growth of **D)** CACO2, **E)** SW403 and **F)** LS513 cells assessed by SRB staining and absorbance (Abs) measurement at the indicated time points after seeding on cell culture plates. The mean (±SEM) of three independent experiments, each with eight replicates is presented. No significant differences were observed (Student's t-test $p>0.05$). Dox -: no doxycycline treatment. Dox +: doxycycline treated (1 μg/mL).

The ability of a single cell to sustain long-term proliferation and **form a colony** is also an important feature of tumorigenesis that contributes to the uncontrolled growth. Two different approaches were used to assess the colony forming capability of the engineered cell line systems. First, a clonogenicity assay was used to investigate possible changes in the long-term proliferative capacity of colon cancer cells on a **solid substrate**. Second, the long-term proliferative capacity of colon cancer cells was assessed on a **semisolid substrate** (soft agar) to investigate the possible role of MYO6 on cell growth without attachment to a basement membrane, a hallmark of carcinogenesis.

The downregulation of MYO6 did not alter the ability of these three colon cancer cell lines to form colonies neither on a solid (**Fig. 38A-C**) nor on a semisolid substrate (**Fig. 38D**). Note that CACO2-sh55 cells were unable to form colonies under the low density seeding condition used; and CACO2 and SW403 cell lines were not able to grow in soft agar.

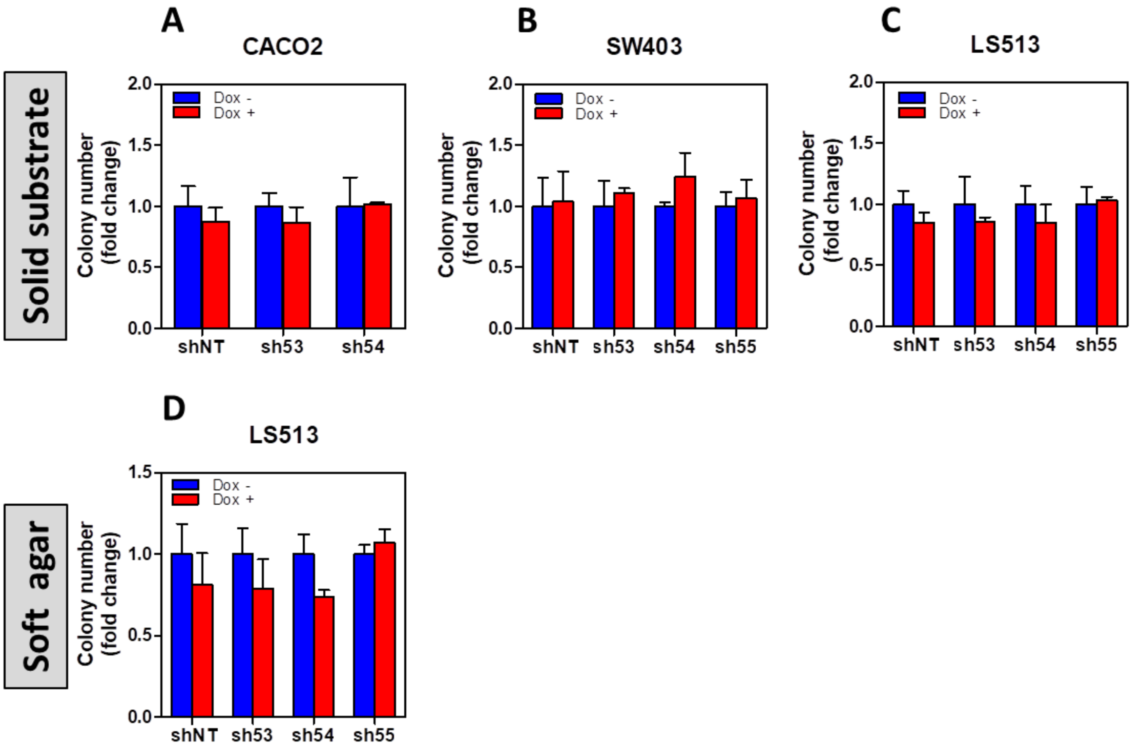

Figure 38: Role of MYO6 on the colony forming ability of colon cancer cells *in vitro*. (A-C) Fold change of the number of colonies formed by **A)** CACO2, **B)** SW403 and **C)** LS513 derivative cells, with (Dox +) and without (Dox -) 1 μg/mL doxycycline, on a solid substrate. **D)** Fold change of the number of colonies observed for LS513 derivative cells, with and without 1 μg/mL doxycycline, on a semisolid substrate (Soft agar). Fold changes are normalized to the number of colonies of the 'no-doxycycline' (Dox -) conditions for each cell line. The mean (±SEM) of three independent experiments each carried out in triplicate is shown. No significant differences were observed (Student's t-test p>0.05).

Next, the possible effect of MYO6 on the growth of colon cancer cells was assessed ***in vivo*** using a subcutaneous xenograft model. sh53 (shRNA against MYO6) and shNT (control) derivative lines from CACO2, SW403 and LS513 were subcutaneously injected in the left and in the right flanks of the NOD/SCID immunodeficient mice, respectively. All animals received doxycycline over the whole experiment (only 'Dox +' conditions) and tumor growth was monitored over time.

Although there was no significant difference in the time required for grafting of the tumors formed by control CACO2-shNT and CACO2-sh53 cells (**Fig. 39B**; Log-rank test p=0.23), reduced MYO6 expression resulted in significantly faster growth of **CACO2** xenografts (**Fig. 39A**), indicating that the loss/reduction of MYO6 expression could play a role in tumor progression. As expected, at the end of the experiment, reduced MYO6 protein expression was confirmed by immunohistochemistry (**Fig. 39C**) in the xenografts formed by the CACO2-sh53 cells compared to the CACO2-shNT control cells.

Two hours before being euthanized, all animals were intraperitoneally injected with 100 mg/Kg of bromodeoxyuridine (BrdU), a synthetic thymidine analog that is incorporated into newly synthesized DNA during S-phase of the cell cycle. In CACO2 xenografts, reduced MYO6 expression was found to be associated with a significant increase in the percentage of proliferating cells (BrdU-positive cells; **Fig. 39D-E**) suggesting that MYO6 regulates the cell division rate *in vivo*. No differences were observed in the percentages of apoptotic cells (active caspase 3-positive cells) between CACO2 xenografts with endogenous and with reduced MYO6 expression (**Fig. 39F-G**).

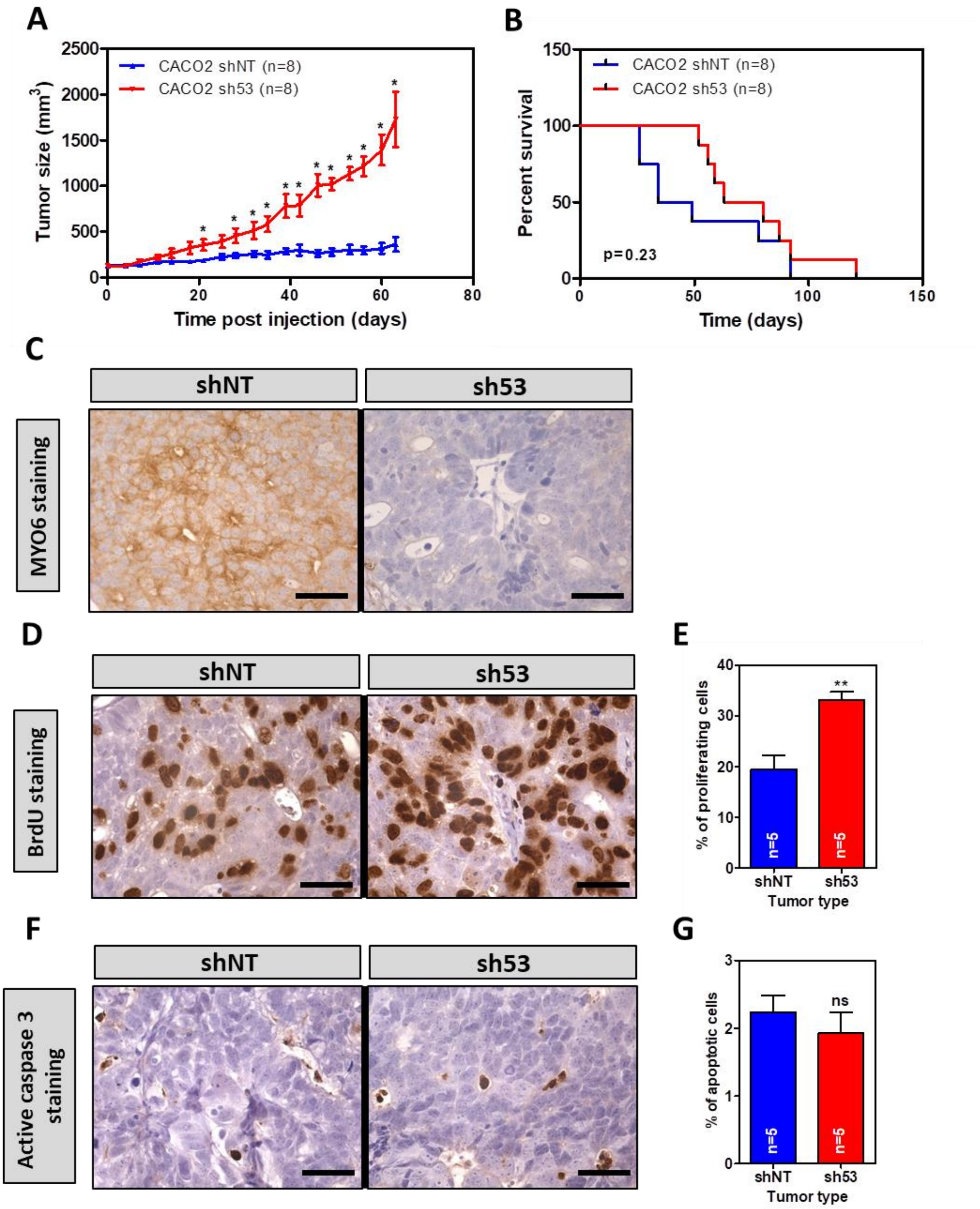

Figure 39: Effects of MYO6 downregulation on the growth of CACO2 cells *in vivo*. A) Growth of CACO2-shNT (control) and CACO2-sh53 cells over time when grown as subcutaneous xenograft tumors in immunodeficient NOD/SCID mice. Animals received doxycycline in the drinking water (1 mg/mL). The average tumor size (±SEM) is shown. n: number of animals per group. **B)** Tumor-free survival of animals injected with CACO2-shNT and CACO2-sh53 cells. Log-rank test p value is shown. **C)** Detection of MYO6 by immunohistochemistry in formalin-fixed, paraffin-embedded xenograft tumor samples from CACO2 derivative shNT and sh53 cell lines. **D)** Detection of proliferating cells in xenograft tumor samples generated from CACO2-shNT and CACO2-sh53 cells, by immunohistochemistry with an antibody against

bromodeoxyuridine (BrdU). **E)** Average (±SEM) percentage of BrdU positive cells in xenograft tumor samples from CACO2-shNT and CACO2-sh53 cells. A minimum of 1,000 cells were scored per tumor sample. **F)** Apoptotic cells were detected in xenograft tumor samples from CACO2-shNT and CACO2-sh53 cells by immunohistochemistry with an antibody against active caspase 3. **G)** Average (±SEM) percentage of apoptotic cells in xenograft tumor samples from CACO2-shNT and CACO2-sh53 cells. A minimum of 1,000 cells were scored per tumor sample. ns: $p>0.05$; *$p<0.05$; **$p<0.01$; Student's t-test. Scale bars: 50 μm.

In **SW403** cell xenografts, reduced expression of MYO6 was also found to increase tumor growth (**Fig. 40A**) further supporting that the loss of MYO6 likely plays an important role in tumor growth *in vivo*. No differences were observed in the time for tumor grafting between SW403-sh53 and control SW403-shNT cells (**Fig. 40B**). Robust MYO6 downregulation was confirmed by immunohistochemistry (**Fig. 40C**) in SW403-sh53 cell xenografts treated with doxycycline but not in the corresponding SW403-shNT control cells.

Moreover, in SW403 xenografts, reduced MYO6 expression was observed to be associated with a significant increase in the percentage of proliferating cells (BrdU-positive cells; **Fig. 40D-E**), further suggesting that the loss of MYO6 affects the proliferation of colon cancer cells *in vivo*. No differences were observed in the percentages of apoptotic cells (active caspase 3-positive cells) between SW403 xenografts with endogenous and reduced MYO6 expression (**Fig. 40F-G**).

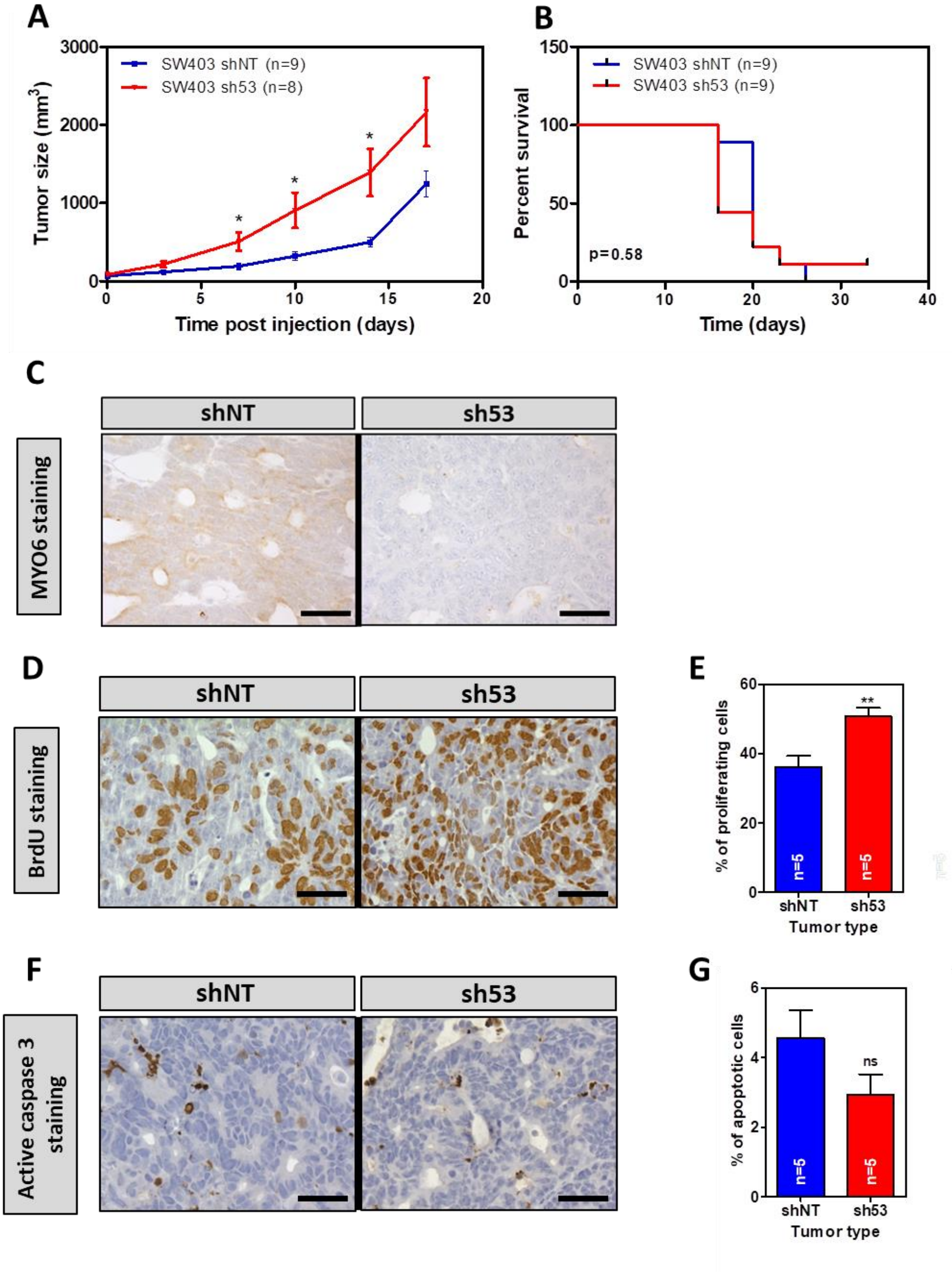

Figure 40: Effects of MYO6 downregulation on the growth of SW403 cells *in vivo*. A) Growth of SW403-shNT (control) and SW403-sh53 cells over time when grown as subcutaneous xenograft tumors in immunodeficient NOD/SCID mice. Animals received doxycycline in the drinking water (1 mg/mL). The average tumor size (±SEM) is shown. n: number of animals per group. **B)** Tumor-free survival of animals injected with SW403-shNT and SW403-sh53 cells. Log-rank test p value is shown. **C)** Detection of MYO6 by immunohistochemistry in formalin-fixed, paraffin-embedded xenograft tumor samples from SW403 derivative shNT and sh53 cell lines. **D)** Detection of proliferating cells in xenograft tumor samples generated from SW403-shNT and SW403-sh53 cells, by immunohistochemistry with an antibody against bromodeoxyuridine (BrdU). **E)** Average (±SEM) percentage of BrdU positive cells in xenograft tumor samples from SW403-shNT and SW403-sh53 cells. A minimum of 1,000 cells were scored per tumor sample. **F)** Apoptotic cells were detected in xenograft tumor samples from SW403-shNT and SW403-sh53 cells, by immunohistochemistry with an antibody against active caspase 3. **G)** Average (±SEM) percentage of apoptotic cells in xenograft tumor samples from SW403-shNT and sh53 cells. A minimum

of 1,000 cells were scored per tumor sample. ns: $p > 0.05$; *$p < 0.05$; **$p < 0.01$; Student's t-test. Scale bars: 50 μm.

However, MYO6 downregulation did not affect the growth of **LS513** xenograft tumors (**Fig. 41A**) although it did accelerate the grafting time of tumors (**Fig. 41B**). MYO6 protein expression was confirmed to be substantially reduced in LS513-sh53 xenograft tumors compared to tumors derived from control SW403-shNT cells under doxycycline treatment, as shown by immunohistochemistry (**Fig. 41C**). In good agreement with this result, the reduction of MYO6 did not change significantly neither the percentage of proliferating cells (BrdU-positive cells; **Fig. 41D-E**) nor the percentage of apoptotic cells (active caspase 3-positive cells; **Fig 41F-G**).

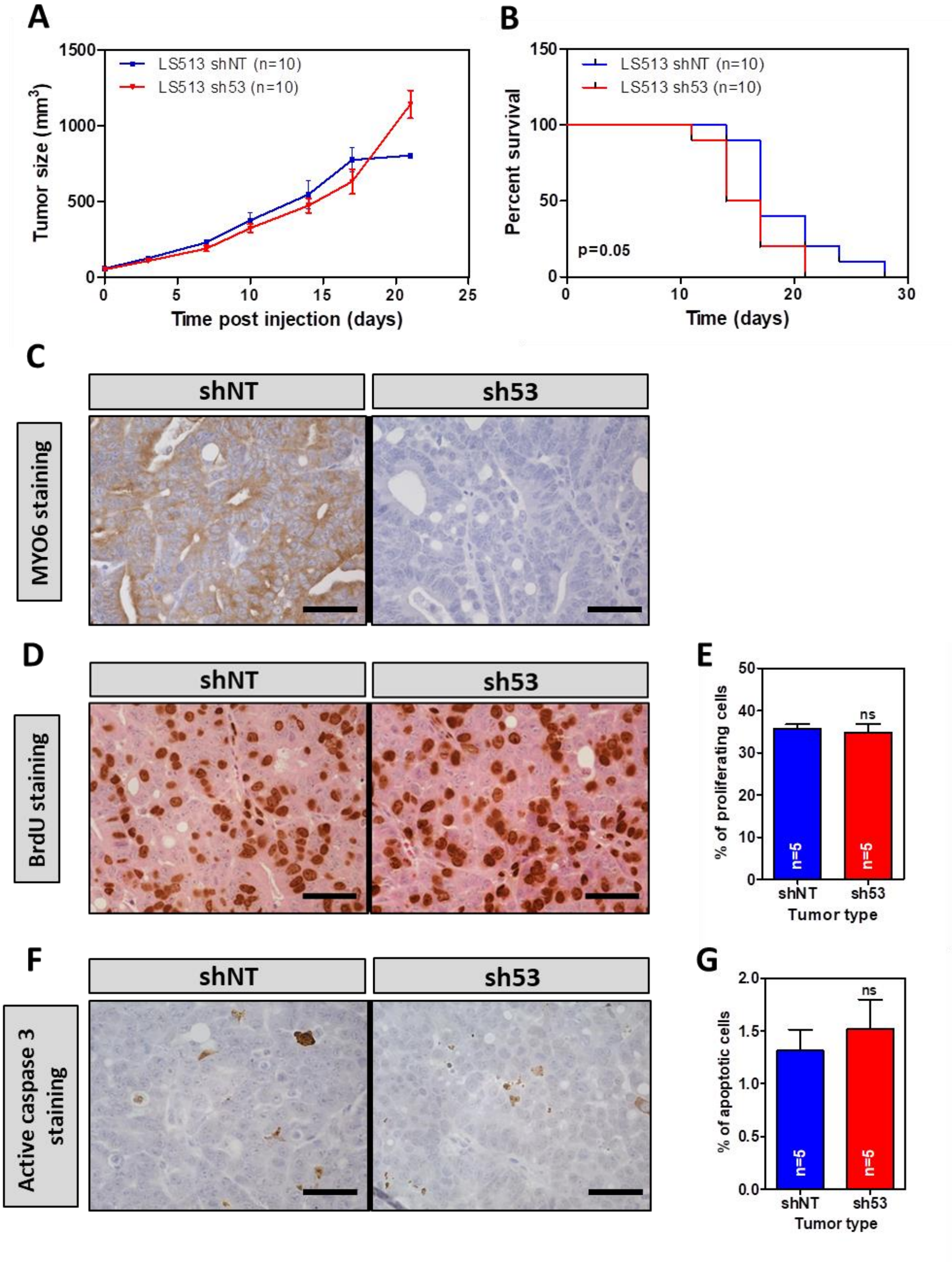

Figure 41: Effects of MYO6 downregulation on the growth of LS513 cells *in vivo*. A) Growth of LS513 shNT (control) and LS513-sh53 cells over time when grown as subcutaneous xenograft tumors in immunodeficient NOD/SCID mice. Animals received doxycycline in the drinking water (1 mg/mL). The average tumor size (±SEM) is shown. n: number of animals per group. **B)** Tumor-free survival of animals injected with LS513-shNT and LS513-sh53 cells. Log-rank test p value is shown. **C)** Detection of MYO6 by immunohistochemistry in formalin-fixed, paraffin-embedded xenograft tumor samples from LS513 derivative shNT and sh53 cell lines. **D)** Detection of proliferating cells in xenograft tumor samples from LS513-shNT and LS513-sh53 cells, by immunohistochemistry with an antibody against bromodeoxyuridine (BrdU). **E)** Average (±SEM) percentage of BrdU positive cells in xenograft tumor samples from LS513-shNT and LS513-sh53 cells. A minimum of 1,000 cells were scored per tumor sample. **F)** Apoptotic cells were detected in xenograft tumor samples from LS513-shNT and LS513-sh53 cells, by immunohistochemistry with an antibody against active caspase 3. **G)** Average (±SEM) percentage of apoptotic cells in xenograft tumor samples from LS513-shNT and LS513-sh53 cells. A minimum of 1,000 cells were scored per tumor sample. ns: p>0.05; Student's t-test. Scale bars: 50 μm.

Collectively, these results demonstrate that reduced MYO6 expression results in significantly increased growth of at least some colon cancer cells and that this is associated with increased proliferation *in vivo*, although MYO6 did not regulate the growth of colon cancer cells *in vitro*.

5. Downregulation of MYO6 expression does not change the metastatic potential of colon cancer cells.

Other hallmark of cancer is the capability of tumor cells to activate invasion and metastasis. During carcinogenesis, tumor cells are able to modify their attachment to other cells and to the extracellular matrix (ECM) and to acquire migration and invasive capacities. Consequently, they first invade surrounding tissues and later distant tissues forming metastasis (Hanahan & Weinberg, 2011).

MYO6 has been involved in ovarian and prostate cancer cells' migration and invasion (Dunn et al., 2006; Yoshida et al., 2004). Therefore, the involvement of MYO6 in the motility and invasiveness of colon cancer cells was studied. In order to investigate the **migration** capability of cells ***in vitro***, a 'wound-healing' assay was first used, in which a confluent culture is scratched creating a region free of cells and repopulation of this area is monitored over time. The migration ability was not affected by MYO6 reduction in LS513 derivative cells (**Fig. 42A**). As CACO2 and SW403 cells show very limited migration capacity to repopulate scratched areas (data not shown), a 'transwell migration' assay was used to assess their migration capability, in which cells are stimulated to migrate towards the lower chamber through a porous membrane by chemoattraction (high concentration of fetal bovine serum). Downregulation of MYO6 in CACO2 and SW403 cells did not affect their migration capacity under these conditions (**Fig. 42B-C**).

A similar transwell assay was used to examine the ***in vitro*** **invasion** capacity of colon cancer cells, but in this case, cells were embedded in a matrix of matrigel, an extracellular matrix secreted by Engelbreth-Holm-Swarm (EHS) mouse sarcoma cells. Therefore, cells had to degrade matrix and invade through it before being able to migrate into the lower chamber of the transwell insert. Invasion capability of CACO2 cells was not affected by reduced MYO6 expression (**Fig. 42D**). SW403 and LS513 cell lines showed very limited invasion capability and changes in the invasive potential could not be assessed under these conditions.

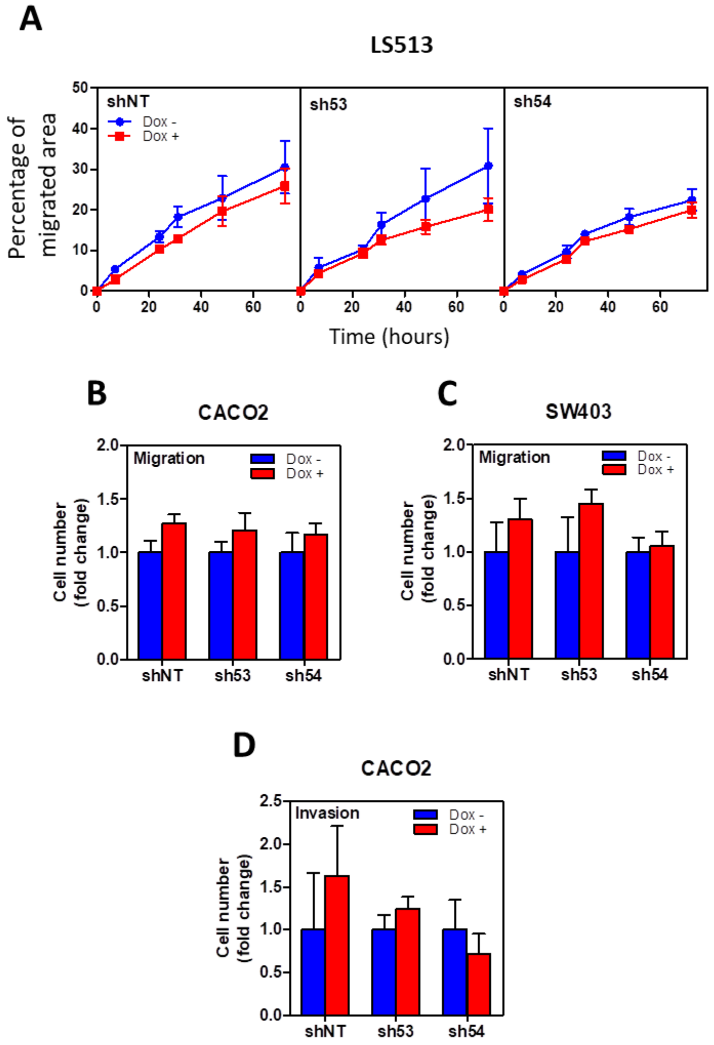

Figure 42: Role of MYO6 downregulation on the migration and invasion capability of colon cancer cells. A) Percentage of the wounded area repopulated by LS513 derivative cells with (Dox +) and without (Dox -) doxycycline (1 µg/mL) at different timepoints, assessed in a wound-healing assay. **(B-C)** Fold change numbers of migrating **B)** CACO2 and **C)** SW403 derivative cells which were treated or not with 1 µg/mL doxycycline and assessed in a Boyden chamber. Fold changes are normalized to the number of colonies of the 'no-doxycycline' conditions for each cell line. **D)** Fold change numbers of matrigel invading CACO2 derivative cells which were treated or not with 1 µg/mL doxycycline. For all the assays the average (±SEM) of three independent experiments each carried out in triplicate is shown. No significant differences were observed (Student's t-test p>0.05).

To further investigate the possible role of MYO6 in migration and invasion, different ***in vivo*** experimental metastasis assays were carried out in NOD/SCID mice. These assays only address the late steps of 'invasion-metastasis cascade', such as survival while being transported in the bloodstream, escape of cells from circulation (extravasation), and growth of cells to form secondary tumors in a new organ environment (Elkin & Vlodavsky, 2001). The most common organs metastasized by colorectal tumors are the liver and the lungs (Qiu, Hu, Yang, Cosgrove, & Xu, 2015; Riihimäki, Hemminki, Sundquist, & Hemminki, 2016). Therefore, experimental models of lung and liver metastasis were carried out to assess the role of MYO6 in the metastatic capacity of colon cancer cells.

A **lung metastasis approach** was carried out for LS513-sh53 cell line, by injecting cells through the tail vain. Following their release into circulation, most cells colonize the lungs, simply because this is the first capillary bed encountered, although some cells could recirculate and be trapped in other organs (Elkin & Vlodavsky, 2001). Cells under doxycycline treatment (Dox +) or not (Dox -) were let to metastasize for 7 weeks. The number and area of microscopic metastases in the lungs were scored in histological sections blinded from the identity of the animal, and no significant differences were observed between animals injected with the control LS513-sh53 (Dox -) or the MYO6 knockdown LS513-sh53 (Dox +) cells (**Fig. 43**). SW403 and CACO2 cell lines did not show any lung metastasizing ability (data not shown).

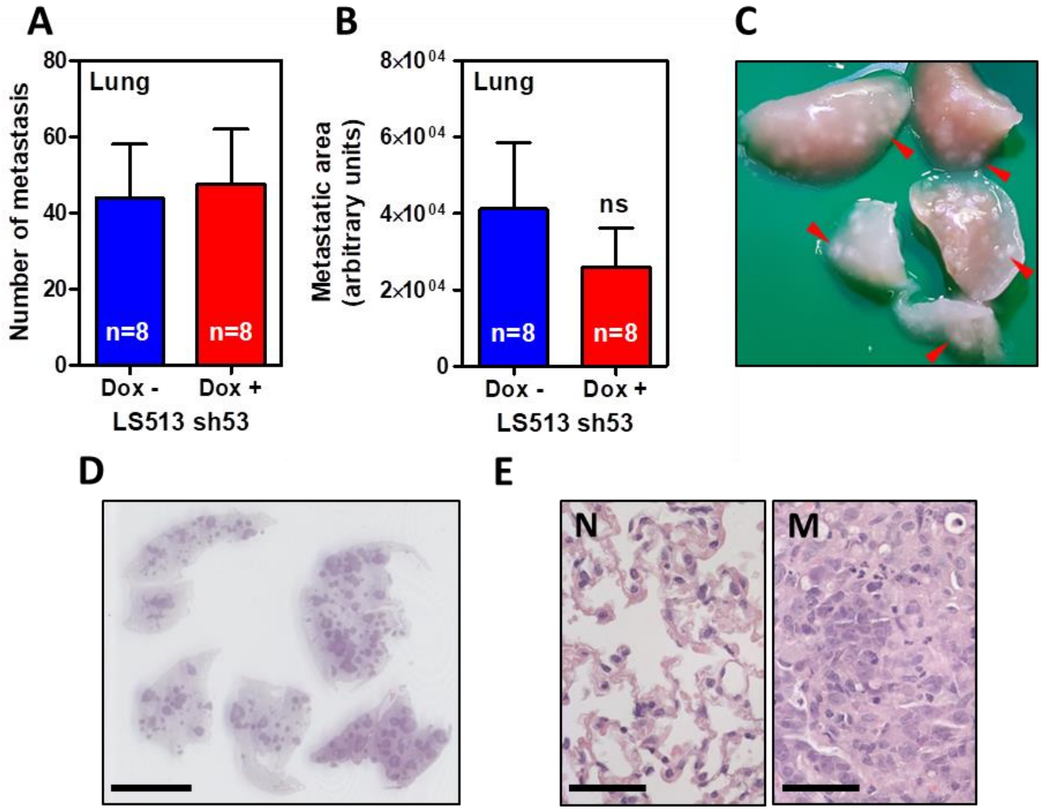

Figure 43: Role of MYO6 in the lung metastasizing capability of LS513 cells. (A-B) Average (±SEM) **A)** number and **B)** area of metastasis formed by LS513-sh53 cells treated (Dox +) or not (Dox -) with doxycycline in lungs of NOD/SCID mice. One formalin-fixed, paraffin-embedded lung sample section was quantified for each animal using ImageJ program. n: number of animals. No significant differences were observed (Student's t-test ns: $p>0.05$). **C)** Representative image of 5 lung-lobes containing lung-metastases (red arrowheads), after mouse dissection. **D)** Representative image of a formalin-fixed, paraffin-embedded lung sample section stained with hematoxylin-eosin. Scale bar: 5 mm. Darker areas represent metastatic areas. **E)** Higher magnification images of lung normal tissue (N) and metastasis (M) from a formalin-fixed, paraffin-embedded lung sample section stained with hematoxylin-eosin. Scale bar: 50 μm. Dox -: no doxycycline treatment. Dox +: doxycycline treated (1 mg/mL in the drinking water).

Next, an experimental model of **liver metastasis** was used to further investigate the role of MYO6 in the metastatic capacity of colon cancer cells. Control (Dox -) or MYO6 knockdown (Dox +) SW403-sh53 cells were injected into the spleen of NOD/SCID immunodeficient mice, thus allowing liver invasion through the splenic vein which connects with the superior mesenteric vein to become the hepatic portal vein (Rajendran et al., 2010; Soares et al., 2014). After 10 weeks, presence of liver metastases was assessed macroscopically under stereomicroscope (**Fig. 44A-B**) and microscopically in histological sections stained with hematoxylin-eosin (**Fig. 44C-D**). Strikingly, no metastases were observed in female mice from both, ‘doxycycling receiving’ (Dox+) and not treated (Dox -) groups. However, a trend towards an increased metastatic incidence was observed in males receiving doxycycline (Dox +) compared to control males (Dox -), although it did not reach statistical significance likely due to the low number of male mice (**Fig. 44E**). However, the liver areas affected by the metastatic lesions formed by SW403-sh53 cells were similar in both doxycycline treated (Dox +) and control (Dox -) animal groups (no statistical analysis can be done due to only one animal presented metastatic lesions in the control group) (**Fig. 44F**). Considering the gender bias, a new liver metastasis experiment should be carried out only using male mice. Although preliminary experiments showed that CACO2 cells do not have liver metastatic capacity under these conditions, LS513 cells were able to metastasize the liver of NOD/SCID mice (preliminary data not shown), and a liver metastasis experiment could be carried out with this cell line to further investigate the role of MYO6 in metastatic potential.

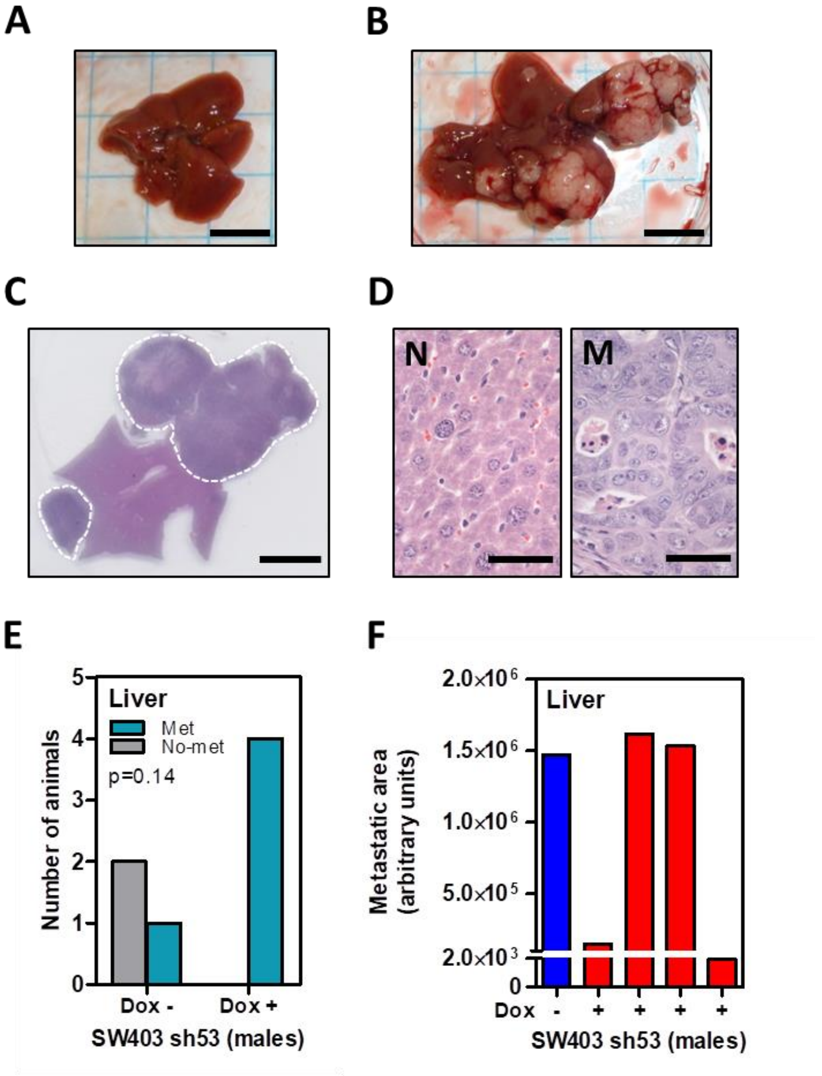

Figure 44: Role of MYO6 in the liver metastasizing capability of SW403 cells. (A-B) Representative images of livers **A)** without metastases or **B)** containing metastases (white masses), after mouse dissection. Scale bars: 1 cm. **C)** Representative image of a formalin-fixed, paraffin-embedded liver section stained with hematoxylin-eosin. Darker areas (circled with white lines) represent metastatic areas. Scale bar: 5 mm. **D)** Higher magnification images of liver normal tissue (N) and metastasis (M) from a formalin-fixed, paraffin-embedded liver sample section stained with hematoxylin-eosin. Scale bars: 50 μm. **E)** Number of male animals with liver metastatic lesions (Met) or without metastasis (No-met) in control (Dox -) or MYO6 knockdown (Dox +) groups. Fisher's exact test p value is shown. **F)** Liver area affected by the metastatic lesions formed by LS513-sh53 cells in each male NOD/SCID mice from control (Dox -; blue columns) or doxycycline receiving (Dox +; red columns) groups (area quantified using ImageJ program). No statistical analysis can be performed, because there is only one animal in the control group. Dox -: no doxycycline treatment. Dox +: doxycycline treated (1 mg/mL in the drinking water).

Collectively, these results indicate that MYO6 does not regulate neither the *in vitro* migration and invasion ability, nor the capacity to metastasize lungs *in vivo* of colon cancer cells, although the loss of MYO6 may increase their ability to metastasize liver.

6. Absence of MYO6 in deficient mice has no effects on intestinal tumorigenesis.

A limitation of *in vitro* experiments is that they do not completely reproduce the complexity of a tumor growing in the host organism, which includes the interaction between tumor and stroma, vascularization, immune system, hormonal signaling and responses, etc. Therefore, to further investigate the implication of MYO6 in intestinal tumorigenesis two different mouse models of intestinal tumorigenesis were used.

Snell's Waltzer mice contain a recessive mutation in *Myo6* gene (*sv*). Homozygous mice for the *sv* mutation present a complete absence of MYO6 protein in the whole body (Avraham et al., 1995). The phenotype of *Myo6*$^{sv/sv}$ mice is characterized by deafness, hyperactivity, jerking movement of the head and a strong tendency to run in circles (Deol & Green, 1966). The absence of MYO6 protein was confirmed in the small intestine of *Myo6*$^{sv/sv}$ mice by immunohistochemistry (**Fig. 45**).

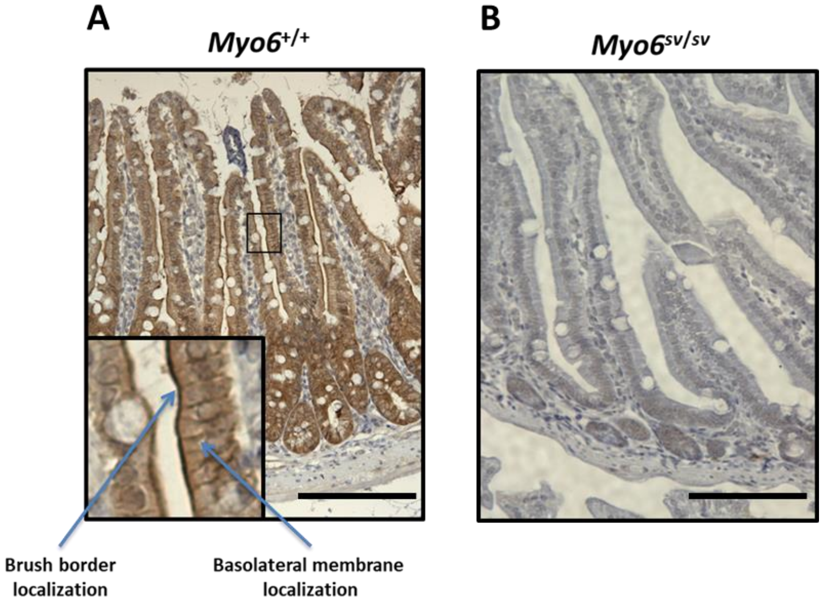

Figure 45: Characterization of *Myo6*$^{sv/sv}$ (Snell's Waltzer) mice. A) MYO6 detection by immunohistochemistry in *Myo6*$^{+/+}$ mouse normal small intestine. Note that MYO6 is mainly localized to the brush border and basolateral membrane of intestinal epithelial cells. **B)** MYO6 immunostaining in *Myo6*$^{sv/sv}$ mouse normal small intestine. Scale bars: 100 μm.

To date, no predisposition to any form of cancer has been reported in *Myo6*$^{sv/sv}$ mice and MYO6 deficient mice have a lifespan comparable to their heterozygous or wild-type littermates, indicating that the absence of MYO6 *per se* most probably does not generate any life shortening disease, such as cancer (Gotoh et al., 2010). Therefore, in order to initiate the oncogenic process and thus, be able to investigate whether the loss of MYO6 affects tumor progression, two different approaches were used: the tumorigenic process was initiated either genetically, using a mutation in the *Apc* gene, or pharmacologically using the intestine-specific azoxymethane (AOM) carcinogen.

The **genetic approach** consisted in crossing mice from the Snell's Waltzer colony with *Apc*$^{\mathrm{Min}}$ (Multiple Intestinal Neoplasia) mice, which carry a heterozygous inactivating mutation in the *Apc* tumor suppressor gene (*Apc*^{Min} mutation) (Su et al., 1992). This mutation, on the C57BL6/J genetic background, leads to the development of multiple tumors (polyps) throughout the intestinal tract (Shoemaker et al., 1998).

Apc^{Min} mutation bearing mice have premature death due to the anemia and intestinal blockage caused by the polyps (Moser et al., 1990). To investigate whether the lack of MYO6 had any additional effect on the lifespan of the animals, **survival differences** between *Apc*^{Min} mice homozygous for the wild-type *Myo6* allele (*Myo6*$^{+/+}$) and homozygous for the inactive Snell's Waltzer *Myo6* allele (*Myo6*$^{\mathrm{sv/sv}}$) were assessed. Kaplan-Meier curves showed that the lifespan of *Apc*$^{Min/+}$ mice was not affected by the absence of MYO6 ($p=0.69$; Log-rank test). The median survival of *Myo6*$^{+/+}$*;Apc*$^{Min/+}$ and *Myo6*$^{sv/sv}$*;Apc*$^{Min/+}$ animals was 168 and 158 days, respectively (**Fig. 46A**).

Nonetheless, to investigate whether MYO6 ablation affected the **tumor number**, **location** and **size** of tumors in *Apc*$^{Min/+}$ mice, an independent group of animals were euthanized at 110 days (16 weeks) of age and their small and large intestines were dissected out and analyzed under a stereomicroscope. No significant differences were observed in the number of large intestinal tumors (**Fig. 46B**) or their size (**Fig. 46C**) between *Myo6*$^{+/+}$*;Apc*$^{Min/+}$ and *Myo6*$^{sv/sv}$*;Apc*$^{Min/+}$ animals. However, a reduction in the number of small intestinal tumors was observed in MYO6 deficient mice (*Myo6*$^{sv/sv}$*;Apc*$^{Min/+}$) compared to control mice (*Myo6*$^{+/+}$*;Apc*$^{Min/+}$) (**Fig. 46D**), although there were no differences in the size of these tumors (**Fig. 46E**). This result was confirmed by scoring the number of small intestinal tumors in hematoxylin-eosin stained histological sections from the same animals (**Fig. 46F-G**). Importantly, a reduction of MYO6 expression was observed in intestinal tumors of *Myo6*$^{+/+}$;*Apc*$^{\mathrm{Min/+}}$ animals compared to their normal intestinal tissue (**Fig. 46H**), which is consistent with the reduced MYO6 expression observed in primary tumors of Dukes' C colorectal cancer patients compared to their normal tissue (**Fig. 28**).

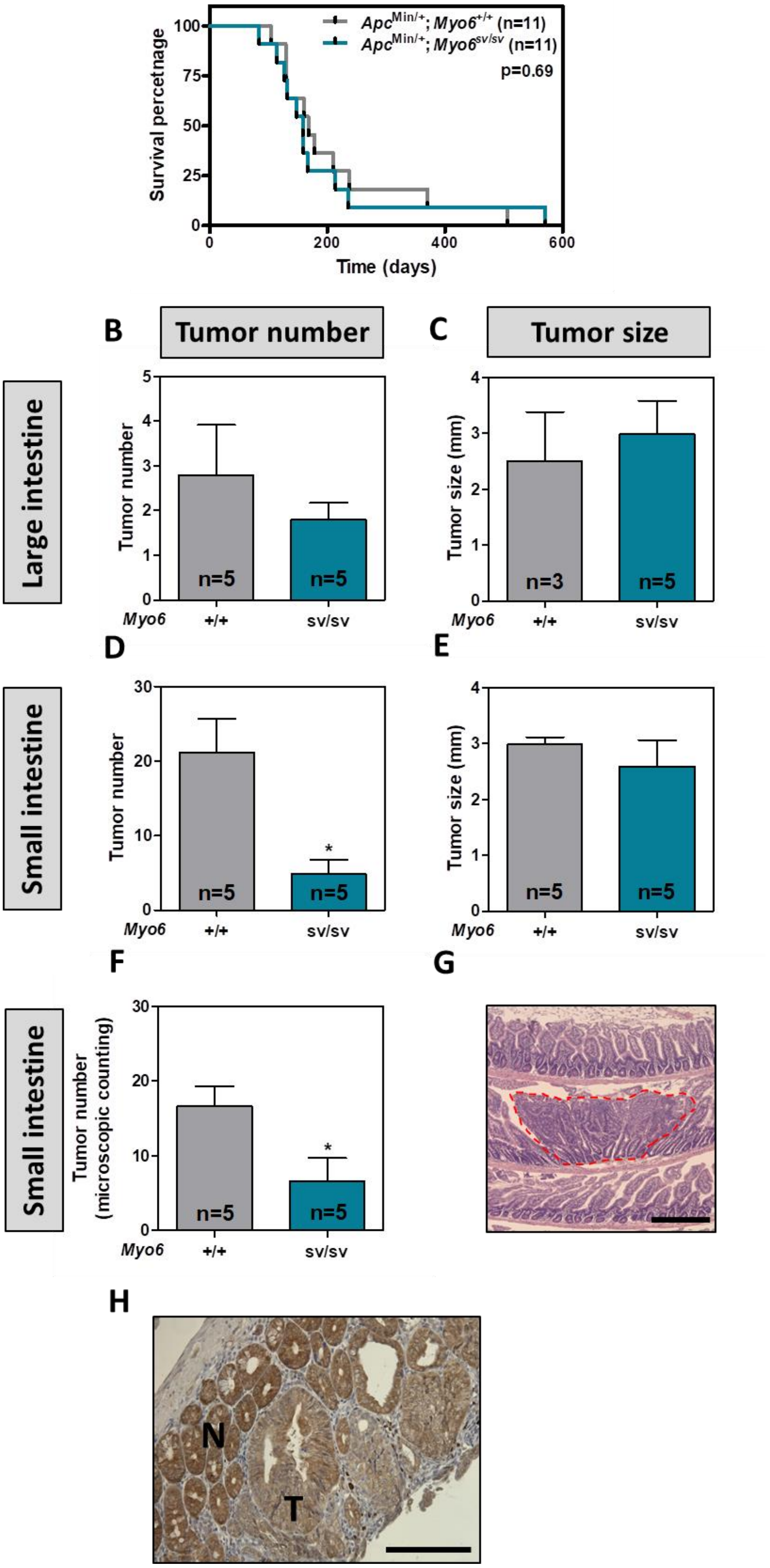

Figure 46: Effects of *Myo6* inactivation on intestinal tumorigenesis in *Apc*$^{Min/+}$ mice. A) Survival curves (Kaplan-Meier curves) of *Apc*$^{Min/+}$ mice which are either wild-type (*Myo6*$^{+/+}$) or knock-out (*Myo6*$^{sv/sv}$) for *Myo6*. n: number of animals. Log-rank test p value is shown. **(B, C)** Average (±SEM) **B)** number and **C)**

size of macroscopically observed tumors in the large intestine of 110 day-old *Apc*$^{\mathrm{Min/+}}$ animals. **(D, E)** Average (±SEM) **D)** number and **E)** size of macroscopically observed tumors in the small intestine of 110 day-old *Apc*$^{\mathrm{Min/+}}$ animals. **F)** Average number (±SEM) of microscopically observed tumors in the small intestine of 110 day-old *Apc*$^{\mathrm{Min/+}}$ animals. n: number of animals. $^{*}p<0.05$; Student's t-test. **G)** Representative image of hematoxylin-eosin stained small intestinal sample from an *Apc*$^{\mathrm{Min/+}}$ mouse. Small intestine appears rolled up longitudinally with the mucosa side inwards (Swiss roll technique). Tumor area is circled with a red line. Scale bar: 400 µm. **H)** MYO6 immunostaining of intestinal tumors from a *Myo6*$^{+/+}$;*Apc*$^{\mathrm{Min/+}}$ mouse. Normal tissue (N) areas in the sample appear with higher staining intensity than tumor areas (T). Scale bar: 100 µm.

To further investigate if the loss of MYO6 affects the intestinal tumor progression, a **pharmacological approach** was also used as an alternative method of tumor initiation, by treating the animals (*Apc*$^{+/+}$) with the intestine-specific carcinogen azoxymethane (AOM) (Mazzolini et al., 2012; Rosenberg, Giardina, & Tanaka, 2009; De Robertis et al., 2011; Bissahoyo et al., 2005). Animals were intraperitoneally injected with AOM weekly for 12 weeks and then, allowed to form tumors for additional 9 weeks. At the end of the experiment, the **number** of intestinal tumors, their **localization** and **size** were analyzed and it was observed that the absence of MYO6 did not alter any of these parameters in the animals treated with AOM (**Fig. 47**).

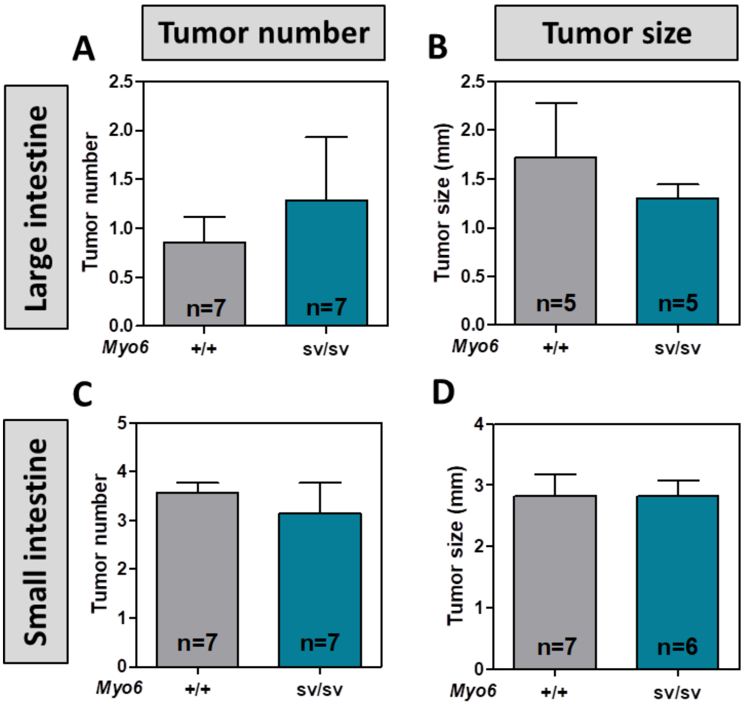

Figure 47: Effects of *Myo6* inactivation on AOM-induced intestinal tumorigenesis. (A, B) Average (±SEM) **A)** number and **B)** size of macroscopically observed tumors in the large intestine of AOM-treated animals. **(C, D)** Average (±SEM) **C)** number and **D)** size of macroscopically observed tumors in the small intestine of AOM-treated animals. n: number of animals. No significant differences were observed (Student's t-test $p>0.05$).

Altogether, these experiments indicate that the absence of MYO6 does not accelerate the tumor progression during the early stages of intestinal tumorigenesis in this specific mouse model. Importantly, it must be taken into consideration that *Myo6*$^{sv/sv}$ mice have significantly reduced body weight compared to *Myo6*$^{+/+}$ mice (**Fig. 48**), a phenotype that could be altering tumor progression in *Myo6*$^{sv/sv}$ animals (Aoi et al., 2010; Colbert et al., 2003; Ju et al., 2008; Kelly et al., 2017; Mehl et al., 2005).

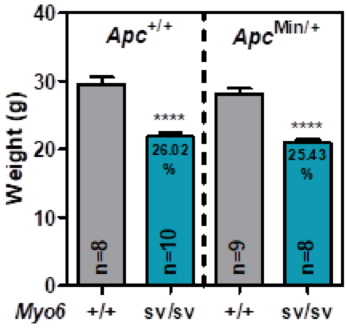

Figure 48: Effects of *Myo6* inactivation in the body weight of mice. Average weight (±SEM) of *Apc*$^{+/+}$ and *Apc*$^{Min/+}$ animals depending on their *Myo6* genotype at 10 weeks of age. n: number of animals. Percentage numbers at the top of the columns indicate percentage of weight reduction compared to their *Myo6*$^{+/+}$ controls. ****p<0.0001; Student's t-test.

7. Absence of MYO6 in mouse intestinal tumor derived organoids increases Wnt signaling.

As mentioned above, effects related to reduced body weight could be modulating intestinal tumorigenesis in Snell's Waltzer mice. Therefore, intestinal organoids derived from these mice were used to further investigate the loss of MYO6 in intestinal tumorigenesis, as an alternative system of an *in vivo* model that permits to avoid confounding effects related to animal weight loss.

Increased proliferation (number of cells in S-phase) was observed in xenografts formed by MYO6 knockdown colon cancer cells in immunodeficient NOD/SCID mice (**Fig. 39 and 40**) and, consistent with the shorter survival of CRC patients with low MYO6 tumor levels (**Fig. 27 and 29**), faster proliferative rates are associated with poor patient prognosis (Al-Sheneber, Shibata, Sampalis, & Jothy, 1993; Mayer et al., 1993; Sinicrope et al., 1999). Because canonical Wnt signaling is a master regulator of proliferation in colon cancer cells, (Sansom et al., 2004; Van de Wetering et al., 2002), the possible involvement of MYO6 in Wnt signaling regulation was investigated. Organoid cells were obtained from small intestinal tumors from *Myo6* wild-type (*Myo6*$^{+/+}$) or *Myo6* knock-out (*Myo6*$^{sv/sv}$) *Apc*$^{Min/+}$ mice. Briefly, small intestines of animals were dissected and areas with tumors were cut. Then, tumors were cut into small pieces and incubated with digestion solution containing 'type I collagenase' and 'type II dispase'. Finally, individual cells were resuspended in medium containing 50% matrigel (an extracellular matrix secreted by Engelbreth-Holm-Swarm (EHS) mouse sarcoma cells), seeded onto plates and allowed to form organoids. Organoid cells were infected with a ‘reporter plasmid’ (7TGC) containing mCherry gene (a type of red fluorescent protein) under SV40 promoter (constitutive expression) which allowed the discrimination between infected and uninfected cells, and green fluorescent protein (GFP) gene under the control of a promoter containing TCF4/β-catenin binding sites, which allowed the quantification of cells with detectable Wnt signaling. The absence of MYO6 was found to significantly increase the percentage of cells with detectable Wnt signaling (percentage of GFP-expressing cells within mCherrry expressing cells) (**Fig. 49A-B**). Moreover, the average levels of Wnt signaling (GFP intensity) were significantly increased in the organoids from *Myo6* knock-out mice (**Fig. 49C**). These results suggested that MYO6 could be a regulator of Wnt signaling in intestinal tumor cells.

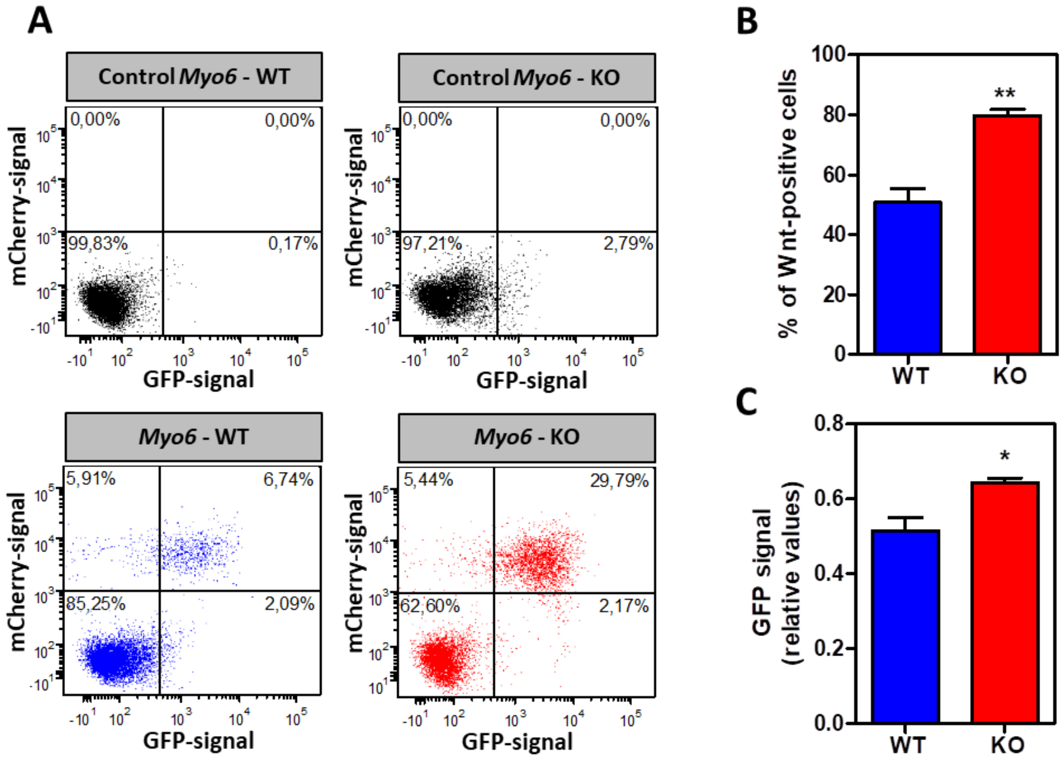

Figure 49: Role of MYO6 on Wnt signaling activation in organoids obtained from small intestinal tumors of $\mathit{Apc}^{Min/+}$ mice. A) Representative FACS dot plots of Wnt signaling detection experiments in murine intestinal tumor organoids. Control organoids represent organoids without ‘reporter plasmid’ (7TGC) infection. mCherry (a type of red fluorescent protein) is constitutively expressed (under SV40 promoter) in organoids infected with the ‘reporter plasmid’, and green fluorescent protein (GFP) is expressed upon Wnt signaling activation. Lower quadrants contain no infected organoid cells. Upper quadrants contain infected organoid cells and the top-right quadrant shows the percentage of organoid cells that are infected and have detectable Wnt signaling levels. **B)** Average percentage of Wnt-positive (mCherry and GFP-positive) organoid-cells derived from *Myo6* wild-type (WT) and *Myo6* knock-out (KO) $\mathit{Apc}^{Min/+}$ mice. **C)** Average relative Wnt signaling levels (mean GFP intensity normalized to mean mCherry intensity) of organoid-cells derived from *Myo6* wild-type (WT) and *Myo6* knock-out (KO) $\mathit{Apc}^{Min/+}$ mice. Average (±SEM) of four independent experiments is shown. *p<0.05; **p<0.01; Student’s t-test.

CHAPTER 5

DISCUSSION

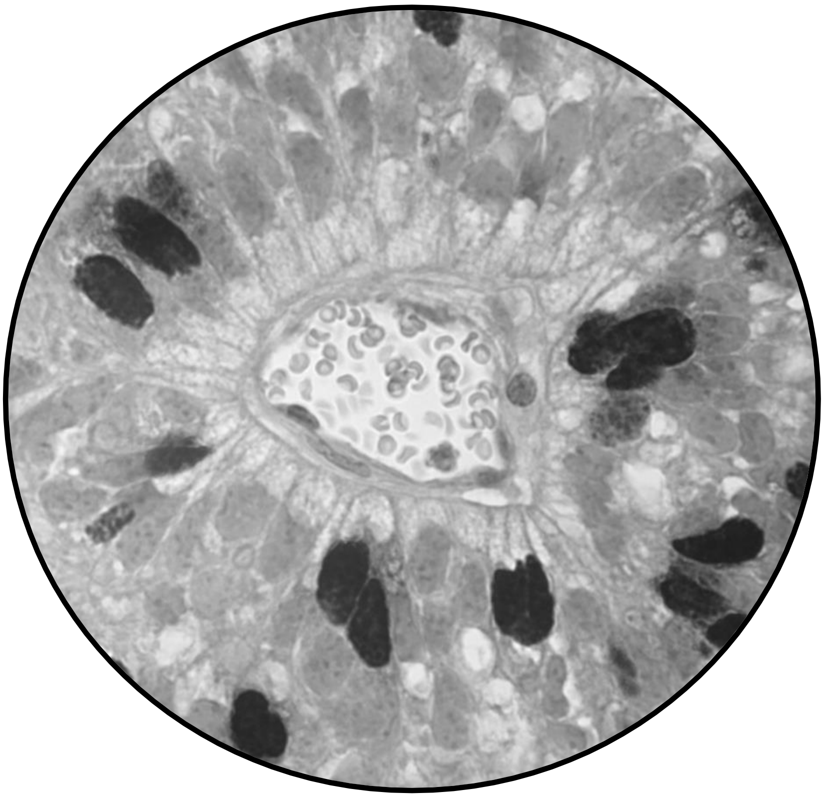

DISCUSSION

Myosin VI is a molecular motor that can anchor cargoes to actin filaments or provide short range trafficking along the actin cytoskeleton by using the energy from ATP hydrolysis (Peckham, 2011). Myosin VI moves towards the minus-end of actin filaments, in the opposite direction to the rest of myosins. Thus, it moves away from the plasma membrane into the cell and away from the surface of internal organelles (Folma Buss & Kendrick-Jones, 2008).

Myosin VI is expressed in most tissues, but its expression varies considerably among them ("The human protein atlas," 2017). Moreover, myosin VI can exist in several isoforms that are expressed in a tissue-specific and dynamic manner. That is, each tissue expresses a different set of isoforms, and the expressed isoforms can vary depending on the conditions and time within the same tissue. This tissue-specific expression of the isoforms likely represents a mechanism to control motor-cargo interactions and their subsequent cellular localization and function, since the isoforms interact with different binding partners (F. Buss et al., 1998; F Buss et al., 2001; T Hasson & Mooseker, 1994; Tumbarello et al., 2013). Myosin VI is highly expressed in the epithelial cells of the small and large intestine, being mainly localized to the apical and basolateral membranes (Hegan et al., 2012).

The trafficking function of myosin VI has been shown to be involved in several cellular processes, such as, endocytosis, endocytic trafficking and recycling of vesicles, autophagy, exocytosis and nuclear transcription; and its anchoring function has been shown to be involved in the maintenance of Golgi complex, cochlear hair-cell sterocilia, enterocytic brush border membrane and adherent-junctions. These functions are accomplished by interacting with different binding partners (Au et al., 2007; F Buss et al., 2001; Fili et al., 2017; Maddugoda et al., 2007; Self et al., 1999; Tumbarello et al., 2012; Warner et al., 2003).

1. MYO6 is an independent marker of prognosis in locally advanced colorectal cancer patients.

Identification of prognostic factors is necessary to predict the outcome of colorectal cancer patients and to decide the best treatment for them. Currently, clinicopathologic staging of colorectal tumors is the most important prognostic factor. The pathologic stage is defined according to the tumor-node-metastasis (TNM) system (**Table 1**), which classifies tumors depending on the invasion depth of the primary tumor through the intestinal wall, as well as, the presence of metastasis in the nearby lymph nodes and/or distant organs (Sobin et al., 2010). Patients from different stages are predicted to have distinct outcomes. However, patients with histopathologically indistinguishable tumors (same stage) can widely vary in their disease recurrence and survival, after surgical and chemotherapeutic treatment. Consequently, there is a large subset of patients who receive treatment from which they do not benefit, but suffer from associated toxicity.

So far, several molecular markers have been described in an attempt to improve prognostic information and predict the benefit derived from systemic treatment. For instance, microsatellite instability (MSI) status and loss of heterozygosity (LOH) of chromosome 18q are considered robust molecular prognostic factors in colorectal cancer patients (Walther et al., 2009). Mutations in *KRAS*, *BRAF*, *APC* and *TP53* have been also identified as prognostic markers (Lech, Słotwiński, Słodkowski, & Krasnodębski, 2016; Walther et al., 2009). However, with the exception of *KRAS* mutations, these markers are not taken into consideration for clinical decision due to the lack of consensus about their true clinical value. Therefore, identification of new colorectal cancer biomarkers that would allow a better prognosis stratification of patients and would help to define more precisely the subset of patients that would benefit the most from the different available therapeutic options is fundamental in order to avoid toxicity from unnecessary treatments.

Here, tumor MYO6 protein and mRNA expression was not associated with clinicopathologic features such as, colorectal cancer patient sex, age, tumor location, histological grade and adjuvant treatment; or molecular features of tumors, such as, DNA replication error status (MSS/MSI), *TP53* status, *KRAS* status and loss of 18q chromosome. Importantly, however, low tumor MYO6 protein and mRNA expression were found to be significantly associated with shorter survival of colorectal cancer patients with locally advanced disease. In addition, MYO6 protein expression was observed to be significantly reduced in primary colorectal tumors compared to normal colonic epithelial cells; and MYO6 expression was further reduced in regional lymph node metastases compared to primary tumors, further indicating that reduced MYO6 expression is associated with poor prognosis in colorectal cancer patients.

Interestingly, a previous report based on the analysis of five public microarray datasets (Sabates-Bellver, Colon; Skrzypczak, Colorectal; Hong, Colorectal; Kaiser, Colon; and TCGA, Colorectal), stated that *MYO6* mRNA expression was increased in colorectal tumors compared to normal colon tissues (You et al., 2016). However, tissue samples selected for these studies were not microdissected and contained multiple cell types that are normally present in the intestinal mucosa or the tumor samples, including blood and lymph vessels, stromal cell or infiltrating lymphocytes. Unlike immunohistochemical studies, transcriptomic high-throughput expression data, such as microarray analysis, assess the levels of gene expression in pooled lysate samples, and the varying amounts of ‘contaminating’ non-epithelial cells can significantly confound the interpretation of gene expression across tumors and especially between normal and tumor tissues. Therefore, gene expression in normal tissues is often underestimated due to the low content of epithelial cells. Immunohistochemical analysis of gene expression using thoroughly validated antibodies allows a trained pathologist to exclude the non-epithelial areas from the analysis and thus, only the expression of the protein in the epithelial cells is taken into consideration for the analysis. Therefore, the reduced MYO6 expression observed here by immunohistochemistry in primary tumors and lymph node metastasis compared to normal colonic epithelial cells is likely more reliable than the reported overexpression assessed by microarray analysis (You et al., 2016).

Collectively, these data demonstrate the prognostic value of MYO6 in colorectal cancer after surgery. Therefore, after independent validation of these results in larger patient cohorts, tumor MYO6 expression could be used as a novel biomarker to predict the probability of disease recurrence and survival of colorectal cancer patients, and thus, to assess the real need for adjuvant chemotherapy, contributing in this way to improve the clinical management of colorectal cancer patients.

2. Generation of isogenic MYO6 knockdown colon cancer cell models.

The MYO6 gene encodes several different isoforms that have been demonstrated to play different roles within the cell. Although not included in this thesis, we did investigate the isoforms expressed in differentiated and undifferentiated colon cancer cells (GenBank references: KY781827 and KY781828) ("NCBI - GenBank," 2017). Despite multiple attempts to overexpress different isoforms of MYO6 using doxycycline-inducible systems, we were unable to ectopically express MYO6 in colon cancer cells, possibly, because MYO6 isoforms' expression/translation is tightly regulated in colon cancer cells. Alternatively, MYO6 knockdown cell models have the advantage of ensuring the silencing of all the MYO6 isoforms expressed in the cell, thus allowing the study all the effects associated with the loss of all the functions of MYO6. However, MYO6 overexpression cell models only allow overexpressing one isoform and it is difficult to predict beforehand which isoform could have a possible involvement in colorectal cancer progression. Interestingly, all engineered MYO6 knockdown cell systems worked well, excepting CACO2-sh55 cell line, which showed limited growth and differentiation capability *in vitro* under the experimental conditions used, for reasons that were not further investigated.

3. MYO6 does not regulate differentiation and polarization in colon cancer cells.

Intestinal epithelial cells possess an asymmetric distribution of components (proteins, lipids, organelles, etc.) along their membranes and within their intracellular spaces, referred as **apical-basal polarity** (Muthuswamy & Xue, 2012). The maintenance of apical-basal polarity is fundamental for their normal physiological functions and tissue integrity, as it allows to properly sense signals that arise from surrounding cells and the microenvironment, and elicit adequate responses. However, when polarity is disrupted cells may become unresponsive to growth inhibitory signals and this may lead to hyperproliferation; may circumvent differentiation and apoptosis; and may increase their migration and invasion capacity. In fact, several proteins that regulate cell polarity have been found to be tumor suppressors and proto-oncoproteins, such as, proteins from the Crumb, PAR and Scrib complexes (Martin-Belmonte & Perez-Moreno, 2012; Wodarz & Näthke, 2007). Loss of apical-basal polarity is commonly observed in advanced tumors but increasing evidence suggests that it can be also an early event in epithelial cancers (Hanahan & Weinberg, 2011; Wodarz & Näthke, 2007).

Establishment of cell polarity depends on **vesicle trafficking and microtubule and actin dynamics** for the correct delivery/localization of cell components (protein, lipids, etc.) within the cell; and on **cell-cell and cell-matrix interactions** to guarantee communication between cells and between cells and extracellular matrix, and to maintain tissue integrity (Muthuswamy & Xue, 2012).

Vesicle trafficking is regulated by several classes of RAB and ARF small GTPase proteins together with the coordinated function of other small GTPases (i.e. RAC, CDC42 and RHO) that are involved in the remodeling of cytoskeletal tracks; and molecular motors, such as kinesins and myosins, which are in charge of vesicle transport (Goldenring, 2013). Loss of components of the vesicle trafficking machinery has been associated with loss of cell polarity and tumor progression. For instance, we have recently shown that RHOA inactivation triggers loss of cell polarity and promotes colorectal cancer progression (Rodrigues et al., 2014). Loss of MYO5B elicits loss of polarity and causes 'microvillus inclusion disease' (Cartón-García et al., 2015; Thoeni et al., 2014); and loss of MYO1A causes also loss of differentiation and polarity leading to intestinal tumor progression (Mazzolini et al., 2012). MYO6 has been shown to participate in the **sorting and delivery of newly-synthesized 'tyrosine motif containing' proteins from the Golgi complex specifically to the basolateral domain** in polarized epithelial cells (Au et al., 2007), suggesting a possible involvement in the maintenance of cell polarity. Apparently, RAB8 recruits MYO6 to the AP-1B sorting compartment via optineurin; and inhibition of MYO6 sorting function causes a reduced and mis-sorted delivery of basolateral proteins, such as LDL, to the apical membrane. Components of this basolateral shorting machinery have been found to be important regulators of cell polarity. Indeed, RAB8-deficient mice showed mislocalization of apical proteins, shortening of apical microvilli and microvillus inclusion disease in enterocytes (Ang, Fölsch, Koivisto, Pypaert, & Mellman, 2003; Takashi Sato et al., 2007); and the intestinal epithelial cells from AP-1B deficient mice presented ectopic microvilli-like structures on the lateral plasma membrane and mislocalization of basolateral membrane proteins (Hase et al., 2013; Mimura et al., 2012).

Here, first, the effects of MYO6 downregulation on the overall differentiation capability of colon cancer cells were investigated by assessing the activity of intestinal brush border hydrolases, which are widely considered as markers of differentiation of colon cancer cells (Matsumoto et al., 1990). Results demonstrated that MYO6 does not regulate the activities of alkaline phosphatase (AP), sucrase-isomaltase (SI) and dipeptidyl peptidase-IV (DPP-IV) enzymes. Therefore, MYO6 is likely not involved in the mechanisms driving their delivery to the apical pole, localization on the membrane and their regulation through endocytosis, either if the differentiation is spontaneous or induced by butyrate. Moreover, it seems that defects in the attachment of microvillar membrane to the underlying cytoskeleton caused by the loss of MYO6 do not affect the proper functioning of these enzymes either. In fact, a previous study reported that expression of AP and SI in the microvilli of enterocytes of Snell's Waltzer mice, which lack MYO6 expression, is not altered (Hegan et al., 2012).

On the other hand, as mentioned above, **cell-cell interactions**, such as, adherens junctions and tight junctions, also contribute to the formation and the maintenance of apical and basolateral domains. Indeed, loss of cell polarity is frequently related to alterations in the attachment to other cells. For instance, loss of overall E-cadherin expression or loss of its normal localization at cell-cell adherens contacts has been associated with tumor progression to a more invasive cancer phenotype (Jeanes et al., 2008). Myosin VI is also known to localize to **adherens junctions**, which suggests another role in regulating cell polarity through the maintenance of cell-cell contacts. In the border cells of *Drosophila* ovaries, myosin VI was found to form a complex with the adhesion proteins E-cadherin and β-catenin, and the absence of myosin VI triggered a reduction of E-cadherin and β-catenin protein levels (Geisbrecht & Montell, 2002).

In mammalian MCF7 breast adenocarcinoma epithelial cells, MYO6 was found to be recruited to adherens contacts as the epithelial monolayers mature, where it formed a complex with E-cadherin and vinculin. Depletion of MYO6 in these cells led to a loss of vinculin from the adherens junctions and a disorganization of perijunctional actin cytoskeleton, which in turn, caused a weakening of cohesive forces of the adhesion complexes (Maddugoda et al., 2007). In fact, loss of vinculin is observed during the development of many cancers, such as squamous carcinoma, rhabdomyosarcoma, breast cancer and colorectal cancer, and has been related to enhanced invasion, metastasis and reduced apoptosis (T. Li et al., 2014).

Therefore, next, the localization of E-cadherin and β-catenin was analyzed in the membrane of differentiated CACO2 cells, in which MYO6 expression is known to increase along with the differentiation process. However, MYO6 reduction did not affect the membrane levels of these proteins, indicating that it is not involved in the basolateral delivery and membrane localization of E-cadherin and β-catenin in colon cancer cells, contrary to shown in border cells of *Drosophila* ovaries. In addition to what observed in MCF7 cells (mentioned above), similar results were previously found in MDCK canine kidney cells, in which localization of E-cadherin was unaffected upon MYO6 dominant negative expression (Au et al., 2007). Moreover, inactivation of MYO6 in CACO2 and MDCK cells did not change their transepithelial electrical resistance (TER) (Au et al., 2007; Chen et al., 2014), which suggests that cell-cell contacts remained unaltered.

Finally, the possible involvement of MYO6 in the LKB1 dependent polarity pathway was investigated by assessing the capacity of LS174T-W4 colon cancer cells to polarize and form apical brush borders after activating LKB1 kinase. LKB1 is a key polarity regulator, mainly of brush border formation and has been shown to have tumor suppressor activity in the intestine (Bardeesy et al., 2002; Herrmann, Byekova, Elmets, & Athar, 2011). The *LKB1* gene is found mutated in the germline of 'Peutz-Jeghers cancer syndrome' patients, which are characterized by the presence of hamartomas in the gastrointestinal tract. However, mutations in *LKB1* gene are rare in sporadic colorectal tumors and epigenetic inactivation is not frequently observed (Trojan, Brieger, Raedle, Esteller, & Zeuzem, 2000; Z.-J. Wang, Taylor, Churchman, Norbury, & Tomlinson, 1998). Thus, downstream effectors of LKB1 or alternative polarization mechanisms are likely to be affected during intestinal tumorigenesis, and contribute to the disruption of cell polarity and differentiation. Here, MYO6 downregulation did not impair the ability of LS174T-W4 cells to polarize and form an apical brush border upon LKB1 activation. This result indicates that MYO6 is not a key downstream effector of LKB1 dependent polarization pathway.

Collectively, these results demonstrate that MYO6 does not play a major role in the regulation of polarization and differentiation of colon cancer cells. In good agreement with these results, MYO6 protein expression in primary colorectal tumors was not associated with tumor grade/differentiation.

MYO6 functions related to the maintenance of cell polarity in normal enterocytes, such as basolateral sorting or microvilli membrane anchoring, were not specifically studied in our colon cancer cells because our aim was to investigate possible alterations in differentiation/polarity that could impact colorectal cancer progression.

4. Loss of MYO6 is important for the growth of colon cancer cells *in vivo*.

MYO6 overexpression has been found to be oncogenic and promote proliferation in cancers such as, hepatocellular carcinoma, breast cancer, gastric cancer, lung cancer and oral squamous carcinoma (Ma et al., 2015; H. Wang et al., 2015; Z. Wang et al., 2016; Yu et al., 2015; X. Zhang et al., 2016).

Here, MYO6 downregulation did not affect the growth and the colony forming ability (neither in solid nor in semisolid substrate) of three different colon cancer cell lines *in vitro*. Strikingly, however, MYO6 knockdown led to a significantly faster growth of CACO2 and SW403 cells when assessed as a subcutaneous xenograft in immunodeficient NOD/SCID mice. Moreover, the increased growth observed was associated with an accelerated rate of cell proliferation, as determined by the percentage of cells incorporating the thymidine analog BrdU during the S-phase of the cell cycle. In addition, although reduced MYO6 did not affect the *in vivo* growth of LS513 cells, it accelerated the grafting time of tumors. The lack of growth differences *in vitro* coupled with the significantly increased growth *in vivo* suggest that the effects of MYO6 knockdown in colon cancer cells are non-cell autonomous. That is, effects related to loss of MYO6 appear to be dependent on an '*in vivo* environment' where, unlike *in vitro* cell cultures, the oxygen, nutrient and growth factor supplies are limited, and cancer cells are in continuous interaction with components of the tumor microenvironment (e.g., stromal cells).

However, the exact mechanisms by which loss of MYO6 accelerates *in vivo* growth of colon cancer cells remain to be elucidated. MYO6 is involved in several cellular processes, such as, endocytosis, secretion, molecule anchoring and nuclear transcription, and thus, loss of MYO6 could promote proliferation by altering different mechanisms. The most predominant MYO6 isoform expressed in enterocytes is the isoform 3 (LI+SI) ("GTEx Portal," 2017), which has been shown to be important for apical endocytosis and endocytic pathway, and for anchoring apical-membrane proteins and the microvillar membrane itself (F Buss et al., 2001; Chen et al., 2014; Hegan et al., 2012). Therefore, MYO6 downregulation in colon cancer cells is likely affecting mainly these specific functions.

Studies have demonstrated that several signaling pathways that control proliferation can be regulated through the endocytosis of their transmembrane receptors, such as Notch or Wnt signaling pathways. Moreover, defects in the endocytosis or in the intracellular pathway that transports the endocytosed receptors to the lysosomes, can lead to an increased signaling activity of transmembrane receptors and consequently to accelerated proliferation (Giebel & Wodarz, 2006). For instance, in *Drosophila melanogaster*, the loss of syntaxin and Rab5, two components of the endocytic vesicle trafficking machinery, leads to an accumulation of membrane receptors, such as Notch signaling receptor, causing an overproliferation of epithelia (Lu & Bilder, 2005). In neural progenitor cells, loss of FilaminA and Formin2, two actin-associated proteins, results in impaired LRP6 endocytosis which leads to canonical Wnt pathway activation and a consequent increase in proliferation (Lian et al., 2016). Moreover, the endocytic adapter protein DAB2, a MYO6 binding partner in clathrin-mediated endocytosis (Morris et al., 2002; Spudich et al., 2007), has been also shown to regulate some receptor-mediated signaling pathways (Fu et al., 2012; Hocevar, Smine, Xu, & Howe, 2001; Hung et al., 2012). For instance, DAB2 inhibits Wnt/β-catenin signaling pathway, by preventing the interaction of Axin with LRP5/6 co-receptors and PP1, or by binding to LRP6 and promoting its endocytosis (Y. Jiang, Prunier, & Howe, 2008; Yong Jiang, He, & Howe, 2012). Indeed, loss of DAB2 has been shown to cause hyperplasia and dysplasia of mouse ovarian surface epithelium (D. H. Yang et al., 2006); and reduced DAB2 expression in lung cancer cells promotes their proliferative and invasive abilities (Xie et al., 2013). Moreover, DAB2 has been found to be frequently lost in human cancers, including colorectal cancer (Z. Zhang, Chen, Tang, & Xie, 2014).

These data suggest that loss of MYO6 could be promoting proliferation in colon cancer cells by impairing endocytosis or endocytic trafficking of membrane receptors and thus, altering the regulation of certain signaling pathways. Moreover, although colon cancer cells have constitutive aberrant activation of the main signaling pathways controlling proliferation, colon cancer cells have been shown to be still responsive to growth factors. For instance, most colon cancer cells present mutations in *APC* or β-catenin genes, and yet, downstream signaling has been found to remain responsive to WNT ligands (Voloshanenko et al., 2013). Furthermore, an increased Wnt signaling activation was observed here in organoids derived from murine intestinal tumors that lack MYO6 compared to wild-type organoids, suggesting that loss of MYO6 could be accelerating proliferation by altering canonical Wnt signaling (Sansom et al., 2004; Van de Wetering et al., 2002).

Nevertheless, as mentioned before, MYO6 is involved in several processes and additional mechanisms could contribute to the observed MYO6-dependent regulation of tumor growth. Further studies are needed to better characterize the molecular mechanisms affected by the downregulation of MYO6 and which MYO6 isoforms are responsible for the observed regulation of tumor growth *in vivo*. Importantly, as MYO6 isoforms are expressed differentially depending on the tissue/organ, MYO6 could be regulating proliferation through distinct mechanisms in the different tissues. Thus, this could explain the opposing effects that the loss of MYO6 causes in different types of cancer.

Surprisingly, however, in a previous report MYO6 downregulation has been shown to reduce proliferation and the colony forming ability of SW1116 colon cancer cells *in vitro* (You et al., 2016). Here, effects of MYO6 knockdown were assessed on the *in vitro* growth of three different colon cancer cells and no changes were observed. SW1116 cells have intermediate MYO6 expression levels (Fig. 30) and, as our cell lines, are ‘microsatellite stable’ (MSS). This discrepancy could be cell-dependent, that is, specific gene mutations/expressions in each cell line could modulate the effects of MYO6 knockdown. Nevertheless, further investigation is needed to characterize how MYO6 regulates proliferation and the mechanisms that are involved.

On the other hand, several studies have demonstrated that rapid tumor proliferation is associated with poor colorectal cancer patient prognosis (Al-Sheneber et al., 1993; Mayer et al., 1993; Sinicrope et al., 1999). Here, loss of MYO6 was observed to accelerate proliferation, which could be responsible for the poor prognosis found in colorectal cancer patients with low tumor MYO6 expression.

5. MYO6 does not regulate the metastatic potential in colon cancer cells.

The acquisition of a motile and invasive phenotype during tumor development leads to the metastatic spread which is often responsible for the death of patients with colorectal cancer (Chamber, Groom, & MacDonald, 2002; Chiang & Massagué, 2008). The gain of this phenotype, a process known as 'epithelial-mesenchymal transition', implies alterations in cell attachment to other cells and to the extracellular matrix, loss of epithelial polarity and acquisition of increased abilities to invade, resist apoptosis and disseminate (Hanahan & Weinberg, 2011).

So far, increased MYO6 expression has been related to a pro-metastatic phenotype in ovarian carcinoma, prostate cancer and lymphoid leukemia. In ovarian cancer cells, inhibition of MYO6 expression impaired *in vitro* migration, and *in vivo* dissemination of intraperitoneally injected ovarian carcinoma cells throughout the peritoneal cavity of nude mice (Yoshida et al., 2004); in prostate cancer cells, the inhibition of MYO6 expression resulted also in an impaired *in vitro* cell migration and in a decreased number of soft agar colonies (Dunn et al., 2006); and in lymphoid leukemia cells MYO6 was found localized in membrane ruffles at the leading edge of motile cells, being important for spontaneous cell migration *in vitro* (Jbireal et al., 2010).

Here, MYO6 downregulation did not affect the migration capability of LS513 colon cancer cells *in vitro*. However, CACO2 and SW403 cells exhibited very limited migration capacity to repopulate scratched culture areas (data not shown) and their migration ability assessed in a 'transwell migration' assay was still low compared to other colon cancer cell lines. Moreover, the *in vitro* matrigel invasion ability of CACO2 cells was not affected either by reduced MYO6 expression. Nevertheless, LS513 and SW403 cells showed very limited invasion capability under the *in vitro* conditions used, and thus, changes in the invasive potential could not be assessed. Overall, these three colon cancer cell lines were not optimal models for the assessment of migration and invasion capabilities *in vitro*. Likely, the lack of a 'real tumor microenvironment', which is known to condition tumor spread, makes cells unable to efficiently migrate/invade *in vitro* under the conditions used (Hanahan & Weinberg, 2011).

In a human body, the invasion and metastasis process consists of several steps and thus, is far more complex than what is recreated in *in vitro* experiments. It begins with local invasion of the tumor, then intravasation of cancer cells into nearby blood and lymphatic vessels, their transit through the lymphatic and hematogenous systems, followed by escape of cancer cells from the lumina of such vessels into the parenchyma of distant tissues (extravasation), the formation of small nodules of cancer cells (micrometastases), and finally the growth of micrometastatic lesions into macroscopic tumors (colonization) (Hanahan & Weinberg, 2011). In order to make a better approximation of the metastasis process as it occurs in colorectal cancer patients and further investigate the possible involvement of MYO6 on it, mouse models of lung and liver metastasis were used. However, these *in vivo* assays only involve the late steps of the 'invasion-metastasis cascade', i.e., from the survival in the bloodstream/lymphatic vessels to the formation of macrometastasis in a new organ environment (Elkin & Vlodavsky, 2001). Results showed that MYO6 inactivation did not affect the capacity of LS513 cells to infiltrate and grow to form metastatic lesions in lungs after being injected intravenously into the bloodstream of immunodeficient mice. However, SW403 and CACO2 cells did not show any lung metastasizing ability and thus, changes in the lung metastatic potential could not be assessed. On the other hand, the ability of SW403 cells to form liver metastasis after being injected into the spleen was found to be dependent on the gender of the animals, so that only male mice showed liver metastatic lesions. Moreover, SW403 cells with reduced MYO6 tended to have increased metastatic potential, as higher number (incidence) of male mice presented liver metastasis compared to animals injected with SW403 cells with endogenous MYO6 expression. However, it did not reach statistical significance likely due to the low number of total animals. Therefore, liver metastasis assay should be repeated again with SW403 cells, increasing the number of male mice in order to have conclusive results about the possible role of MYO6 in liver metastatic potential. Moreover, LS513 cells were found to have liver metastasizing ability (data not shown) and thus, a full experiment could be carried out to further investigate MYO6 involvement in liver metastasis.

Altogether, the results obtained so far, show that MYO6 does not regulate the metastatic ability of the colon cancer cells studied. This is in contrast with earlier results obtained in ovarian cancer, prostate cancer and lymphoid leukemia, in which overexpression of MYO6 was shown to promote migration and invasion. A previous study revealed that MYO6 isoform 2 (without large insert and with small insert) was almost exclusively overexpressed in ovarian tumors being responsible for increased migratory capacity. Moreover, only certain types of cancers were found to positively select this isoform (Wollscheid et al., 2016). However, in epithelial cells from the colon, the predominant isoforms detected are the 3 (LI+SI) and 5 (no inserts), although it cannot be excluded the presence of other isoforms (www.gtexportal.org/home/) ("GTEx Portal," 2017). Therefore, if colon cancer cells do not strongly express isoform 2 either, which seems to be regulating the migration and invasion potential, no changes should be expected in the metastatic ability of cells when downregulating MYO6 expression. On the other hand, in prostate cancer cells, MYO6 overexpression was found to enhance the secretion of 'prostate-specific antigen' (PSA), a protein that increases cellular migration by promoting epithelial-mesenchymal cell transition and by cleaving extracellular matrix proteins (Puri et al., 2010). As PSA is specifically expressed in prostate tissue, MYO6 roles seem to be also conditioned by the tissue specific protein expressions. Therefore, the opposite MYO6 effects (oncogenic/tumor suppressor) found on distinct cancer types could be explained by the different expression of MYO6 isoforms and tissue context.

Intriguingly, although no changes in the metastatic potential of colon cancer cells were observed when MYO6 expression was downregulated, MYO6 expression was found to be reduced in lymph node metastasis compared to primary colorectal tumors. Several reasons could explain this situation: 1) As shown in MCF7 epithelial breast adenocarcinoma cells (Maddugoda et al., 2007), loss of MYO6 in colorectal tumors could facilitate their migration and invasion by weakening cohesive forces between cells and not by modulating directly such processes. However, this possible effect caused by loss of MYO6 cannot be properly assessed neither in the *in vitro* nor in the *in vivo* experiments that were performed. 2) On the other hand, the metastatic potential of colon cancer cells was found to vary depending on the type of organ to be colonized, as observed for SW403 cells or as previously reported (Wagner, Toth, Steele, & Thomas, 1992). In our study, metastases in the lymph nodes were assessed, which imply a completely different tissue compared to lung and liver tissues. Thus, reduced MYO6 expression could be promoting metastasis in a tissue specific manner. 3) Finally, deregulation of other proteins, in addition to being responsible for the increased metastatic potential of colorectal cancers to colonize lymph nodes, could also induce a reduction of MYO6 expression, thus, making MYO6 reduction to be a consequence instead of being causative.

6. Absence of MYO6 does not promote intestinal tumorigenesis in Snell's Waltzer mice.

In order to overcome the intrinsic limitations of *in vitro* experimentation with cell line models and extend our study of the role of MYO6 on the tumorigenic process in the context of a full organism, a *Myo6* knock-out mouse model was used (*Myo6*$^{sv/sv}$; Snell's Waltzer). The phenotype of *Myo6*$^{sv/sv}$ mice is characterized by deafness, hyperactivity, jerking movement of the head and a strong tendency to run in circles (Deol & Green, 1966). Moreover, *Myo6*$^{sv/sv}$ mice were observed to have significantly reduced body weight compared to wild-types, likely due to the inherent hyperactivity, as previously shown for other circling mice (J. W. Lee et al., 2001).

Here, the absence of MYO6 did not accelerate the intestinal tumorigenic process neither in *Apc*$^{\mathrm{Min/+}}$ or AOM-treated mice. However, previous reports have shown that physical activity can reduce the number and size of intestinal polyps in *Apc*$^{\mathrm{Min/+}}$ mice (Colbert et al., 2003; Mehl et al., 2005), and also the number of tumors or aberrant crypt foci (ACF) in the colon of AOM-treated mice (Aoi et al., 2010; Ju et al., 2008; Kelly et al., 2017), independently of whether the physical activity causes a body weight reduction or not. Therefore, considering that high physical activity and concomitant reduced body weight are associated with smaller and less abundant intestinal tumors in mice, the possible oncogenic effects caused by the absence of MYO6 could be confounded by the effects of the hyperactivity shown in Snell's Waltzer mice. Moreover, differences in the number of small intestinal tumors between *Myo6* knock-out and wild-type mice in the genetic approach but not in the pharmacological approach, could be due to differences in the mechanisms of tumor initiation or because of the differential impact of the hyperactive phenotype on the oncogenic process initiated by *Apc*$^{\mathrm{Min}}$ mutations or by AOM treatment.

Collectively, these results indicate that the absence of MYO6 does not accelerate tumor progression during the early stages of intestinal tumorigenesis in this specific mouse model. However, results should be considered inconclusive because of the confounding effects caused by the inactivation of MYO6 in other organs (i.e., the inner ear) in the Snell's Waltzer mouse model used.

In an attempt to avoid the unwanted effects associated with MYO6 inactivation in other organs, organoid cultures were generated from intestinal tumors of *Apc*$^{Min/+}$ mice that were either WT (*Myo6*$^{+/+}$) or KO (*Myo6*$^{sv/sv}$) for *Myo6*. First, murine tumor organoids were stably transduced with a Wnt reporter construct, and increased Wnt activity was observed in *Myo6* KO organoid cells compared to *Myo6* WT organoids. Further characterization of the phenotypic changes in these tumor organoids is currently ongoing in the laboratory, aimed at 1) assessing proliferation changes; 2) changes in the expression of a panel of Wnt target genes; and 3) growth of organoid cells in a model of orthotopic cecum implantation in *Myo6* wild-type host mice.

In conclusion, despite the oncogenic activity of MYO6 in other tumor types, here, MYO6 was shown to have a tumor suppressor activity in colorectal cancer due to its role in growth regulation *in vivo*. Moreover, MYO6 expression was demonstrated to be frequently reduced in primary tumors and lymph node metastasis; and low expression of MYO6 in primary tumors was found to be associated with poor colorectal cancer patient prognosis. We hypothesize that the different expression of MYO6 isoforms (types and levels) in the different tissues/organs is responsible for the divergent roles of MYO6 in the tumorigenic process of different organs. In fact, MYO6 is overexpressed in ovarian and prostate cancers compared to normal tissues and high MYO6 expression in these cancers correlates with poor patient prognosis (“The cancer genome atlas,” 2017). However, which MYO6 isoform and which function is responsible for the growth changes observed in colorectal tumors remains to be fully elucidated. Here, some MYO6 functions that could be involved in colorectal cancer progression have been discussed. However, other functions, such as, the recently discovered nuclear transcription regulating function could also contribute to tumor progression. Finally, the investigation of the effects of the loss of MYO6 on intestinal tumorigenesis in an alternative mouse model with intestinal-specific MYO6 inactivation is necessary to confirm our results of MYO6 as a possible tumor suppressor.

This study constitutes the first demonstration of the possible tumor suppressor role of MYO6 in colorectal cancer and highlights the divergent roles of MYO6 in the tumorigenic process of different organs.

CHAPTER 6

CONCLUSIONS

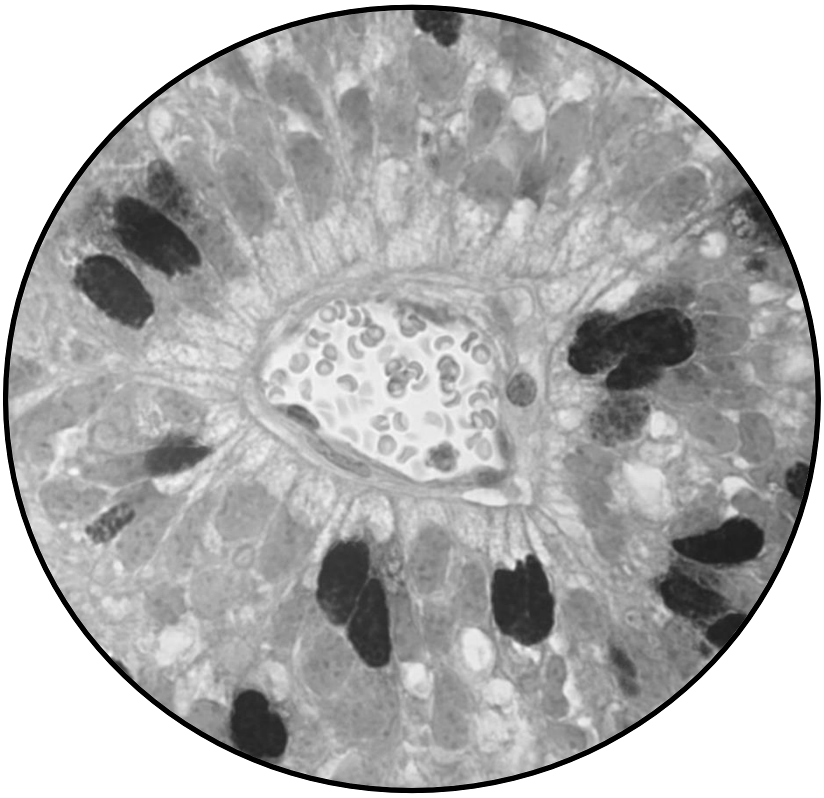

CONCLUSIONS

Unconventional myosins have been found to be deregulated in several types of cancer. Myosin VI is involved in vesicle trafficking in several cellular processes, such as endocytosis and exocytosis, and also participates in the anchoring of cargos to the actin cytoskeleton. Myosin VI deregulation has been reported to alter motility, invasion and proliferation in several cancers, but the role of MYO6 in colorectal cancer has not been investigated in depth. In this study, the functional relevance of the loss of MYO6 in colorectal cancer was investigated.

The main findings of this study are as follows:

- Low MYO6 tumor expression is associated with shorter disease-free and overall survival of patients with locally advanced colorectal cancer.
- Inactivation of MYO6 does not affect the differentiation or polarization of colon cancer cells.
- Inactivation of MYO6 in colon cancer cells does not affect their growth *in vitro*, but can increase their growth *in vivo* (xenograft models).
- Inactivation of MYO6 does not significantly alter the metastatic potential of colon cancer cells.
- Absence of MYO6 in *Apc*$^{\mathrm{Min/+}}$ or AOM-treated mice does not accelerate the intestinal tumor progression in Snell’s Waltzer mouse model.
- Absence of MYO6 in organoids derived from mouse small intestinal tumors increased the transcriptional activity of a Wnt signaling reporter construct.

This study indicates a possible tumor suppressor role of MYO6 in the progression of colorectal cancer which contrasts with the current literature that tends to consider MYO6 as an oncogene, and highlights the divergent roles of MYO6 in the tumorigenic process depending on the type of organ/tissue.

BIBLIOGRAPHY

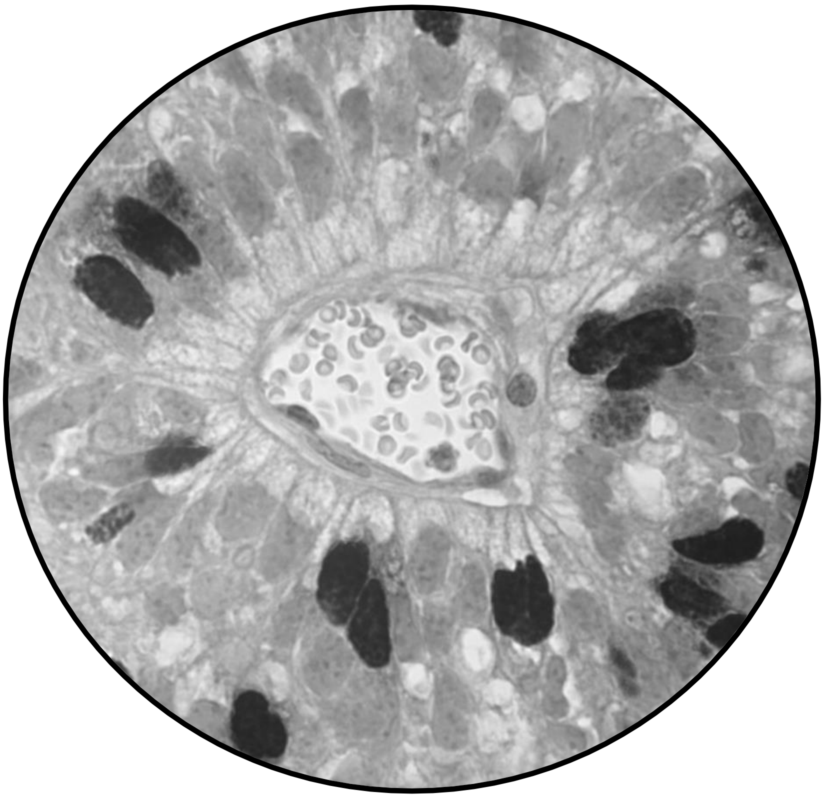

BIBLIOGRAPHY

Ahmed, Z. M., Morell, R. J., Riazuddin, S., Gropman, A., Shaukat, S., Ahmad, M. M., … Wilcox, E. R. (2003). Mutations of MYO6 are associated with recessive deafness, DFNB37. *American Journal of Human Genetics*, *72*(5), 1315–1322. http://doi.org/10.1086/375122

Al-Sheneber, I. F., Shibata, H. R., Sampalis, J., & Jothy, S. (1993). Prognostic significance of proliferating cell nuclear antigen expression in colorectal cancer. *Cancer*, *71*(6), 1954–9.

Albertson, R., Riggs, B., & Sullivan, W. (2005). Membrane traffic: A driving force in cytokinesis. *Trends in Cell Biology*, *15*(2), 92–101. http://doi.org/10.1016/j.tcb.2004.12.008

Alkowari, M. K., Vozzi, D., Bhagat, S., Krishnamoorthy, N., Morgan, A., Hayder, Y., … Abdulhadi, K. (2017). Targeted sequencing identifies novel variants involved in autosomal recessive hereditary hearing loss in Qatari families. *Mutation Research - Fundamental and Molecular Mechanisms of Mutagenesis*, *800–802*, 29–36. http://doi.org/10.1016/j.mrfmmm.2017.05.001

Altman, D., Sweeney, H. L., & Spudich, J. A. (2004). The mechanism of myosin VI translocation and its load-induced anchoring. *Cell*, *116*(5), 737–749. http://doi.org/doi.org/10.1016/S0092-8674(04)00211-9

American Cancer Society. (2018a). Survival Rates for Colorectal Cancer, by Stage. Retrieved February 21, 2018, from https://www.cancer.org/cancer/colon-rectal-cancer/detection-diagnosis-staging/survival-rates.html

American Cancer Society. (2018b). Treatment of Colon Cancer, by Stage. Retrieved February 21, 2018, from https://www.cancer.org/cancer/colon-rectal-cancer/treating/by-stage-colon.html

Ang, A. L., Fölsch, H., Koivisto, U. M., Pypaert, M., & Mellman, I. (2003). The Rab8 GTPase selectively regulates AP-1B-dependent basolateral transport in polarized Madin-Darby canine kidney cells. *Journal of Cell Biology*, *163*(2), 339–350. http://doi.org/10.1083/jcb.200307046

Aoi, W., Naito, Y., Takagi, T., Kokura, S., Mizushima, K., Takanami, Y., … Yoshikawa, T. (2010). Regular exercise reduces colon tumorigenesis associated with suppression of iNOS. *Biochemical and Biophysical Research Communications*, *399*(1), 14–19. http://doi.org/10.1016/j.bbrc.2010.07.023

Arango, D., Laiho, P., Kokko, A., Alhopuro, P., Sammalkorpi, H., Salovaara, R., … Aaltonen, L. A. (2005). Gene-expression profiling predicts recurrence in Dukes' C colorectal cancer. *Gastroenterology*, *129*(3), 874–884. http://doi.org/10.1053/j.gastro.2005.06.066

Arden, S. D., Puri, C., Sui-Yan Au, J., Kendrick-Jones, J., & Buss, F. (2007). Myosin VI Is Required for Targeted Membrane Transport during Cytokinesis. *Molecular Biology of the Cell*, *18*, 4750–4761. http://doi.org/10.1091/mbc.E07

Arjonen, A., Kaukonen, R., Mattila, E., Rouhi, P., Högnäs, G., Sihto, H., … Ivaska, J. (2014). Mutant p53 – associated myosin-X upregulation promotes breast cancer invasion and metastasis. *Journal of Clinical Investigation*, *124*(3), 1069–1082. http://doi.org/10.1172/JCI67280DS1

Aschenbrenner, L., Lee, T., & Hasson, T. (2003). Myo6 Facilitates the Translocation of Endocytic

Vesicles from Cell Peripheries, *14*(July), 2728–2743. http://doi.org/10.1091/mbc.E02

ATCC. (2017). Retrieved May 15, 2018, from https://www.lgcstandards-atcc.org/en.aspx

Au, J. S. Y., Puri, C., Ihrke, G., Kendrick-Jones, J., & Buss, F. (2007). Myosin VI is required for sorting of AP-1B-dependent cargo to the basolateral domain in polarized MDCK cells. *Journal of Cell Biology*, *177*(1), 103–114. http://doi.org/10.1083/jcb.200608126

Avraham, K. B., Hasson, T., Steel, K. P., Kingsley, D. M., Russell, L. B., Mooseker, M. S., … Jenkins, N. A. (1995). The mouse Snell's waltzer deafness gene encodes an unconventional myosin required for structural integrity of inner ear hair cells. *Nature Genetics*, *11*(4), 369–75. http://doi.org/doi:10.1038/ng1295-369

Baas, A. F., Kuipers, J., van der Wel, N. N., Batlle, E., Koerten, H. K., Peters, P. J., & Clevers, H. C. (2004). Complete polarization of single intestinal epithelial cells upon activation of LKB1 by STRAD. *Cell*, *116*, 457–466. http://doi.org/10.1016/S0092-8674(04)00114-X

Bahloul, A., Chevreux, G., Wells, A. L., Martin, D., Nolt, J., Yang, Z., … Sweeney, H. L. (2004). The unique insert in myosin VI is a structural calcium-calmodulin binding site. *Proceedings of the National Academy of Sciences of the United States of America*, *101*(14), 4787–4792. http://doi.org/10.1073/pnas.0306892101

Barber, T. D., Mcmanus, K., Yuen, K. W. Y., Reis, M., Parmigiani, G., Shen, D., … Hieter, P. (2008). Chromatid cohesion defects may underlie chromosome instability in human colorectal cancers. *Proceedings of the National Academy of Sciences of the United States of America*, *105*(9), 3443–3448. http://doi.org/10.1073/pnas.0712384105.

Bardeesy, N., Sinha, M., Hezel, A. F., Signoretti, S., Hathaway, N. A., Sharpless, N. E., … DePinho, R. A. (2002). Loss of the Lkb1 tumour suppressor provokes intestinal polyposis but resistance to transformation. *Nature*, *419*(6903), 162–167. http://doi.org/10.1038/nature01045

Barker, N., Ridgway, R. A., van Es, J. H., van de Wetering, M., Begthel, H., van den Born, M., … Clevers, H. (2009). Crypt stem cells as the cells-of-origin of intestinal cancer. *Nature*, *457*(7229), 608–611. http://doi.org/10.1038/nature07602

Batlle, E., Henderson, J. T., Beghtel, H., Van den Born, M. M. W., Sancho, E., Huls, G., … Clevers, H. (2002). β-catenin and TCF mediate cell positioning in the intestinal epithelium by controlling the expression of EphB/EphrinB. *Cell*, *111*(2), 251–263. http://doi.org/10.1016/S0092-8674(02)01015-2

Batters, C., Brack, D., Ellrich, H., Averbeck, B., & Veigel, C. (2016). Calcium can mobilize and activate myosin-VI. *Proceedings of the National Academy of Sciences*, *113*(9), E1162–E1169. http://doi.org/10.1073/pnas.1519435113

Bissahoyo, A., Pearsall, R. S., Hanlon, K., Amann, V., Hicks, D., Godfrey, V. L., & Threadgill, D. W. (2005). Azoxymethane is a genetic background-dependent colorectal tumor initiator and promoter in mice: Effects of dose, route, and diet. *Toxicological Sciences*, *88*(2), 340–345. http://doi.org/10.1093/toxsci/kfi313

Biswas, S., Davis, H., Irshad, S., Sandberg, T., Worthley, D., & Leedham, S. (2015). Microenvironmental control of stem cell fate in intestinal homeostasis and disease. *Journal of Pathology*, *237*(2), 135–145. http://doi.org/10.1002/path.4563

Boland, C. R., & Goel, A. (2010). Microsatellite Instability in Colorectal Cancer.

Gastroenterology, *138*(6), 2073–2087. http://doi.org/10.1053/j.gastro.2009.12.064

Bose, A., Robida, S., Furcinitti, P. S., Chawla, A., Fogarty, K., Corvera, S., & Czech, M. P. (2004). Unconventional myosin Myo1c promotes membrane fusion in a regulated exocytic pathway. *Molecular and Cellular Biology*, *24*(12), 5447–5458. http://doi.org/10.1128/MCB.24.12.5447-5458.2004

Brenner, H., Kloor, M., & Pox, C. P. (2014). Colorectal cancer. *The Lancet*, *383*(9927), 1490–1502. http://doi.org/10.1016/S0140-6736(13)61649-9

Budczies, J., Klauschen, F., & Denkert, C. (2013). Cutoff Finder. Retrieved April 28, 2018, from http://molpath.charite.de/cutoff/

Bunn, R. C., Jensen, M. A., & Reed, B. C. (1999). Protein interactions with the glucose transporter binding protein GLUT1CBP that provide a link between GLUT1 and the cytoskeleton. *Molecular Biology of the Cell*, *10*(4), 819–32. http://doi.org/10.1091/mbc.10.4.819

Buss, F., Arden, S. D., Lindsay, M., Luzio, J. P., & Kendrick-Jones, J. (2001). Myosin VI isoform localized to clathrin-coated vesicles with a role in clathrin-mediated endocytosis. *The EMBO Journal*, *20*(14), 3676–84. http://doi.org/10.1093/emboj/20.14.3676

Buss, F., & Kendrick-Jones, J. (2008). How are the cellular functions of myosin VI regulated within the cell? *Biochemical and Biophysical Research Communications*, *369*(1), 165–75. http://doi.org/10.1016/j.bbrc.2007.11.150

Buss, F., Kendrick-Jones, J., Lionne, C., Knight, A. E., Côté, G. P., & Luzio, J. P. (1998). The localization of myosin VI at the golgi complex and leading edge of fibroblasts and its phosphorylation and recruitment into membrane ruffles of A431 cells after growth factor stimulation. *The Journal of Cell Biology*, *143*(6), 1535–45.

Buss, F., Luzio, J. P., & Kendrick-jones, J. (2002). Myosin VI, an Actin Motor for Membrane Traffic and Cell Migration. *Traffic*, *3*(12), 851–858. http://doi.org/doi.org/10.1034/j.1600-0854.2002.31201.x

Buss, F., Spudich, G., & Kendrick-jones, J. (2004). M YOSIN VI : Cellular Functions and Motor Properties. *Annual Review of Cell and Developmental Biology*, *20*, 649–676. http://doi.org/10.1146/annurev.cellbio.20.012103.094243

Cao, R., Chen, J., Zhang, X., Zhai, Y., Qing, X., Xing, W., … Zhu, X. (2014). Elevated expression of myosin X in tumours contributes to breast cancer aggressiveness and metastasis. *British Journal of Cancer*, *111*(3), 539–550. http://doi.org/10.1038/bjc.2014.298

Cartón-García, F., Overeem, A. W., Nieto, R., Bazzocco, S., Dopeso, H., Macaya, I., … Arango, D. (2015). Myo5b knockout mice as a model of microvillus inclusion disease. *Scientific Reports*, *5*, 12312. http://doi.org/10.1038/srep12312

Caswell, P., & Norman, J. (2008). Endocytic transport of integrins during cell migration and invasion. *Trends in Cell Biology*, *18*(6), 257–263. http://doi.org/10.1016/j.tcb.2008.03.004

Chamber, A. F., Groom, A. C., & MacDonald, I. C. (2002). Dissemination and growth of cancer cells in metastatic sites. *Nature Reviews Cancer*, *2*(8), 563–572. http://doi.org/10.1038/nrc865

Chantret, I., Barbat, A., Dussaulx, E., Brattain, M. G., & Zweibaum, A. (1988). Epithelial Polarity, Villin Expression, and Enterocytic Differentiation of Cultured Human Colon Carcinoma Cells: A Survey of Twenty Cell Lines. *Cancer Research*, *48*(7), 1936–1942.

Chen, T., Hubbard, A., Murtazina, R., Price, J., Yang, J., Cha, B., … Donowitz, M. (2014). Myosin VI mediates the movement of NHE3 down the microvillus in intestinal epithelial cells. *Journal of Cell Science*, *127*(16), 3535–45. http://doi.org/10.1242/jcs.149930

Chhabra, E. S., & Higgs, H. N. (2007). The many faces of actin: matching assembly factors with cellular structures. *Nature Cell Biology*, *9*(10), 1110–1121. http://doi.org/10.1038/ncb1007-1110

Chiang, A. C., & Massagué, J. (2008). Molecular Basis of Metastasis. *New England Journal of Medicine*, *359*(26), 2814–2823. http://doi.org/10.1056/NEJMra0805239

Chibalina, M. V, Poliakov, A., Kendrick-Jones, J., & Buss, F. (2010). Myosin VI and optineurin are required for polarized EGFR delivery and directed migration. *Traffic (Copenhagen, Denmark)*, *11*(10), 1290–303. http://doi.org/10.1111/j.1600-0854.2010.01101.x

Chibalina, M. V, Puri, C., Kendrick-Jones, J., & Buss, F. (2009). Potential roles of myosin VI in cell motility. *Biochemical Society Transactions*, *37*(Pt 5), 966–70. http://doi.org/10.1042/BST0370966

Chibalina, M. V, Seaman, M. N. J., Miller, C. C., Kendrick-Jones, J., & Buss, F. (2007). Myosin VI and its interacting protein LMTK2 regulate tubule formation and transport to the endocytic recycling compartment. *Journal of Cell Science*, *120*(Pt 24), 4278–4288. http://doi.org/10.1242/jcs.014217

Choi, B. Y., Park, G., Gim, J., Kim, A. R., Kim, B. J., Kim, H. S., … Park, W. Y. (2013). Diagnostic Application of Targeted Resequencing for Familial Nonsyndromic Hearing Loss. *PLoS ONE*, *8*(8), 1–8. http://doi.org/10.1371/journal.pone.0068692

Chung, Y. S., Song, I. S., Erickson, R. H., Sleisenger, M. H., & Kim, Y. S. (1985). Effect of growth and sodium butyrate on brush border membrane-associated hydrolases in human colorectal cancer cell lines. *Cancer Research*, *45*(7), 2976–2982.

Clevers, H., & Batlle, E. (2006). EphB/EphrinB receptors and Wnt signaling in colorectal cancer. *Cancer Research*, *66*(1), 2–5. http://doi.org/10.1158/0008-5472.CAN-05-3849

Clevers, H., & Batlle, E. (2013). SnapShot: The intestinal crypt. *Cell*, *152*(5), 1198–1198.e2. http://doi.org/10.1016/j.cell.2013.02.030

Clevers, H. C., & Bevins, C. L. (2013). Paneth cells: maestros of the small intestinal crypts. *Annual Review of Physiology*, *75*, 289–311. http://doi.org/10.1146/annurev-physiol-030212-183744

Colbert, L. H., Mai, V., Perkins, S. N., Berrigan, D., Lavigne, J. A., Wimbrow, H. H., … Hursting, S. D. (2003). Exercise and intestinal polyp development in APCMin mice. *Medicine and Science in Sports and Exercise*, *35*(10), 1662–1669. http://doi.org/10.1249/01.MSS.0000089349.54813.41

Compton, C. C. (2003). Colorectal Carcinoma: Diagnostic, Prognostic, and Molecular Features. *Modern Pathology*, *16*(4), 376–388. http://doi.org/10.1097/01.MP.0000062859.46942.93

Crawley, S. W., Mooseker, M. S., & Tyska, M. J. (2014). Shaping the intestinal brush border. *Journal of Cell Biology*, *207*(4), 441–451. http://doi.org/10.1083/jcb.201407015

Cronin, M. A., Diao, F., & Tsunoda, S. (2004). Light-dependent subcellular translocation of Gqalpha in Drosophila photoreceptors is facilitated by the photoreceptor-specific myosin III NINAC. *Journal of Cell Science*, *117*(20), 4797–4806. http://doi.org/10.1242/jcs.01371

Crosnier, C., Stamataki, D., & Lewis, J. (2006). Organizing cell renewal in the intestine: stem cells, signals and combinatorial control. *Nature Reviews. Genetics*, *7*(5), 349–59. http://doi.org/10.1038/nrg1840

Dance, A. L., Miller, M., Seragaki, S., Aryal, P., White, B., Aschenbrenner, L., & Hasson, T. (2004). Regulation of myosin-VI targeting to endocytic compartments. *Traffic (Copenhagen, Denmark)*, *5*(10), 798–813. http://doi.org/10.1111/j.1600-0854.2004.00224.x

Davies, R. J., Miller, R., & Coleman, N. (2005). Colorectal cancer screening: prospects for molecular stool analysis. *Nature Reviews. Cancer*, *5*(3), 199–209. http://doi.org/10.1038/nrc1545

De Lanerolle, P. (2012). Nuclear actin and myosins at a glance. *Journal of Cell Science*, *125*(21), 4945–4949. http://doi.org/10.1242/jcs.099754

De Robertis, M., Massi, E., Poeta, M. L., Carotti, S., Morini, S., Cecchetelli, L., … Fazio, V. M. (2011). The AOM/DSS murine model for the study of colon carcinogenesis: From pathways to diagnosis and therapy studies. *Journal of Carcinogenesis*, *10*, 9. http://doi.org/10.4103/1477?3163.78279

Deol, M. S., & Green, M. C. (1966). Snell's Waltzer, a new mutation affecting behavior and the inner ear in the mouse. *Genetics Research*, *8*, 339–345.

Dippold, H. C., Ng, M. M., Farber-Katz, S. E., Lee, S. K., Kerr, M. L., Peterman, M. C., … Field, S. J. (2009). GOLPH3 Bridges Phosphatidylinositol-4- Phosphate and Actomyosin to Stretch and Shape the Golgi to Promote Budding. *Cell*, *139*(2), 337–351. http://doi.org/10.1016/j.cell.2009.07.052

Doherty, G. J., & McMahon, H. T. (2009). Mechanisms of endocytosis. *Annual Review of Biochemistry*, *78*, 857–902. http://doi.org/10.1146/annurev.biochem.78.081307.110540

Drake, R. L., Vogl, W., & Mitchell, A. W. M. (2006). *Gray. Anatomía para estudiantes*. S.A. ELSEVIER ESPAÑA.

Dukes, C. E. (1932). The classification of cancer of the rectum. *Journal of Pathological Bacteriology*, *35*, 323–332. http://doi.org/10.1007/BF02989012

Dunn, T. A., Chen, S., Faith, D. A., Hicks, J. L., Platz, E. A., Chen, Y., … Luo, J. (2006). A novel role of myosin VI in human prostate cancer. *The American Journal of Pathology*, *169*(5), 1843–1854. http://doi.org/10.2353/ajpath.2006.060316

Elkin, M., & Vlodavsky, I. (2001). Tail Vein Assay of Cancer Metastasis. *Current Protocols in Cell Biology*, 19.2.1-19.2.7. http://doi.org/10.1002/0471143030.cb1902s12

Ensembl. (2018). Retrieved April 9, 2018, from https://www.ensembl.org/Homo_sapiens/Gene/Summary?db=core;g=ENSG00000196586;r=6:75749192-75919537;t=ENST00000369985

Fearon, E. R. (2011). Molecular Genetics of Colorectal Cancer. *Annual Review of Pathology*, *6*, 479–507. http://doi.org/10.1146/annurev-pathol-011110-130235

Fearon, E. R., & Vogelstein, B. (1990). A genetic model for colorectal tumorigenesis. *Cell*, *61*(5), 759–767. http://doi.org/10.1016/0092-8674(90)90186-I

Feldman, M., Friedman, L. S., & Sleisenger, M. H. (2002). *Sleisenger and Fordtran's Gastrointestinal and Liver Disease: Pathophysiology/Diagnosis/Management* (7th editio, Vol. 2). Philadelphia, Pennsylvania: Saunders Elsevier.

Ferlay, J., Steliarova-Foucher, E., Lortet-Tieulent, J., Rosso, S., Coebergh, J. W. W., Comber, H., … Bray, F. (2013). Cancer incidence and mortality patterns in Europe: estimates for 40 countries in 2012. *European Journal of Cancer (Oxford, England : 1990)*, *49*(6), 1374–403. http://doi.org/10.1016/j.ejca.2012.12.027

Fernandez, L. P., Milne, R. L., Pita, G., Floristan, U., Sendagorta, E., Feito, M., … Ribas, G. (2009). Pigmentation-related genes and their implication in malignant melanoma susceptibility. *Experimental Dermatology*, *18*(7), 634–642. http://doi.org/10.1111/j.1600-0625.2009.00846.x

Fielding, A. B., Schonteich, E., Matheson, J., Wilson, G., Yu, X., Hickson, G. R. X., … Gould, G. W. (2005). Rab11-FIP3 and FIP4 interact with Arf6 and the exocyst to control membrane traffic in cytokinesis. *The EMBO Journal*, *24*(19), 3389–3399. http://doi.org/10.1038/sj.emboj.7600803

Fili, N., Hari-Gupta, Y., dos Santos, Á., Cook, A., Poland, S., Ameer-Beg, S. M., … Toseland, C. P. (2017). NDP52 activates nuclear myosin VI to enhance RNA polymerase II transcription. *Nature Communications*, *8*(1), 1871. http://doi.org/10.1038/s41467-017-02050-w

Fodde, R., Kuipers, J., Rosenberg, C., Smits, R., Kielman, M., Gaspar, C., … Clevers, H. (2001). Mutations in the APC tumour suppressor gene cause chromosomal instability. *Nature Cell Biology*, *3*(4), 433–438. http://doi.org/10.1038/35070129

Fu, L., Rab, A., Tang, L. P., Rowe, S. M., Bebok, Z., & Collawn, J. F. (2012). Dab2 is a key regulator of endocytosis and post-endocytic trafficking of the cystic fibrosis transmembrane conductance regulator. *Biochemical Journal*, *441*(2), 633–643. http://doi.org/10.1042/BJ20111566

Fuerer, C., & Nusse, R. (2010). Lentiviral vectors to probe and manipulate the Wnt signaling pathway. *PLoS ONE*, *5*(2), e9370. http://doi.org/10.1371/journal.pone.0009370

Geisbrecht, E. R., & Montell, D. J. (2002). Myosin VI is required for E-cadherin-mediated border cell migration. *Nature Cell Biology*, *4*(8), 616–620. http://doi.org/10.1038/ncb830

GenBank. (2017). Retrieved April 9, 2018, from www.ncbi.nlm.nih.gov/nuccore/KY781827

Gerald, N. J., Damer, C. K., O'Halloran, T. J., & De Lozanne, A. (2001). Cytokinesis failure in clathrin-minus cells is caused by cleavage furrow instability. *Cell Motility and the Cytoskeleton*, *48*(3), 213–223. http://doi.org/10.1002/1097-0169(200103)48:3<213::AID-CM1010>3.0.CO;2-V

Gibbs, D., Kitamoto, J., & Williams, D. S. (2003). Abnormal phagocytosis by retinal pigmented epithelium that lacks myosin VIIa, the Usher syndrome 1B protein. *Proceedings of the National Academy of Sciences*, *100*(11), 6481–6486. http://doi.org/10.1073/pnas.1130432100

Giebel, B., & Wodarz, A. (2006). Tumor Suppressors: Control of Signaling by Endocytosis. *Current Biology*, *16*(3), 91–92. http://doi.org/10.1016/j.cub.2006.01.025

Glotzer, M. (2005). The molecular requirements for cytokinesis. *Science*, *307*(5716), 1735–1739. http://doi.org/10.1126/science.1096896

Goldenring, J. R. (2013). A central role for vesicle trafficking in epithelial neoplasia: Intracellular highways to carcinogenesis. *Nature Reviews Cancer*, *13*(11), 813–820. http://doi.org/10.1038/nrc3601

Gonsalvez, G. B., Urbinati, C. R., & Long, R. M. (2005). RNA localization in yeast: moving towards a mechanism. *Biology of the Cell*, *97*(1), 75–86. http://doi.org/10.1042/BC20040066

Gotoh, N., Yan, Q., Du, Z., Biemesderfer, D., Kashgarian, M., Mooseker, M. S., & Wang, T. (2010). Altered renal proximal tubular endocytosis and histology in mice lacking myosin-VI. *Cytoskeleton (Hoboken, N.J.)*, *67*(3), 178–192. http://doi.org/10.1002/cm.20435

Green, R. A., & Kaplan, K. B. (2003). Chromosome instability in colorectal tumor cells is associated with defects in microtubule plus-end attachments caused by a dominant mutation in APC. *Journal of Cell Biology*, *163*(5), 949–961. http://doi.org/10.1083/jcb.200307070

Green, R. A., Wollman, R., & Kaplan, K. B. (2005). APC and EB1 Function Together in Mitosis to Regulate Spindle Dynamics and Chromosome Alignment. *Molecular Biology of the Cell*, *16*, 4609–4622. http://doi.org/10.1091/mbc.E05-03-0259

Griffiths, G., & Simons, K. (1986). The trans Golgi Network: Sorting at the Exit Site of the Golgi Complex. *Science*, *234*(4775), 438–443. http://doi.org/DOI: 10.1126/science.2945253

GTEx Portal. (2017). Retrieved May 29, 2018, from https://www.gtexportal.org/home/gene/MYO6

Gupton, S. L., & Waterman-Storer, C. M. (2006). Spatiotemporal Feedback between Actomyosin and Focal-Adhesion Systems Optimizes Rapid Cell Migration. *Cell*, *125*(7), 1361–1374. http://doi.org/10.1016/j.cell.2006.05.029

Hallett, R. M., Dvorkin-Gheva, A., Bane, A., & Hassell, J. A. (2012). A gene signature for predicting outcome in patients with basal-like breast cancer. *Scientific Reports*, *2*(227), 1–8. http://doi.org/10.1038/srep00227

Hamer, H. M., Jonkers, D., Venema, K., Vanhoutvin, S., Troost, F. J., & Brummer, R. J. (2008). Review article: The role of butyrate on colonic function. *Alimentary Pharmacology and Therapeutics*, *27*(2), 104–119. http://doi.org/10.1111/j.1365-2036.2007.03562.x

Hanahan, D., & Weinberg, R. A. (2000). The Hallmarks of Cancer. *Cell*, *100*(1), 57–70. http://doi.org/10.1016/S0092-8674(00)81683-9

Hanahan, D., & Weinberg, R. A. (2011). Hallmarks of cancer: the next generation. *Cell*, *144*(5), 646–674. http://doi.org/10.1016/j.cell.2011.02.013

Haq, A. I., Schneeweiss, J., Kalsi, V., & Arya, M. (2009). The Dukes staging system: a cornerstone in the clinical management of colorectal cancer. *The Lancet Oncology*, *10*(11), 1128. http://doi.org/10.1016/S1470-2045(09)70157-3

Hase, K., Nakatsu, F., Ohmae, M., Sugihara, K., Shioda, N., Takahashi, D., … Ohno, H. (2013). AP-1B-mediated protein sorting regulates polarity and proliferation of intestinal epithelial cells in mice. *Gastroenterology*, *145*(3), 625–635.

http://doi.org/10.1053/j.gastro.2013.05.013

Hasson, T. (2003). Myosin VI: two distinct roles in endocytosis. *Journal of Cell Science*, *116*(Pt 17), 3453–3461. http://doi.org/10.1242/jcs.00669

Hasson, T., & Mooseker, M. S. (1994). Porcine myosin-VI: Characterization of a new mammalian unconventional myosin. *The Journal of Cell Biology*, *127*(2), 425–440. http://doi.org/10.1083/jcb.127.2.425

Heasman, S. J., & Ridley, A. J. (2008). Mammalian Rho GTPases: new insights into their functions from in vivo studies. *Nature Reviews. Molecular Cell Biology*, *9*(9), 690–701. http://doi.org/10.1038/nrm2476

Hegan, P. S., Giral, H., Levi, M., & Mooseker, M. S. (2012). Myosin VI is required for maintenance of brush border structure, composition, and membrane trafficking functions in the intestinal epithelial cell. *Cytoskeleton (Hoboken, N.J.)*, *69*(4), 235–51. http://doi.org/10.1002/cm.21018

Heidrych, P., Zimmermann, U., Kuhn, S., Franz, C., Engel, J., Duncker, S. V., … Knipper, M. (2009). Otoferlin interacts with myosin VI: Implications for maintenance of the basolateral synaptic structure of the inner hair cell. *Human Molecular Genetics*, *18*(15), 2779–2790. http://doi.org/10.1093/hmg/ddp213

Herrmann, J. L., Byekova, Y., Elmets, C. A., & Athar, M. (2011). Liver Kinase B1 (LKB1) in the pathogenesis of epithelial cancers. *Cancer Letters*, *306*(1), 1–9. http://doi.org/10.1016/j.canlet.2011.01.014

Hilgert, N., Topsakal, V., van Dinther, J., Offeciers, E., Van de Heyning, P., & Van Camp, G. (2008). A splice-site mutation and overexpression of MYO6 cause a similar phenotype in two families with autosomal dominant hearing loss. *European Journal of Human Genetics*, *16*(5), 593–602. http://doi.org/10.1038/sj.ejhg.5202000

Hocevar, B. A., Smine, A., Xu, X. X., & Howe, P. H. (2001). The adaptor molecule disabled-2 links the transforming growth factor β receptors to the Smad pathway. *EMBO Journal*, *20*(11), 2789–2801. http://doi.org/10.1093/emboj/20.11.2789

Howitt, M. R., Lavoie, S., Michaud, M., Blum, A. M., Tran, S. V., Weinstock, J. V., … Artis, D. (2016). Tuft cells, taste-chemosensory cells, orchestrate parasite type 2 immunityin the gut. *Science*, *351*(6279), 1329–1333. http://doi.org/10.1126/science.aaf1648

Humphries, A., & Wright, N. a. (2008). Colonic crypt organization and tumorigenesis. *Nature Reviews. Cancer*, *8*(6), 415–24. http://doi.org/10.1038/nrc2392

Hung, W. S., Huang, C. L., Fan, J. T., Huang, D. Y., Yeh, C. F., Cheng, J. C., & Tseng, C. P. (2012). The endocytic adaptor protein Disabled-2 is required for cellular uptake of fibrinogen. *Biochimica et Biophysica Acta - Molecular Cell Research*, *1823*(10), 1778–1788. http://doi.org/10.1016/j.bbamcr.2012.06.008

Isaji, M., Lenartowska, M., Noguchi, T., Frank, D. J., & Miller, K. G. (2011). Myosin VI regulates actin structure specialization through conserved cargo-binding domain sites. *PloS One*, *6*(8), e22755. http://doi.org/10.1371/journal.pone.0022755

Issa, J. P. (2004). CpG island methylator phenotype in cancer. *Nature Reviews. Cancer*, *4*(12), 988–993. http://doi.org/10.1038/nrc1507

Issa, J. P. (2008). Colon cancer: It's CIN or CIMP. *Clinical Cancer Research*, *14*(19), 5939–5940. http://doi.org/10.1158/1078-0432.CCR-08-1596

Jbireal, J. M. A., Strell, C., Niggemann, B., Zänker, K., & Entschladen, F. (2010). The selective role of myosin VI in lymphoid leukemia cell migration. *Leukemia Research*, *34*(12), 1656–1662. http://doi.org/10.1016/j.leukres.2010.04.018

Jeanes, A., Gottardi, C., & Yap, A. (2008). Cadherins and cancer: how does cadherin dysfunction promote tumor progression? *Oncogene*, *27*(55), 6920–6929. http://doi.org/10.1038/onc.2008.343

Jiang, Y., He, X., & Howe, P. H. (2012). Disabled-2 (Dab2) inhibits Wnt/β2-catenin signalling by binding LRP6 and promoting its internalization through clathrin. *EMBO Journal*, *31*(10), 2336–2349. http://doi.org/10.1038/emboj.2012.83

Jiang, Y., Prunier, C., & Howe, P. H. (2008). The inhibitory effects of Disabled-2 (Dab2) on Wnt signaling are mediated through Axin. *Oncogene*, *27*(13), 1865–1875. http://doi.org/10.1038/sj.onc.1210829

Jonsdottir, G. A., & Li, R. (2004). Dynamics of yeast Myosin I: evidence for a possible role in scission of endocytic vesicles. *Current Biology*, *14*(17), 1604–1609. http://doi.org/10.1016/j.cub.2004.08.055

Ju, J., Nolan, B., Cheh, M., Bose, M., Lin, Y., Wagner, G. C., & Yang, C. S. (2008). Voluntary exercise inhibits intestinal tumorigenesis in Apc(Min/+) mice and azoxymethane/dextran sulfate sodium-treated mice. *BMC Cancer*, *8*, 316. http://doi.org/10.1186/1471-2407-8-316

Jung, E. J., Liu, G., Zhou, W., & Chen, X. (2006). Myosin VI is a mediator of the p53-dependent cell survival pathway. *Molecular and Cellular Biology*, *26*(6), 2175–2186. http://doi.org/10.1128/MCB.26.6.2175-2186.2006

Kaplan, K. B., Burds, A. A., Swedlow, J. R., Bekir, S. S., Sorger, P. K., & Näthke, I. S. (2001). A role for the Adenomatous Polyposis Coli protein in chromosome segregation. *Nature Cell Biology*, *3*(4), 429–432. http://doi.org/10.1038/35070123

Kelly, S. A., Zhao, L., Jung, K. C., Hua, K., Threadgill, D. W., Kim, Y., … Pomp, D. (2017). Prevention of tumorigenesis in mice by exercise is dependent on strain background and timing relative to carcinogen exposure. *Scientific Reports*, *7*, 43086. http://doi.org/10.1038/srep43086

Kim, Y. S., & Ho, S. B. (2010). Intestinal goblet cells and mucins in health and disease: Recent insights and progress. *Current Gastroenterology Reports*, *12*(5), 319–330. http://doi.org/10.1007/s11894-010-0131-2

Komaba, S., Inoue, A., Maruta, S., Hosoya, H., & Ikebe, M. (2003). Determination of human myosin III as a motor protein having a protein kinase activity. *Journal of Biological Chemistry*, *278*(24), 21352–21360. http://doi.org/10.1074/jbc.M300757200

Krendel, M., & Mooseker, M. S. (2005). Myosins: tails (and heads) of functional diversity. *Physiology (Bethesda, Md.)*, *20*, 239–51. http://doi.org/10.1152/physiol.00014.2005

Kwon, T.-J., Oh, S.-K., Park, H.-J., Sato, O., Venselaar, H., Choi, S. Y., … Choi, J. Y. (2014). The effect of novel mutations on the structure and enzymatic activity of unconventional myosins associated with autosomal dominant non-syndromic hearing loss. *Open Biology*, *4*(7), 140107 (1-8). http://doi.org/10.1098/rsob.140107

Ladinsky, M. S., Mastronarde, D. N., McIntosh, J. R., Howell, K. E., & Staehlin, L. A. (1999). Golgi structure in three dimensions: functional insights from the normal rat kidney cell. *The Journal of Cell Biology*, *144*(6), 1135–1149. http://doi.org/10.1083/jcb.144.6.1135

Lamb, C. A., Yoshimori, T., & Tooze, S. A. (2013). The autophagosome: origins unknown, biogenesis complex. *Nature Reviews Molecular Cell Biology*, *14*(12), 759–774. http://doi.org/10.1038/nrm3696

Lan, L., Han, H., Zuo, H., Chen, Z., Du, Y., Zhao, W., … Zhang, Z. (2010). Upregulation of myosin Va by snail is involved in cancer cell migration and metastasis. *International Journal of Cancer*, *126*(1), 53–64. http://doi.org/10.1002/ijc.24641

Langford, G. M. (2002). Myosin-V, a versatile motor for short-range vesicle transport. *Traffic*, *3*(12), 859–865. http://doi.org/10.1034/j.1600-0854.2002.31202.x

Lech, G., Słotwiński, R., Słodkowski, M., & Krasnodębski, I. W. (2016). Colorectal cancer tumour markers and biomarkers: Recent therapeutic advances. *World Journal of Gastroenterology*, *22*(5), 1745–1755. http://doi.org/10.3748/wjg.v22.i5.1745

Lee, J. W., Lee, E. J., Hong, S. H., Chung, W. H., Lee, H. T., Lee, T. W., … Ryoo, Z. Y. (2001). Circling mouse: possible animal model for deafness. *Comparative Medicine*, *51*(6), 550–554.

Lee, S. J., & Montell, C. (2004). Light-dependent translocation of visual arrestin regulated by the NINAC myosin III. *Neuron*, *43*(1), 95–103. http://doi.org/10.1016/j.neuron.2004.06.014

Lehner, B., Sandner, B., Marschallinger, J., Lehner, C., Furtner, T., Couillard-Despres, S., … Aigner, L. (2011). The dark side of BrdU in neural stem cell biology: Detrimental effects on cell cycle, differentiation and survival. *Cell and Tissue Research*, *345*(3), 313–328. http://doi.org/10.1007/s00441-011-1213-7

Li, Q., & Sarna, S. K. (2009). Nuclear Myosin II Regulates the Assembly of Preinitiation Complex for ICAM-1 Gene Transcription. *Gastroenterology*, *137*(3), 1051–1060. http://doi.org/10.1053/j.gastro.2009.03.040

Li, T., Guo, H., Song, Y., Zhao, X., Shi, Y., Lu, Y., … Wu, K. (2014). Loss of vinculin and membrane-bound β-catenin promotes metastasis and predicts poor prognosis in colorectal cancer. *Molecular Cancer*, *13*(1), 1–15. http://doi.org/10.1186/1476-4598-13-263

Lian, G., Dettenhofer, M., Lu, J., Downing, M., Chenn, A., Wong, T., & Sheen, V. (2016). Filamin A- and formin 2-dependent endocytosis regulates proliferation via the canonical Wnt pathway. *Development*, *143*(23), 4509–4520. http://doi.org/10.1242/dev.139295

Lindsay, A. J., & McCaffrey, M. W. (2009). Myosin Vb localises to nucleoli and associates with the RNA polymerase I transcription complex. *Cell Motility and the Cytoskeleton*, *66*(12), 1057–1072. http://doi.org/10.1002/cm.20408

Lo, C.-M., Buxton, D. B., Chua, G. C. H., Dembo, M., Adelstein, R. S., & Wang, Y.-L. (2004). Nonmuscle Myosin IIB Is Involved in the Guidance of Fibroblast Migration. *Molecular Biology of the Cell*, *15*(3), 982–989. http://doi.org/10.1091/mbc.E03-06-0359

Loikkanen, I., Toljamo, K., Hirvikoski, P., Väisänen, T., Paavonen, T. K., & Vaarala, M. H. (2009).

Myosin VI is a modulator of androgen-dependent gene expression. *Oncology Reports*, *22*, 991–995. http://doi.org/10.3892/or_00000526

Lu, H., & Bilder, D. (2005). Endocytic control of epithelial polarity and proliferation in Drosophila. *Nature Cell Biology*, *7*(12), 1132–1139. http://doi.org/10.1038/ncb1324

Ma, X., Yan, J., Chen, W., Du, P., Xie, J., Yu, H., & Wu, H. (2015). Knockdown of myosin VI inhibits proliferation of hepatocellular carcinoma cells in vitro. *Chemical Biology & Drug Design*, *86*(4), 723–730. http://doi.org/10.1111/cbdd.12544

Maddugoda, M. P., Crampton, M. S., Shewan, A. M., & Yap, A. S. (2007). Myosin VI and vinculin cooperate during the morphogenesis of cadherin cell-cell contacts in mammalian epithelial cells. *Journal of Cell Biology*, *178*(3), 529–540. http://doi.org/10.1083/jcb.200612042

Majewski, L., Nowak, J., Sobczak, M., Karatsai, O., Havrylov, S., Lenartowski, R., … Redowicz, M. J. (2018). Myosin VI in the nucleus of neurosecretory PC12 Cells: Stimulation-dependent nuclear translocation and interaction with nuclear proteins. *Nucleus*, *9*, 125–141. http://doi.org/10.1080/19491034.2017.1421881

Majewski, Ł., Sobczak, M., Havrylov, S., Jóźwiak, J., & Rędowicz, M. J. (2012). Dock7: A GEF for Rho-family GTPases and a novel myosin VI-binding partner in neuronal PC12 cells. *Biochemistry and Cell Biology*, *90*(4), 565–574. http://doi.org/10.1139/o2012-009

Malvezzi, M., Bertuccio, P., Rosso, T., Rota, M., Levi, F., La Vecchia, C., & Negri, E. (2015). European cancer mortality predictions for the year 2015: Does lung cancer have the highest death rate in EU women? *Annals of Oncology*, *26*(4), 779–786. http://doi.org/10.1093/annonc/mdv001

Malvezzi, M., Carioli, G., Bertuccio, P., Rosso, T., Boffetta, P., Levi, F., … Negri, E. (2016). European cancer mortality predictions for the year 2016 with focus on leukaemias. *Annals of Oncology*, *27*(4), 725–731. http://doi.org/10.1093/annonc/mdw022

Marcus, L., Lemery, S. J., Khasar, S., Wearne, E., Helms, W. S., Yuan, W., … Pazdur, R. (2017). FDA approval summary: TAS-102. *Clinical Cancer Research*, *23*(12), 2924–2927. http://doi.org/10.1158/1078-0432.CCR-16-2157

Mariadason, J. M., Bordonaro, M., Aslam, F., Shi, L., Kuraguchi, M., Velcich, A., & Augenlicht, L. H. (2001). Down-regulation of β-Catenin TCF Signaling Is Linked to Colonic Epithelial Cell Differentiation. *Cancer Research*, *61*, 3465–3471.

Mariadason, J. M., Rickard, K. L., Barkla, D. H., Augenlicht, L. H., & Gibson, P. R. (2000). Divergent phenotypic patterns and commitment to apoptosis of Caco-2 cells during spontaneous and butyrate-induced differentiation. *Journal of Cellular Physiology*, *183*(3), 347–354. http://doi.org/10.1002/(SICI)1097-4652(200006)183:3<347::AID-JCP7>3.0.CO;2-W

Markowitz, S. D., & Bertagnolli, M. M. (2009). Molecular Basis of Colorectal Cancer. *The New England Journal of Medicine*, *361*(25), 2449–2460. http://doi.org/10.1056/NEJMra0804588.

Markowitz, S. D., Dawson, D. M., Willis, J., & Willson, J. K. V. (2002). Focus on colon cancer. *Cancer Cell*, *1*(3), 233–236. http://doi.org/doi.org/10.1016/S1535-6108(02)00053-3

Mármol, I., Sánchez-de-Diego, C., Pradilla Dieste, A., Cerrada, E., & Rodriguez Yoldi, M. J.

(2017). Colorectal Carcinoma: A General Overview and Future Perspectives in Colorectal Cancer. *International Journal of Molecular Sciences*, *18*(1), 197. http://doi.org/10.3390/ijms18010197

Martin-Belmonte, F., & Perez-Moreno, M. (2012). Epithelial cell polarity, stem cells and cancer. *Nature Reviews Cancer*, *12*(1), 23–38. http://doi.org/10.1038/nrc3169

Maru, Y., Orihashi, K., & Hippo, Y. (2016). Lentivirus-Based Stable Gene Delivery into Intestinal Organoids. *Gastrointestinal Physiology and Diseases*, *1422*, 13–21. http://doi.org/10.1007/978-1-4939-3603-8_2

Masters, T. A., Kendrick-Jones, J., & Buss, F. (2016). Calcium gets myosin VI ready for work. *Proceedings of the National Academy of Sciences*, *113*(9), 2325–2327. http://doi.org/10.1073/pnas.1600725113

Matsumoto, H., Erickson, R. H., Gum, J. R., Yoshioka, M., Gum, E., & Kim, Y. S. (1990). Biosynthesis of Alkaline-Phosphatase During Differentiation of the Human Colon Cancer Cell-Line Caco-2. *Gastroenterology*, *98*(5), 1199–1207. http://doi.org/10.1016/0016-5085(90)90334-W

Maupin, P., Phillips, C. L., Adelstein, R. S., & Pollard, T. D. (1994). Differential localization of myosin-II isozymes in human cultured cells and blood cells. *Journal of Cell Science*, *107*(11), 3077–3090.

Maxfield, F., & McGraw, T. (2004). Endocytic recycling. *Nature Reviews Molecular Cell Biology*, *5*(2), 121–32. http://doi.org/10.1038/nrm1315

Mayer, A., Masafumi, T., Fritz, E., Schellander, G., Kofler, K., & Ludwig, H. (1993). The prognostic significance of proliferating cell nuclear antigen, epidermal growth factor receptor, and mdr gene expression in colorectal cancer. *Cancer*, *71*(8), 2454–2460. http://doi.org/10.1002/1097-0142(19930415)71:8<2454::AID-CNCR2820710805>3.0.CO;2-2

Mazzolini, R., Dopeso, H., Mateo-lozano, S., Chang, W., Rodrigues, P., & Bazzocco, S. (2012). Brush border Myosin Ia has tumor suppressor activity in the intestine. *Proceedings of the National Academy of Sciences*, *109*, 1530–1535. http://doi.org/10.1073/pnas.1108411109

McDonald, S. A. C., Preston, S. L., Lovell, M. J., Wright, N. A., & Jankowski, J. A. Z. (2006). Mechanisms of disease: from stem cells to colorectal cancer. *Nature Clinical Practice. Gastroenterology & Hepatology*, *3*(5), 267–274. http://doi.org/10.1038/ncpgasthep0473

Medema, J. P., & Vermeulen, L. (2011). Microenvironmental regulation of stem cells in intestinal homeostasis and cancer. *Nature*, *474*(7351), 318–26. http://doi.org/10.1038/nature10212

Meerbrey, K. L., Hu, G., Kessler, J. D., Roarty, K., Li, M. Z., Fang, J. E., … Elledge, S. J. (2011). The pINDUCER lentiviral toolkit for inducible RNA interference in vitro and in vivo. *Proceedings of the National Academy of Sciences*, *108*(9), 3665–3670. http://doi.org/10.1073/pnas.1019736108

Mehl, K. A., Davis, J. M., Clements, J. M., Berger, F. G., Pena, M. M., & Carson, J. A. (2005). Decreased intestinal polyp multiplicity is related to exercise mode and gender in ApcMin/+ mice. *Journal of Applied Physiology*, *98*(6), 2219–2225. http://doi.org/10.1152/japplphysiol.00975.2004

Melchionda, S., Ahituv, N., Bisceglia, L., Sobe, T., Glaser, F., Rabionet, R., … Gasparini, P. (2001). MYO6, the human homologue of the gene responsible for deafness in Snell's waltzer mice, is mutated in autosomal dominant nonsyndromic hearing loss. *American Journal of Human Genetics*, *69*(3), 635–640. http://doi.org/10.1086/323156

Menke, V., Van Zoest, K. P. M., Moons, L. M. G., Pot, R. G. J., Siersema, P. D., Kuipers, E. J., & Kusters, J. G. (2012). Myo9B is associated with an increased risk of Barrett's esophagus and esophageal adenocarcinoma. *Scandinavian Journal of Gastroenterology*, *47*(12), 1422–1428. http://doi.org/10.3109/00365521.2012.722673

Millo, H., Leaper, K., Lazou, V., & Bownes, M. (2004). Myosin VI plays a role in cell-cell adhesion during epithelial morphogenesis. *Mechanisms of Development*, *121*(11), 1335–1351. http://doi.org/10.1016/j.mod.2004.06.007

Mimura, M., Masuda, A., Nishiumi, S., Kawakami, K., Fujishima, Y., Yoshie, T., … Yoshida, M. (2012). AP1B plays an important role in intestinal tumorigenesis with the truncating mutation of an APC gene. *International Journal of Cancer*, *130*(5), 1011–1020. http://doi.org/10.1002/ijc.26131

Mischel, P. S., Shai, R., Shi, T., Horvath, S., Lu, K. V., Choe, G., … Nelson, S. F. (2003). Identification of molecular subtypes of glioblastoma by gene expression profiling. *Oncogene*, *22*(15), 2361–2373. http://doi.org/10.1038/sj.onc.1206344

Miyagawa, M., Naito, T., Nishio, S., Kamatani, N., & Usami, S. (2013). Targeted Exon Sequencing Successfully Discovers Rare Causative Genes and Clarifies the Molecular Epidemiology of Japanese Deafness Patients. *PLoS ONE*, *8*(8), 1–11. http://doi.org/10.1371/journal.pone.0071381

Miyagawa, M., Nishio, S., Kumakawa, K., & Usami, S. (2015). Massively Parallel DNA Sequencing Successfully Identified Seven Families With Deafness-Associated MYO6 Mutations: The Mutational Spectrum and Clinical Characteristics. *Annals of Otology, Rhinology & Laryngology*, *124*, 148S–157S. http://doi.org/10.1177/0003489415575055

Miyoshi, H., & Stappenbeck, T. S. (2013). In vitro expansion and genetic modification of gastrointestinal stem cells as organoids. *Nat Protocols*, *8*(12), 2471–2482. http://doi.org/10.1038/nprot.2013.153

Mohiddin, S. A., Ahmed, Z. M., Griffith, A. J., Tripodi, D., Friedman, T. B., Fananapazir, L., & Morell, R. J. (2004). Novel association of hypertrophic cardiomyopathy, sensorineural deafness, and a mutation in unconventional myosin VI (MYO6). *Journal of Medical Genetics*, *41*(4), 309–314. http://doi.org/10.1136/jmg.2003.011973

Moran, G. W., Leslie, F. C., Levison, S. E., Worthington, J., & McLaughlin, J. T. (2008). Enteroendocrine cells: neglected players in gastrointestinal disorders? *Therapeutic Advances in Gastroenterology*, *1*(1), 51–60. http://doi.org/10.1177/1756283X08093943

Morris, S. M., Arden, S. D., Roberts, R. C., Kendrick-Jones, J., Cooper, J. A., Luzio, J. P., & Buss, F. (2002). Myosin VI binds to and localises with Dab2, potentially linking receptor-mediated endocytosis and the actin cytoskeleton. *Traffic*, *3*(5), 331–41. http://doi.org/doi.org/10.1034/j.1600-0854.2002.30503.x

Morriswood, B., Ryzhakov, G., Puri, C., Arden, S. D., Roberts, R., Dendrou, C., … Buss, F. (2007). T6BP and NDP52 are myosin VI binding partners with potential roles in cytokine signalling and cell adhesion. *Journal of Cell Science*, *120*(Pt 15), 2574–85.

http://doi.org/10.1242/jcs.007005

Moser, A. R., Pitot, H. C., & Dove, W. F. (1990). A Dominant Mutation That Predisposes Intestinal Neoplasia in the Mouse. *Science*, *247*(4940), 322–324. http://doi.org/10.1126/science.2296722

Mouradov, D., Sloggett, C., Jorissen, R. N., Love, C. G., Li, S., Burgess, A. W., … Sieber, O. M. (2014). Colorectal cancer cell lines are representative models of the main molecular subtypes of primary cancer. *Cancer Research*, *74*(12), 3238–3247. http://doi.org/10.1158/0008-5472.CAN-14-0013

Mukherjea, M., Llinas, P., Kim, H. J., Travaglia, M., Safer, D., Ménétrey, J., … Sweeney, H. L. (2009). Myosin VI Dimerization Triggers an Unfolding of a Three-Helix Bundle in Order to Extend Its Reach. *Molecular Cell*, *35*(3), 305–315. http://doi.org/10.1016/j.molcel.2009.07.010

Muthuswamy, S. K., & Xue, B. (2012). Cell Polarity as a Regulator of Cancer Cell Behavior Plasticity. *Annual Review of Cell and Developmental Biology*, *28*(1), 599–625. http://doi.org/10.1146/annurev-cellbio-092910-154244

Muzny, D. M., Bainbridge, M. N., Chang, K., Dinh, H. H., Drummond, J. a., Fowler, G., … Thomson., E. (2012). Comprehensive molecular characterization of human colon and rectal cancer. *Nature*, *487*(7407), 330–337. http://doi.org/10.1038/nature11252

Nagafuchi, A., & Takeichi, M. (1989). Transmembrane control of cadherin-mediated cell adhesion: a 94 kDa protein functionally associated with a specific region of the cytoplasmic domain of E-cadherin. *Cell Regulation*, *1*(1), 37–44. http://doi.org/10.1091/mbc.1.1.37

Nakano, T., Tani, M., Nishioka, M., Kohno, T., Otsuka, A., Ohwada, S., & Yokota, J. (2005). Genetic and epigenetic alterations of the candidate tumor-suppressor gene MYO18B, on chromosome arm 22q, in colorectal cancer. *Genes Chromosomes and Cancer*, *43*(2), 162–171. http://doi.org/10.1002/gcc.20180

Nash, J. E., Appleby, V. J., Corrêa, S. A. L., Wu, H., Fitzjohn, S. M., Garner, C. C., … Molnár, E. (2010). Disruption of the interaction between myosin VI and SAP97 is associated with a reduction in the number of AMPARs at hippocampal synapses. *Journal of Neurochemistry*, *112*(3), 677–690. http://doi.org/10.1111/j.1471-4159.2009.06480.x

NCBI - GenBank. (2017). Retrieved May 27, 2018, from https://www.ncbi.nlm.nih.gov/genbank/

Nishioka, M., Kohno, T., Tani, M., Yanaihara, N., Tomizawa, Y., Otsuka, A., … Yokota, J. (2002). MYO18B, a candidate tumor suppressor gene at chromosome 22q12.1, deleted, mutated, and methylated in human lung cancer. *Proceedings of the National Academy of Sciences*, *99*(19), 12269–12274. http://doi.org/10.1073/pnas.192445899

Noguchi, T., Lenartowska, M., & Miller, K. G. (2006). Myosin VI Stabilizes an Actin Network during Drosophila Spermatid Individualization. *Molecular Biology of the Cell*, *17*(6), 2559–2571. http://doi.org/10.1091/mbc.E06-01-0031

Ohashi, S., Koike, K., Omori, A., Ichinose, S., Ohara, S., Kobayashi, S., … Anzai, K. (2002). Identification of mRNA/protein (mRNP) complexes containing Purα, mStaufen, Fragile X Protein, and myosin Va and their association with rough endoplasmic reticulum equipped with a kinesin motor. *Journal of Biological Chemistry*, *277*(40), 37804–37810.

http://doi.org/10.1074/jbc.M203608200

Olson, A. (2006). RNAi Codex: a portal/database for short-hairpin RNA (shRNA) gene-silencing constructs. *Nucleic Acids Research*, *34*(90001), D153–D157. http://doi.org/10.1093/nar/gkj051

Oonk, A. M. M., Leijendeckers, J. M., Lammers, E. M., Weegerink, N. J. D., Oostrik, J., Beynon, A. J., … Pennings, R. J. E. (2013). Progressive hereditary hearing impairment caused by a MYO6 mutation resembles presbyacusis. *Hearing Research*, *299*, 88–98. http://doi.org/10.1016/j.heares.2012.12.015

Paddison, P. J., Cleary, M., Silva, J. M., Chang, K., Sheth, N., Sachidanandam, R., & Hannon, G. J. (2004). Cloning of short hairpin RNAs for gene knockdown in mammalian cells. *Nature Methods*, *1*(2), 163–167. http://doi.org/10.1038/nmeth1104-163

Pancione, M., Remo, A., & Colantuoni, V. (2012). Genetic and epigenetic events generate multiple pathways in colorectal cancer progression. *Pathology Research International*, *2012*, 509348. http://doi.org/10.1155/2012/509348

Peckham, M. (2011). Coiled coils and SAH domains in cytoskeletal molecular motors. *Biochemical Society Transactions*, *39*(5), 1142–8. http://doi.org/10.1042/BST0391142

Penengo, L., Mapelli, M., Murachelli, A. G., Confalonieri, S., Magri, L., Musacchio, A., … Schneider, T. R. (2006). Crystal Structure of the Ubiquitin Binding Domains of Rabex-5 Reveals Two Modes of Interaction with Ubiquitin. *Cell*, *124*(6), 1183–1195. http://doi.org/10.1016/j.cell.2006.02.020

Philimonenko, V. V., Janáček, J., Harata, M., & Hozák, P. (2010). Transcription-dependent rearrangements of actin and nuclear myosin I in the nucleolus. *Histochemistry and Cell Biology*, *134*(3), 243–249. http://doi.org/10.1007/s00418-010-0732-8

Pino, M. S., & Chung, D. C. (2010). The Chromosomal Instability Pathway in Colon Cancer. *Gastroenterology*, *138*(6), 2059–2072. http://doi.org/10.1053/j.gastro.2009.12.065

Pinto, D., & Clevers, H. (2005). Wnt, stem cells and cancer in the intestine. *Biology of the Cell*, *97*(3), 185–196. http://doi.org/10.1042/BC20040094

Pollard, T. D., & Borisy, G. G. (2003). Cellular motility driven by assembly and disassembly of actin filaments. *Cell*, *112*(4), 453–465. http://doi.org/10.1016/S0092-8674(03)00120-X

Porter, A. G., & Jänicke, R. U. (1999). Emerging roles of caspase-3 in apoptosis. *Cell Death and Differentiation*, *6*(2), 99–104. http://doi.org/10.1038/sj.cdd.4400476

Post, P. L., Bokoch, G. M., & Mooseker, M. S. (1998). Human myosin-IXb is a mechanochemically active motor and a GAP for rho. *Journal of Cell Science*, *111*, 941–950. Retrieved from http://www.ncbi.nlm.nih.gov/pubmed/9490638

Preston, S. L., Wong, W. M., Chan, A. O. O., Poulsom, R., Jeffery, R., Goodlad, R. A., … Wright, N. A. (2003). Bottom-up histogenesis of colorectal adenomas: Origin in the monocryptal adenoma and initial expansion by crypt fission. *Cancer Research*, *63*(13), 3819–3825. http://doi.org/63:3819-3825

Puri, C., Chibalina, M. V, Arden, S. D., Kruppa, A. J., Kendrick-Jones, J., & Buss, F. (2010). Overexpression of myosin VI in prostate cancer cells enhances PSA and VEGF secretion, but has no effect on endocytosis. *Oncogene*, *29*(2), 188–200.

http://doi.org/10.1038/onc.2009.328

Puthalakath, H., Villunger, A., O'Reilly, L. A., Beaumont, J. G., Coultas, L., Cheney, R. E., … Strasser, A. (2001). Bmf: A proapoptotic BH3-only protein regulated by interaction with the myosin V actin motor complex, activated by anoikis. *Science*, *293*(5536), 1829–1832. http://doi.org/10.1126/science.1062257

Qiu, M., Hu, J., Yang, D., Cosgrove, D. P., & Xu, R. (2015). Pattern of distant metastases in colorectal cancer : a SEER based study. *Oncotarget*, *6*(36), 1–9. http://doi.org/10.18632/oncotarget.6130

Quintero, O. A., DiVito, M. M., Adikes, R. C., Kortan, M. B., Case, L. B., Lier, A. J., … Cheney, R. E. (2009). Human Myo19 Is a Novel Myosin that Associates with Mitochondria. *Current Biology*, *19*(23), 2008–2013. http://doi.org/10.1016/j.cub.2009.10.026

Rajagopalan, H., Nowak, M. A., Vogelstein, B., & Lengauer, C. (2003). The significance of unstable chromosomes in colorectal cancer. *Nature Reviews. Cancer*, *3*(9), 695–701. http://doi.org/10.1038/nrc1165

Rajendran, S., Salwa, S., Gao, X., Tabirca, S., O'Hanlon, D., O'Sullivan, G. C., & Tangney, M. (2010). Murine bioluminescent hepatic tumour model. *Journal of Visualized Experiments : JoVE*, (41), 5–7. http://doi.org/10.3791/1977

Rao, M. V., Engle, L. J., Mohan, P. S., Yuan, A., Qiu, D., Cataldo, A., … Nixon, R. A. (2002). Myosin Va binding to neurofilaments is essential for correct myosin Va distribution and transport and neurofilament density. *Journal of Cell Biology*, *159*(2), 279–289. http://doi.org/10.1083/jcb.200205062

Reck-Peterson, S. L., Provance, D. W., Mooseker, M. S., & Mercer, J. A. (2000). Class V myosins. *Biochimica et Biophysica Acta - Molecular Cell Research*, *1496*(1), 36–51. http://doi.org/10.1016/S0167-4889(00)00007-0

Reinhard, J., Scheel, A. A., Diekmann, D., Hall, A., Ruppert, C., & Bähler, M. (1995). A novel type of myosin implicated in signalling by rho family GTPases. *The EMBO Journal*, *14*(4), 697–704. http://doi.org/10.1002/j.1460-2075.1995.tb07048.x

Reya, T., & Clevers, H. (2005). Wnt signalling in stem cells and cancer. *Nature*, *434*(7035), 843–50. http://doi.org/10.1038/nature03319

Ridley, A. J. (2003). Cell Migration: Integrating Signals from Front to Back. *Science*, *302*(5651), 1704–1709. http://doi.org/10.1126/science.1092053

Riihimäki, M., Hemminki, A., Sundquist, J., & Hemminki, K. (2016). Patterns of metastasis in colon and rectal cancer. *Scientific Reports*, *6*(1), 29765. http://doi.org/10.1038/srep29765

RNAi Central shRNA retriever. (2009). Retrieved April 5, 2017, from http://cancan.cshl.edu/RNAi_central/RNAi.cgi?type=shRNA

RNAi Codex. (2009). Retrieved April 4, 2017, from http://cancan.cshl.edu/cgi-bin/Codex/Codex.cgi

Rodrigues, P., Macaya, I., Bazzocco, S., Mazzolini, R., Andretta, E., Dopeso, H., … Arango, D. (2014). RHOA inactivation enhances Wnt signalling and promotes colorectal cancer. *Nature Communications*, *5*, 5458. http://doi.org/10.1038/ncomms6458

Rosenberg, D. W., Giardina, C., & Tanaka, T. (2009). Mouse models for the study of colon carcinogenesis. *Carcinogenesis*, *30*(2), 183–196. http://doi.org/10.1093/carcin/bgn267

Rosenblatt, J., Cramer, L. P., Baum, B., & McGee, K. M. (2004). Myosin II-dependent cortical movement is required for centrosome separation and positioning during mitotic spindle assembly. *Cell*, *117*(3), 361–372. http://doi.org/10.1016/S0092-8674(04)00341-1

Ross, M. E., Zhou, X., Song, G., Shurtleff, S. A., Girtman, K., Song, W. Kg., … Downing, J. R. (2003). Classification of pediatric acute lymphoblastic leukemia by gene expression profiling. *The American Society of Hematology*, *102*(8), 2951–2959. http://doi.org/10.1182/blood-2003-01-0338.

Sahlender, D. A., Roberts, R. C., Arden, S. D., Spudich, G., Taylor, M. J., Luzio, J. P., … Buss, F. (2005). Optineurin links myosin VI to the Golgi complex and is involved in Golgi organization and exocytosis. *The Journal of Cell Biology*, *169*(2), 285–95. http://doi.org/10.1083/jcb.200501162

Saitoh, T., Takemura, S., Ueda, K., Hosoya, H., Nagayama, M., Haga, H., … Takahashi, M. (2001). Differential localization of non-muscle myosin II isoforms and phosphorylated regulatory light chains in human MRC-5 fibroblasts. *FEBS Letters*, *509*(3), 365–369. http://doi.org/10.1016/S0014-5793(01)03186-6

Sakurai, K., Hirata, M., Yamaguchi, H., Nakamura, Y., & Fukami, K. (2011). Phospholipase Cδ3 is a novel binding partner of myosin VI and functions as anchoring of myosin VI on plasma membrane. *Advances in Enzyme Regulation*, *51*(1), 171–81. http://doi.org/10.1016/j.advenzreg.2010.09.014

Salles, F. T., Andrade, L. R., Tanda, S., Grati, M., Plona, K. L., Gagnon, L. H., … Berryman, M. a. (2014). CLIC5 stabilizes membrane-actin filament linkages at the base of hair cell stereocilia in a molecular complex with radixin, taperin, and myosin VI. *Cytoskeleton (Hoboken, N.J.)*, *71*(1), 61–78. http://doi.org/10.1002/cm.21159

Sambuy, Y., De Angelis, I., Ranaldi, G., Scarino, M. L., Stammati, A., & Zucco, F. (2005). The Caco-2 cell line as a model of the intestinal barrier: influence of cell and culture-related factors on Caco-2 cell functional characteristics. *Cell Biology and Toxicology*, *21*(1), 1–26. http://doi.org/10.1007/s10565-005-0085-6

Sanggaard, K. M., Kjaer, K. W., Eiberg, H., Nürnberg, G., Nürnberg, P., Hoffman, K., … Tranebjærg, L. (2008). A novel nonsense mutation in MYO6 is associated with progressive nonsyndromic hearing loss in a Danish DFNA22 family. *American Journal of Medical Genetics, Part A*, *146*(8), 1017–1025. http://doi.org/10.1002/ajmg.a.32174

Sansom, O. J., Reed, K. R., Hayes, A. J., Ireland, H., Brinkmann, H., Newton, I. P., … Winton, D. J. (2004). Loss of Apc in vivo immediately perturbs Wnt signaling, differentiation, and migration. *Genes and Development*, *18*(12), 1385–1390. http://doi.org/10.1101/gad.287404

Sato, T., Es, J. H. Van, Snippert, H. J., Stange, D. E., Vries, R. G., Born, V. Den, … Clevers, H. (2011). Paneth cells constitute the niche for Lgr5 stem cells in intestinal crypts. *Nature*, *469*(7330), 415–418. http://doi.org/10.1038/nature09637

Sato, T., Mushiake, S., Kato, Y., Sato, K., Sato, M., Takeda, N., … Harada, A. (2007). The Rab8 GTPase regulates apical protein localization in intestinal cells. *Nature*, *448*(7151), 366–369. http://doi.org/10.1038/nature05929

Schepers, A., & Clevers, H. (2012). Wnt Signaling, Stem Cells, and Cancer of the Gastrointestinal Tract. *Cold Spring Harbor Perspectives in Biology*, *4*(4), a007989. http://doi.org/10.1101/cshperspect.a007989

Scholey, J. M., Brust-Mascher, I., & Mogilner, A. (2003). Cell division. *Nature*, *422*(6933), 746–752. http://doi.org/10.1038/nature01599

Schweitzer, J. K., & D'Souza-Schorey, C. (2002). Localization and activation of the ARF6 GTPase during cleavage furrow ingression and cytokinesis. *Journal of Biological Chemistry*, *277*(30), 27210–27216. http://doi.org/10.1074/jbc.M201569200

Scott, C. C., Vacca, F., & Gruenberg, J. (2014). Endosome maturation, transport and functions. *Seminars in Cell & Developmental Biology*, *31*, 2–10. http://doi.org/10.1016/j.semcdb.2014.03.034

Seiler, C., Ben-David, O., Sidi, S., Hendrich, O., Rusch, A., Burnside, B., … Nicolson, T. (2004). Myosin VI is required for structural integrity of the apical surface of sensory hair cells in zebrafish. *Developmental Biology*, *272*(2), 328–38. http://doi.org/10.1016/j.ydbio.2004.05.004

Self, T., Sobe, T., Copeland, N. G., Jenkins, N. A., Avraham, K. B., & Steel, K. P. (1999). Role of myosin VI in the differentiation of cochlear hair cells. *Developmental Biology*, *214*(2), 331–41. http://doi.org/10.1006/dbio.1999.9424

Servier Medical Art. (2004). Retrieved April 25, 2018, from https://smart.servier.com/category/anatomy-and-the-human-body/digestive-system/

Shearer, A. E., DeLuca, A. P., Hildebrand, M. S., Taylor, K. R., Gurrola, J., Scherer, S., … Smith, R. J. H. (2010). Comprehensive genetic testing for hereditary hearing loss using massively parallel sequencing. *Proceedings of the National Academy of Sciences*, *107*(49), 21104–21109. http://doi.org/10.1073/pnas.1012989107

Shih, I. M., Wang, T. L., Traverso, G., Romans, K., Hamilton, S. R., Ben-Sasson, S., … Vogelstein, B. (2001). Top-down morphogenesis of colorectal tumors. *Proceedings of the National Academy of Sciences of the United States of America*, *98*(5), 2640–5. http://doi.org/10.1073/pnas.051629398

Shoemaker, A. R., Moser, A. R., Midgley, C. A., Clipson, L., Newton, M. A., & Dove, W. F. (1998). A resistant genetic background leading to incomplete penetrance of intestinal neoplasia and reduced loss of heterozygosity in ApcMin/+ mice. *Proceedings of the National Academy of Sciences*, *95*(18), 10826–10831.

Sinicrope, F. A., Hart, J., Hsu, H. A., Lemoine, M., Michelassi, F., & Stephens, L. C. (1999). Apoptotic and mitotic indices predict survival rates in lymph node-negative colon carcinomas. *Clinical Cancer Research*, *5*(7), 1793–1804.

Skehan, P., Storeng, R., Scudiero, D., Monks, A., McMahon, J., Vistica, D., … Boyd, M. R. (1990). New colorimetric cytotoxicity assay for anticancer-drug screening. *Journal of National Cancer Institute*, *82*(13), 1107–1112. http://doi.org/doi.org/10.1093/jnci/82.13.1107

Skop, A. R., Bergmann, D., Mohler, W. A., & White, J. G. (2001). Completion of cytokinesis in C. elegans requires a brefeldin A-sensitive membrane accumulation at the cleavage furrow apex. *Current Biology*, *11*(10), 735–746. http://doi.org/10.1016/S0960-9822(01)00231-7

Soares, K. C., Foley, K., Olino, K., Leubner, A., Mayo, S. C., Jain, A., … Zheng, L. (2014). A preclinical murine model of hepatic metastases. *Journal of Visualized Experiments : JoVE*, (91), 51677. http://doi.org/10.3791/51677

Sobin, L. H., Gospodarowicz, M. K., & Wittekind, C. H. (2010). TNM classification of malignant tumors. 7th ed. Oxford: Wiley-Blackwell; 2010. *TNM Classification of Malignant Tumors. 7th Ed.*, 349–445. http://doi.org/10.1016/B978-1-4377-0272-9.50014-0

Song, C. F., Sader, K., White, H., Kendrick-Jones, J., & Trinick, J. (2010). Nucleotide-dependent shape changes in the reverse direction motor, myosin VI. *Biophysical Journal*, *99*(10), 3336–3344. http://doi.org/10.1016/j.bpj.2010.09.014

Spink, B. J., Sivaramakrishnan, S., Lipfert, J., Doniach, S., & Spudich, J. A. (2008). Long single alpha-helical tail domains bridge the gap between structure and function of myosin VI. *Nature Structural & Molecular Biology*, *15*(6), 591–7. http://doi.org/10.1038/nsmb.1429

Spudich, G., Chibalina, M. V, Au, J. S.-Y., Arden, S. D., Buss, F., & Kendrick-Jones, J. (2007). Myosin VI targeting to clathrin-coated structures and dimerization is mediated by binding to Disabled-2 and PtdIns(4,5)P2. *Nature Cell Biology*, *9*(2), 176–83. http://doi.org/10.1038/ncb1531

Standring, S., Borley, N. R., Collins, P., Crossman, A. R., Gatzoulis, M. A., Healy, J. C., … Wigley, C. B. (2008). *Gray's anatomy: the anatomical basis of clinical practice.* (40th editi). Elsevier, New York.

Stoffel, E. M., & Kastrinos, F. (2014). Familial colorectal cancer, beyond lynch syndrome. *Clinical Gastroenterology and Hepatology*, *12*(7), 1059–1068. http://doi.org/10.1016/j.cgh.2013.08.015

Strickland, L. I., & Burgess, D. R. (2004). Pathways for membrane trafficking during cytokinesis. *Trends in Cell Biology*, *14*(3), 115–118. http://doi.org/10.1016/j.tcb.2004.01.006

Su, L. K., Kinzler, K. W., Vogelstein, B., Preisinger, A. C., Moser, A. R., Luongo, C., … Dove, W. F. (1992). Multiple intestinal neoplasia caused by a mutation in the murine homolog of the APC gene. *Science (New York, N.Y.)*, *256*(5057), 668–70. http://doi.org/10.1126/science.1350108

Subramani, S., & Malhotra, V. (2013). Non-autophagic roles of autophagy-related proteins. *EMBO Reports*, *14*(2), 143–151. http://doi.org/10.1038/embor.2012.220

Sweeney, H. L., Park, H., Zong, A. B., Yang, Z., Selvin, P. R., & Rosenfeld, S. S. (2007). How myosin VI coordinates its heads during processive movement. *The EMBO Journal*, *26*(11), 2682–2692. http://doi.org/10.1038/sj.emboj.7601720

Syamaladevi, D. P., Spudich, J. A., & Sowdhamini, R. (2012). Structural and functional insights on the Myosin superfamily. *Bioinformatics and Biology Insights*, *6*, 11–21. http://doi.org/10.4137/BBI.S8451

TCGA Colon and Rectal Cancer (COADREAD) - Xena Functional Genomics Explorer. (2016). Retrieved April 28, 2018, from https://xenabrowser.net/

Terese Winslow LLC. (2014). Retrieved April 4, 2017, from www.teresewinslow.com

The cancer genome atlas. (2017). Retrieved June 14, 2018, from https://cancergenome.nih.gov/

The human protein atlas. (2017). Retrieved May 27, 2018, from https://www.proteinatlas.org/ENSG00000196586-MYO6/tissue

Thoeni, C. E., Vogel, G. F., Tancevski, I., Geley, S., Lechner, S., Pfaller, K., … Huber, L. A. (2014). Microvillus Inclusion Disease: Loss of Myosin Vb Disrupts Intracellular Traffic and Cell Polarity. *Traffic*, *15*(1), 22–42. http://doi.org/10.1111/tra.12131

Togo, T., & Steinhardt, R. A. (2004). Nonmuscle Myosin IIA and IIB Have Distinct Functions in the Exocytosis-dependent Process of Cell Membrane Repair. *Molecular Biology of the Cell*, *15*(2), 688–695. http://doi.org/10.1091/mbc.E03-06-0430

Tokuo, H., & Ikebe, M. (2004). Myosin X transports Mena/VASP to the tip of filopodia. *Biochemical and Biophysical Research Communications*, *319*(1), 214–220. http://doi.org/10.1016/j.bbrc.2004.04.167

Tomatis, V. M., Papadopulos, A., Malintan, N. T., Martin, S., Wallis, T., Gormal, R. S., … Meunier, F. A. (2013). Myosin VI small insert isoform maintains exocytosis by tethering secretory granules to the cortical actin. *Journal of Cell Biology*, *200*(3), 301–320. http://doi.org/10.1083/jcb.201204092

Trojan, J., Brieger, A., Raedle, J., Esteller, M., & Zeuzem, S. (2000). Promoter and Allelic Loss At Chromosome 19P13 . 3 in Sporadic Colorectal Cancer. *Gut*, *47*(2), 272–276.

Tumbarello, D. A., Kendrick-Jones, J., & Buss, F. (2013). Myosin VI and its cargo adaptors - linking endocytosis and autophagy. *Journal of Cell Science*, *126*(Pt 12), 2561–70. http://doi.org/10.1242/jcs.095554

Tumbarello, D. A., Waxse, B. J., Arden, S. D., Bright, N. a, Kendrick-Jones, J., & Buss, F. (2012). Autophagy receptors link myosin VI to autophagosomes to mediate Tom1-dependent autophagosome maturation and fusion with the lysosome. *Nature Cell Biology*, *14*(10), 1024–1035. http://doi.org/10.1038/ncb2589

Tuxworth, R. I., Weber, I., Wessels, D., Addicks, G. C., Soll, D. R., Gerisch, G., & Titus, M. A. (2001). A role for myosin VII in dynamic cell adhesion. *Current Biology*, *11*(5), 318–329. http://doi.org/10.1016/S0960-9822(01)00097-5

Tyska, M. J., Mackey, A. T., Huang, J.-D., Copeland, N. G., Jenkins, N. A., & Mooseker, M. S. (2005). Myosin-1a is critical for normal brush border structure and composition. *Molecular Biology of the Cell*, *16*(5), 2443–57. http://doi.org/10.1091/mbc.E04-12-1116

Tyska, M. J., & Mooseker, M. S. (2004). A role for myosin-1A in the localization of a brush border disaccharidase. *Journal of Cell Biology*, *165*(3), 395–405. http://doi.org/10.1083/jcb.200310031

UniProt. (2014). Retrieved April 9, 2018, from www.uniprot.org

Valdembri, D., Caswell, P. T., Anderson, K. I., Schwarz, J. P., König, I., Astanina, E., … Serini, G. (2009). Neuropilin-1/GIPC1 signaling regulates alpha5beta1 integrin traffic and function in endothelial cells. *PLoS Biology*, *7*(1), e25. http://doi.org/10.1371/journal.pbio.1000025

Van de Wetering, M., Sancho, E., Verweij, C., De Lau, W., Oving, I., Hurlstone, A., … Clevers, H. (2002). The β-catenin/TCF-4 complex imposes a crypt progenitor phenotype on colorectal cancer cells. *Cell*, *111*(2), 241–250. http://doi.org/10.1016/S0092-8674(02)01014-0

Van Roy, F., & Berx, G. (2008). The cell-cell adhesion molecule E-cadherin. *Cellular and*

Molecular Life Sciences, *65*(23), 3756–3788. http://doi.org/10.1007/s00018-008-8281-1

Varadi, A., Tsuboi, T., & Rutter, G. A. (2005). Myosin Va Transports Dense Core Secretory Vesicles in Pancreatic MIN6 B-Cells. *Molecular Biology of the Cell*, *16*(6), 2670–2680. http://doi.org/10.1091/mbc.E04-11-1001

Vickaryous, N., Polanco-Echeverry, G., Morrow, S., Suraweera, N., Thomas, H., Tomlinson, I., & Silver, A. (2008). Smooth-muscle myosin mutations in hereditary non-polyposis colorectal cancer syndrome. *British Journal of Cancer*, *99*(10), 1726–1728. http://doi.org/10.1038/sj.bjc.6604737

Voloshanenko, O., Erdmann, G., Dubash, T. D., Augustin, I., Metzig, M., Moffa, G., … Boutros, M. (2013). Wnt secretion is required to maintain high levels of Wnt activity in colon cancer cells. *Nature Communications*, *4*, 2610. http://doi.org/10.1038/ncomms3610

Vona, B., Müller, T., Nanda, I., Neuner, C., Hofrichter, M. A. H., Schröder, J., … Haaf, T. (2014). Targeted next-generation sequencing of deafness genes in hearing-impaired individuals uncovers informative mutations. *Genetics in Medicine*, *16*(12), 945–953. http://doi.org/10.1038/gim.2014.65

Vreugde, S., Ferrai, C., Miluzio, A., Hauben, E., Marchisio, P. C., Crippa, M. P., … Biffo, S. (2006). Nuclear Myosin VI Enhances RNA Polymerase II-Dependent Transcription. *Molecular Cell*, *23*(5), 749–755. http://doi.org/10.1016/j.molcel.2006.07.005

Wagner, H. E., Toth, C. A., Steele, G. D., & Thomas, P. (1992). Metastatic potential of human colon cancer cell lines: relationship to cellular differentiation and carcinoembryonic antigen production. *Clinical & Experimental Metastasis*, *10*(1), 25–31. Retrieved from http://www.ncbi.nlm.nih.gov/pubmed/1733644

Walther, A., Johnstone, E., Swanton, C., Midgley, R., Tomlinson, I., & Kerr, D. (2009). Genetic prognostic and predictive markers in colorectal cancer. *Nature Reviews in Cancer*, *9*(7), 489–499. http://doi.org/nrc2645 [pii]\r10.1038/nrc2645

Wang, D., Zhu, L., Liao, M., Zeng, T., Zhuo, W., Yang, S., & Wu, W. (2016). MYO6 knockdown inhibits the growth and induces the apoptosis of prostate cancer cells by decreasing the phosphorylation of ERK1/2 and PRAS40. *Oncology Reports*, 1285–1292. http://doi.org/10.3892/or.2016.4910

Wang, H., Wang, B., Zhu, W., & Yang, Z. (2015). Lentivirus-Mediated Knockdown of Myosin VI Inhibits Cell Proliferation of Breast Cancer Cell. *Cancer Biotherapy and Radiopharmaceuticals*, *30*(8), 330–335. http://doi.org/10.1089/cbr.2014.1759

Wang, Z.-J., Taylor, F., Churchman, M., Norbury, G., & Tomlinson, I. (1998). Genetic Pathways of Colorectal Carcinogenesis Rarely Involve the PTEN and LKB1 Genes Outside the Inherited Hamartoma Syndromes. *The American Journal of Pathology*, *153*(2), 363–366. http://doi.org/10.1016/S0002-9440(10)65579-4

Wang, Z., Ying, M., Wu, Q., Wang, R., & Li, Y. (2016). Overexpression of myosin VI regulates gastric cancer cell progression. *Gene*, *593*(1), 100–109. http://doi.org/10.1016/j.gene.2016.08.015

Warner, C. L., Stewart, A., Luzio, J. P., Steel, K. P., Libby, R. T., Kendrick-Jones, J., & Buss, F. (2003). Loss of myosin VI reduces secretion and the size of the Golgi in fibroblasts from Snell's waltzer mice. *The EMBO Journal*, *22*(3), 569–79. http://doi.org/10.1093/emboj/cdg055

Waterman-Storer, C., Duey, D. Y., Weber, K. L., Keech, J., Cheney, R. E., Salmon, E. D., & Bement, W. M. (2000). Microtubules remodel actomyosin networks in Xenopus egg extracts via two mechanisms of F-actin transport. *Journal of Cell Biology*, *150*(2), 361–376. http://doi.org/10.1083/jcb.150.2.361

Weidberg, H., Shvets, E., & Elazar, Z. (2011). Biogenesis and Cargo Selectivity of Autophagosomes. *Annual Review of Biochemistry*, *80*, 125–156. http://doi.org/10.1146/annurev-biochem-052709–094552

Weitz, J., Koch, M., Debus, J., Höhler, T., Galle, P. R., & Büchler, M. W. (2005). Colorectal cancer. *Lancet*, *365*(9454), 153–65. http://doi.org/10.1016/S0140-6736(05)17706-X

Wells, A. L., Lin, A. W., Chen, L. Q., Safer, D., Cain, S. M., Hasson, T., … Sweeney, H. L. (1999). Myosin VI is an actin-based motor that moves backwards. *Nature*, *401*(6752), 505–8. http://doi.org/10.1038/46835

Wilson, G. M., Fielding, A. B., Simon, G. C., Yu, X., Andrews, P. D., Hames, R. S., … Prekeris, R. (2005). The FIP3-Rab11 Protein Complex Regulates Recycling Endosome Targeting to the Cleavage Furrow during Late Cytokinesis. *Molecular Biology of the Cell*, *16*(2), 849–860. http://doi.org/10.1091/mbc.E04-10-0927

Wodarz, A., & Näthke, I. (2007). Cell polarity in development and cancer. *Nature Cell Biology*, *9*(9), 1016–24. http://doi.org/10.1038/ncb433

Wollscheid, H. P., Biancospino, M., He, F., Magistrati, E., Molteni, E., Lupia, M., … Polo, S. (2016). Diverse functions of myosin VI elucidated by an isoform-specific α-helix domain. *Nature Structural and Molecular Biology*, *23*(4), 300–308. http://doi.org/10.1038/nsmb.3187

Wu, H., Nash, J. E., Zamorano, P., & Garner, C. C. (2002). Interaction of SAP97 with minus-end-directed actin motor myosin VI: Implications for AMPA receptor trafficking. *Journal of Biological Chemistry*, *277*(34), 30928–30934. http://doi.org/10.1074/jbc.M203735200

Wu, X., Rao, K., Bowers, M. B., Copeland, N. G., Jenkins, N. A., & Hammer, J. A. (2001). Rab27a enables myosin Va-dependent melanosome capture by recruiting the myosin to the organelle. *Journal of Cell Science*, *114*(Pt 6), 1091–1100. http://doi.org/10.1091/mbc.11.2.691

Xie, X. M., Zhang, Z. Y., Yang, L. H., Yang, D. L., Tang, N., Zhao, H. Y., … Wang, E. H. (2013). Aberrant hypermethylation and reduced expression of disabled-2 promote the development of lung cancers. *International Journal of Oncology*, *43*(5), 1636–1642. http://doi.org/10.3892/ijo.2013.2084

Yanaihara, N., Nishioka, M., Kohno, T., Otsuka, A., Okamoto, A., Ochiai, K., … Yokota, J. (2004). Reduced expression of MYO18B, a candidate tumor-suppressor gene on chromosome ARM 22Q, in ovarian cancer. *International Journal of Cancer*, *112*(1), 150–154. http://doi.org/10.1002/ijc.20339

Yang, D. H., Fazili, Z., Smith, E. R., Cai, K. Q., Klein-Szanto, A., Cohen, C., … Xu, X. X. (2006). Disabled-2 heterozygous mice are predisposed to endometrial and ovarian tumorigenesis and exhibit sex-biased embryonic lethality in a p53-Null background. *American Journal of Pathology*, *169*(1), 258–267. http://doi.org/10.2353/ajpath.2006.060036

Yang, T., Wei, X., Chai, Y., Li, L., & Wu, H. (2013). Genetic etiology study of the non-syndromic deafness in Chinese Hans by targeted next-generation sequencing. *Orphanet Journal of*

Rare Diseases, *8*(1), 85–93. http://doi.org/10.1186/1750-1172-8-85

Yang, Z., & Klionsky, D. J. (2010). Mammalian autophagy: core molecular machinery and signaling regulation. *Current Opinion in Cell Biology*, *22*(2), 124–131. http://doi.org/10.1016/j.ceb.2009.11.014.Mammalian

Yoshida, H., Cheng, W., Hung, J., Montell, D., Geisbrecht, E., Rosen, D., … Naora, H. (2004). Lessons from border cell migration in the Drosophila ovary: A role for myosin VI in dissemination of human ovarian cancer. *Proceedings of the National Academy of Sciences of the United States of America*, *101*(21), 8144–8149. http://doi.org/10.1073/pnas.0400400101

You, W., Tan, G., Sheng, N., Gong, J., Yan, J., Chen, D., … Wang, Z. (2016). Downregulation of myosin VI reduced cell growth and increased apoptosis in human colorectal cancer. *Acta Biochimica et Biophysica Sinica*, *48*(5), 430–436. http://doi.org/10.1093/abbs/gmw020

Yu, H., Zhu, Z., Chang, J., Wang, J., & Shen, X. (2015). Lentivirus-Mediated Silencing of Myosin VI Inhibits Proliferation and Cell Cycle Progression in Human Lung Cancer Cells. *Chemical Biology & Drug Design*, *86*(4), 606–613. http://doi.org/10.1111/cbdd.12528

Zhang, H., Berg, J. S., Wang, Y., Lång, P., Sousa, A. D., Bhaskar, A., … Strömblad, S. (2004). Myosin-X provides a motor-based link between integrins and the cytoskeleton. *Nature Cell Biology*, *6*(6), 523–531. http://doi.org/10.1038/ncb1136

Zhang, X., Huang, Z., Hu, Y., & Liu, L. (2016). Knockdown of Myosin 6 inhibits proliferation of oral squamous cell carcinoma cells. *Journal of Oral Pathology & Medicine*, *45*(40), 740–745. http://doi.org/10.1111/jop.12448

Zhang, Z., Chen, Y., Tang, J. J., & Xie, X. (2014). Frequent loss expression of dab2 and promotor hypermethylation in human cancers: A meta-analysis and systematic review. *Pakistan Journal of Medical Sciences*, *30*(2), 432–437. http://doi.org/10.12669/pjms.302.4486

Zhu, X., Zeng, X., Huang, B., & Hao, S. (2004). Actin is closely associated with RNA polymerase II and involved in activation of gene transcription. *Biochemical and Biophysical Research Communications*, *321*(3), 623–630. http://doi.org/10.1016/j.bbrc.2004.05.229